Migraine pathophysiology: NR2A/SFKs signaling in cortical spreading depression

Thesis submitted in accordance with the requirements of the University of Liverpool for the degree of Doctor in Philosophy by Fan Bu

Primary supervisor: Dr. Minyan Wang

Co-supervisor: Professor John Paul Quinn

Molecular and Clinical Pharmacology

Institute of Translational Medicine

Faculty of Health and Life Sciences

University of Liverpool

UK

May 2017

Acknowledgement

First of all, my deepest gratitude goes first and foremost to Dr. Minyan Wang, my primary supervisor, for her constant guidance, encouragement and patience. She has walked me through all the stages of research and thesis writing. Without her illuminating supervision and instruction, this thesis could not have reached its present form. Her earnest and rigorous attitude always transcends academia and provides a quest for my life.

Second, I would like to express my heartfelt gratitude to my co-supervisor Professor John Paul Quinn, who has the attitude and the substance of a real scientist, for his enthusiasm and inclusion.

I am greatly indebted to my father and mother Xiaojun Bu and Min Du, who have provided me through moral, emotional and financial support in my life. I am also grateful to my other family members who have supported me along the way.

In addition, my thanks would go to my beloved wife Tingting Zhang and son Chong Bu for their loving considerations and great confidence in me all through these years. Send out my endless love to you!

Furthermore, I owe my sincere gratitude to all the fellow and friends for their help during my Ph.D. study, especially Yan Wang for her guidance in IHC, Yanli Li for her guidance in CSD recording in chick retina, and Ying Zhu and Mingming Yuan for their support in qPCR process. I am also grateful for providing NVP-AAM077 from Dr. Yi Li at Department of Chemistry, XJTLU, and for developing the script of Labview software from Dr. Shangbin Chen at Wuhan National Laboratory for Optoelectronics, Huazhong University of Science and Technology.

Finally, I would like to thank to XJTLU research development fund and Wangwenli Charitable Foundation for financial support.

Key words

Migraine, cortical spreading depression, NR2A, sarcoma family kinases, pannexin1, calcitonin gene-related peptide

Abstract

Cortical spreading depression (CSD) is a propagating neuronal/glial excitation, followed by depression in cerebral cortex and subcortical regions. It is known to be the underlying cause of migraine with aura in humans. CSD can also lead to migraine-like behavior by triggering pannexin1 (Panx1) channels opening and induce the release of calcitonin gene-related peptide (CGRP) that plays a key player in migraine patients. Increasing evidence points to an essential role of NR2A-containing NMDA receptors in CSD propagation *in vitro*; however whether NR2A also mediates CSD genesis and its downstream signaling associated with CSD is unknown. The purpose of this thesis is to clarify the contribution of NR2A-containing receptors to CSD propagation and determine their role in CSD genesis *in vivo*, and if so, to further explore the mechanism underlying the action of NR2A relevant to Panx1 channels opening and CGRP gene expression in rats. In the present study, CSD was induced both *in vitro* and *in vivo*. Multi-disciplinary methods were used including electrophysiology and intrinsic optical imaging for CSD recording, western blot, immunoprecipitation and immunohistochemistry for protein detection, and qPCR for gene expression analysis.

The results demonstrated that NR2A-containing receptor inhibition using NR2A-preferring antagonist, TCN-201, suppressed CSD propagation in a concentration-dependent manner in the chick retina. In addition, both the NR2A antagonists, NVP-AAM077 and TCN-201, concentration-dependently suppressed

CSD genesis but not propagation in the microdialysis-based CSD model in rats. Differently, perfusion of 0.3 nmol NVP-AAM077 into contralateral cerebroventricle considerably suppressed CSD propagation in rats. These data suggests a key role of NR2A in mediating both CSD genesis and propagation.

Further mechanism study showed that CSD not only promoted sarcoma family kinases (SFKs) activation, but also SFKs-Panx1 interaction and neuronal Panx1 channels opening in the ipsilateral cortex of rats. Corresponds to this finding, inhibition of SFKs by intracerebroventricle (*i.c.v.*) perfusion of 2.5 nmol PP2 not only attenuated both SFKs activation and Panx1 channels opening induced by CSD, but also suppressed CSD propagation. Furthermore, the CSD-induced SFKs activation, SFKs-Panx1 interaction and neuronal Panx1 channels opening were significantly suppressed under NR2A inhibition by *i.c.v.* perfusion of 0.3 nmol NVP-AAM077. Finally, pre-treatment with 0.3 nmol NVP-AAM077 prevented the elevation of CGRP mRNA 24 hour after multiple CSD in the ipsilateral visual cortex of rats.

In summary, this study provides strong evidence that NR2A-containing NMDA receptors contribute to CSD genesis and propagation, and reveals a previously unknown migraine mechanism of NR2A involving SFKs, Panx1 and CGRP during CSD, i.e. NR2A regulates single CSD-induced opening of neuronal Panx1 channels via coupling activated SFKs to Panx1 in cortex, and that NR2A regulates multiple CSD-induced CGRP gene expression in visual cortex. These findings provide new insights into CSD involving NR2A-containing receptor and downstream signals. Selectively antagonizing these elements might constitute a highly specific strategy treating migraine and other diseases associated with CSD.

List of Contents

Chapter 1 General introduction

1.1 Cortical spreading depression

1.1.1 Definition and brief history of its discovery

Cortical spreading depression (CSD) is a temporary excitation of synaptic activity followed by depression that propagates slowly (~ 3 mm/min) across the unilateral cerebral cortex and subcortical regions (Somjen, 2005). CSD was first described by Leão as an unexpected silencing of the ongoing electrical activity from the cortical surface of anesthetized rabbits, when he wanted to study the cortical electrogram of experimental epilepsy (Leao, 1944b) in 1944. Leão further recorded the negative slow potential change, including a depolarization followed by prolonged repolarization, associated with CSD from the cortical surface using string galvanometer and vacuum tube amplifier in 1947 (Leao, 1947). From then on, increasing studies have been attempting to explain its mechanism although it still remains far from clear.

1.1.2 Key features of CSD

Neurons and especial their proximal dendrites are the main active players of neuronal hyperexcitability, which is considered as the initiation of CSD (Dreier, 2011). However, the process of CSD is not only a local, temporary disruption of ionic homeostasis in neurons but also relevant to glia cells, e.g. microglia (Pusic et al., 2014) and astrocyte (Seidel and Shuttleworth, 2011, Seidel et al., 2016).

The experimental CSD can be triggered by electrical pulses, alkaline pH, low osmolarity, mechanical stimuli such as pressure on or puncture of the cerebral cortex, and a variety of chemicals such as K^+, N-methyl-D-aspartic (NMDA) or glutamate (Smith et al., 2006), in which the high-K^+ is used as one of the most common triggers for inducing single (Bolay et al., 2002) and multiple (Godukhin and Obrenovitch, 2001) CSD by either topical (Godukhin and Obrenovitch, 2001)

or through microdialysis (Obrenovitch et al., 1993) application for the study of both CSD genesis and propagation.

CSD is known to be associated with various physiological changes not only in the central nervous system (CNS), e.g. cortex (Feuerstein et al., 2016)and thalamus (Tepe et al., 2015), but also in the peripheral nervous system (PNS), e.g. trigeminal ganglion (Smith et al., 2006), in different species and humans (Somjen et al., 1992, Bowyer et al., 1999a, Bowyer et al., 1999b, Smith et al., 2000).

1.1.2.1 Changes in cerebral blood flow

Leão (Leao, 1944a) first described the dilation of pial blood vessels accompanying CSD in 1944, which is further examined using hydrogen clearance method (Matsushima et al., 1996), laser Doppler flowmetry (Back et al., 1994) and blood-oxygen level-dependent (BOLD) contrast (Cao et al., 1999). The regional cerebral blood flow (CBF) change response to CSD is typically composed of four distinct vasomotor phases: i) an initial hypoperfusion coincident with the depolarization of CSD; ii) a rapid hyperemia during and after the repolarization of CSD; iii) a smaller hyperemia followed the first hyperemia; and iv) a prolonged oligemia lasting an hour or more (Ayata and Lauritzen, 2015). Meanwhile, the regional CBF is not changed at any time in subcortical regions by either single or multiple CSD (Kuge et al., 2000).

Various vasoactive substances being released from, or produced by, brain cells is likely to be the underlying mechanisms of CBF change during CSD. These mainly include calcitonin gene-related peptide (CGRP), glutamate, acetycholine (ACh), cGMP and ATP (Colonna et al., 1994, Basarsky et al., 1999, Rodrigues and Martins-Ferreira, 1980, Read et al., 2001, Schock et al., 2007). For example, topical administration of CGRP, an extremely potent dilator of brain vessels (Arulmani et al., 2004) on meninges strongly increases dural blood flow (Levy et al., 2005), while CGRP receptor antagonist not only suppresses CSD (Tozzi et al., 2012) but also attenuates pial dilation induced by CSD (Colonna et al., 1994). It is known that glutamate receptor activation leads to vasodilation (Fergus and Lee, 1997), and that glutamate also triggers CSD (Lauritzen et al., 1988), which could

in part support the contribution of glutamate receptor to the CSD-induced CBF response. Because both NMDA (Peeters et al., 2007) and non-NMDA (i.e. α-amino-3-hydroxy-5-methyl-4-isoxazolepropionic acid, AMPA) (Holland et al., 2010) subtypes of glutamate receptors antagonists inhibit the CBF change, whereas only NMDA subtype suppresses CSD (Nellgard and Wieloch, 1992, Peeters et al., 2007), it possibly appears that the vasomotion response to glutamate via NMDA receptor mechanism under CSD condition.

CSD-induced vascular response may proceed independently via its direct vascular conduction. This notion is supported by the following evidences. Firstly, dilation of arterioles on the cortical surface propagates at a greater velocity than the underlying CSD wave and spread into areas not reached by CSD wave (Brennan et al., 2007). Secondly, multiple CSD waves induce an additional spontaneous CBF changes that spread to the contralateral cortex (Eftekhari, 2016). However, since CSD can proceed without alteration in the absence of the vascular response (Dahlem and Muller, 2000), the vascular response is apparently not essential for CSD process.

1.1.2.2 Changes in cellular ionic homeostasis and energy metabolism

The CSD phenomenon is associated with transient, localized redistribution of ions between the extracellular and intracellular. The extracellular concentration of K^+ rapidly rises and reaches levels as high as 30-60 mM. At the same time, the extracellular Na^+ and Cl^- levels decrease to approximately 50-70 mM as these ions enter cells and cause the neuronal excitation followed by depolarization and a period of electrical silence. Ca^{2+} enters after the outward movement of K^+, resulting in a net decrease in extracellular Ca^{2+} to approximately 0.2-0.8 mM (Pietrobon and Moskowitz, 2014). Selective blocking of ion channels, e.g. Na^+ channel, depresses CSD (Tozzi et al., 2012), while increasing the concentration of K^+ in the perfusion medium restores CSD propagation (Obrenovitch and Zilkha, 1995). In the absence of Ca^{2+} in the perfusion medium, the initiation of CSD is completely prevented (Obrenovitch et al., 1993). All of the above evidences suggest the critical roles of ions in CSD. These fluxes also result in a transient

cellular swelling and an accompanying decrease in the volume of extracellular fluid (Zhou et al., 2010). Additionally, pH selective microelectrode in the extracellular space shows a rapid transient alkalinisation followed by a large, prolonged acidification (Mutch and Hansen, 1984).

It is well established that CSD stimulates energy demand (Krivanek, 1961, Mies and Paschen, 1984, Mayevsky and Weiss, 1991), which is directly linked to the disruption of the K^+ and Na^+ gradients across the cellular membrane because restoration from the ionic homeostasis requires energy (Hansen and Lauritzen, 1984). During this process, CSD-induced rise in cerebral metabolic rate of O_2 ($CMRO_2$) supports the increased Na^+-K^+-ATPase activity for transporting Na^+ out of, and K^+ into, the cells (Cruz et al., 1999), which uses more glucose (Shinohara et al., 1979) and lactate efflux (Cruz et al., 1999). The accumulation of intercellular Ca^{2+} during CSD may trigger an increase in $CMRO_2$ via the uniporter of Ca^{2+} in the membrane of mitochondria (Zhou et al., 2010). CSD can also activate glycolytic pathways. For example, CSD is accompanied with the rise of lactate and reduction of glycogen in the brain (Lauritzen et al., 1990). The activation of glycolytic pathway is also consistent with intracellular alkalinisation of astrocytes during CSD (Chesler and Kraig, 1987), which promotes the glycogen phosphorylase and lactate production (Hof et al., 1988, Cruz et al., 1999).

1.1.2.3 Changes in neurotransmitters and receptors

CSD is known to be associated plenty of neurotransmitters and receptors. Neurotransmitters mainly include glutamate, ACh, dopamine, CGRP, NO, gamma-aminobutyric acid (GABA) and serotonin (5-HT) (Fabricius et al., 1993, Yavich and Ylinen, 2005, Shi et al., 2010, Read et al., 1997, Storer and Goadsby, 1997, Rodrigues et al., 1988). The release of these neurotransmitters correlates with the dramatic changes in extracellular and intracellular ions during CSD and they play important roles in the initiation of CSD. For example, the concentration of glutamate in dialysate samples from cortex increases during CSD (Fabricius et al., 1993) and glutamate is required for CSD genesis (Van Harreveld, 1959,

Lauritzen, 1994, Smith et al., 2006). CSD initiation is known to attribute to glutamate actin on NMDA receptor, but not the other two ionotropic glutamate receptors, AMPA and Kainite (KA) receptors. This is supported by that: (i) NMDA, the specific agonist of NMDA receptor has similar effect with glutamate on eliciting CSD (Curtis and Watkins, 1961), which is in line with that inhibition of NMDA receptor but not AMPA receptor or KA receptor suppresses CSD (Smith et al., 2006); (ii) activation of AMPA receptor prevents, but not facilitates NMDA-induced CSD (Addae et al., 2000). In addition, CGRP receptor is proved involving into CSD as BIBN4096, the small molecular inhibitor of CGRP receptor, suppresses CSD propagation in the chick retina (Wang et al., 2016a). By contrast, $GABA_A$ receptor α2 subtype is considered as negative regulator in mediating CSD because both $GABA_A$ receptor and the α2 subtype-preferring positive modulators suppress CSD propagation in the retina model (Wang et al., 2015). Furthermore, local inhibition of NO synthesis delays the genesis of CSD repolarization in rats (Wang et al., 2003). These evidences suggest a complex phenomenon resulting from the interaction of various processes in CSD initiation, and that diverse cellular elements involve in different properties of CSD.

1.1.2.4 Changes in gene expression

CSD can cause changes in the expression of a large number of genes mainly associated with neuroinflammation, apoptosis and synaptic transmission (Choudhuri et al., 2002, Sintas et al., 2016). For example, the gene related to L-type calcium channels are upregulated 2 hours after multiple CSD induction in the brain of mouse (Choudhuri et al., 2002). 24 hours after multiple CSD, there is an increase in mRNA level of CGRP in discrete cortex of rats (Yan Wang, 2016), whereas the content of AMPA receptor is reduced (Chazot et al., 2002). The fact that certain genes associated with hormonal stimulus, apoptosis and interleukin signaling induced by multiple CSD are not altered by anti-CSD drugs, e.g. topiramate and valproate, in cortex of rats (Sintas et al., 2016), represents the needs for exploring targets associated with CSD in migraine therapy.

1.2. Clinical relevance of CSD

1.2.1. Migraine and CSD

Migraine is a disabling neurovascular disorder characterized by severe, episodic and unilateral headache lasting hours to days, affects an estimated 16% of the population worldwide (Lauritzen, 1994, Tfelt-Hansen, 2010) and up to 25% of migraineurs experience transient focal neurologic symptoms (aura), including visual disturbance, unilateral paresthesias, motor symptoms, and language disturbances (Viana et al., 2016). The initiation of a migraine attack is frequently associated with a wide variety of internal and external triggers such as stress, hormonal fluctuations, sleep disturbances, and meal skipping. The accumulating evidences are in favour of, although still be debated, the neural and vascular mechanisms underlying migraine with or without aura (Hargreaves, 2007, Cutrer, 2010). With respect to this theory, the brain state of altered excitability and the abnormal brain vascular state is capable of activating the trigeminal vascular system, meningeal nociceptors and then leading to the onset of headache (Noseda and Burstein, 2013).

It is generally recognized that single CSD causes migraine aura, and is proposed as the putative mechanism of migraine headache (Hadjikhani et al., 2001, Smith et al., 2006, Ayata, 2010). In 1941 Lashley firstly described a scotomas invasion during migraine headache (Lashley, 1941). A dozen years later, Milner stated a possible correspondence between migraine aura and CSD because of the striking similarity of the time courses between the scintillating scotomas and Leão's spreading depression (Milner, 1958). This opinion is further supported by the clinical study in which spontaneous and exercise-triggered migraine aura can be acquired by magnetic resonance imaging (MRI) before and during the BOLD changes and headache phase (Hadjikhani et al., 2001). In addition, CSD causes large rise in vasoactive neuropeptides such as substance P, CGRP and vessel dilation in rodents (Noseda and Burstein, 2013), activates meningeal nociceptors and the central trigeminovascular neurons (Zhang et al., 2011, Zhang et al., 2010). Furthermore, CSD triggers migraine-like behavior in mice (Karatas et al., 2013).

Specifically, CSD activates the pannexin1 (Panx1) channels with subsequent sustained release of high-mobility group box 1 (HMGB1) from neurons. HMGB1 release promotes inflammation stress via translocation of nuclear factor-κB into nucleus of astrocytes followed by the formation of cytokines, prostanoids and inducible NO from glia limitans and, hence, causes trigeminovascular activation, vessel dilation and headache-like headache in mice. However, how CSD leading to migraine still needs to be further elucidated.

1.2.2. *Stroke, brain injury and CSD*

In addition to migraine, CSD is also associated with stroke and traumatic brain injury (TBI). Stroke is the rapid loss of brain function due to disturbance in the blood supply to the brain. This can be due to ischemia caused by blockade of blood vessel, or hyperaemia caused by hypertension (Cahill et al., 2006). Spontaneous CSD-like depolarization can be observed in the vicinity areas of ischemic infarct in cortex (Strong et al., 1983) and subcortical regions (Dreier, 2011). CSD represents as an irreversible depolarization at the region where suffers persistent hypoxia or hypoglycemia (Farkas et al., 2010). CSD can cause ischemic cell death following the onset of spreading depolarization (Dreier et al., 1998). CSD also occurs following acute TBI that often accompanied with hemorrhage (Dreier, 2011, Hartings et al., 2009). Whereas the pattern of TBI-triggered CSD is heterogeneous and influenced by many factors, a common feature is that multiple CSD events are observed lasting hours to days in patients (Lauritzen et al., 2011) and also in some, but not all, animal TBI models (Hartings et al., 2016). It is worthy to mention that whether the TBI-induced CSD aggravates brain injury is still controversial. Baumgarten group found that the additional CSD has no effect on injury volume at 24 hours (Lauritzen and Hansen, 1992). A different result is obtained in an *in vitro* model, where the single CSD wave caused by trauma enlarged the volume of cortical damage compared with the traumatic cortex without CSD (von Baumgarten et al., 2008), suggesting that both single and multiple CSD may worse TBI.

1.3. NMDA receptor signaling in CNS diseases

1.3.1 NMDA receptor properties and distribution

Glutamate is the one of main excitatory neurotransmitters in the CNS and can bind to its specific glutamate receptors (Flores-Soto et al., 2012). The large family of excitatory glutamate receptors is classified as metabotropic and ionotropic receptors, in which NMDA receptor constitutes the ionotropic subfamily identified by specific molecular composition and unique pharmacological properties (Dingledine et al., 1999).

It is widely accepted that NMDA receptor forms tetrameric structures (Michaelis, 1998) by combinations of different subunits: NR1, NR2 (A-D) and NR3 (A and B). Functional NMDA receptor is generally formed by heterotetramers comprising of two mandatory NR1 subunits and two functional NR2 subunits (Sasaki et al., 2002, Flores-Soto et al., 2012). These NMDA receptor subunits share a common membrane topology characterized by an amino-terminal extracellular domain; a ligand binding domain; a transmembrane region formed by 4 hydrophobic segments, and a carboxyl tail domain in the intracellular region, which varies in size depending upon the subunit and provides multiple sites of interaction with numerous intracellular proteins. Activation of NMDA receptor requires simultaneous binding by glutamate and glycine (or D-serine) as agonists, and the depolarisation of the cell membrane (Lynch and Guttmann, 2001). The agonist binding domain binds glycine in NR1 and NR3, whereas glutamate binds with NR2 subunit (Furukawa et al., 2005). Once the receptor is activated, its affinity for endogenous pore blocker Mg^{2+} is reduced and therefore permeability of Ca^{2+} increased.

The four NR2 subunits show a distinct distribution in the CNS, e.g. NR2A is ubiquitously expressed in synapses, while NR2B is enriched in extra-synaptically in the forebrain of adult rat (Watanabe et al., 1994, Sanz-Clemente et al., 2013). Besides that, NMDA receptor is also widely distributed in PNS and other organs including lungs and liver (Nasstrom et al., 1993).

1.3.2 NMDA-containing receptor and CSD

NMDA receptor contributes to CSD genesis, as evidenced by that CSD can be blocked by the antagonists of NMDA receptor MK-801 (Peeters et al., 2007, Bu et al., 2016) and ketamine (Hernandez-Caceres et al., 1987), and partially suppressed by L-701,324 (Obrenovitch and Zilkha, 1996a) and memantine (Peeters et al., 2007). MK-801 is not considered as an anti-CSD candidate for the migraine treatment because of its unacceptable side effects caused by the blockade of normal neuronal function (Chen and Lipton, 2005, Chen and Lipton, 2006). Ketamine, another noncompetitive antagonist only shows efficacy in reducing the aura symptoms but fails to reduce the pain severity resulting from familial hemiplegic migraine in a small clinical trial (Kaube et al., 2000). Differently, memantine can reduce the headache frequency when given as a preventive treatment of refractory migraine in an open-label study (Bigal et al., 2008). Nevertheless, a randomized, placebo-controlled trial is required for further confirmation and that the side effects, although generally mild, but of high ratio, e.g. somnolence (25%), asthenia (11%) and anxiety (11%) still need to be considered (Huang et al., 2014).

NR2B subunit also involves in mediating CSD. Inhibitory effect of NR2B preferring antagonists, e.g. CP-101 606, ifenprodil and Ro 25-6981 are observed to suppress CSD in rats (Menniti et al., 2000, Faria and Mody, 2004, Peeters et al., 2007). However, mediation of NR2A-containing receptor to CSD is still a matter of debate, which is shown as that BOLD accompanied with CSD is not altered by NR2A antagonist in rats (Shatillo et al., 2015); In contrast, NR2A inhibition suppresses the propagation of CSD in the chick retina (Wang et al., 2012). In that case, the involvement of NR2A-containing receptor in CSD needs to be further investigated.

1.3.3 Key signaling associated with NMDA receptor

Multiple cell signaling is associated with NMDA receptor, which is implicated in many neuropathological states (Farinelli et al., 2009, Kemp and McKernan, 2002, Sheng and Kim, 2002, Salter and Kalia, 2004) (Figure 1). Among these, the second messenger is probably one of the best understood. For example, glutamate

toxicity is capable of Ca^{2+} influx through NMDA receptor and leads to neuronal death (Chen et al., 1997). NMDA receptor activation also stimulates neuronal nitric oxide synthase (nNOS) (Garthwaite et al., 1988, Bredt and Snyder, 1992), which may be the underlying cause of the NO formation-induced rapid recovery from the depolarization of CSD (Wang et al., 2003). In addition, cytoplasmic scaffolding protein and kinases are also implicated in the NMDA receptor signaling. For instance, NMDA receptor contributes to the amplitude of CSD by interacting with postsynaptic density protein (PSD)95 (Kucharz et al., 2016). Uncoupling NMDA receptor-NADH dehydrogenase subunit 2 (ND2) complex from SFKs relieves neuropathic pain (Liu et al., 2008). Activation of NMDA receptor can couple SFKs to Panx1 channels during neuronal excitotoxicity (Weilinger et al., 2016). Furthermore, the NMDA receptor also regulates gene expression of neurotransmitters. For example, the elevation of CGRP mRNA can be prevented by NMDA receptor blocker kynurenic acid in peripheral and central nervous systems in nitroglycerin-induced migraine model in rats (Greco et al., 2016).

NR2 subunits, especially 2A and 2B, largely determine the distinct pharmacological and pathological properties of NMDA receptor (Cull-Candy and Leszkiewicz, 2004, Paoletti and Neyton, 2007, Gielen et al., 2009). For instance, NR2A promotes the surface insertion of GluR1 into cell membrane in mature cultured hippocampal neurons, whereas NR2B prevents it (Kim et al., 2005). Selectively blocking NR2A prevents the generation of epilepsy and the development of mossy fiber sprouting in the kindling and pilocarpine epileptic models of rats, whereas inhibition of NR2B has no effect (Liu et al., 2007). In addition, activation of NR2A generates resistance to ischemia by elevating cyclic-AMP response element activity levels, and this effect can be abolished by NR2A antagonist NVP-AAM077 (Terasaki et al., 2010).

1.3.3.1 Sarcoma family kinases

SFKs is a family of non-receptor protein tyrosine kinases and first identified as the proto-oncogenes that has been linked with the development and progression of

cancer (Martin, 2001). Five members of the Src family kinases are expressed in the mammalian CNS - Src, Fyn, Yes, Lck and Lyn. These kinases range in size from 52 to 62 kDa, and are mainly comprised by four domains: three homologous domains Src homology (SH)1, SH2 and SH3 domains, and a SH4 domain that is a short sequence at the amino N-terminus of the protein for anchoring the protein to cell membrane. The SH1 domain contains the 'activation loop' including a tyrosine residue at 416 amino acid that confers the catalytic activity by autophosphorylation. Between the SH3 and SH4 domains is the unique domain that is variable between the subtypes of SFKs. (Salter and Kalia, 2004).

SFKs widely participant in a variety of physiological and pathological conditions e.g. memory, inflammatory, ischemia, epilepsy and neuropathic pain (Roskoski, 2004, Yeatman, 2004, Salter and Kalia, 2004). For example, peripheral nerve injury activates SFKs in the lumbar spinal cord, and intrathecal administration of SFKs inhibitor suppresses mechanical hypersensitivity in the nerve-injured mice (Katsura et al., 2006). In addition, SFKs activity increases during ischemia (Takagi et al., 1999), and that inhibition of SFKs suppresses neuronal depolarization when the tissue exposures to anoxia (Weilinger et al., 2012). Given ischemia and migraine have the similar part in pathophysiological characters, e.g. the spreading depolarization (Kurth et al., 2012), it is plausible to propose that SFKs are also activated by CSD and mediate CSD in turn.

It is known that NMDA receptor can directly interact with SFKs (Salter and Kalia, 2004). For instance, SFKs are coupled to NMDA receptor through ND2 (Gingrich et al., 2004). Uncoupling Src from NMDA receptor complex relieves inflammatory and neuropathic pain (Liu et al., 2008). In addition, NR2A is subjected to phosphorylation for regulating the function of receptor (Cheung and Gurd, 2001, Wang et al., 2014b). For instance, the Y1325 and Y1387 amino acid at C-terminus of NR2A is phosphorylated by intracellular SFKs, which promotes the receptor current (Yang and Leonard, 2001). However, whether SFKs involve NR2A signaling associated with CSD is unknown.

1.3.3.2 Pannexin1 channels

Panx family is a class of plasma membrane spanning proteins that presumably form a hexameric, non-selective ion channel and made up by 3 isoforms: Panx1, Panx2, and Panx3 (Isakson and Thompson, 2014). Similar to the connexins, the secondary structure of Panx contains four transmembrane segments, two extracellular loops and one intracellular, with its amino N- and C- terminus at the intracellular space. However, Panx notably does not form endogenous gap junctions due to the N-linked glycosylation preventing docking of Panx channels from adjacent cells (MacVicar and Thompson, 2010).

Panx family is abundantly expressed in the CNS of mammals in many types of cells, e.g. microglia, astrocytes, oligodendrocytes and neurons, in which Panx1 channels are the most-studied member to date (Wang et al., 2014a). Panx1 has high permeability to small molecules (up to 1.5 kDa), ATP, Ca^{2+}, glutamate and some inflammatory mediators. It can be activated by several mechanisms, such as mechanical stimulation, increases of extracellular K^{+}, proteolytic cleavage of its C-terminus, raising of the intracellular Ca^{2+}, and several intracellular signaling (Penuela et al., 2013).

Panx1 channels have considerable correlation with NMDA receptors in multiple neurological diseases, including epilepsy (Clasadonte et al., 2013), migraine (Karatas et al., 2013) and ischemia stoke (Weilinger et al., 2012). For example, Panx1 channels opening is triggered by NMDA receptor stimulation and contributes to the epileptiform seizure in the hippocampus (Thompson et al., 2008) and rhythmic neuronal discharge in the seizure susceptible brain (Hellier et al., 2009). In addition, CSD triggers headache-like behavior via activating Panx1 channels, which can be prevented by NMDA receptor blocker (Karatas et al., 2013). Furthermore, activation of NMDA receptor causes excitotoxicity via coupling SFKs to Panx1 channels in both ischemic *in vitro* and *in vivo* models (Weilinger et al., 2012, Weilinger et al., 2016), raising the possibility that NMDA receptor also mediates CSD-induced Panx1 channels opening via SFKs.

Herein, I propose that NR2A-containing receptor may regulate CSD-induced coupling of activated SFKs to Panx1 channels. The hypothesis is mainly supported by the following observations: (i) NR2A plays a crucial role in

mediating CSD propagation in chick retina (Wang et al., 2012); (ii) NMDA receptor contributes to CSD-induced Panx1 opening (Karatas et al., 2013); (iii) NMDA receptor activation couples SFKs to Panx1 channels in ischemic model (Weilinger et al., 2012, Weilinger et al., 2016); and (iv) NR2A, SFKs and Panx1 co-localize in postsynaptic dense area (Sugrue et al., 1990, Zoidl et al., 2007, Sanz-Clemente et al., 2013).

1.3.3.3 Calcitonin gene-related peptide

CGRP, a 37-amino acid peptide, is consists of two forms of αCGRP and βCGRP (Wimalawansa et al., 1990) that share >90% homology and differ by only three amino acids in the human, bearing similar biological activities (Steenbergh et al., 1986). It is generally considered that αCGRP is the principal form found in both CNS and PNS , whereas βCGRP is found mainly in the enteric nervous system (Mulderry et al., 1985). CGRP is known to mediate neurogenic inflammation, modulate nociceptive input (Russo, 2015) and act as a vasodilator (Brain et al., 1985).

Both clinical and preclinical studies support CGRP as a key player in migraine (Russo, 2015, Edvinsson, 2008). CGRP levels are elevated in both the serum and cerebral spinal fluid (CSF) of migraineurs (van Dongen et al., 2016) and that intravenous CGRP administration to migraineurs is sufficient to elicit a migraine-like headache (Hansen et al., 2010, Lassen et al., 2002). Similarly, CGRP receptor antagonists and anti-CGRP antibodies reduce the headache days per month in patients with episodic migraine (Bigal et al., 2015, Edvinsson, 2015, Vecsei et al., 2015). Experimental studies show that intracerebroventricular (*i.c.v.*) perfusion of CGRP promotes the behavioral sensitivity to light in transgenic CGRP-sensitized mice. It suggests a central mechanism of CGRP in mediating the photophobia of migraine. Additionally, multiple, but not single CSD can elevate the contents of CGRP mRNA in motor, somatosensory and visual cortices of the ipsilateral hemisphere in rats (Wang et al., 2016b), implying an underlying relationship between CGRP expression and chronic migraine that is characterized by frequency progressively migraine attack over months or years (Lipton et al.,

2004). The fact that inhibition of CGRP prevents the post-traumatic headache in mice suggests a critical role of CGRP in the consequence of TBI (Bree and Levy, 2016), another disease accompanies with multiple CSD (Hartings et al., 2016). However, the mechanism of CSD-induced CGRP gene expression needs to be addressed.

There is a link between NMDA receptor and CGRP. Firstly, perfusion of NMDA receptor antagonists, MK-801 and AP-5, prevent capsaicin-induced CGRP release in the spinal cord of rats (Garry et al., 2000). Secondly, the endogenous NMDA receptor antagonist, kynurenic acid abolishes the headache-like behavior and importantly reduces CGRP mRNA level in the trigeminal ganglion, medulla pons and cervical spinal cord in a nitroglycerin-induced migraine model of rat (Greco et al., 2016). These data suggest that NMDA receptor may influence CGRP gene expression in the cortical regions in response to CSD. In that case, it is reasonable to propose that NR2A may be a mechanism by which the levels of CGRP induced by multiple CSD in discrete cortices become elevated for a prolonged period in chronic migraine and TBI patients.

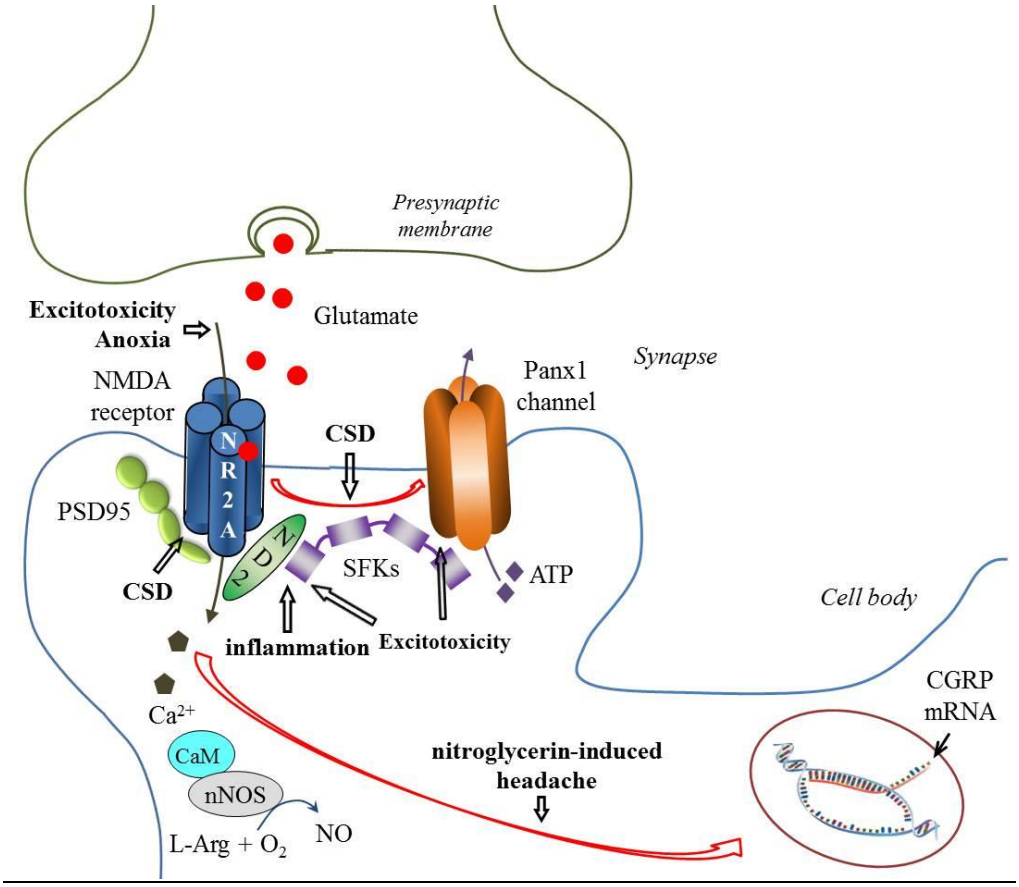

Figure 1. Schematic diagram of key signaling associated with NMDA receptor in terms of both protein and gene levels in multiple diseases. Abbreviations: CaM, Calmodulin; CGRP, Calcitonin gene-related peptide; CSD, cortical spreading depression; ND2, NADH dehydrogenase subunit 2; NMDA, N-methyl-D-aspartic acid; nNOS, neuronal nitric oxide synthase; Panx1, pannexin1; PSD, Postsynaptic density protein; SFKs, sarcoma family kinases.

1.4. *Overall aim*

The overall aim of this thesis is to understand the migraine pathophysiology by investigating whether NR2A-containing NMDA receptor contributes to the genesis and propagation of CSD, and its downstream signaling pathways involving Panx1 channels opening via activating SFKs, and CGRP gene expression. Specific objectives will be introduced in details in the following chapters.

Chapter 2 Material and methods

2.1 Animals

All animal procedures were approved by the Ethical Review Panels of Soochow University and performed in accordance with the associated guidelines. All efforts were made to minimize animal suffering to reduce the number of animals used. *In vitro* experiments were performed on male chicks (*n* = 14, WuXi Yangzichang Ltd, Wuxi, China) with the age of 8-28 days. *In vivo* experiments were performed on male Sprague Dawley rats (*n* = 85, 322.98 ± 43.08 g, mean ± SD, Shanghai SLAC Laboratory Animal Corporation Ltd, Shanghai, China). All animals were housed for at least 7 days before use on a 12 h light/dark cycle with food and water available ad libitum.

2.2 In vitro experiment

The chick retina preparation was regarded as an effective *in vitro* model for my study objective, because: (i) CSD waves can be repeatedly induced by K^+ over several hours (Sheardown, 1993, Hanke and de Lima, 2008); (ii) the intrinsic optical signal of CSD waves can be observed and recorded (Dahlem and Muller, 2000, Dahlem et al., 2003, Farkas et al., 2008), and the signal is very similar to that from the electrophysiological recording both *in vitro* and *in vivo* (Peixoto et al., 2001, Farkas et al., 2008); (iii) is appropriated in testing the NMDA receptor pharmacology of CSD (Sheardown, 1993, Kertesz et al., 2010), which is found to be very similar to that in mammal (Gill et al., 1992, Kertesz et al., 2010); (iv) enables several concentrations of chemicals are tested in one preparation, and the concentrations at target level are known.

The CSD model in our setting up is validated as inhibition of NR2A-containing receptor by NVP-AAM077 suppressed the magnitude and propagation of CSD in concentration-dependent manner in the chick retina (Jia et al., 2015), which is quite similar to the previous description (Wang et al., 2012).

2.2.1 Surgical preparation

As previously described (Farkas et al., 2008), chicks were killed by cervical dislocation, decapitated, and the left eye dissected rapidly. The eye was cut at the equator, the vitreous humour sucked away. The posterior eyecup was placed in a tissue chamber and weighed down to keep it submerged in the medium. Unless otherwise stated, the chamber was perfused with Ringer's solution (concentrations in mM: 100 NaCl, 6 KCl, 1 $MgSO_4$, 30 $NaHCO_3$, 1 NaH_2PO_3, 1 $CaCl_2$ and 20 glucose; bubbled with 95% O_2 and 5% CO_2; pH 7.3) using a peristaltic pump (Minipuls3, Gilson, France). The perfusion rate was 0.5 ml/min and the medium volume in the chamber kept constant by a suction pump (BT100-1L, Longer Pump Ltd, China). The tissue was allowed to recover by perfusion of Ringer's solution for 30 minutes before inducing the 1st CSD. The temperature was kept at 32 ℃ by temperature control system (Figure 2).

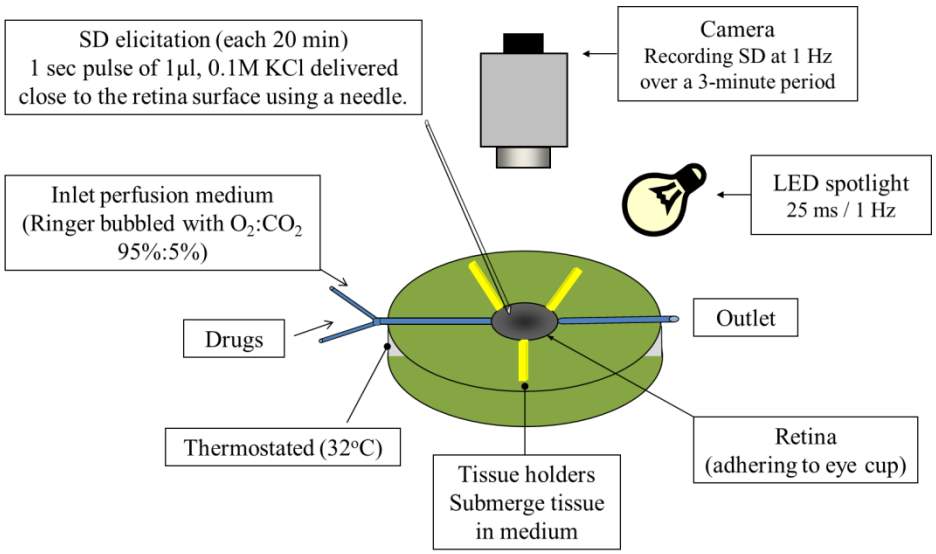

Figure 2. Diagram showing CSD model based on intrinsic optical imaging in chick retina.

2.2.2 SD induction

One CSD was induced as previously described (Wang et al., 2015). Briefly, 1 µl of KCl at 0.1 M was topically perfused at the edge of eyecup by 1 second through a

30 gauge needle with flat head connected to a 25 µl volume microsyringe (Hamilton, Bonaduz, Switzerland) (Figure 3).

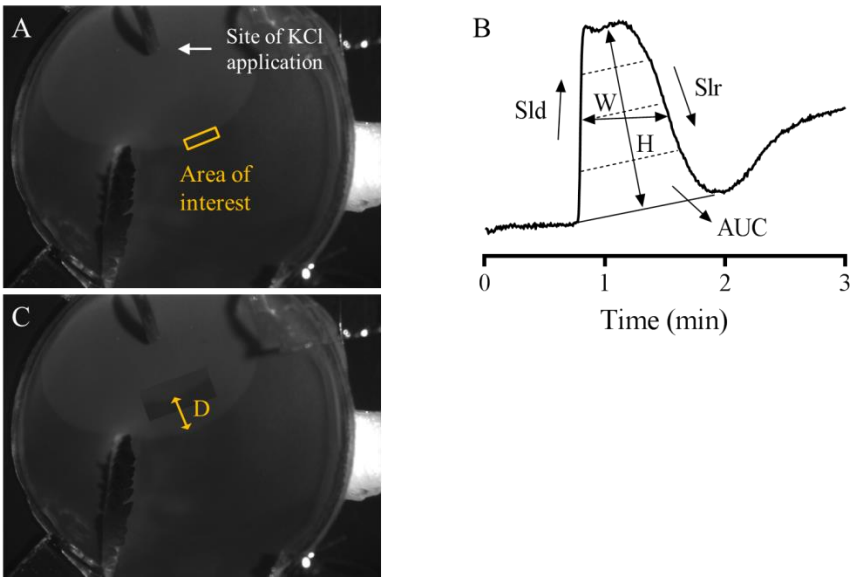

Figure 3. Representative image (A and C) and plot of CSD propagation wave (B) induced by high-K^+ in the chick retina. The same area of interest (rectangle within left picture, AOI) was selected and used for all pictures of the sequence under study. All the averaged gray levels within the AOI were plotted against time to generate the CSD wave (B). Area under the curve (AUC), height (H), width at half height (WHH), maximum slope of depolarization (Sld) and maximum slope of repolarization (Slr) of CSD wave were determined to quantify CSD magnitude. Propagation rate was calculated as indicated by the distance (D) between two CSD wave fronts within the same AOI dividing the time duration to quantify drug effect on tissue excitability to CSD.

2.2.3 *Intrinsic optical imaging of CSD*

The retina was illuminated for 25 milli-seconds (ms) every 1 Hz using a high-power LED spotlight (625 nm peak wavelength, SLS-0307-A, Mightex, Pleasanton, USA) and the illumination was driven by a computer-controlled power supply (Sirius LED controller, SLC-SA04-U, Mightex, USA). The

reflected light was simultaneously recorded with a monochrome camera (QIC-F-M-12, Media Cybernetics, UK) used at a maximal spatial resolution. Image sequences were taken at 1 Hz over a 3-minute period, started as CSD was elicited. Camera exposure and illumination were synchronized using the same external trigger (TG5011, TTi, UK). Image Pro Plus 7.0 software was used for image acquisition, storage and analysis (Figure 4).

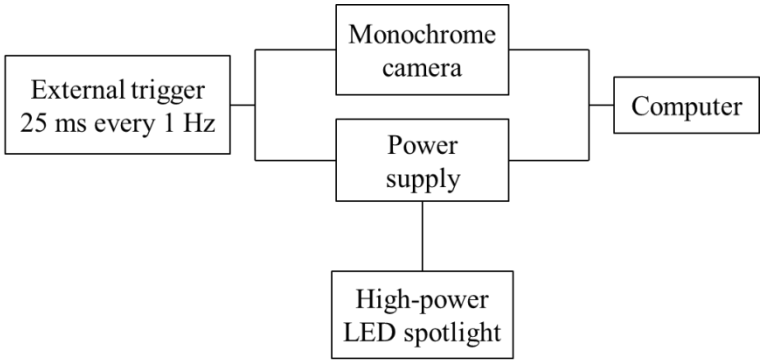

Figure 4. Schematic presentation of the electronic devices used for the recording of optical imaging of CSD synchronously with external spotlight triggering.

2.2.4 Agents administered and experimental design

To further validate whether NR2A inhibition could suppress CSD propagation, TCN-201 was used at the concentration range selected to NR2A, and two groups were designed: (i) TCN-201 at 1, 3 and 9 μM dissolved in 0.01%, 0.03% and 0.1% dimethylsulfoxide (DMSO) in respective order (n = 6); (ii) DMSO at 0.01%, 0.03% and 0.1% as TCN-201 vehicle control group (n = 8); It should be noted, the maximum solubility of TCN-201 was determined to be 9 μM in 0.1% DMSO, the maximum concentration in Ringer's solution without affecting retinal CSD per our investigation (Wang et al., 2015). In each experiment, ten CSD episodes were induced with 20 minutes interval for recovery. Two separate CSDs was for each of the different and consecutive tests: (i) initial Ringer's control; (ii) low concentration of chemical or vehicle; (iii) medium concentration of chemical or vehicle; (vi) high concentration of chemical of vehicle; (v) post-treatment with Ringer's control (i.e. drug removal). For each test sequence, the perfusion medium

was changed immediately after the end of the 2nd, 4th, 6th, and 8th CSD recording when required, such that the preparation was adequately perfused with the proper drug or vehicle or Ringer's medium for the subsequent test (Figure 5).

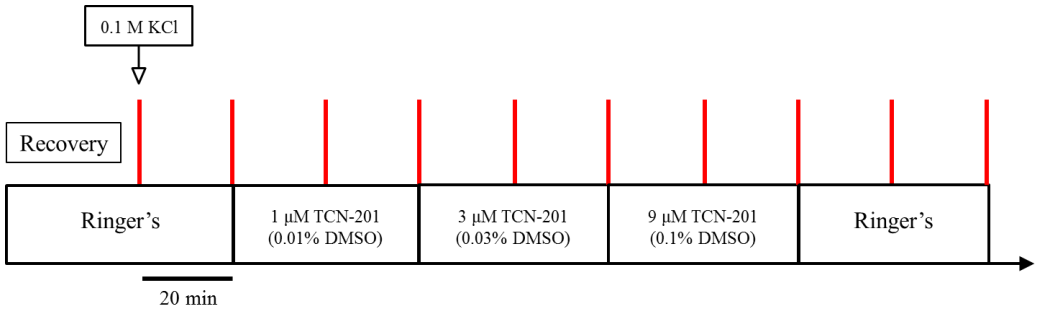

Figure 5. Experimental protocol for investigating the effect of TCN-201 to CSD propagation in chick retina. Two groups were designed with DMSO control and chemical groups. In each experiment, ten repeated CSDs were induced by high-K^+ with 20 minutes recovery. Two separate CSDs were for each of the different and consecutive test. Each CSD was recorded for 3 minutes at the start of high-K^+ perfusion. Chemicals at 3 different concentrations were applied 40 minutes before and during the 4nd, 6rd and 8th CSD.

2.2.5 *Data presentation and statistical analysis*

As reported previously (Wang et al., 2012), for each 360-frame sequence, an area of interest (AOI) parallel to the CSD wave front was delineated manually (Figure 2.2.2). For each image within the sequence, the gray levels of the pixels constituting the AOI were plotted against the time as an indicator to characterize CSD. Excel program was used to determine (i) area under the curve (AUC, gray levels×minute) of CSD wave; (ii) height (H, changes of gray levels changes of gray levels), the differences of gray levels between peak point and midpoint of base line of CSD wave; (iii) width at half height (WHH, second); (iv) maximum slope of depolarization (Sld, changes of gray levels/minute); (v) maximum slope of repolarization (Slr, changes of gray levels/minute). AUC, H, WHH, Sld and Slr were used as the index reflecting the magnitude of propagating CSD (Figure 3 B). (vi) propagation rate (mm/minute), the velocity of each CSD wave in each CSD

episode, calculated as indicated by the distance (D) between two CSD wave fronts within the same AOI at the two different time points dividing the time duration to quantify drug effect on tissue excitability to CSD (Figure 3 C). The average of CSD in each episode was used for quantified analysis. The calculated values within each different test were averaged and all corresponding data was given as mean ± SD in percentages of their respective baselines. Mann-Whitney test and Wilcoxon matched-pairs test were used for data analysis. Differences were considered significant when $^{*}p < 0.05$, $^{**}p < 0.01$ and $^{***}p < 0.001$.

2.3 In vivo experiment

2.3.1 Surgical preparation

Rat was anaesthetised with isoflurane (5% for induction, 2.5-3.5% during the surgery, 1-1.5% for maintenance) in O_2:N_2O (50:100 cc/min), with the animal breathing spontaneously. The anaesthetic depth was monitored and adjusted by observation of the electroencephalogram (EEG) and state of the animal. The suitable anaesthesia was reflected by regular breathing, absence of whisker movements, and unresponsive to tail pinches. Rectal temperature of animal was maintained at 37°C throughout the experiment using temperature control system (TC-10, npi, Germany).

Rat was fixed on stereotaxic apparatus (Model 900, KOPF, USA) after deeply anaesthesia. After making an incision in the scalp along sagittal direction and blunt separating soft tissues, parietal bone was exposed. Several bur holes were drilled on the parietal bone by dental-feinmechanik dental drill (D-3000 hannover 91, OTTO MUSS) for CSD induction, CSD recording and drugs administration. The coordinates would be introduced in the corresponding sections. Unless otherwise stated, these bur holes were kept moisture with artificial cerebral spinal fluid (ACSF) throughout the experiment. Further experimental procedure was carried out at least one hour stabilization after the surgery.

2.3.2 Microdialysis-based CSD experiment

The unique microdialysis probe incorporating a recording electrode (0.25 mm external diameter, ME-H1, Applied Neuroscience, UK) was used to investigate the effect of NR2A-containing receptor antagonists on CSD genesis (Figure 6). It can simultaneously perform the following operations within the same cortical region (Obrenovitch et al., 1993): (i) induction of CSD by perfusion of high-K^+ medium; (ii) quantitative recording of electrophysiological variables of CSD; (iii) local application of chemicals. The co-localized manipulation at the site of CSD recording is especially suitable to the pharmacology of CSD genesis. In addition, this technique enables several concentrations of chemicals to be applied in one preparation. One more important advantage is that allow us to predict the concentration of chemicals perfused into the cortex more precisely.

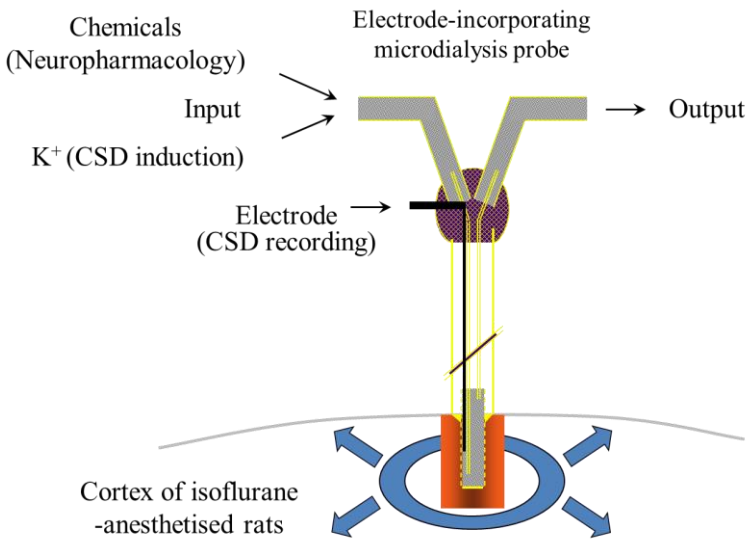

Figure 6. Illustration of the experimental strategy relying on the use of microdialysis probes incorporating an electrode for elicitation of CSD by high-K^+ medium, recoding of CSD and pharmacology study in rat.

2.3.2.1 CSD induction

The microdialysis probe was implanted into right cortex 1.3-1.4 mm deep from

the cortical surface through a bur (0.8 mm inner diameter) at the coordinate of 2 mm posterior and 2 mm lateral to Bregma (Figure 7) and held on parietal bone by acrylic acid dental cement (Shanghai Medical Instruments Co. Ltd., China). Unless otherwise stated, the microdialysis probe was perfused with ACSF (composition in mM: 125 NaCl, 2.5 KCl, 1.18 $MgCl_2$, 1.26 $CaCl_2$; pH 7.3 adjusted with 1 M NaOH, not buffered) at 1 μl/minute with a syringe pump (CMA100, CMA/Microdialysis, Sweden). For eliciting CSD, a medium containing 250 mM K^+ (composition in mM: 2.5 NaCl, 250 KCl, 1.18 $MgCl_2$, 1.26 $CaCl_2$; pH 7.3 adjusted with 1 M NaOH, not buffered) was used. It is noted that a higher concentration of K^+ at 250 mM was required to induce CSD (Bu et al., 2016) compared to 160 mM employed when halothane was used as the anaesthetic (Wang et al., 2003). This difference in K^+ requirement could be due to the anaesthetics (isoflurane *vs* halothane) having different effects on CSD. Indeed, different inhalational anaesthetics have been reported to show slightly different degrees of inhibitory effect on CSD (Piper and Lambert, 1996), but this effect can be neglected as all experiments carried out under the same anesthetic condition.

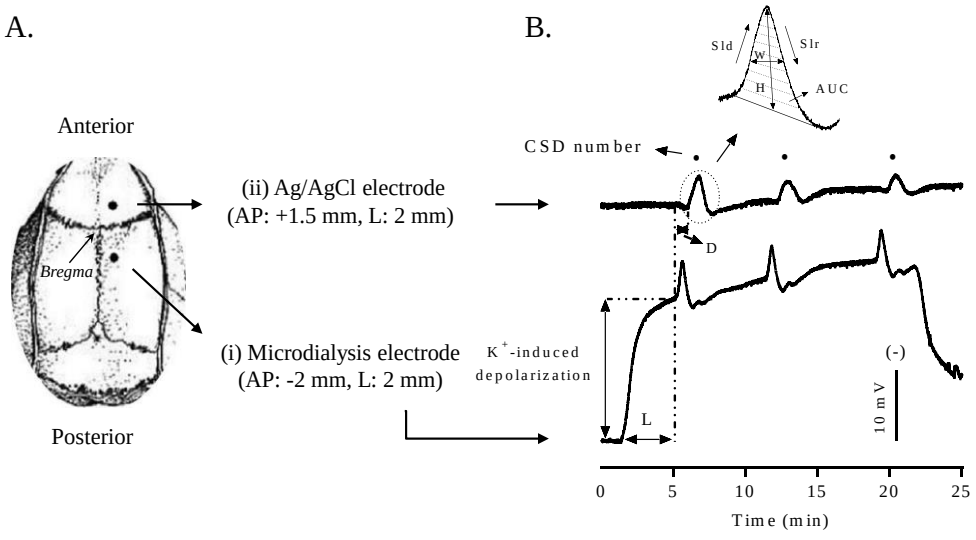

Figure 7. Schematic representation of electrode implantation sites (A) and representative traces in direct current (DC) potential of CSD (B) induced by perfusion of 250 mM KCl through the microdialysis probe in the isoflurane-anaesthetised rat. CSD wave in the genesis site was recorded through the microdialysis probe implanted at 2 mm posterior to Bregma in the right cortex.

CSD propagation wave was simultaneously recorded through the Ag/AgCl electrode implanted in the ipsilateral cortex at 1.5 mm anterior to Bregma. Chemicals were perfused through the microdialysis probe for pharmacology study. Area under the curve (AUC, dotted line), height (H), width at half height (WHH), maximum slope of depolarization (Sld) and maximum slope of repolarization (Slr) of CSD wave were determined to indicate CSD magnitude. CSD latency (L) and CSD number were used to assess the susceptibility of the cortex to K^+ induced CSD. Both CSD magnitude and susceptibility of cortex to CSD were used to reflect the genesis of CSD. Propagation rate was used to assess the propagation of CSD as calculated by the distance dividing by the time delay (D).

2.3.2.2 CSD recording

The microdialysis probe incorporating a recording electrode was used for recording CSD genesis (Figure 7 A). For recording CSD propagation, an Ag/AgCl recording electrode (0.1 mm external diameter, Applied Neuroscience, UK) was implanted into the ipsilateral cortex 0.9 mm deep from the cortical surface through a bur hole (0.8 mm inner diameter) at the coordinate of 1.5 mm anterior and 2 mm lateral to Bregma (Figure 7 A) and held by electrode holder (8309003, CMA, Sweden). Ag/AgCl reference electrode (Applied Neuroscience, London, UK) was placed under the scalp of rat.

2.3.2.3 Agents administered and experimental design

The following five series of experiment were carried out to examine the effect of NR2A-containing receptor antagonists NVP-AAM077 and TCN-201 on CSD genesis and propagation. The known non-competitive NMDA receptor antagonist, MK-801, was used for model validation (Obrenovitch and Zilkha, 1996a). The concentration ranges of chemicals were carefully selected to ensure their selectivity for each targeting (Ogden and Traynelis, 2011). These series are: (i) ACSF as the NVP-AAM077 and MK-801 vehicle group (n = 6); (ii) MK-801 (M107, Sigma-Aldrich, n = 6); (iii) NVP-AAM077 (n = 6, synthesized by Yi Li in Department of Chemistry, XJTLU, China), a small molecule compound (542.14

KDa) that can competitively act on glutamate pocket of NMDA receptors with 10 to 100-fold selectivity for NR2A over other subunits of NMDA receptors (Auberson et al., 2002, Liu et al., 2004, Neyton and Paoletti, 2006); (iv) DMSO at 0.05%, 0.15% and 0.5% as the TCN-201 vehicle group in respective order (n = 6). Our preliminary experiment demonstrated that DMSO at 0.5% is the maximum concentration in ACSF without affecting CSD in microdialysis-based CSD model; (v) TCN-201 (4154, Tocris, n = 6), a small compound (461.89 KDa) that can noncompetitively act on the glycine binding domains of dimer interface of NR1 and NR2A (Bettini et al., 2010, Ogden and Traynelis, 2011) with 300-fold selectivity for NR2A over other subunits of NMDA receptors in transfected HEK 293T cells (Bettini et al., 2010). It should be noted that the microdialysis probe used in this study has 10~20% recovery rate, i.e. the ratio of the drug penetration through the semi-permeable membrane of the probe into the cortex relative to its original concentration. For instance, an estimation of 5~10 μM of TCN-201 were expected to diffuse into the cortical tissue surrounding the implantation site of microdialysis probe when the maximum concentration at 50 μM was applied.

Five consecutive CSD episodes in each experiment for NVP-AAM077 and MK-801 testing were elicited by perfusion of K^+-medium through microdialysis probes for 20 minutes followed by 40 minutes ACSF perfusion to allow tissues recovery. These episodes were: (i) initial ACSF control; (ii) low concentration of the drug or ACSF; (iii) medium concentration of the drug or ACSF; (iv) high concentration of the drug or ACSF; (v) post-treatment with ACSF solution. The drug at each concentration (0.3, 1, 3 μM for NVP-AAM077 or 3, 10, 30 μM for MK-801) was perfused through microdialysis probes for 20 minutes before and during K^+-medium perfusion for the 2nd, 3rd and 4th CSD episodes (Figure 8).

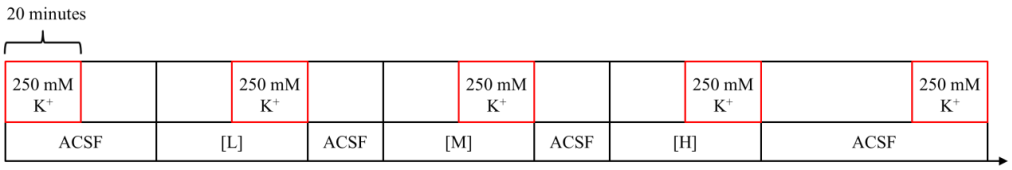

Figure 8. Experimental protocol for investigating effect of NVP-AAM077 and MK-801 to CSD in microdialysis-based CSD model of the rat. Three groups were

designed with ACSF control group and two chemicals groups. In each experiment, 5 repeated CSD episodes were induced by K^+-medium for 20 minutes, each followed by 40-minutes recovery. Chemicals at 3 different concentrations (L, M and H) were applied 20 minutes before and during the 2nd, 3rd and 4th episodes.

For testing the effect of TCN-201 on CSD genesis, the 5th episode, i.e. the effect of post-treatment with ACSF to CSD, was not performed given the non-competitive character of drug. TCN-201 (5, 15, 50 μM) at each concentration was perfused through microdialysis probes for 40 minutes before and 20 minutes during K^+-medium perfusion for the 2nd, 3rd and 4th CSD episodes (Figure 9). My preliminary study showed that the concentration of 50μM is the maximal solubility of TCN-201 in 0.5% DMSO.

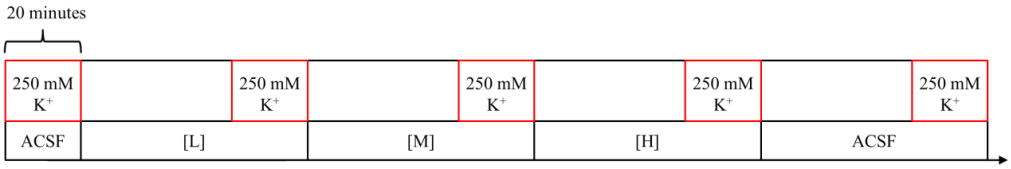

Figure 9. Experimental protocol for investigating effect of TCN-201 to CSD in microdialysis-based CSD model of the rat. Two groups were designed with DMSO control and chemical groups. In each experiment, 4 repeated CSD episodes were induced by K^+-medium for 20 minutes, each followed by 40-minutes recovery. Drugs at 3 different concentrations (L, M and H) were applied 40 minutes before and 20 minutes during the 2nd, 3rd and 4th CSD episodes.

2.3.3 Intracerebroventricular perfusion experiment

2.3.3.1 CSD induction

CSD was induced by 1 μl of KCl at 3 M topically perfused onto cortical surface with dura intact for 5 minutes through a bur hole (1 mm inner diameter) on right

parietal bone at 5 mm posterior and 2 mm lateral to Bregma (Figure 10 A and C). This 5-minute duration of KCl was perfused so that one CSD wave could be elicited under the experimental condition with dura intact and anesthetics applied (Yan Wang, 2016). After CSD induction, the high-K^+ was quickly replaced by ACSF, allowed quick recovery of the tissue.

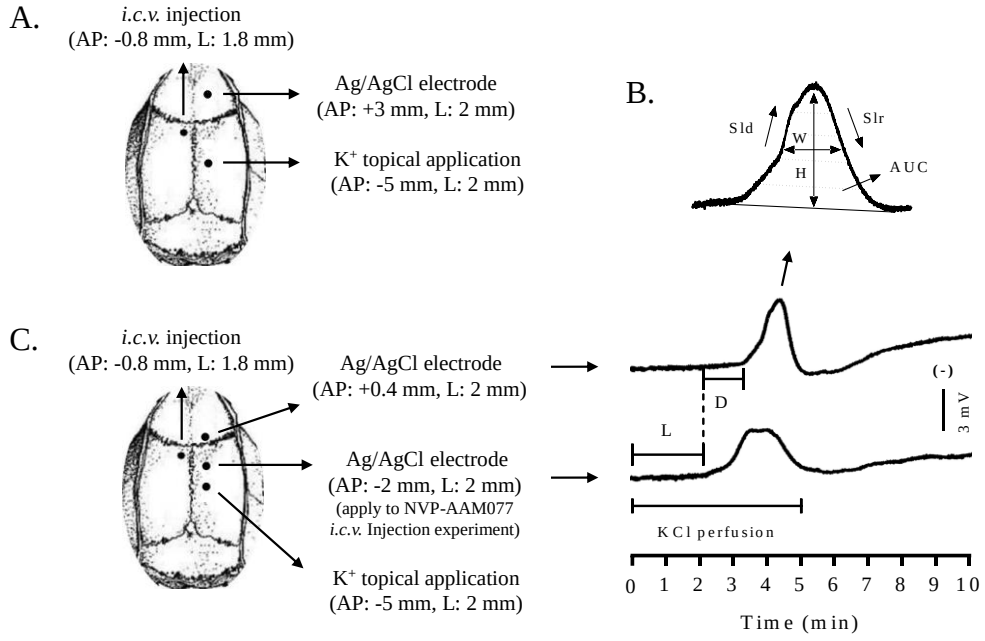

Figure 10. Schematic representation of electrode implantation sites (A and C) and representative traces in DC potential of CSD (B) induced by 3 M KCl through topical application in the anaesthetised rat. (A and C) In the *i.c.v.* based experiments, CSD was induced by topical application of high-K^+ onto the cortical surface with dura intact at 5 mm posterior to Bregma of right parietal bone. CSD propagation wave was recorded at different coordinates of ipsilateral cortical side in separated sets of experiment: (i) at 3 mm anterior to Bregma for following investigation of protein and gene expression (A); (ii) at 0.4 mm anterior to Bregma for following investigation of effect of PP2 to CSD-induced Panx1 opening using immunohistochemistry (IHC) (C); (iii) at 2 mm posterior plus 0.4 mm anterior to Bregma for following investigation of effect of NVP-AAM077 to CSD-induced Panx1 channels opening using IHC (C). The chemicals were *i.c.v.* perfused into contralateral ventricle through a cannula implanted (A and C). Area under the curve (AUC, dotted line), height (H), width at half height (WHH),

maximum slope of depolarization (Sld) and maximum slope of repolarization (Slr) of CSD wave were determined to indicate CSD magnitude. CSD latency (L) was indicated as the time difference between the start of high-K^+ topical application and the start of depolarization of the 1st CSD wave. L and CSD number were used to assess the susceptibility of the cortex to CSD. CSD propagation rate was used to assess the propagation of CSD as calculated by the distance dividing the time delay (D).

2.3.3.2 Agents administered

To ensure chemicals diffusing to distant cortical layers with predictable concentrations, a set of *in vivo* experiment by perfusion of chemicals into the contralateral ventricle was designed. A stainless steel cannula (inner diameter: 0.38 mm, 62002, RWD Life Science, China) was implanted into contralateral ventricle 3.5 mm deep from the cortical surface trough a bur hole (1 mm inner diameter) at 0.8 mm posterior and 1.8 mm lateral to Bregma and held in place by holder (Figure 10 A and C). A matched stainless steel inner pipe (62202, RWD Life Science, China) connecting to a 25 μl volume microsyringe via PE tubing (62302, RWD Life Science, China) was inserted into lateral ventricle through cannula for *i.c.v.* perfusion. A syringe pump was used to deliver precise micro-perfusion.

NVP-AAM077

For selective inhibition of NR2A, NVP-AAM077 at 30 μM in ACSF was *i.c.v.* perfused at 1 μl/minute for 10 minutes. In this case, total 0.3 nmol NVP-AAM077 was perfused into cerebral ventricle.

PP2

For selective inhibition of SFKs, PP2, a small-molecule modulator that directly bind to the catalytic domain of SFKs and thereby block phosphoryl transfer (Salter and Kalia, 2004), at 500 μM in 50% DMSO was *i.c.v.* perfused at 0.5 μl/minute for 10 minutes. In this case, total 2.5 nmol PP2 was perfused into

cerebral ventricle. PP3, the inactive analog of PP2 was used as negative control.

The amount of drugs were applied by referencing that only 1/100-1/200 of insulin could diffuse into contralateral cortex 30-120 minutes after *i.c.v.* perfusion (Proescholdt et al., 2000), and at the resulting estimated concentration, NVP-AAM077 and PP2 in cortical tissue is selective for NR2A (Bu et al., 2016) and SFKs (Bain et al., 2003) respectively.

Propidium iodide

Propidium iodide (PI) is a membrane-impermeable fluoroprobe with a molecular mass of 668.4 Da; it may pass through megachannels and fluoresces in a way by interacting with nucleic acids (Thompson et al., 2006). It is known that single or multiple CSD can induce PI staining in neurons in mice (Yildirim et al., 2015), which can be prevented by Panx1 inhibitors carbenoxolone, probenecid, ^{10}Panx or siRNA. In addition, PI staining is not anesthetic-specific, e.g. isoflurane anesthesia, which also inhibits gap junctions, did not significantly affect PI labeling (Karatas et al., 2013), suggesting that PI is appropriate for indicating CSD-induced Panx1 channels opening in our preparation.

Previously, it was demonstrated that neuronal PI uptake reached maximum 5 minutes after CSD in ipsilateral cortex if contralateral *i.c.v.* perfusion of 0.5 μg PI 2 minutes before CSD induction in mice (Karatas et al., 2013). Similar with the previous study, 5 minutes before CSD induction, total 2 μg PI (1 mg/ml) or ACSF (vehicle control) was *i.c.v.* perfused at 0.5 μl/minute for 4 minutes, to indicate the CSD-induced Panx1 opening in our experiment. The heart of rat was then perfused by 4% paraformaldehyde fixative (PFA) 5 minutes after CSD induction.

Signs indicative of successful *i.c.v.* perfusion included: (i) needle track connecting to cerebral ventricle; (ii) wide diffusion of PI in ventricle in the case of PI was applied in experiment (Figure 11).

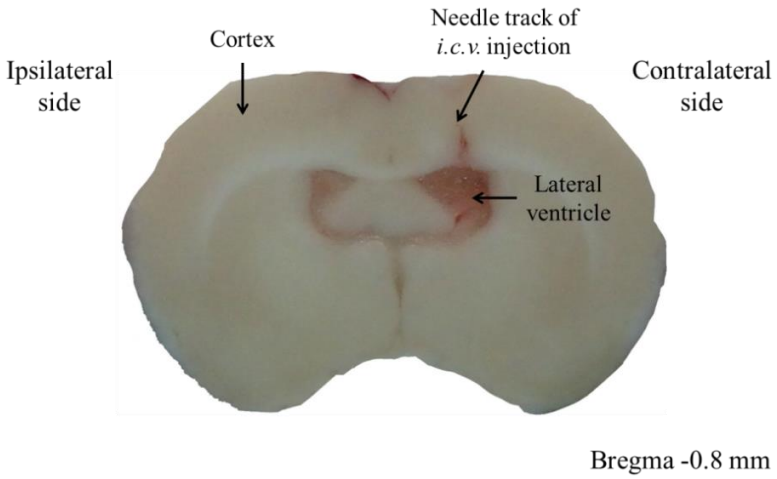

Figure 11. Histological verification of successful *i.c.v.* perfusion. The representative diagram shows coronal section at 0.8 mm posterior to Bregma. Red track shows the position of cannula implantation for *i.c.v.* perfusion. The dissolved PI by cerebrospinal fluid in ventricle shows in red.

2.3.3.3 CSD recording by Ag/AgCl electrodes

One or two Ag/AgCl recording electrode(s) were implanted into the ipsilateral cortex (0.9 mm deep from the cortical surface) through bur holes (0.8 mm inner diameter) drilled on parietal bone and held by electrode holders at different coordinates for CSD recording. The coordinates are: (i) for electrophysiological experiments followed by western blot and qPCR, one electrode was implanted at 2 mm lateral and 3 mm anterior to Bregma (Figure 10 A); (ii) for investigating the effect of NVP-AAM077 on CSD propagation and CSD-induced Panx1 channels opening, two electrodes were implanted at both 0.4 mm anterior and 2 mm posterior, and 2 mm lateral to Bregma (Figure 10 C); (iii) for investigating the effect of PP2 on CSD propagation and CSD-induced Panx1 channels opening, only one electrode was implanted at 2 mm lateral and 0.4 mm anterior to Bregma (Figure 10 C). Ag/AgCl reference electrode was placed under the scalp of rat.

2.3.3.4 Experimental design

Six series experiments were designed:

Series 1: In order to investigate whether NR2A inhibition could suppress CSD propagation and CSD-induced Panx1 channels opening, overall two CSD episodes were elicited at 40-minute intervals and three groups were designed: (i) NVP-AAM077 was administrated immediately after the 1st CSD episode (n = 6); (ii) CSD group (n = 7), and (iii) sham group in the absence of high-K^+ application (n = 6). ACSF but not NVP-AAM077 was used in CSD and sham groups. PI was administrated 5 minutes before the 2nd CSD episode in all groups. Rat heart was perfused immediately 5 minutes after the 2nd CSD episode for immunohistochemistry (IHC) experiment in order to make sure that the ipsilateral cortex is invaded by CSD (de Lima et al., 2009) (Figure 12).

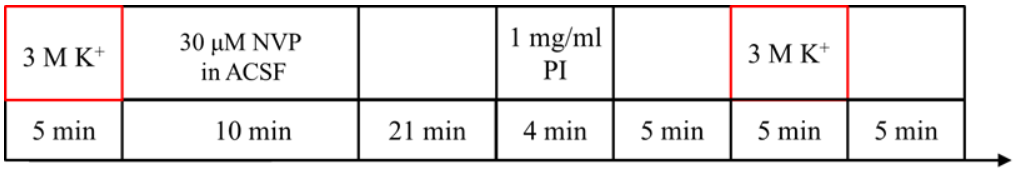

Figure 12. Experimental protocol for investigating whether *i.c.v.* perfusion of NVP-AAM077 suppresses CSD propagation and CSD-induced Panx1 channels opening in the rats. Two repeated CSD episodes were induced by topical application of high-K^+ for 5 minutes with 40-minutes interval for drug and control groups, whereas in the absence of CSD was carried out as sham in each experiment. 10 µl NVP-AAM077 at 30 µM (ACSF as control) was *i.c.v.* perfused 30 minutes before the 2nd CSD episode in drug group. 2 µ PI (1mg/ml) was *i.c.v.* perfused 5 minutes before the 2nd CSD episode in all groups.

The previous study showed that PI update was returned in 30 minutes after CSD in ipsilateral cortex, compared with the group without CSD elicitation in mice (Karatas et al., 2013), suggesting that the Panx1 activation induced by the 1st CSD episode would not influence the subsequent PI uptake induced by the 2nd CSD episode in our preparation.

In order to minimize animal use, 5 rats from CSD group and 6 rats from the sham group were also used for series 4 (see below).

Series 2: In order to detect whether CSD could induce SFKs phosphorylation at Y416 amino acid, and that CSD propagation and SFKs phosphorylation could be prevented by SFKs inhibitor, one CSD episode was elicited and four groups were designed: (i) SFKs selective inhibitor, PP2 was *i.c.v.* perfused starting from 120 minutes before CSD induction (n = 6); (ii) PP3 was administrated as the negative control (n = 6); (iii) ACSF was perfused in the CSD control group (n = 5); (iv) ACSF was applied in the absence of CSD induction in the sham group (n = 3). Cortical tissue was rapidly dissected 5 minutes after CSD induction for western blot (Figure 13).

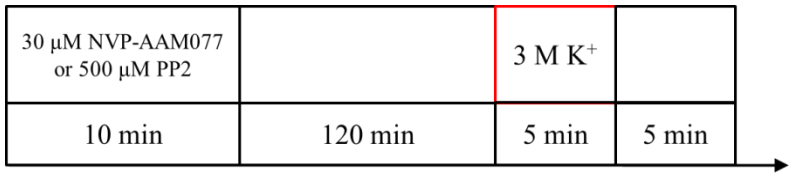

Figure 13. Experimental protocol for investigating the effect of PP2 and NVP-AAM077 on CSD propagation and CSD-induced protein expression. In each experiment, 5 μl PP2 (500 μM) or 10 μl NVP-AAM077 (30 μM) was *i.c.v.* perfused 120 before topical application of high-K^+. ACSF (as control for NVP-AAM077) or PP3 (as control for PP2) was perfused into contralateral ventricle was carried out in control group. *I.c.v.* perfusion of ACSF without topical application of high-K^+ was applied in sham group.

In order to minimize animal use, some rats from this series were also used for series 3-5 (see below): 3 rats from the sham group and 3 from CSD group were used for subsequent cortex dissection in series 4. Three rats from PP3 and 3 from PP2 groups were used for subsequent animal perfusion, followed by IHC in series 5. All 5 rats in the CSD group and 3 rats in the sham group were also used for series 3.

Series 3: In order to examine whether NR2A inhibition could suppress both CSD-induced SFKs activation and CSD-induced interaction of SFKs and Panx1, three groups were designed with the protocol kept the same as that in series 2

except that NVP-AAM077 (n = 5), but not PP2 or PP3, was administrated. ACSF was perfused in the presence of high-K^+ as the CSD group and in absence of high-K^+ in the sham group (Figure 13).

It needs to mention that as the preliminary study showed that there was no difference in CSD induction and Panx1 channels opening between two different perfusion rate of ACSF at 0.5 μl/minute and 1 μl/minute, the sham and CSD groups from series 1 was therefore used in this series in order to minimize the animal use.

Series 4: In order to test whether CSD could induce Panx1 expression, two groups were considered: (i) CSD group; (ii) sham group (Figure 13).

Series 5: In order to examine whether SFK inhibition could suppress CSD-induced Panx1 opening, four groups were designed. The protocol was the same as that in series 1 except that both PP2 and PP3, but not NVP-AAM077, were applied respectively starting from 120 minutes before CSD induction to allow drugs sufficiently entering into the cell (Figure 14).

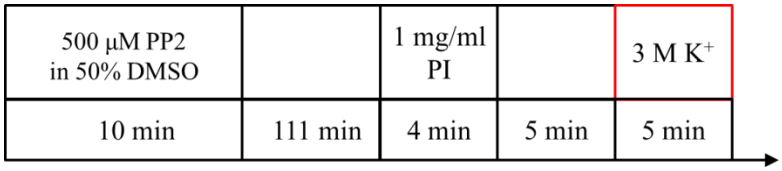

Figure 14. Experimental protocol for investigating whether *i.c.v.* perfusion of PP2 could suppress CSD propagation and CSD-induced Panx1 channels opening in rats. One CSD episode was induced by topical application of high-K^+ for 5 minutes in drug and control groups, whereas in the absence of high-K^+ was carried out as sham in each experiment. 5 μl PP2 at 500 μM (PP3 as control) was *i.c.v.* perfused 120 before CSD induction. 2 μ PI (1mg/ml) was *i.c.v.* perfused 5 minutes before CSD induction in all groups.

Series 6: In order to examine whether NR2A inhibition could suppress CSD-induced CGRP gene expression, 5 repeated CSD episodes with 40-minutes

interval were induced and three groups were designed: (i) NVP-AAM077 group (n = 5). NVP-AAM077 was administrated before the 1st high-K^+ application. (ii) CSD group (n = 3) and (iii) sham group in the absence of high-K^+ application (n = 3). ACSF but not NVP-AAM077 was applied in CSD and sham groups (Figure 15). The electrode was removed and wound sutured 5 minutes after the 5th CSD episode. Ibuprofen (5-10 mg) and mupirocin ointment (0.4-0.8 mg) were applied on the wound. 24 hours after the 5th CSD episode, rat was re-anaesthetized and ipsilateral motor, somatosensory and visual cortices were dissected and store at -80℃.

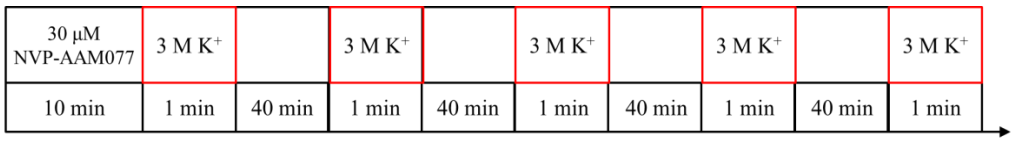

Figure 15. Experimental protocol for investigating the effect of NVP-AAM077 on CSD-induced CGRP mRNA expression in rats. Five repeated CSD episodes were induced by high-K^+ for 1 minute with 40-minutes interval in drug and control groups, whereas in the absence of high-K^+ was performed as sham. 10 μl NVP-AAM077 (30 μM) were *i.c.v.* perfused immediately before the 1st high-K^+ application. ACSF but not NVP-AAM077 was applied in control and sham groups.

2.3.4 Electronic devices setup

Both EEG and direct current (DC) potential were derived from the potential between the recording electrode (the electrode built into the microdialysis probe in microdialysis experiment or the anterior Ag/AgCl recording electrode in *i.c.v.* experiment) and the Ag/AgCl reference electrode (Obrenovitch et al., 1993).

As reported previously (Wang et al., 2003), EEG and DC signals were first amplified with a high-impedance input, AC/DC pre-amplifier (NL834, Neurolog System, Digitimer Ltd., UK). The alternating current component in the 1-30 Hz window provided the EEG (overall ×5000 amplification) and the 0-30 Hz window

provided the extracellular DC potential (overall ×250 amplification). The recorded EEG variables were monitored by a digital oscilloscope (DS1000B, RIGOL, China). All the recorded variables were continuously digitised, displayed and recorded by a computer using Labview 11.0 via an analogue/digital-converter (USB6009, NI Instruments, USA) during experiment (Figure 16).

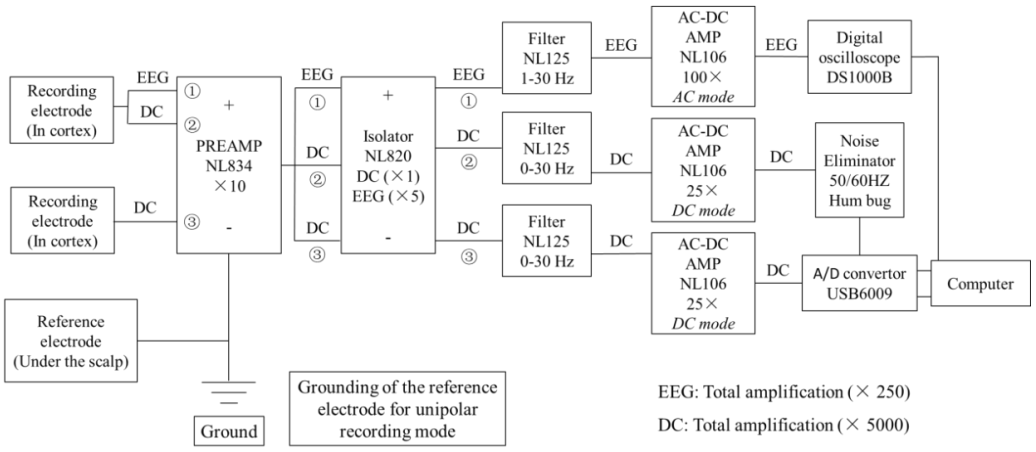

Figure 16. Schematic presentation of the electronic devices used for the recording of DC and EEG activity with microdialysis probe and Ag/AgCl electrode. Pre-amplifier (PREAMP), AC (alternating current), DC (direct current).

In the microdialysis-based experiment, the spreading depolarization wave of CSD at the induction site was recognized as a transient, negative shift superimposed on the sustained shift resulting from the imposed high extracellular K^+ concentration (Figure 7 B). The spreading depolarization wave of CSD at the propagation site was recognized by a transient, negative shift but in the absence of the sustained depolarization shift (Figure 7 B and Figure 10 B).

2.3.5 Data presentation and statistical analysis

Details on CSD number, latency, area under the curve (AUC), height (H), width at half height (WHH), maximum slope of depolarization (Sld), maximum slope of repolarization (Slr), and propagation rate were quantified as that described

previously (Bu et al., 2016, Wang et al., 2003). Labview program was used to determine (i) CSD number in each episode; (ii) Latency (minute), the time required to elicit the 1st CSD wave from the start of depolarization induced by K^+-medium through microdialysis probe or from the start of topical perfusion of K^+ on cortical surface. CSD number and latency were used to reflect tissue susceptibility to CSD; (iii) AUC (mV × minutes); (iv) H (mV), the distance between peak point and midpoint of base line of curve; (v) WHH (second); (vi) Sld (mV/minute); (vii) Slr (mV/minute). AUC, H, WHH, Sld and Slr were used to reflect the magnitude of CSD waves. Both tissue susceptibility to CSD and CSD magnitude were accessed to reflect the genesis of CSD. (viii) Propagation rate (mm/minute), the velocity of each CSD wave, to reflect the propagation of CSD (Figure 7 B and Figure 10 B). In the case of CSD wave was completely abolished by chemicals, the latency was counted as 20 minutes if K^+-medium perfused through microdialysis probe or 10 minutes if K^+ perfused onto cortical surface; AUC, H, WHH, Sld, Slr and propagation rate were counted as zero when CSD waves were abolished; The average of each CSD parameter in each episode was used for quantified analysis.

All values were given in mean ± SEM. Unpaired t-test, paired t-test, and One-way ANOVA with subsequent Bonferonni test were used for data analysis if data obeys normal distribution. The significant difference was showed as $^{*}p < 0.05$, $^{**}p < 0.01$ and $^{***}p < 0.001$.

2.4 *Immunohistochemistry analysis of protein changes*

2.4.1 Sample preparation

CSD-induced Panx1 channels opening under SFKs or NR2A inhibition was detected using IHC. After being deeply anesthetized with 5% isoflurane in N_2O (150 cc/min), rats were transcardially perfused by sodium phosphate buffer (PBS) (09-8912-100, Medicago) for 20 minutes at 8 ml/minute, followed by 4% PFA in PBS for 10 min at 4 ml/min using peristaltic pump (FH-100, Thermo Scientific). Brain was quickly removed, and post-fixed in 4% PFA overnight followed by

cryoprotected in 30% (w/v) sucrose solution for 48 hours. 20 μm thick coronal sections close to coordinates (0.4 mm anterior to Bregma), where motor, somatosensory and cingulate cortices could be seen, were cut in cryostat (CM1950, Leica) and stored in -80°C.

2.4.2 Immunohistochemistry

In order to label neurons, brain slices were incubated with NeuN monoclonal antibody (anti-mouse, #MAB377, Millipore) (Wolf et al., 1996). Briefly, slices were incubated in 0.3% Trition ×100 in PBS for permeabilization for 30 minutes at room temperature (RT) and blocked with 5% goat serum (AR0009, Boster Biology, China) in PBS for 1 hour to reduce non-specific binding. Sections were then exposed to the NeuN antibody at 1:1000 incubation with blocking solution overnight at 4℃, followed by a fluorescently-labeled (488) secondary antibody (A11029, Invitrogen) at 1:500 in blocking solution for 1 hour at RT. Immuno-negative control was performed by staining of NeuN antibody in rat purkinje cells (Wolf et al., 1996). Additionally, the secondary antibody only was performed for further confirming the specificity of NeuN antibody.

2.4.3 Data presentation and statistical analysis

NeuN at 488 nm and PI staining at 535 nm were detected under the fluorescence microscope (Eclipse Ni-U, Nikon). Labeled cells were counted on one microscopic field at 400 × magnification on 2 neighboring coronal sections from each ipsilateral cortex of the rat. The differential cortical layers were positioned under the guidance of anatomical microstructure of rat neocortex (DeFelipe et al., 2002) (Figure 35 A). The number of labeled cells in the selected fields was averaged by one blinded observer for subsequent data analysis. All values were given in mean ± SEM. Unpaired t-test was used for data analysis if data obeys normal distribution. Mann-Whitney test was used for data analysis if data obeys abnormal distribution. Differences were considered significant when $^{*}p < 0.05$, $^{**}p < 0.01$ and $^{***}p < 0.001$.

2.5 Western blotting analysis of protein changes

2.5.1 Protein preparation

The CSD ipsilateral cortex without PI staining was homogenized in the presence of protease inhibitor (Complete EASYpacks, 04693116001, Roche) and phosphatase inhibitor (#5870, CST) using a tissue ruptor (9001272, GIAGEN) on ice for subsequent detection of SFKs phosphorylation. Total protein was harvested from supernatant after tissue lysate was centrifuged at 13,000 rpm for 10 minutes at 4℃. Protein concentrations were determined using Bicinchoninic acid Protein Assay Kit (P0010, Beyotime).

2.5.2 Western blotting

Protein (30 μg for Panx1, 80 μg for PY416 SFKs, SFKs and β-actin) were denatured with 4×NuPAGE® LDS Sample Buffer (NP0007, Invitrogen) and 2% SDS by boiling for 5 minutes, then separated on a 10% sodium dodecyl sulfate–polyacrylamide gel, subsequently transferred onto nitrocellulose membranes (66485, Pall Corporation). Non-specific binding was blocked with 5% milk in tris-buffered saline with Tween-20 (TBST) for 1 hour at RT.

In order to detect the expression of Panx1 (~45 kDa), membranes were incubated with Panx1 monoclonal antibody (anti-rabbit, LS-C138631, LSBio) at 1:30000 overnight at 4℃. Once excess primary antibody was washed off by TBST, membranes were incubated with heavy+light chains horseradish peroxidase-labeled secondary antibody (AB10058, Sangon Biotech) at 1:5000 for 1 hour at RT. Protein bands were detected by Western bright enhanced chemiluminuscence working solution (K-12045-D50, Advansta) and exposed on Kodak medical X-ray film (XBT-1, Kodak).

β-actin (~45 kDa), was detected as the reference (Wang et al., 2016a) after that the nitrocellulose membrane stripped by 0.2 M NaOH for 15 minutes at 37℃. Stripping was to avoid any interruption from Panx1 as they have similar

molecular weight. The membrane was then washed out using TBST and the same process was repeated starting from non-specific binding blocking by 5% milk except that β-actin monoclonal antibody (anti-rabbit, #4970, CST) at 1:1000, but not Panx1 antibody was used.

In order to detect the level of SFKs (~ 60 kDa) phosphorylation post CSD and effects of SFKs or NR2A inhibition on CSD-induced SFKs activity, membranes were divided into two parts for detecting PY416 SFKs, a strong indicator of SFKs activation (Smart et al., 1981), and β-actin respectively. After non-specific binding blocking, membranes were incubated with the PY416 SFKs (anti-rabbit, #6943, CST, for detecting effect of PP2 on CSD-induced SFKs phosphorylation; anti-rabbit, #2101, CST, for detecting effect of NVP-AAM077 on CSD-induced SFKs phosphorylation) antibody at 1:500 and β-actin antibody at 1:1000 overnight at 4℃ respectively. The same process for incubation of secondary antibody and detection of chemilluminescence were performed as that for Panx1 detection. Additionally, total SFKs was also detected by repeating the same process starting from membranes stripping except that SFKs monoclonal antibody (anti-rabbit, #2109, CST) but not β-actin antibody was used. The specificity of primary antibodies was examined in full gels before formal experiments. The secondary antibody only was performed for further confirmation. The stripping process followed secondary antibody only was performed to test whether previous primary antibody was stripped clearly.

2.5.3 Co-immunoprecipitation

In order to examine interaction of PY416 SFKs and Panx1 in the cortex, co-immunoprecipitation (co-IP) was performed using Pierce Classic IP Kit (26146, Thermo Fisher). Briefly, 300 μg protein was pre-cleaned by 20 μl control agarose resin, eluted at 1000 ×g for 1 minute, then incubated with 100 μl buffer of 0.02 μg Panx1 antibody and 10 μl A/G protein agarose resin for 2 hours at 4℃. The bound resin was separated from the mixture at 1000 ×g for 1 minute and washed in IP Lysis/Wash buffer following three times centrifugation at 1000 ×g prior to western blotting. Nitrocellulose membrane was then incubated with PY416 SFKs

monoclonal antibody (anti-rabbit, #6943, CST) at 1:500 followed by light chain only horseradish peroxidase-labeled secondary antibody (D110059, Sangon Biotech) at 1:5000 for SFKs detection. After stripping, Panx1 was detected by incubation with Panx1 antibody at 1:30000 as that described above except that light chain only but not light+heavy chains secondary antibody was used. Western blotting without IP'd purification was performed as the positive control. Control agarose resin that would not interact with primary antibody was used as the negative control for IP'd purification.

2.5.4 Data presentation and statistical analysis

The grey value of signal was quantified using Image J software and normalized to β-actin for data comparison. The values were given in percentages of basal level, i.e. the averaged value of sham group. All values were given in mean ± SEM. Unpaired t-test was used for data analysis if data obeys normal distribution. Mann-Whitney test was used for data analysis if data obeys abnormal distribution. Differences were considered significant when $^{*}p < 0.05$ and $^{**}p < 0.01$.

2.6 Gene expression

2.6.1 RNA extraction

Trizol reagent (T9424, Sigma-Aldrich) was used to extract mRNA following the manufacturer's instruction. Briefly, 50-100 mg tissue was homogenized in 1 ml Trizol reagent and 200 μl chloroform and, shook vigorously for 15 seconds. After 8 minutes incubation at RT, samples were centrifuged at 12000 ×g for 15 minutes at 4℃, separating phase into three layers: (i) RNA-containing colorless aqueous upper layer; (ii) a thin middle interphase layer and (iii) a bottom DNA-and-protein-containing red organic layer. The upper layer was carefully transferred into a new microfuge tube. 500 μl of isopropanol was added per 1 ml of Trizol reagent. Stand for 8 minutes and then centrifuge at 12000 ×g for 10 minutes at 4℃. After discarding the supernatant, RNA pellet was washed by 1 ml 75%

molecular grade ethanol (per 1 ml Trizol used in the initial step). Samples were centrifuged at 7500 ×g for 5 minutes at 4℃. The supernatant was discarded and the RNA pellet was air dried at room temperature. Finally, the RNA pellet was re-suspended in 10-40 µl nuclease free water and incubated on a heat block at 55℃ for 10 minutes. After complete dissolution, RNA concentration was measured by Nanodrop for later cDNA synthesis.

RNA concentration was measured by Nanodrop 2000c (Thermo Scientific). The sample reader was washed with nuclease free water and dried with KimWipe. Following the instruction of the software, the Nanodrop was set to RNA. 1 µl of elution nuclease free water was loaded and set as blank. 1 µl of sample was loaded and the absorbance measured. The absorbance of UV light by nucleic acid at 260 nm depends on their concentration. After reading completion, the RNA concentration in ng/µl was obtained. The quality of the RNA was also assessed by the Nanodrop through measuring the ratios of A260/A280 and A260/A230; expected values for high RNA purity are approximately 2.0 and 2.0-2.2, respectively.

2.6.2 *cDNA preparation*

The GoScript Reverse Transcription System (A5001, Promega) was used for first strand cDNA synthesis from total RNA following the manufacturer's protocol. Briefly, 1µg RNA was used for each sample in the reverse transcriptase reaction, mixed in a PCR tube with the following components (Table 1):

Component	Volume
RNA (up to 1 µg)	x µl
Random primers (0.5 µg/reaction)	1 µl
Oligo$(dT)_{15}$ Primers (0.5 µg/reaction)	1 µl
Nuclease free water	x µl
Final volume	5 µl

Table 1. Reagents components for reverse transcription step one.

The mixture was incubated at 70℃ for 5 minutes, immediately cooled down on ice, and added the following reverse transcription mix (Table 2) to a final 20 µl reaction volume.

Component	Volume	Final concentration
GoScript 5X reaction buffer	4 µl	1x
MgCl2 (25 mM)	4 µl	5 mM
PCR nucleotide mix (10 mM of each dNTP)	1 µl	0.5 mM
Recombinant RNasin Rinonuclease inhibitor (40 U/µl)	0.5 µl	1 U/µl
GoScript Reverse Transcriptase	1 µl	-
Nuclease free water	4.5 µl	-
Final volume	15 µl	

Table 2. Reagents components for reverse transcription step two.

The final reaction mixture was incubated as following: at 25℃ for 5 minutes for primer annealing; at 42℃ for 60 minutes for extension; finally at 70℃ for 15 minutes to inactivate the reverse transcriptase. The cDNA was stored at -20℃ for later use.

2.6.3 *Real-time quantitative PCR detecting system (qPCR)*

QPCR was used to detect gene expression of CGRP. Two housekeeping genes, peptidylprolyl isomerase A (PPIA) and ACTB, rather than a single housekeeping gene were used in this study as reference for reliable result. Primers (forward, reverse) were: PPIA (NM_017101.1) 5'TTGCTGCAGACATGGTCAAC3', 5'TGTCTGCAAACAGCTCGAAG3'; ACTB (NM_001101.3) 5'ACGGTCAGGTCATCACTATGG3', 5'AGCCACCAATCCACACAG3'; and CGRP: (NM_001033953.2) 5'AACCTTGGAAAGCAGCCCAGGCATG3', 5'GTGGGCACAAAGTTGTCCTTCACCA3'. QPCR was performed using GoTaq qPCR Master Mix (Promega) following the manufacturer's instruction.

The reaction component (Table 3) is:

Component	Volume (*n*=1)	Final concentration
2× GoTaq qPCR Master Mix	10 µl	0.025 U/µl
cDNA template	×µl	-
Forward primer	0.3 µl	0.33 µM
Reverse primer	0.3 µl	0.33 µM
Nuclease free water	X µl	-
Final volume	20 µl	

Table 3. Reagents component for qPCR.

Analysis was performed on 7500 fast Real-Time PCR system (Applied BiosystemsTM Waltham, MA, USA) with the following thermal cycling conditions (Table 4):

	Cycling Program	Cycles
Hot-start Activation	95 ℃ for 2 min	1
Denaturation	95 ℃ for 15 s	40
Anealing/Extension	60 ℃ for 1 min	
Dissociation	60-95 ℃	1

Table 4. QPCR running setting up.

2.6.4 *Data presentation and statistical analysis*

Samples were analyzed by the relative fold change ($2^{-\Delta\Delta Ct}$ method) normalized to the ipsilateral sham tissue. In detail, the individual CGRP mRNA levels were normalized to the product-based geometric mean of the two reference genes (Vandesompele et al., 2002), calculated as the square-root of the product of the reference genes (PPIA ×ACTB), i.e.

① $$\text{Individual CGRP mRNA levels} = 2^{-\Delta Ct(CGRP)\sqrt{Ct(PPIA)*Ct(\beta-actin)}}$$

In the next step, the individual CGRP fold change was obtained from dividing ① by the average of ① of sham samples, i.e.

$$\text{CGRP fold change} = 2^{-\Delta(\text{individual})\Delta(\text{average})\text{Ct}}$$

Formula 2.6.4. $2^{-\Delta\Delta Ct}$ method for calculating relative gene expression.

Mann-Whitney test was used for data analysis. Differences were considered significant when $^{*}p < 0.05$.

Chapter 3 NR2A contributes to CSD genesis and propagation in rats

The previous study shows that NR2A inhibition by NVP-AAM077 suppresses the propagation of CSD in the chick retina (Wang et al., 2012). However, an opposite opinion showed that NR2A antagonist TCN-201 applied through intraperitoneal injection don't alter the BOLD accompanied with CSD in rats (Shatillo et al., 2015). To further investigate whether NR2A could contribute CSD propagation, I examined the effect of bath application of TCN-201 on CSD propagation in chick retina. In addition, I explored whether NR2A inhibition by NVP-AAM077 and TCN-201 could suppress CSD genesis and propagation in microdialysis-based CSD model in rats. Finally, the involvement of NR2A in CSD propagation was further determined by *i.c.v.* perfusion of NVP-AAM077 in rats.

3.1 Objectives

3.1.1 *To investigate whether NR2A inhibition could suppress CSD propagation in chick retina*

3.1.2 *To validate microdialysis-based CSD model under isoflurane anaesthesia in rats*

3.1.3 *To investigate whether NR2A inhibition could suppress CSD genesis in microdialysis-based CSD model*

3.1.4 *To investigate whether NR2A inhibition could suppress CSD propagation in microdialysis-based CSD model*

3.1.5 *To investigate whether i.c.v. perfusion of NR2A antagonist could suppress CSD propagation in rats*

3.2 Results

3.2.1 *TCN-201 suppressed CSD propagation in chick retina*

In the DMSO group, the AUC, H, WHH, Sld, Slr and propagation rate of CSD had no significant change throughout the experiment (n = 8, Figure 17). Compared with the control group, TCN-201 suppressed AUC, WHH, Sld and propagation rate and increased Slr of CSD in a concentration-dependent manner. At the maximum concentration tested (9 μM), the AUC, WHH, Sld and propagation rate were significantly reduced to 73.8% (n = 6, $^{***}p < 0.001$, Figure 17 A), 76.10% (n = 6, $^{***}p < 0.001$, Figure 17 C), 79.91% (n = 6, $^{**}p < 0.01$, Figure 17 D) and 72.77±4.09 (n = 6, $^{***}p < 0.001$, Figure 17 F) of initial level in respective order, meanwhile Slr was increased to 124.30% (n = 6, $^{*}p < 0.05$, Figure 17 E) of initial level in respective order. This inhibitory effect slightly but not significantly recovered after drug removal. H was not altered at any concentration of drug we tested (n = 6, Figure 17 B).

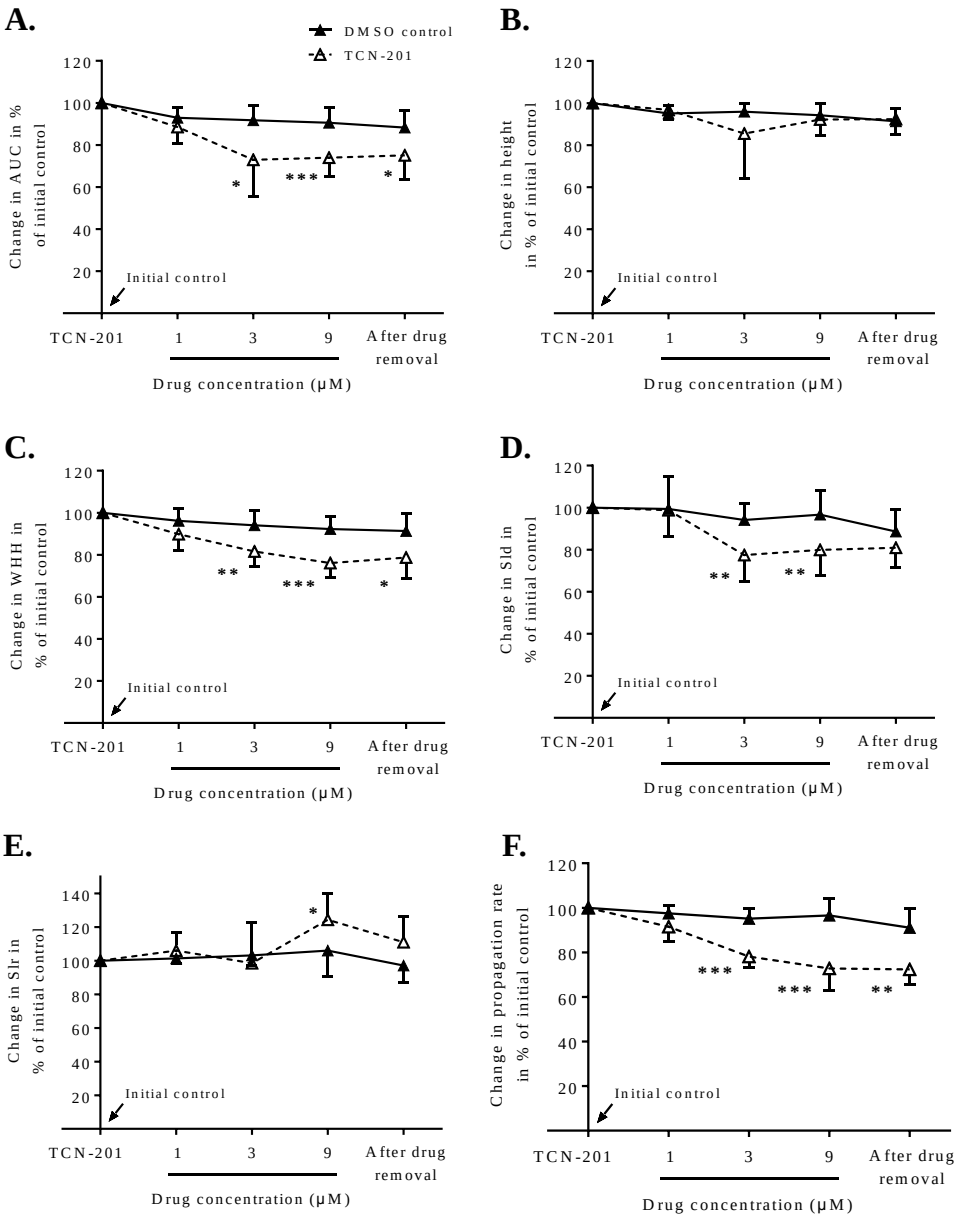

Figure 17. Effects of TCN-201 on the magnitude (A-E) and propagation rate (F) of CSD induced by high-K^+ in the chick retina. Data was plotted as percentage of their initial levels and indicated as mean ± SD. Mann-Whitney test with two-tailed calculation was used for significance between DMSO (n = 8) and TCN-201 (n = 6) groups ($^{*}p < 0.05$, $^{**}p \leq 0.01$, $^{***}p \leq 0.001$). Wilcoxon matched pairs test with two-tailed calculation was used to test whether tissue was restored after drug removal.

3.2.2 Validation of microdialysis-based CSD model under isoflurane anaesthesia in rats.

In the control group, 250 mM K^+ induced CSD was recorded at genesis site throughout experiment (ACSF, Figure 18). The average number, latency and the magnitude of the 1st CSD episode were 3.0 ± 0.86 (n = 6, Figure 19 A), 6.53 ± 1.93 minutes (n = 6, 19 B) and 4.95 ± 1.06 mV × minute (n = 6, Figure 20 A) in respective order. No significant difference in any parameter was observed over the 5 CSD episodes.

To validate the CSD model under anesthesia with isoflurane, the NMDA receptor antagonist, MK-801, with known anti-CSD effect (Obrenovitch and Zilkha, 1996a, Marrannes et al., 1988, Wang et al., 2012), was examined through the microdialysis probe. At CSD genesis site, the CSD number, latency and magnitude had no difference in the 1st episode compared to the control (ACSF) group (Figure 19 A and B, Figure 20 A). MK-801 suppressed CSD genesis in a concentration dependent manner (Figure 18). MK-801 at 30 μM completely abolished CSD in 5 out of 6 experiments during the 20-minute (Table 5). CSD number significantly reduced to 0.67 ± 0.33 compared to 2.5 ± 0.62 of the control group (n = 6, $^{*}p < 0.05$, Figure 19 A). At this concentration of MK-801, CSD latency (7.52 ± 1.41 minutes) increased 2.5-folds compared to the control group (18.49 ± 1.51 minutes) (n = 6, $^{***}p < 0.001$, Figure 19 B). This inhibitory effect on CSD was persistent after the drug removal (i.e. in the 5th CSD episode).

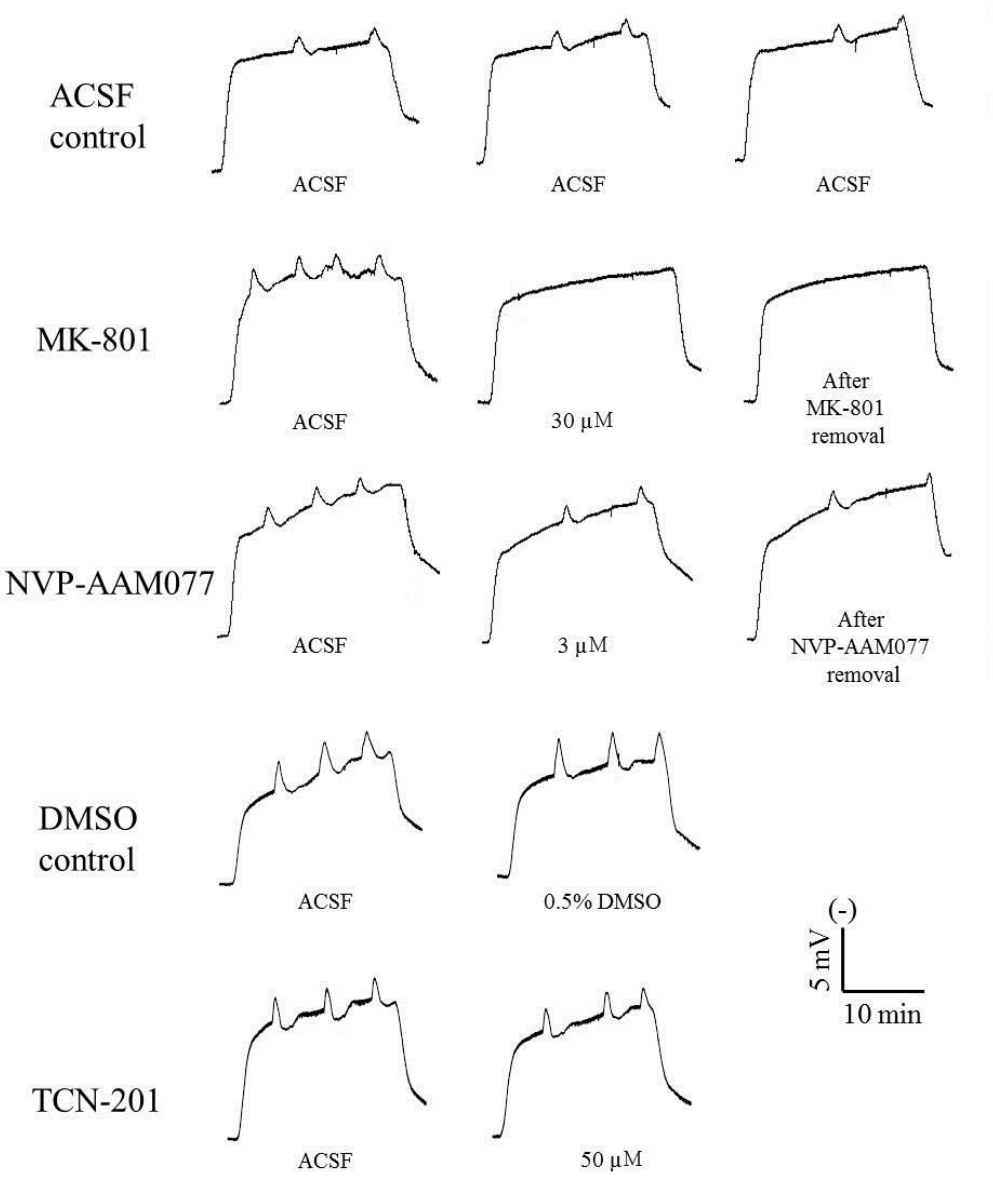

Figure 18. Representative CSD traces of the effects of MK-801, NVP-AAM077 and TCN-201 on tissue susceptibility to CSD induced by K^+-medium perfused through the microdialysis probe. ACSF group set as control for MK-801 and NVP-AAM077 groups. DMSO group set as control for TCN-201 group.

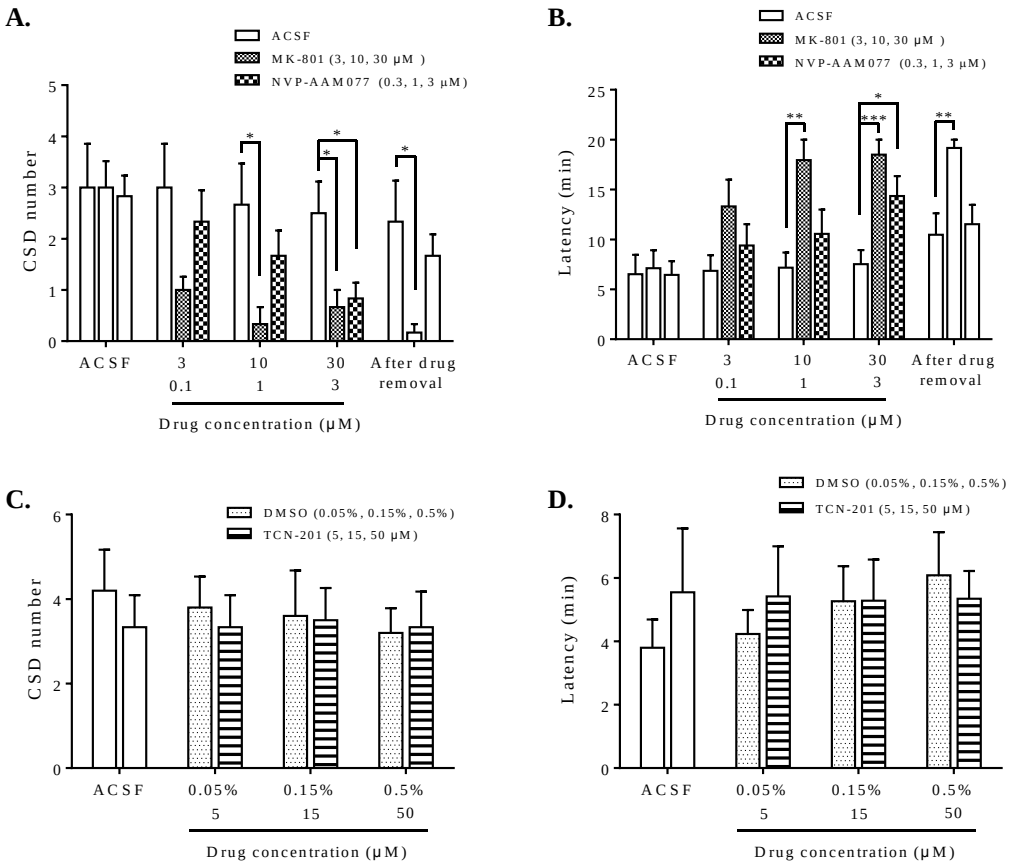

Figure 19. Effects of MK-801, NVP-AAM077 and TCN-201 on tissue susceptibility to CSD induced by K^+-medium perfused through the microdialysis probe. ACSF group (n = 6) set as control for MK-801 (n = 6) and NVP-AAM077 (n = 6) groups (A and B). DMSO group (n = 7) set as control of TCN-201 (n = 6) (C and D). All the values given were means ± SEM. One-way ANOVA test was used for statistics among ACSF, MK-801 and NVP-AAM077 groups with subsequent Bonferonni test for significance between control and drug treatment groups ($^{*}p < 0.05$, $^{**}p \leq 0.01$, $^{***}p \leq 0.001$). Unpaired t-test with two-tailed calculation was used to test for significance between DMSO and TCN-201 groups. Paired t-test with one-tailed calculation was used to test whether tissue was restored after drug removal between the 4th and 5th CSD episodes.

Groups	Number of tested animals	Number of tested animals in which CSD was completely blocked
ACSF Control	6	0
MK-801	6	5
NVP-AAM077	6	2
DMSO Control	6	0
TCN-201	6	0

Table 5. The number of animals in which CSD was completely blocked by MK-801, NVP-AAM077 and TCN-201 in microdialysis-based model. ACSF group set as control for MK-801 and NVP-AAM077 groups. DMSO group set as control for TCN-201 group.

3.2.3 NR2A inhibition suppressed CSD genesis in microdialysis-based CSD model

To investigate whether NR2A inhibition could suppress the susceptibility of cortical tissue to CSD, the effect of NR2A antagonists NVP-AAM077 and TCN-201 on CSD number and latency were examined by local perfused at where CSD generated through microdialysis probe. In the NVP-AAM077 group, the CSD number and latency in the 1st episode were 2.83 ± 0.40 (n = 6) and 6.45 ± 1.37 minutes (n = 6) in respective order, which had no significant difference compared with control group (Figure 19 A and B). NVP-AAM077 at 0.3, 1 and 3 μM concentration-dependently reduced CSD number (Figure 18). At the highest concentration applied, the reduction in CSD number reached significance (0.83 ± 0.31, n = 6) compared with that of control group (2.53 ± 0.62, n = 6, $^{*}p < 0.05$, Figure 19 A), and completely abolished CSD in 2 out of 6 experiments during 20-minute (Table 5). Conversely to CSD number, NVP-AAM077 at 3 μM significantly prolonged CSD latency to 13.94 ± 2.23 minutes (n = 6) compared with the corresponding control (7.52 ± 1.41 minutes, n = 6, $^{*}p < 0.05$, Figure 19 B). There was no significant recovery on CSD number and latency after the drug removal.

In DMSO control group, the CSD number and latency in the 1st episode were 4.2 ± 0.97 (n = 5, Figure 19 C) and 3.80 ± 0.89 minutes (n = 7, Figure 19 D). DMSO at 0.05%, 0.15% or 0.5% had no significant effect on these parameters when compared among episodes. In the TCN-201 group, the CSD number and latency in the 1st episode were 3.3 ± 0.76 (n = 5) and 5.55 ± 2.01 minutes (n = 6), which had no significant difference compared with the corresponding control group (Figure 18, Figure 19 C and D). Contrary to NVP-AAM077, TCN-201 didn't alter either CSD number (n = 6) or latency (n = 6) even at 50 μM compared to control group (Figure 19 C and D).

To investigate whether NR2A inhibition could suppress the magnitude of CSD, the effect of NR2A antagonists NVP-AAM077 and TCN-201 on AUC, H, WHH, Sld and Slr of CSD were examined by local perfused at CSD genesis site through microdialysis probes. In the ACSF group, the AUC, H, WHH, Sld and Slr in the 1st episode were 4.95 ± 1.06 mV × minutes (n = 6, Figure 20 A), 6.12 ± 0.91 mV (n = 6, Figure 20 C), 36.05 ± 3.21 seconds (n = 6, Figure 20 E), 31.74 ± 5.40 mV/minute (n = 6, Figure 20 G) and 19.92 ± 2.02 mV/minute (n = 6, Figure 20 I) in respective order. There was no significant difference in any of these parameters over the 5 repeated CSD episodes. Under NVP-AAM077 application, the AUC, H, WHH and Sld waves were concentration-dependently reduced. Compared with control (ACSF) group, NVP-AAM077 at 3 μM significantly reduced AUC from 5.20 ± 0.94 mV × minutes to 2.36 ± 0.79 mV × minutes (n = 6, $^{*}p < 0.01$, Figure 20 A), H from 6.35 ± 0.82 mV to 3.55 ± 1.17 mV (n = 6, $^{*}p < 0.01$, Figure 20 C), WHH from 36.92 ± 2.09 seconds to 21.02 ± 7.15 seconds (n = 6, $^{*}p < 0.01$, Figure 20 E) and Sld from 21.11 ± 3.92 mV/minute to 13.12 ± 4.45 mV/minute (n = 6, $^{*}p < 0.01$, Figure 20 G), whereas Slr was not altered (n = 6, Figure 20 I). There was no significant recovery on AUC, H, WHH and Sld of CSD after the drug removal.

In DMSO group, the AUC, H, WHH, Sld and Slr of CSD in the 1st episode were 4.81 ± 0.38 mV × minutes (n = 6, Figure 20 B), 5.02 ± 0.62 mV (n = 5, Figure 20 D), 37.059 ± 2.92 seconds (n = 5, Figure 20 F), 30.28 ± 3.34 mV/minute (n = 5, Figure 20 H) and 20.30 ± 3.14 mV/minute (n = 6, Figure 20 J) in respective order. DMSO at 0.05%, 0.15% or 0.5% had no significant effect on these parameters

when compared among episodes. In the TCN-201 group, the AUC and Sld were concentration-dependently reduced. Compared with control group, TCN-201 at 50 μM reduced the magnitude from 5.15 ± 0.62 mV × minutes to 3.69 ± 0.36 mV × minutes (n = 6, $^{*}p$ = 0.043, Figure 20 B), and Sld from 30.22 ± 2.3 mV/minute to 25.26 ± 1.99 mV/minute (n = 6, $^{*}p$ = 0.043, Figure 20 H), whereas H, WHH or Slr was not altered (n = 6, Figure 20 D, F and J).

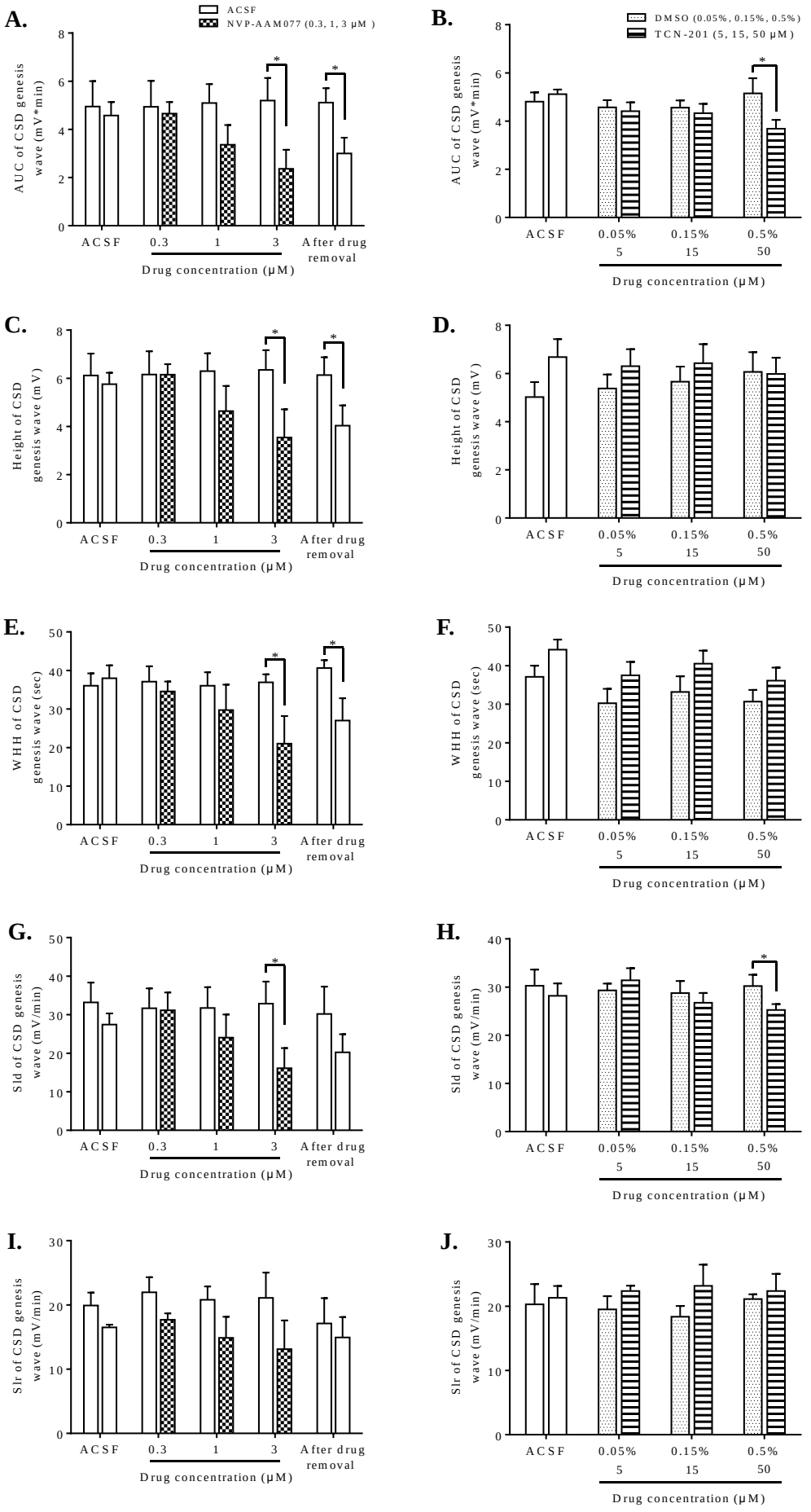
A.
ACSF
NVP-AAM077 (0.3, 1, 3 μM)
AUC of CSD genesis wave (mV*min)
ACSF
0.3
1
3
After drug removal
Drug concentration (μM)
B.
DMSO (0.05%, 0.15%, 0.5%)
TCN-201 (5, 15, 50 μM)
AUC of CSD genesis wave (mV*min)
ACSF
0.05%
0.15%
0.5%
5
15
50
Drug concentration (μM)
C.
Height of CSD genesis wave (mV)
D.
Height of CSD genesis wave (mV)
E.
WHH of CSD genesis wave (sec)
F.
WHH of CSD genesis wave (sec)
G.
Sld of CSD genesis wave (mV/min)
H.
Sld of CSD genesis wave (mV/min)
I.
Slr of CSD genesis wave (mV/min)
J.
Slr of CSD genesis wave (mV/min)

Figure 20. Effects of NVP-AAM077 (A, C, E, G, I) and TCN-201 (B, D, F, H, J) perfused through the microdialysis probe on the magnitude of CSD genesis waves. All the values shown were means ± SEM. Unpaired t-test with two-tailed calculation was used for statistical analysis for significance between the control and chemical treatment groups, i.e. ACSF (n = 6) vs NVP-AAM077 (n = 6), and DMSO (n = 6) vs TCN-201 (n = 6) ($^{*}p < 0.05$). Paired t-test with one-tailed calculation was used to test whether tissue was restored after drug removal between the 4th and 5th CSD episodes for NVP-AAM077 testing.

3.2.4 CSD propagation was not altered by NR2A inhibition in microdialysis-based CSD model.

To investigate whether NR2A inhibition could suppress CSD propagation, the effect of NR2A antagonists NVP-AAM077 and TCN-201 on AUC, H, WHH, Sld and Slr of CSD propagation wave and CSD propagation rate were examined by local perfusion of chemicals at CSD genesis site through microdialysis probe. In the ACSF group, the AUC, H, WHH, Sld and Slr and CSD propagation rate in the 1st episode were 4.62 ± 0.73 mV × minutes (n = 6, Figure 21 A), 6.19 ± 1.07 mV (n = 6, Figure 21 C), 41.14 ± 31.73 seconds (n = 6, Figure 21 E), 21.24 ± 53.55 mV/minute (n = 6, Figure 21 G), 18.94 ± 2.66 mV/minute (n = 6, Figure 21 I) and 7.09 ± 0.63 mm/minute (n = 6, Figure 22 A). No parameter was altered over the 5 repeated CSD episodes. In the NVP-AAM077 group, no significant difference was observed in any parameter of CSD in the 1st episode when compared with control (ACSF) group (n = 6, Figure 21 A, C, E, G and I, Figure 22 A). Contrary to the effect of NVP-AAM077 on CSD genesis, NVP-AAM077 didn't alter any parameter of propagating CSD at all concentrations we tested compared to control group (n = 6, Figure 21 A, C, E, G and I, Figure 22 A).

In DMSO group, the AUC, H, WHH, Sld and Slr of propagating CSD and CSD propagation rate in the 1st episode were 3.69 ± 0.28 mV × minutes (n = 5, Figure 21 B), 4.12 ± 0.38 mV (n = 3, Figure 21 D), 40.02 ± 3.43 seconds (n = 3, Figure 21 F), 16.41 ± 1.54 mV/minute (n = 3, Figure 21 H), 17.6 ± 1.19 mV/minute (n = 3, 21 J) and 6.53 ± 0.83 mm/minute (n = 5, Figure 22 B) in respective order.

DMSO at 0.05%, 0.15% or 0.5% had no significant effect on these parameters when compared among episodes. In the TCN-201 group, there was no significant difference in these parameters of CSD in the 1st episode compared with control group (*n* = 3-5, Figure 21 B, D, F, H and J, Figure 22 B). Similarly with the effect of NVP-AAM077 to CSD propagation, TCN-201 didn't alter any parameter of propagating CSD as well compared to control group (*n* = 3-5, Figure 21 B, D, F, H and J, Figure 22 B).

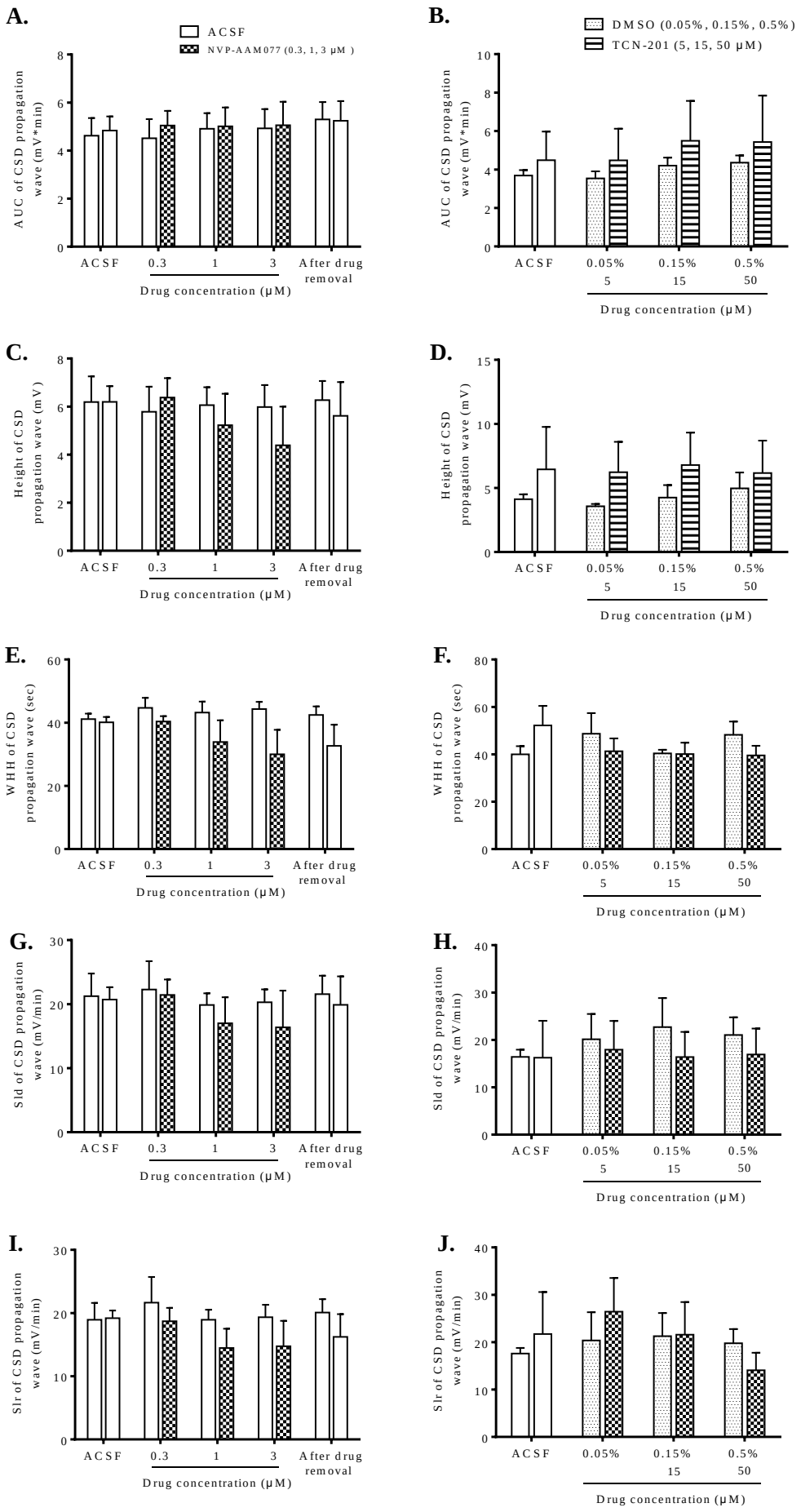
A.
ACSF
NVP-AAM077 (0.3, 1, 3 μM)
AUC of CSD propagation wave (mV*min)
ACSF
0.3
1
3
After drug removal
Drug concentration (μM)
B.
DMSO (0.05%, 0.15%, 0.5%)
TCN-201 (5, 15, 50 μM)
AUC of CSD propagation wave (mV*min)
ACSF
0.05%
0.15%
0.5%
5
15
50
Drug concentration (μM)
C.
Height of CSD propagation wave (mV)
D.
Height of CSD propagation wave (mV)
E.
WHH of CSD propagation wave (sec)
F.
WHH of CSD propagation wave (sec)
G.
Sld of CSD propagation wave (mV/min)
H.
Sld of CSD propagation wave (mV/min)
I.
Slr of CSD propagation wave (mV/min)
J.
Slr of CSD propagation wave (mV/min)

Figure 21. Effects of NVP-AAM077 (A, C, E, G, I) and TCN-201 (B, D, F, H, J) perfused through the microdialysis probe on the magnitude of CSD propagation waves. All the values shown were means ± SEM. Unpaired t-test with two-tailed calculation was used for statistical analysis for significance between the control and chemicals treatment groups, i.e. ACSF (n = 6) vs NVP-AAM077 (n = 6), and DMSO (n = 5) vs TCN-201 (n = 5). Paired t-test with one-tailed calculation used to test whether tissue was restored after drug removal between the 4th and 5th CSD episodes for NVP-AAM077 testing.

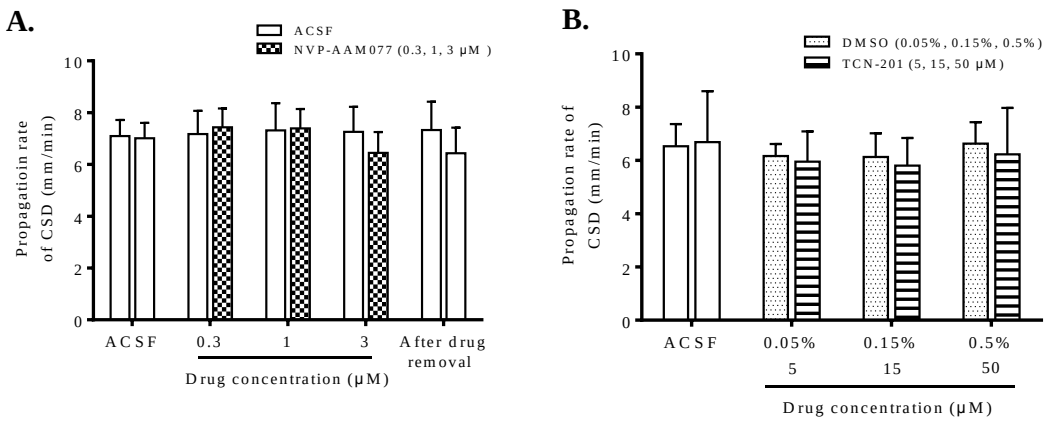

Figure 22. Effects of NVP-AAM077 (A) and TCN-201 (B) perfused through the microdialysis probe on propagation rate of CSD. All the values shown were means ± SEM. Unpaired t-test with two-tailed calculation was used for statistical analysis for significance between the control and drug treatment groups, i.e. ACSF (n = 6) vs NVP-AAM077 (n = 6), and DMSO (n = 6) vs TCN-201 (n = 4). Paired t-test with one-tailed calculation was used to test whether tissue was restored after drug removal between the 4th and 5th CSD episodes for NVP-AAM077 testing.

3.2.5 *NR2A inhibition by i.c.v. perfusion of NVP-AAM077 suppressed CSD propagation in rats*

Distinct from that of CSD genesis, NVP-AAM077 was unable to alter CSD propagation in the microdialysis-based CSD model (Figure 21 and 22). I assumed that should be caused by that locally perfused chemical couldn't diffuse to the remote site where CSD propagation waves were recorded. To allow chemical

diffusing to distant cortical region, contralateral ventricle perfusion was performed for further investigating the effect of NR2A inhibition on CSD propagation.

In the ACSF group, the AUC, H, WHH, Sld and Slr of propagating CSD at the anterior recording site (0.4 mm anterior to Bregma) in the 1st episode were 5.67 ± 0.64 mV × minutes, 7.94 ± 1.43 mV, 41.83 ± 2.64 seconds, 29.94 ± 4.38 mV/minute and 22.79 ± 3.57 mV/minute (n = 6, Figure 23 A-E). There was no change of these parameters throughout the experiment. In NVP-AAM077 group, the AUC, H, WHH, Sld and Slr at the same coordinate in the 1st episode have no difference with that of control group (n = 6, Figure 23 A-E). In contrast to that perfused via microdialysis, *i.c.v.* perfusion of 0.3 nmol NVP-AAM077 significantly suppressed the AUC of CSD propagation wave. In the NVP-AAM077 group, the AUC was reduced to 4.20 ± 0.80 mV × minutes compared to 6.37 ± 0.50 mV × minutes in the control group (n = 6, $^{*}p < 0.05$, Figure 23 A). H, WHH, Sld or Slr was not altered compared to the control group (n = 6, Figure 23 B-E). Similarly, the suppressive effect of NVP-AAM077 on the AUC of CSD propagation waves was also observed at 2 mm posterior to Bregma; whereas H, WHH, Sld or Slr was not altered at the same coordinate as well (data not shown).

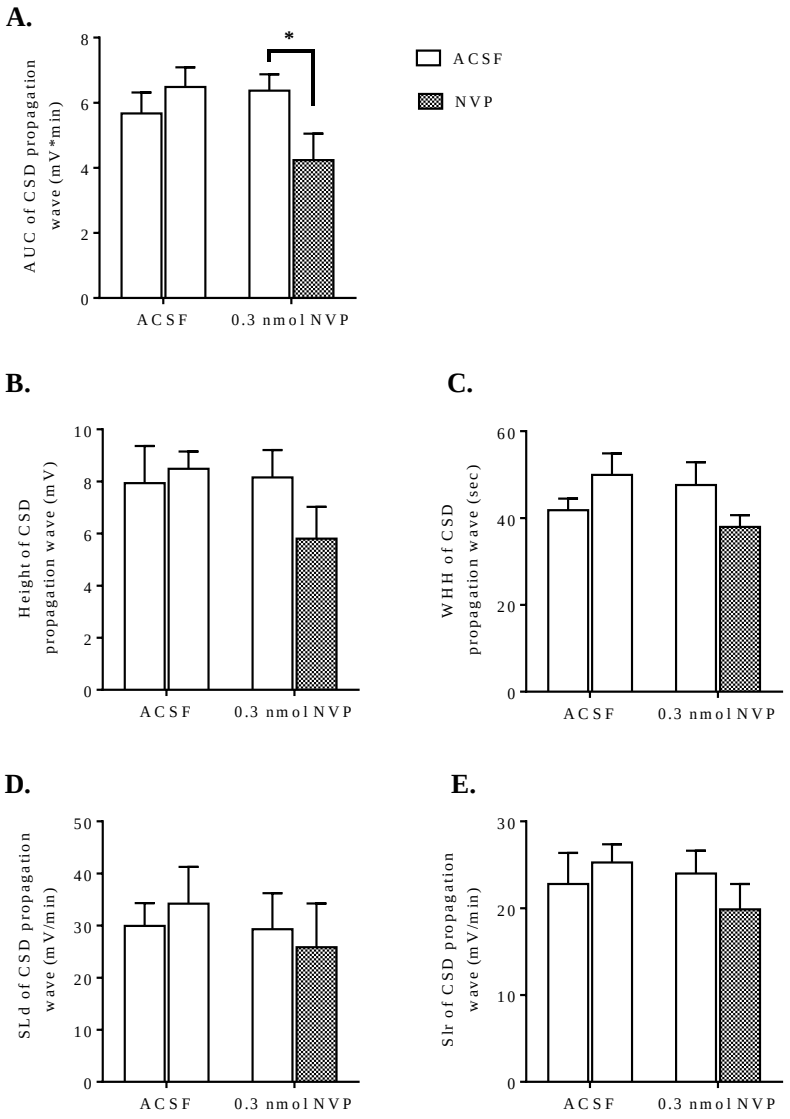

Figure 23. Effects of NVP-AAM077 perfused into the left lateral ventricle on the magnitude of CSD propagation waves at 0.4 mm anterior to Bregma. All the values shown were means ± SEM. Unpaired t-test with two-tailed calculation was used for statistical analysis for significance between the drug (n = 6) and control group (n = 6) ($^{*}p < 0.05$).

In the ACSF group, the propagation rate of CSD in the 1st episode was 4.01 ± 0.21 mm/minute (n = 6). There was no change of these parameters throughout the experiment. In NVP-AAM077 group, the propagation rate in the 1st episode was 4.47 ± 0.79 mm/minute, which have no difference with that of control group (n = 6, Figure 24). Interestingly, *i.c.v.* perfusion of 0.3 nmol NVP-AAM077

significantly suppressed CSD propagation rate from 4.03 ± 0.37 mm/minute to 2.64 ± 0.27 mm/minute compared to the control group (n = 6, $^{**}p < 0.01$, Figure 24).

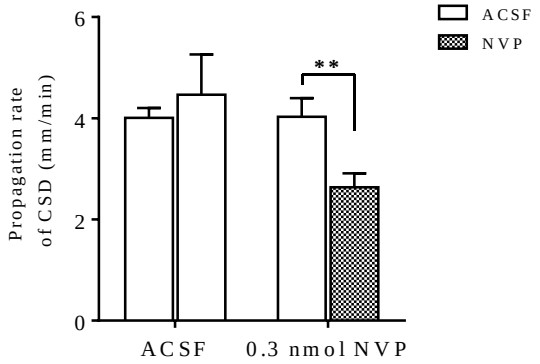

Figure 24. Effects of NVP-AAM077 perfused into the left lateral ventricle on the propagation rate of CSD. All the values shown were means ± SEM. Unpaired t-test was used for statistical analysis for significance between the drug (n = 6) and control group (n = 6) ($^{**}p < 0.05$).

3.3 Discussion

The main findings of this chapter are that NR2A-containing NMDA receptors not only contribute to CSD genesis but also CSD propagation *in vivo*, which was supported by that NR2A-containing receptor antagonists NVP-AAM077 and TCN-201 suppressed CSD genesis, while *i.c.v.* perfusion of NVP-AAM077 suppressed CSD propagation in rats and bath application of TCN-201 suppressed CSD propagation in the chick retina.

Validation of microdialysis-based CSD model under isoflurane anaesthesia

Several studies report that inhalational anaesthetics suppress CSD (Piper and Lambert, 1996, Kudo et al., 2008). In this study, I still consider isoflurane anesthesia, but not pentobarbitone, which has the least action on CSD (Kitahara et al., 2001), for studying genesis and propagation of CSD based on the following reasons: (i) the *in vivo* experiment lasted almost 7 hours, whereas barbiturates

usually only maintain anesthesia from several minutes to 4 hours (Norn et al., 2015), which don't meet our requirement; (ii) isoflurane has been widely used in other studies for studying CSD (Peeters et al., 2007, Chang et al., 2010, Unekawa et al., 2012, Shatillo et al., 2015); indeed, isoflurane provide a stable and consistent depth of anesthesia throughout the experiment and the concentration can be adjusted according to surgical and CSD recording procedures under study; whereas barbiturates generally result in uneven levels of anesthesia; (iii) under isoflurane anaesthesia, the profound inhibitory effects of MK-801 on CSD magnitude and susceptibility of the cortex to CSD (Figure 19 and Figure 20) are consistent with those reported previously (Obrenovitch and Zilkha, 1996b, Willette et al., 1994); (iv) the fact that genesis or propagation of CSD was not altered in the control group yet was suppressed by NVP-AAM077 and TCN-201, suggesting that the suppression of CSD is due to NR2A inhibition, rather than isoflurane. Collectively, the above evidence validates that the *in vivo* study under isoflurane anaesthesia is feasible and valid for assessing CSD genesis and propagation for NMDA receptor pharmacology.

NR2A-containing receptors mediate both CSD genesis and propagation

NVP-AAM077 markedly suppressed K^+-induced CSD number and increased CSD latency when perfused via microdialysis probe at 3 μM (Figure 19). The reduced cortical susceptibility to CSD under NR2A inhibition extended our previous finding on the crucial role NR2A-containing receptors in mediating CSD propagation (Wang et al., 2012). However, TCN-201 at 50 μM didn't alter the CSD number and latency, which is likely attributed to the low efficacy of TCN-201 and the limitation of its maximal solubility in DMSO.

Surprisingly, local application of NVP-AAM077 at 3 μM or TCN-201 at 50 μM through the microdialysis probe did not alter the magnitude of CSD propagation wave and propagation rate in the rats (Figure 21 and 22). That is on contrast to that are observed in chick retina, in which both NVP-AAM077 (Wang et al., 2012) and TCN-201 (Figure 17) are effective in suppressing CSD propagation rate and magnitude. I suspect that this negative result *in vivo* may be attributed to the fact that the recording site of CSD propagation waves was not exposed to chemicals

that were locally perfused at the CSD elicitation site. To clarify whether inhibition of NR2A could be effective in CSD propagation *in vivo*, contralateral ventricle perfusion of NVP-AAM077 was considered as this would allow the drug to diffuse to distant cortex following cerebrospinal fluid flow. In this study, as expected, *i.c.v.* perfusion of 0.3 nmol NVP-AAM077 markedly suppressed the magnitude (Figure 23) and propagation rate of CSD (Figure 24), confirming the mediation of NR2A to CSD propagation.

The importance of NR2A in CSD propagation is supported by the action of TCN-201 (Figure 17), which has 300-fold selectivity to NR2A compared with NR2B-containing receptors (Bettini et al., 2010). Indeed, at the medium concentration of 3 μM of the drug applied, suppressive effects on both magnitude and propagation rate of CSD propagation wave were observed in chick retina (Figure 17). As the chick retina is devoid of blood vessel, the fact that the inhibitory effect of TCN-201 on CSD propagation under this study suggests an involvement of neuronal mechanism under NR2A inhibition. Interestingly, this data on TCN-201 in chick retina is in contrast to a recent study employing BOLD fMRI approach, which shows that TCN-201 is ineffective in CSD BOLD response in rats (Shatillo et al., 2015). The discrepancy may be attributed to different methods applied for CSD recording: BOLD fMRI (Shatillo et al., 2015) that is largely based on brain-specific hemodynamic responses versus intrinsic optical signal that is based on neuronal activity of chick retina. Whether TCN-201 could alter CSD propagation *in vivo* using an electrophysiology approach where neuronal activities could be monitored remains to be further investigated. It is worthy to mention that the efficacy of TCN-201 against CSD propagation in chick retina is >30-fold lower than that of NVP-AAM077 (Wang et al., 2012). This suggests that a much higher concentration of TCN-201 may be needed for sufficient binding to its receptors in future *in vivo* studies for effectiveness of the drug on CSD. Further studies using NR2A knockout animals will help to elucidate the role of NR2A in CSD.

Elucidation of the inhibitory effects of NVP-AAM077 and TCN-201 on CSD *in vivo* suggests that such drug-alike candidates targeting NR2A may constitute a highly specific strategy with better efficacy and safety profile for treating CSD

associated migraine aura, relative to non-subtype selective NMDA receptors (Wang et al., 2012). This possibility is likely due to the following reasons: (i) NVP-AAM077 suppresses CSD in chick retina with approximately 320-fold more potency, while TCN-201 with approximately 20-fold more potency than memantine (Peeters et al., 2007), a clinically acceptable drug for treating migraines (Huang et al., 2014); (ii) partial inhibition of CSD by both NVP-AAM077 and TCN-201 in rats is also observed with the uncompetitive NMDA receptor antagonist, memantine (Peeters et al., 2007, Chen and Lipton, 2005); (iii) the rapid reversibility of NVP-AAM077 after the drug withdrawal resulting from its competitive antagonism supports a likely better safety profile; (iv) the high NR2A-preferring character of TCN-201, i.e. > 300 folds selectivity to NR2A compared with NR2B-containing receptors, supports a likely less side-effect profile.

Possible mechanism contributing to NR2A in mediating CSD

The present data suggests that activation of NR2A-containing receptors contribute to CSD genesis and propagation. There are several mechanisms which may explain the nature of CSD modulation by NVP-AAM077 and TCN-201 *in viv*o and *in vitro*. It is likely that inhibition of CSD magnitude under NR2A inhibition is attributed to their ability to desensitize neurons as NVP-AAM077 competitively blocks steady-state NR1/NR2A receptor currents from a cortical neuron (Noh et al., 2009); and TCN-201 accelerates NR1/NR2A receptor deactivation (Hansen et al., 2012). In addition, NR2A activation permitting calcium ion influx in neurons (von Engelhardt et al., 2007) may get involved in mediating CSD, which is supported, in part, by the increased calcium influx triggers CSD and accelerates CSD propagation in rats (Torrente et al., 2014). Furthermore, the role of NR2A in CSD may be associated with its interaction with PSD95. This assumption is supported by that uncoupling PSD95 from NR2A suppresses the magnitude of CSD in chick retina (unpublished from our group), which is similar with that interrupting the interaction of NMDA receptors and PSD95 suppressed the magnitude of CSD in cortex of mice (Kucharz et al., 2016). Finally, it is plausible to suppose that the contribution of NR2A to CSD may be relevant to SFKs as several tyrosine residues in the C-terminal tails of NR2A can be phosphorylated

by SFKs, e.g. Y1325 and Y1387 (Salter and Kalia, 2004).

In summary, the present data provides strong evidence on a critical role of NR2A in CSD genesis and propagation *in vivo* and also suggests that drugs preferably antagonizing NR2A-containing NMDA receptor may constitute a highly specific strategy with fewer side effects for treating CSD associated migraine aura.

Chapter 4 SFKs activation involving CSD can be regulated by NR2A

Given that SFKs can potentiate the current of NR2A-containing receptor via phosphorylating the Y1325 and Y1387 amino acids in the C-terminal sequence of NR2A (Yang and Leonard, 2001) and that SFKs can be activated by exogenous NMDA during anoxia (Weilinger et al., 2012), SFKs may also possess unidentified function during CSD. This chapter aims to explore if NR2A signaling involves SFKs in the evolution of migraine. The following question will be addressed: Do SFKs mediate CSD in rats? Does CSD induce SFKs activation? Can the CSD-induced SFKs activation be regulated by NR2A?

4.1 Objectives

4.1.1 To investigate whether CSD could activate SFKs

4.1.2 To investigate whether SFKs inhibitor could prevent CSD-induced SFKs activation

4.1.3 To investigate whether SFKs inhibitor could suppress CSD propagation.

4.1.4 To investigate whether inhibition of NR2A could suppress CSD-induced SFKs activation

4.2 Results

4.2.1 CSD induced ipsilateral cortical SFKs activation

A unique band was observed at 60 kDa after incubating PY416 SFKs or total SFKs antibody with the protein from the sham group (Figure 25 A and B). In addition, the background was clean if incubating protein with secondary antibody only for the process of PY416 SFKs detection, or for total SFKs detection after

stripping (Figure 25 C and D), suggesting the immunoreactive specificities of PY416 SFKs and total SFKs in our preparation.

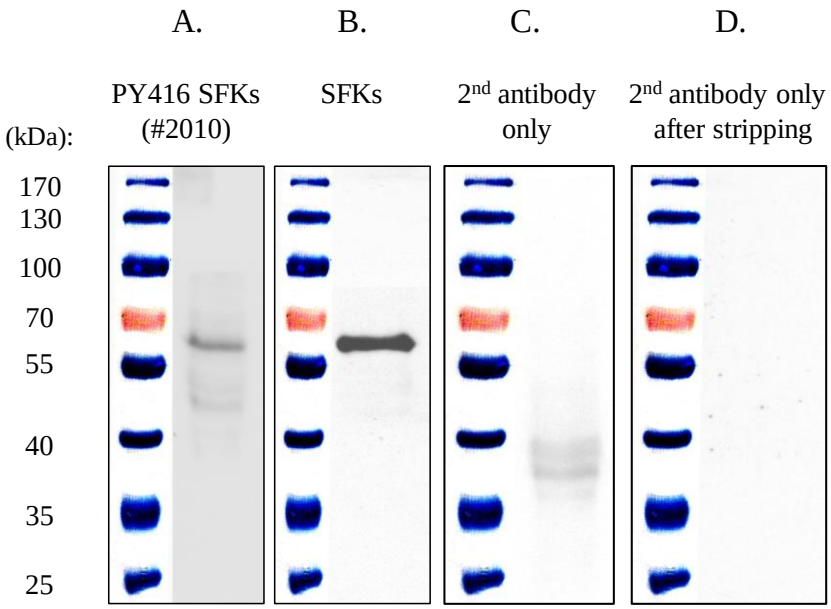

Figure 25. Control study for the specificities of PY416 SFKs and total SFKs antibodies, which indicated by the 60 kDa protein bands from the cortical tissue by western blot (A and B). There was no striking band observed in the absence of primary antibodies before (C) or after (D) stripping.

In the sham group, the relative intensity of phosphorylated SFKs at Y416 and total SFKs were 0.43 ± 0.06 and 1.59 ± 0.58 respectively (n = 3, Figure 27). In the CSD group (n = 5), the relative intensity of phosphorylated SFKs in the ipsilateral cortex was 1.60 ± 0.17, which was significantly increased when compared with that of the sham group (n = 3, $^{**}p < 0.01$, Figure 26 and 27). By contrast, the level of total SFKs was 1.82 ± 0.52, which had not different from that of sham group (n = 5, Figure 27).

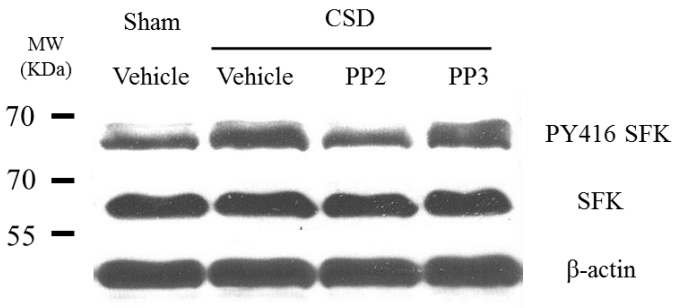

Figure 26. Representative immunoblotting of PY416 SFKs and total SFKs in the ipsilateral cortex of rats treated with ACSF, PP3 or PP2 in response to CSD. Equal loading of samples was indicated by the β-actin bands. Phospho-Y416 levels indicated activated SFKs and total SFKs levels indicated SFKs expression. Samples from the sham group set as control.

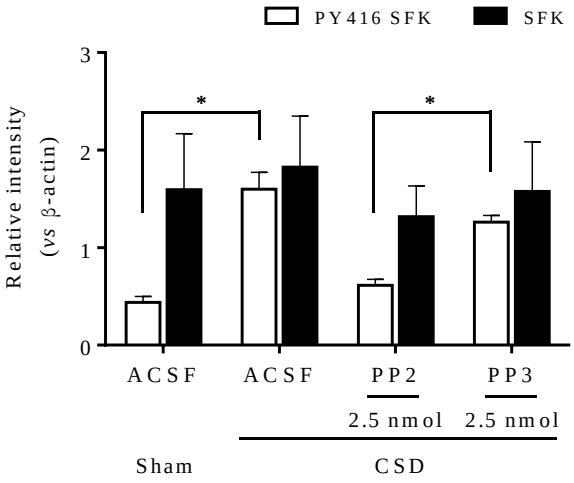

Figure 27. Quantitative analysis of relative intensity of ipsilateral cortical PY416 SFKs and total SFKs normalized to β-actin after CSD treated with ACSF or 2.5 nmol PP2 or PP3 *i.c.v.* perfused in rats. All the values were shown as means ± SEM. Mann-Whitney test was used for comparison the relative intensity of PY416 SFKs and total SFKs between two independent groups. $^{*}p < 0.05$ when compared between sham (n = 3) and CSD (n = 5) groups with two-tailed calculation, and that compared between PP2 (n = 3) and PP3 (n = 3) groups with one-tailed calculation.

4.2.2 SFKs inhibitor prevented CSD-induced SFKs activation

In the PP3 group, the level of phosphorylated SFKs in the ipsilateral cortex was 1.26 ± 0.07, which had different from that of CSD group (n = 3). Similarly, total SFKs level was not altered by 2.5 nmol PP3 (n = 3, Figure 26 and 27). In the PP2 group, the level of phosphorylated SFKs was reduced to 0.61 ± 0.06. This reduction was significantly different from that of the PP3 group (n = 3, $^{*}p < 0.05$, Figure 26 and 27). On contrary, the level of total SFKs was not altered by PP2 compared with PP3 group (n = 3, Figure 26 and 27).

4.2.3 SFKs inhibitor suppressed CSD

In the PP3 control group, high-K^{+} induced CSD was identified by a transient negative shift of DC potential in all rats (Figure 28). The CSD number (n = 5, Figure 29 A) and latency (n = 4, Figure 29 B) were 1.60 ± 0.25 and 1.37 ± 0.27 minutes in respective order. The SFKs inhibitor, PP2, at 2.5 nmol perfused into the contralateral ventricle significantly prolonged CSD latency when compared to that of PP3 group with prolonged to 3.08 ± 0.52 minutes (n = 5, $^{*}p < 0.05$, Figure 29 B). PP2 slightly reduced CSD number but this reduction did not reach significance (n = 5, Figure 29 A).

In addition, in the PP3 control group, the AUC, H, WHH, Sld and Slr of propagating CSD were 10.04 ± 0.64 mV × minute, 11.26 ± 0.98 mV, 47.55 ± 8.80 seconds, 71.49 ± 14.90 mV/minute and 25.40 ± 2.79 mV/minute respectively (n = 5, Figure 29 C-G). PP2 at 2.5 nmol significantly suppressed the AUC when compared to that of PP3 group with AUC reduced to 7.63 ± 0.43 mV × minute (n = 5, $^{*}p < 0.05$, Figure 29 C). The H, WHH, Sld and Slr were not altered by PP2 (n = 5, Figure 29 D-G).

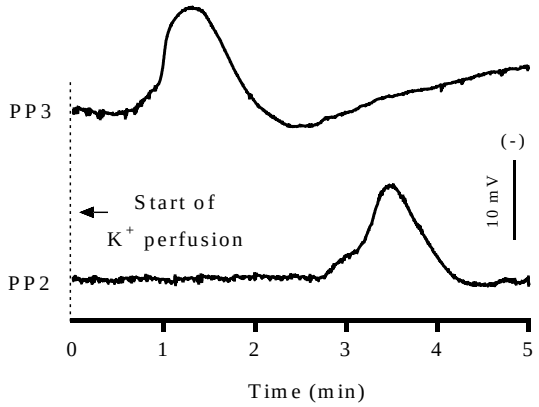

Figure 28. Representative traces in DC potential indicating CSD wave after *i.c.v.* perfusion of 2.5 nmol SFKs inhibitor PP2 or PP3 as inactive analog.

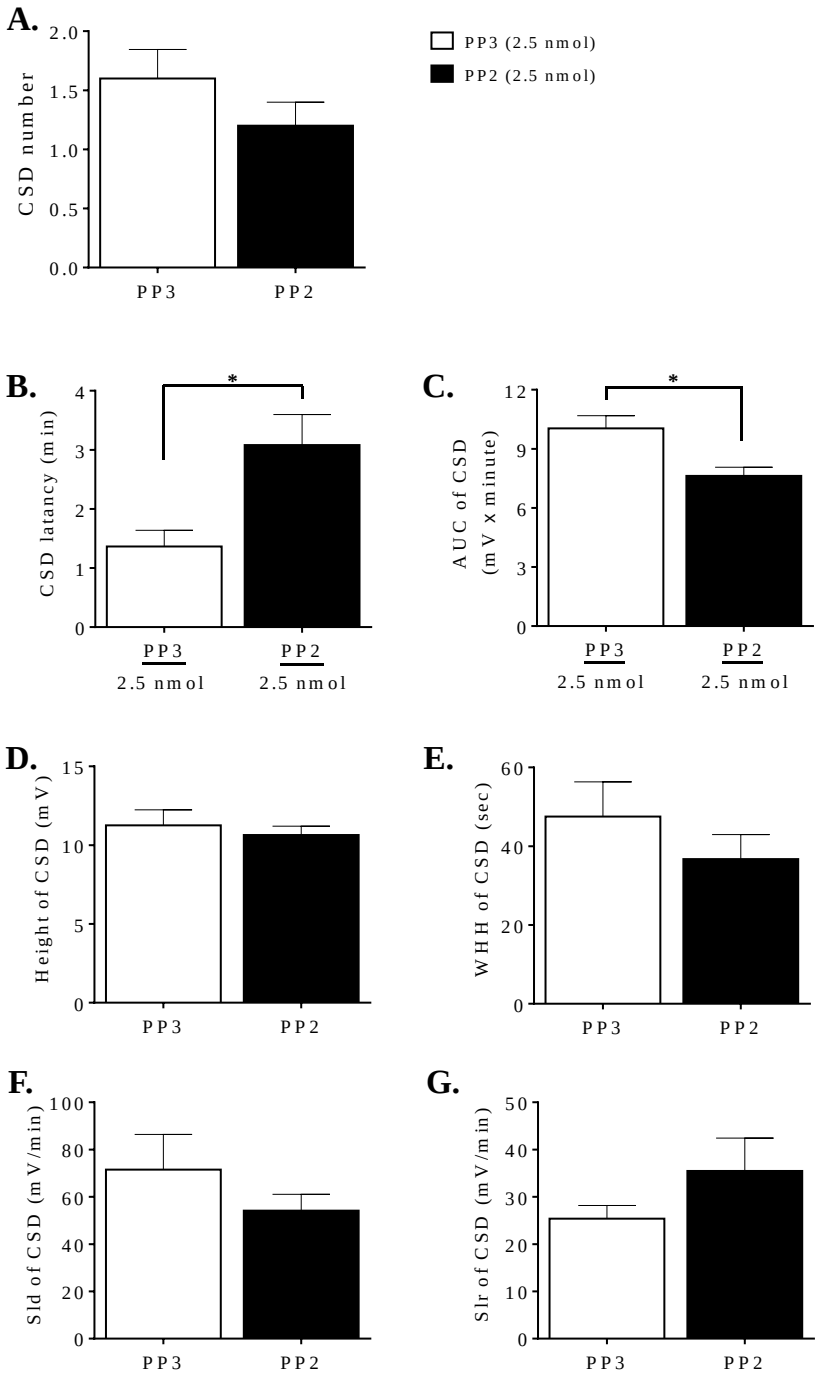

Figure 29. Effects of PP2 perfused into the left lateral ventricle on the cortical susceptibility to CSD and the magnitude of CSD propagation waves. All the values shown were means ± SEM. Unpaired t-test with two-tailed calculation was used for statistical analysis for significance between the drug (n = 5) and control (n = 5) group ($^{*}p < 0.05$).

4.2.4 NR2A antagonist suppressed CSD-induced SFKs activation

In the sham group, both PY416 SFKs and total SFKs were detected in CSD ipsilateral cortex at the size of 60 KDa (Figure 30). The relative intensity of phosphorylated SFKs and total SFKs were 0.37 ± 0.03 and 0.81 ± 0.05 respectively (n = 3, Figure 31). As described above, CSD significantly increased the level of phosphorylated SFKs to 0.69 ± 0.11 (n = 5, $^{*}p < 0.05$), whereas the total SFKs was not altered (n = 5, Figure 31).

Similar as PP2 (Figure 27), in the NVP-AAM077 group, the level of phosphorylated SFKs induced by CSD was markedly reduced to 0.35 ± 0.04 when compared with that of CSD group (n = 5, $^{*}p < 0.05$, Figure 31). However, reduction of total SFKs in the CSD ipsilateral cortex was not observed (n = 5, Figure 31).

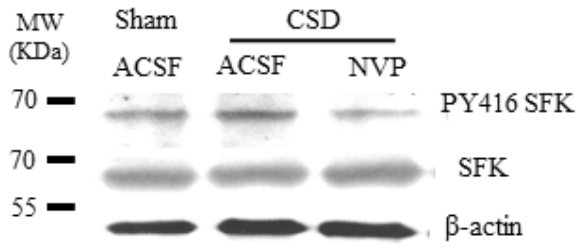

Figure 30. Representative immunoblotting of ipsilateral cortical PY416 SFKs and total SFKs in rats treated with ACSF or NVP-AAM077 (0.3 nmol) in the presence of CSD. Samples from the sham group were used as the control. Equal loading was indicated by β-actin bands. PY416 levels indicated the activated SFKs and that total SFKs level indicated SFKs expression.

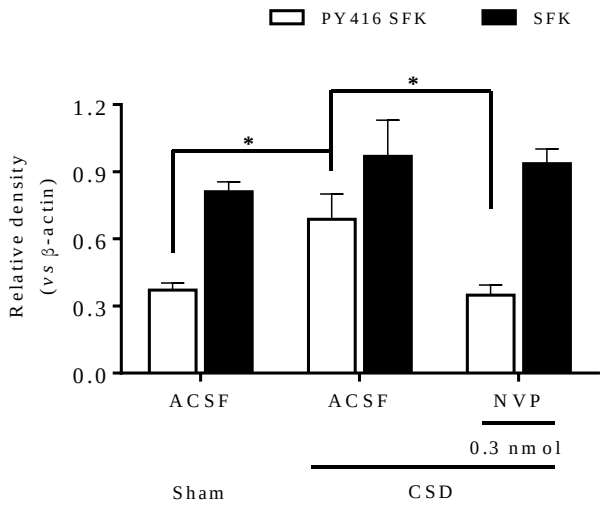

Figure 31. Quantitative analysis of relative intensity of PY416 SFKs and total SFKs normalized to β-actin after CSD treated with ACSF or NVP-AAM077 (0.3 nmol). All the values shown were means ± SEM. Mann-Whitney test with one-tailed calculation was used for statistical analysis between sham (n = 3) and CSD (n = 5) group ($^{*}p < 0.05$). Unpaired t-test with two-tailed calculation was used for statistical analysis between CSD and NVP-AAM077 (n = 5) group ($^{*}p < 0.05$).

4.3 Discussion

The key finding in this study are that SFKs activity plays an important role in mediating CSD. This is supported by that ipsilateral cortical SFKs phosphorylation at active site Y416 was elevated in response to CSD, which is prevented by the SFKs inhibitor, PP2 that is *i.c.v.* perfused into rats (Figure 26 and 27). Additionally, SFKs are found to be a key modulator of CSD propagation as inhibition of SFKs by PP2 suppresses both CSD magnitude and cortical susceptibility to CSD (Figure 29). Furthermore, both CSD-induced SFKs activation (Figure 31) and CSD propagation (Figure 23 and 24) was suppressed by NR2A antagonist NVP-AAM077.

Mechanism of SFKs-mediating CSD

Although the mechanism of action of SFKs associated with CSD is not fully

known, it is likely to involve the interaction of NR2A-containing NMDA receptors for the following reasons: (i) both SFKs inhibition (Figure 29) and NR2A inhibition (Bu et al., 2016) were found to suppress CSD propagation; (ii) CSD-induced SFKs activation can be prevented by NR2A antagonist (Figure 31); (iii) several amino acid sites of NR2A subunit can be phosphorylated by SFKs (Cheung and Gurd, 2001); (iv) Src potentiates the currents of recombinant NR1/2A receptor by reducing the affinity of NR2A for Zn^{2+} (Kohr and Seeburg, 1996), a NR2A preferring antagonist (Gielen et al., 2009, Paoletti and Neyton, 2007) that is known to reduce CSD propagation in rats (Aiba et al., 2012); (v) SFKs interacting with NMDA receptors is known to be via PSD95 in the model of chronic pain (Salter and Pitcher, 2012). Uncoupling interaction of PSD95 and NMDA receptors can suppress CSD amplitude in rats (Kucharz et al., 2016), which is in line with that interrupting the direct interaction of PSD95 and NR2A suppressed CSD magnitude in chick retina (unpublished data). The above evidences prompt a functional positive loop comprising SFKs and NR2A in mediating CSD, in which CSD-induced SFKs activation further promotes CSD propagation via NR2A.

SFKs may also mediate CSD through P2X7 receptor for the following evidences: (i) SFKs can be regulated by P2X7 receptor in glia in the CNS (Bravo et al., 2015); and (ii) anti-P2X7 receptor antibody suppresses the cortical susceptibility to CSD and the magnitude of CSD in rats (unpublished from our group), which is in line with the inhibitory effect of SFKs inhibitor on CSD.

It is necessary to discuss that migraine aura in believed to involve only a single CSD event (Smith et al., 2006) and the experimental protocol in this chapter was designed to elicit one single CSD, despite this occasionally 2 CSD waves were seen due to variation of individual rat cortex susceptibility to the 5-minutes KCl application. This finding therefore provides evidence linking CSD and SFKs activity that may contribute to migraine pathogenesis.

In summary, this data extends a previous study that synaptic Src phosphorylation was observed in the rat hippocampal slice following NMDA signaling (Weilinger et al., 2016) and adds insight into SFKs activation that is one of the most

important mechanisms for a number of neuro-pathological conditions related to inflammatory response (Okutani et al., 2006), cerebral ischemia (Zhang et al., 2007, Kumar et al., 2014) and stroke (Weilinger et al., 2012, Weilinger et al., 2016). Selectively targeting SFKs may represent a promising alternative for prophylactic treatment of migraine aura and headache.

Chapter 5 SFKs contribute to CSD-induced Panx1 channels opening

Previous study shows that anoxia causes Panx1 channels opening via activating SFKs (Weilinger et al., 2012). In addition, CSD can trigger neuronal Panx1 channels opening (Karatas et al., 2013). It suggests that SFKs may also play a role during CSD. The activation of SFKs by CSD (Chapter 4) further raises the possibility that CSD may trigger Panx1 channels opening via SFKs.

5.1 Objectives

5.1.1 *To investigate whether CSD could induce Panx1 expression in cortex of rats.*

5.1.2 *To investigate whether CSD could induce neuronal Panx1 opening in cingulate, motor and somatosensory cortices.*

5.1.3 *To investigate whether SFKs inhibition could suppress CSD-induced neuronal Panx1 opening in the discrete cortices.*

5.2 Results

5.2.1 *Panx1 protein expression was not altered by CSD.*

A unique band was observed at 45 kDa after incubating Panx1 antibody with the protein from the sham group (Figure 32), suggesting the immunoreactive specificity of Panx1 in our preparation, and that Panx1 channel expression in the cerebral hemispheres.

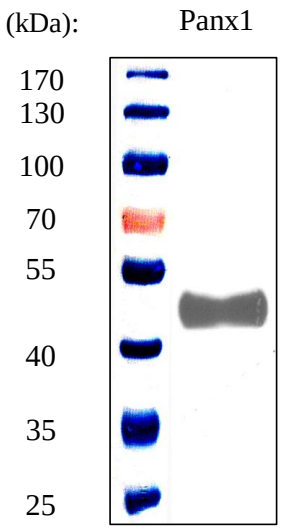

Figure 32. Control study for the specificity of Panx1 antibody. Panx1 was indicated by the 45 kDa protein band from the cortical tissue by western blot.

In the sham group, the level of Panx1 was 1.02 ± 0.08 in the ipsilateral cortex (*n* = 3). Panx1 expression level was not altered after CSD with 1.15 ± 0.19 (*n* = 3, Figure 33 and 34).

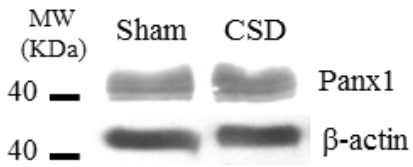

Figure 33. Representative immunoblotting of Panx1 in ipsilateral cortex with or without CSD.

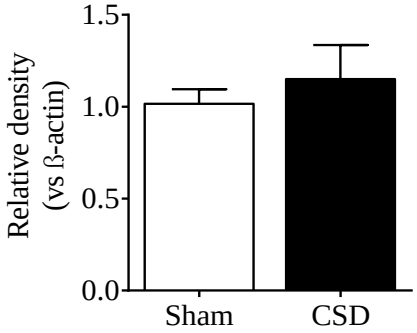

Figure 34. No change in Panx1 protein expression was detected after CSD. All the values shown were means ± SEM. Mann-Whitney test with two-tailed calculation was used for significance between sham (n = 3) and CSD (n = 3) groups.

5.2.2 *CSD triggered neuronal Panx1 opening in cingulate, motor and somatosensory cortices.*

In the formal experiment, Panx1 in layers V and VI of cortex was selected for investigating the activity of channels, based on the following reasons: (i) The number of PI-positive cells (per mm^2) was significantly increased in the V and VI layers of cortex after CSD (n = 6), compared with the sham group (n = 4, $^{*}p < 0.05$, $^{**}p < 0.01$, Figure 35 B and C); and (ii) the previous study shows a preferential distribution of Panx1 in the V and VI layers of cortex (Zoidl et al., 2007).

In addition, the distribution of PI uptake in V and VI layers of different coordinates of ipsilateral cortex also was investigated given the limited time of PI diffusion in brain in 5 minutes after CSD induction. Compared with the sham group (n = 2), CSD-induced PI staining was increased between 0.4 mm anterior and 2 mm posterior to Bregma in ipsilateral cortex. Differently, at the remote regions, i.e. 3-5 mm posterior to Bregma, the PI uptake was not altered (n = 2, Figure 35 D). Therefore, PI staining would be investigated in the V and VI layers of ipsilateral cortex at 0.4 mm anterior to Bregma in our formal experiment.

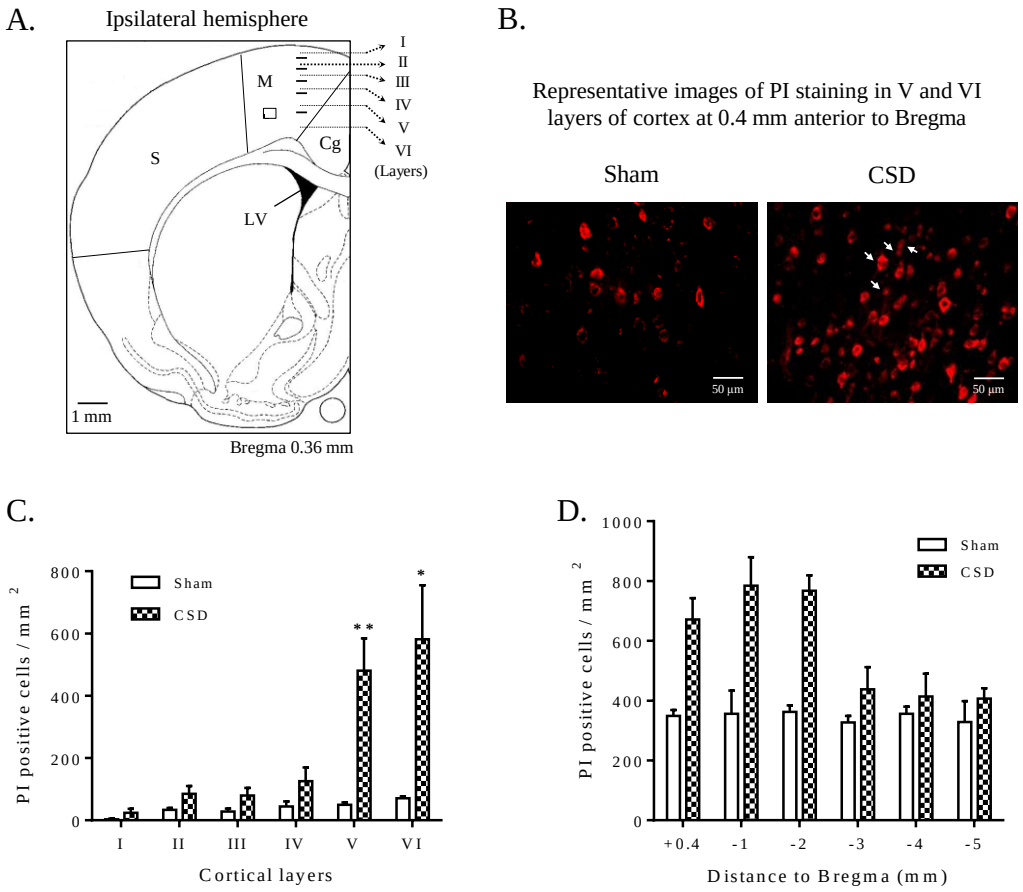

Figure 35. The distribution of CSD-induced PI staining in ipsilateral cortex of the rats. (A) Schematic representation of coronal section of unilateral hemisphere. S = somatosensory cortex, M = motor cortex, Cg = cingulate cortex, LV = lateral ventricle. I–VI indicate the different cortical layers. Dotted line in a box shows the selected field for panel (B). (B) Representative images of CSD-induced PI staining (red fluorescence) in layers V and VI of the ipsilateral motor cortices at 0.4 mm anterior to Bregma at 400× magnification. Representative PI-positive cells were indicated by arrows shown in the field indicating Panx1 channels opening. (C) Statistical analysis of CSD-induced PI staining in the layers I–VI of ipsilateral cortices at 0.4 mm anterior to Bregma. (D) Statistical analysis of CSD-induced PI staining in the layers V and VI of ipsilateral cortices between 0.4 mm anterior to 5 mm posterior to Bregma. All the values shown are means ± SEM. Unpaired t-test with one-tailed calculation was used for statistical analysis between groups ($^{*}p < 0.05$, $^{**}p < 0.01$).

NeuN was used for neurons labeling. The preliminary experiments suggest the

specific immunoreactivity of NeuN to neurons as there were striking nuclear and cytoplasmic staining in cortical cells and cerebellar granule (Figure 36 left and middle columns), but not in cerebellar Purkinje cells (Figure 36 middle column) in the presence of NeuN antibody. It is similar with the previous study (Wolf et al., 1996). In addition, no cell staining was observed under primary antibody omission condition in cortex as negative control (Figure 36 right column).

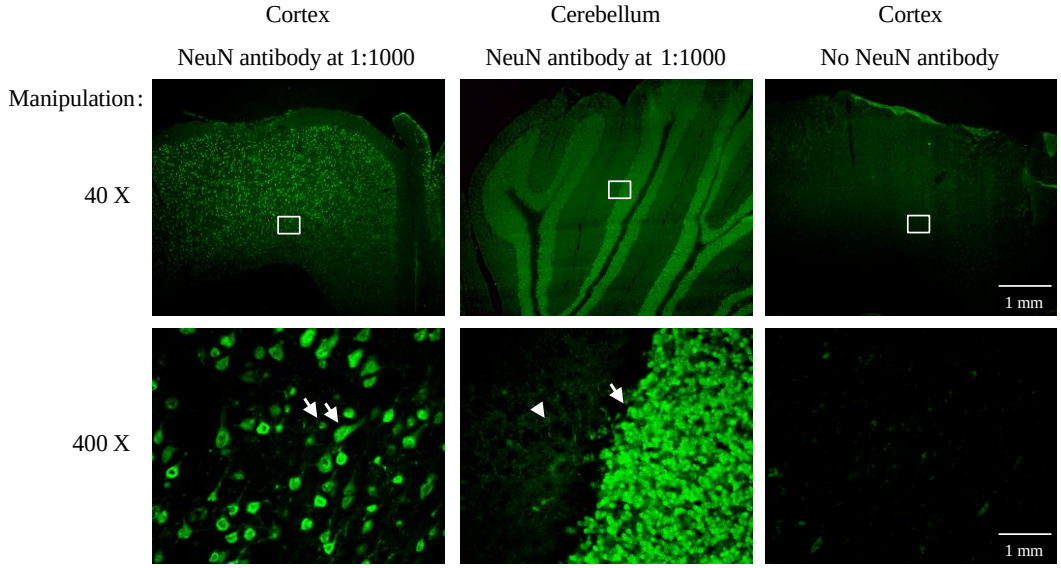

Figure 36. Coronal section with or without NeuN antibody at 1:1000 for testing the specificity of immunoreactivity. There are striking nuclear and cytoplasmic immuno-staining of neurons (arrow) in cortex and granule cells in cerebellum but not Purkinje cells (arrow head) in cerebellum in the presence of NeuN antibody. Granule cells and Purkinje cells in cerebellum were carried out as immuno-postive and –negative control for NeuN staining respectively. No cell staining was observed under primary antibody omission condition in cortex. The 400 × field comes from the area where is selected by white box from the 40 × field.

In the sham group, the average number of PI positive cells in cingulate, motor and somatosensory cortices was 424.3 ± 100.30 per mm^2 (n = 6), 210.0 ± 58.99 per mm^2 (n = 6) and 129.2 ± 26.39 per mm^2 (n = 4, Figure 37 and 38). The PI positive cells content in motor and somatosensory cortices was similar; whereas the cingulate had higher number in the sham group with 2-3 folds compared with that

of motor and somatosensory cortices respectively (Figure 38). Following CSD, the number of PI positive cells was significantly increased to 787.6 ± 46.81 per mm^2 (n = 6, $^{**}p < 0.01$), 660.9 ± 43.92 per mm^2 (n = 5, $^{***}p < 0.001$) and 569.3 ± 41.21 per mm^2 (n = 6, $^{***}p < 0.001$) in the ipsilateral cingulate, motor and somatosensory cortices compared to the sham group (Figure 38).

In the sham group, the number of NeuN positive cells in ipsilateral cingulate, motor and somatosensory cortices were 1118 ± 48.65 per mm^2, 847.60 ± 88.60 per mm^2, 877.7 ± 102.1 per mm^2 in respective order (Figure 37 and 39). There was no significant different in NeuN positive cells content after CSD or PP3, PP2 administration in these cortical regions (Figure 37 and 39).

Similar with PI positive cells, the number of PI/NeuN double staining cells were significantly increased by CSD in ipsilateral cingulate (600.9 ± 42.49 per mm^2, n = 6, $^{**}p < 0.01$), motor (667.3 ± 37.91 per mm^2, n = 5, $^{***}p < 0.001$) and somatosensory cortices (544.6 ± 25.20 per mm^2, n = 6, $^{***}p < 0.001$) compared to that in sham group with 319.0 ± 67.43 per mm^2 (n = 6), 90.05 ± 16.36 per mm^2 (n = 6) and 72.22 ± 18.56 per mm^2 (n = 4, Figure 40).

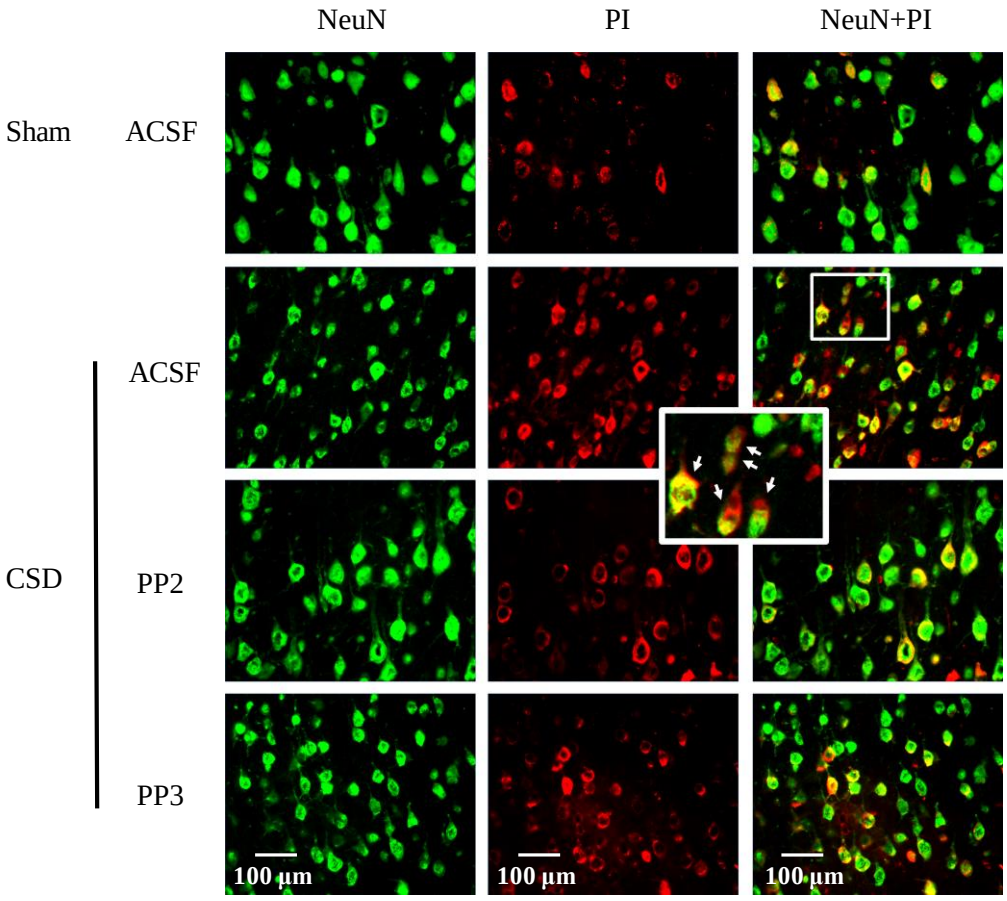

Figure 37. Representative images of CSD-induced PI staining (labeled in red) of NeuN positive cells (labeled in green) in cortical layers V and VI of ipsilateral motor cortex treated with ACSF or 2.5 nmol PP3 or 2.5 nmol PP2 in 1/20 mm^2. PI positive neurons (labeled in yellow) were indicated by arrows shown in the insert indicating neuronal Panx1 channel opening.

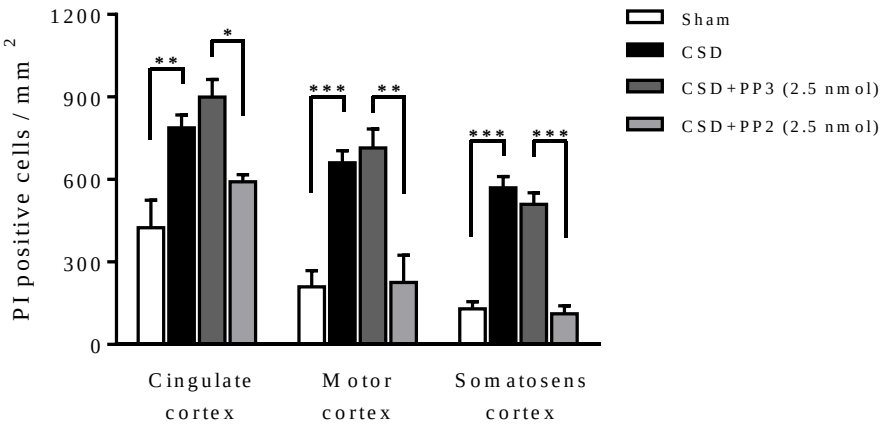

Figure 38. Effects of PP2 (2.5 nmol) on PI positive cells in cingulate, motor and somatosensory cortices in the presence of CSD. All the values shown were means ± SEM. $^{**}p < 0.01$, $^{***}p < 0.001$, unpaired t-test with two-tailed calculation was used for comparing PI staining between sham ($n = 6$) and CSD ($n = 6$) groups. $^{*}p < 0.05$, $^{**}p < 0.01$, $^{***}p < 0.001$, Mann-Whitney test with one-tailed calculation was used for statistical analysis for CSD vs PP3 ($n = 3$) groups, and PP3 vs PP2 ($n = 3$) groups.

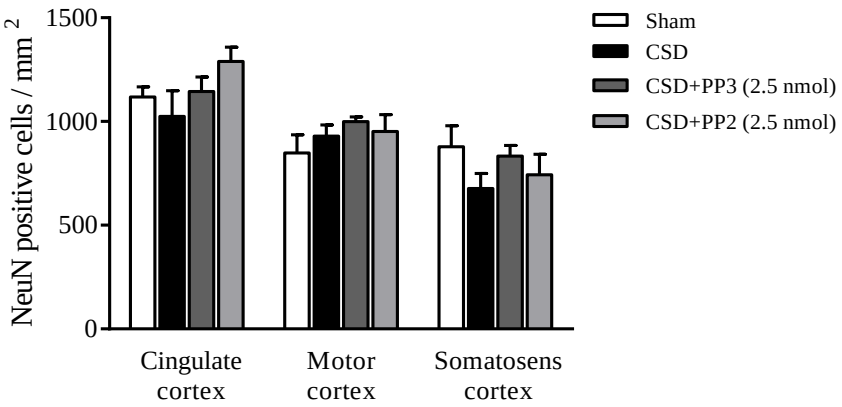

Figure 39. Effects of PP2 (2.5 nmol) on NeuN positive cells in cingulate, motor and somatosensory cortices in the presence of CSD. All the values shown were means ± SEM. Unpaired t-test with two-tailed calculation was used for comparing NeuN staining between sham ($n = 6$) and CSD ($n = 6$) groups. Mann-Whitney test with two-tailed calculation was used for significance between CSD ($n = 6$) and PP3 ($n = 3$), and that between PP3 and PP2 ($n = 3$).

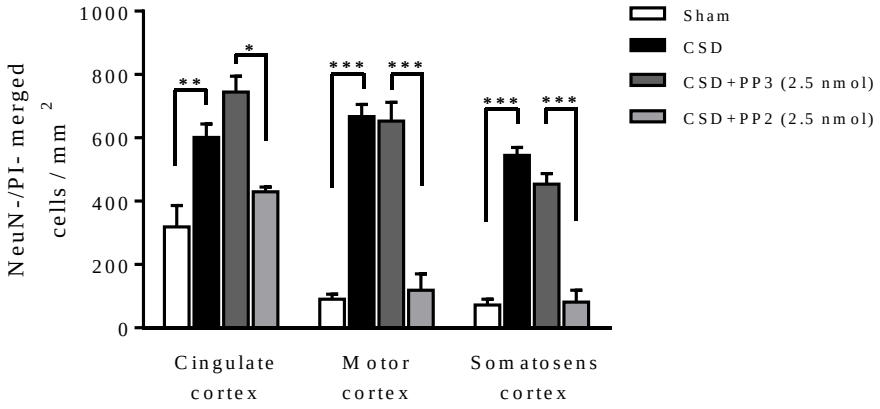

Figure 40. Effects of PP2 (2.5 nmol) on PI positive neurons in cingulate, motor and somatosensory cortices in the presence of CSD. All the values shown were means ± SEM. $^{**}p < 0.01$, $^{***}p < 0.001$, unpaired t-test with two-tailed calculation was used for comparing neuronal PI staining between sham (n = 6) and CSD (n = 6) groups. $^{*}p < 0.05$, $^{***}p < 0.001$, Mann-Whitney test with one-tailed calculation was used for statistical analysis for CSD vs PP3 (n = 3) groups, and PP3 vs PP2 (n = 3) groups.

5.2.3 SFKs inhibitor suppressed CSD-induced neuronal Panx1 channels opening in cingulate, motor and somatosensory cortices.

In the PP3 group, the number of PI positive cells was similar with that in CSD group in ipsilateral cingulate, motor and somatosensory cortices (Figure 38), indicating PP3 has no effect on CSD-induced Panx1 channels opening. Interestingly, CSD-induced PI staining was significantly reduced to 591.8 ± 25.35 (n = 3, $^{*}p < 0.05$), 225.9 ± 98.19 per mm^2 (n = 3, $^{**}p < 0.01$) and 111.1 ± 29.39 per mm^2 (n = 3, $^{***}p < 0.001$) by 2.5 nmol PP2 in cingulate, motor and somatosensory cortices in respective order when compared with that of PP3 group with 899.9 ± 63.17 per mm^2 (n = 3), 714.7 ± 68.59 per mm^2 (n = 3) and 509.2 ± 41.86 per mm^2 (n = 3, Figure 38).

Similar with PI positive cells, the number of PI/NeuN double staining cells were not altered by 2.5 nmol PP3 compared to CSD group in these cortical regions (Figure 40). However, 2.5 nmol PP2 significantly reduced CSD-induced number

of PI positive neurons to 424 ± 12.96 per mm^2 (n = 3, $^{*}p < 0.05$), 118.5 ± 51.85 per mm^2 (n = 3, $^{***}p < 0.001$) and 81.47 ± 37.58 per mm^2 (n = 3, $^{***}p < 0.001$) in ipsilateral cingulate, motor and somatosensory cortices when compared with that of PP3 group with 744.37 ± 50.10 per mm^2 (n = 3), 652.5 ± 59.69 per mm^2 (n = 3) and 453.7 ± 33.38 per mm^2 (n = 3) in respective order (Figure 40).

5.3 Discussion

The present results demonstrate that CSD-induced SFKs activation contributes to neuronal Panx1 channels opening in cortex. This is supported by that SFKs inhibitor suppressed single CSD-induced neuronal PI uptake in the ipsilateral cingulate, motor and somatosensory cortices; meanwhile the total Panx1 expression was not altered.

CSD-induced Panx1 channel opening in discrete cortical regions

The distribution of single CSD-activated Panx1 channels in the ipsilateral cingulate, motor and somatosensory cortices, extends the early study showing that CSD-induced Panx1 channels opening in cortex (Karatas et al., 2013). The fact of the levels of activated Panx1 are increased in multiple cortical regions (Figure 38 and 40) indicates that the elevation is attributed to CSD rather than mechanical stimulation by surgery that is known one of the underlying causes of Panx1 activation (Bravo et al., 2015). Interestingly, Panx1 channels are activated by CSD in the cingulate cortex is not supported by the previous observation that the depolarization of CSD waves is less efficient in the middle cortical regions (e.g. cingulate cortex), compared with the lateral regions (Eiselt et al., 2004). It is likely that the degree of Panx1 channels opening is not correlated to the magnitude of CSD. Given that PI uptake is not sensitive to CSD in the regions away from PI perfusion site in my result (Figure 35 D), whether Panx1 is also activated by CSD in those cortical regions still needs further investigation.

It is necessary to mention that both single and multiple CSD can trigger PI uptake in cortical NeuN (immuno-react with neurons) but not in ALDH1L1 (immuno-react with astrocyte) positive cells in isoflurane anaesthetic mice

(Karatas et al., 2013), which supports our study that the CSD-induced Panx1 activation is of neuron original in discrete cortices to some extent.

The mediation of SFKs to CSD-induced Panx1 channels opening

A key finding in this study is that CSD triggers neuron al Panx1 opening via SFKs. I speculate CSD could couple SFKs to Panx1 for channel opening for the following reasons: (i) SFKs contributes to CSD-induced neuronal Panx1 channels opening in the discrete cortices; (ii) both Panx1 channels and SFKs are expressed in postsynaptic region (Thomas and Brugge, 1997, Bravo et al., 2015) and have a physical interaction in hippocampus (Weilinger et al., 2016); (iii) a putative phosphorylation site at Y308 of Panx1 matched consensus sequence for SFKs function to anoxia-induced Panx1 channels opening (Weilinger et al., 2012). These evidences prompt us that CSD may also recruit SFKs to activate Panx1 channels by a physical interaction.

It needs to mention that the SFKs inhibitor PP2 can't discriminate the different members of SFKs (Hanke et al., 1996, Liu et al., 1999). Because the commercial antibodies or inhibitors of different members of SFKs are unavailable, I didn't investigate the involvement of subtypes of SFKs in Panx1 channels opening induced by CSD. Further investigation is required in the future.

In conclusion, I identified a mechanism through which SFKs activation induced by CSD leads to the opening of Panx1 channels. Given the important role of Panx1 in CSD-induced headache-like behavior (Karatas et al., 2013), this work that links SFKs and Panx1 channels may represent a new insight into migraine pathology.

Chapter 6 NR2A contributes to CSD-induced Panx1 channels opening and the interaction of SFKs and to Panx1

The above research demonstrates that (i) NR2A-containing receptors contribute to CSD-induced SFKs activation and (ii) CSD triggers Panx1 channels opening via SFKs in the ipsilateral cortex. In this study, I aim to investigate whether NR2A could contribute to CSD-induced Panx1 channels opening. In addition, given that NMDA receptor/SFKs/Panx1 complex functions during anoxia (Weilinger et al., 2016), it is reasonable to propose that NR2A may also regulate CSD-induced Panx1 channels opening via coupling SFKs to Panx1.

6.1 Objectives

6.1.1 *To investigate whether NR2A inhibitor could suppress CSD-induced neuronal Panx1 channels opening in discrete cortices.*

6.1.2 *To investigate whether CSD could induce the interaction of SFKs and Panx1.*

6.1.3 *To investigate whether NR2A inhibitor could suppress CSD-induced interaction of SFKs and Panx1.*

6.2 Results

6.2.1 *NR2A antagonist suppressed CSD-induced neuronal Panx1 channels opening in cingulate, motor and somatosensory cortices.*

In the CSD group, the number of NeuN positive cells in ipsilateral cingulate, motor and somatosensory cortices were 1024 ± 124.2 per mm^2, 929.4 ± 54.4 per mm^2 and 677.7 ± 72.49 per mm^2 in respective order (Figure 41 and 42). There was no significant different in NeuN positive cells content after 0.3 nmol

NVP-AAM077 administration in these cortical regions (Figure 42).

As described above (Figure 38), the number of PI positive cells were 787.6 ± 46.81 per mm^2 (n = 6), 660.9 ± 43.92 per mm^2 (n = 5) and 569.3 ± 41.21 per mm^2 (n = 6) in the ipsilateral cingulate, motor and somatosensory cortices of CSD group in respective order (Figure 43). 0.3 nmol NVP-AAM077 significantly prevented the CSD-induced PI staining in motor and somatosensory cortices. In the NVP-AAM077 group, the level of CSD-induced PI positive cells reduced to 308.1 ± 57.86 per mm^2 (n = 5, $^{**}p < 0.01$) and 294.6 ± 22.96 per mm^2 (n = 4, $^{**}p < 0.01$) in respective order (Figure 43). However, the content of PI staining in cingulate cortex was not altered by NVP-AAM077 (n = 4, Figure 43).

Similarly, reduction of number of PI/NeuN double staining cells was also observed in ipsilateral motor and somatosensory cortex with *i.c.v.* administration of 0.3 nmol NVP-AAM077 (Figure 44). In NVP-AAM077 group, these value were 228.8 ± 72.66 per mm^2 (n = 5) and 355.2 ± 72.76 per mm^2 (n = 5), which is significantly different from that of the CSD group with 667.3 ± 37.91 per mm^2 (n = 5, $^{***}p < 0.001$) and 544.6 ± 25.20 per mm^2 (n = 6, $^{**}p < 0.01$, Figure 44). By contrast, the level of CSD-induced PI positive neurons in cingulate cortex (n = 6) was not altered by NVP-AAM077 (n = 4, Figure 44).

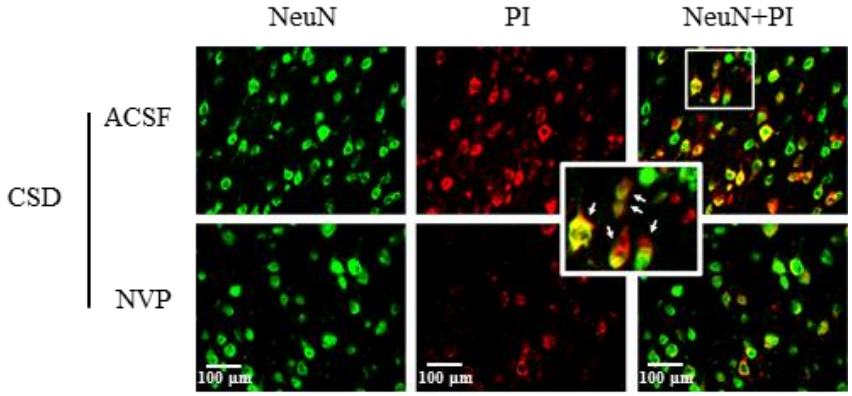

Figure 41. Representative images of CSD-induced PI staining (labeled in red) on NeuN positive cells (labeled in green) in layers V and VI of motor cortex of rats treated with ACSF or NVP-AAM077 (0.3 nmol) in 1/20 mm^2. PI-/NeuN double

staining (labeled in yellow) was pointed by arrows in the insert.

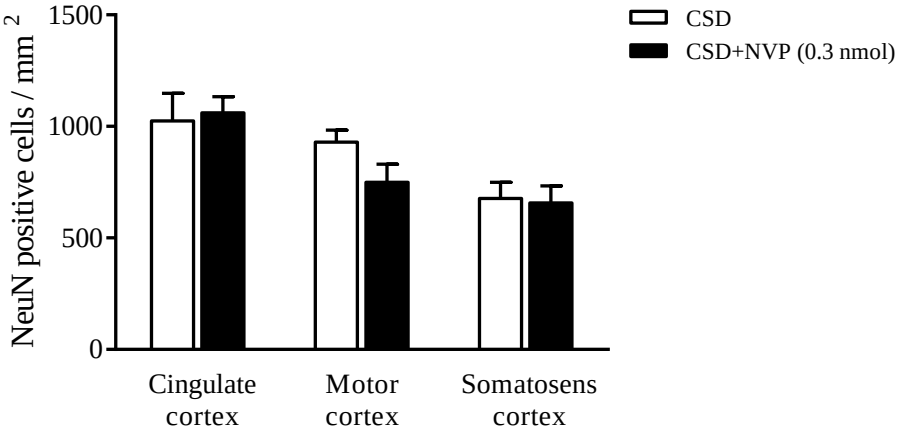

Figure 42. Effect of NVP-AAM077 (0.3 nmol) on NeuN staining in the presence of CSD in cingulate, motor and somatosensory cortices. All values shown were means ± SEM. Unpaired t-test with two-tailed calculation was used for statistical analysis for significance between CSD (n = 6) and NVP-AAM077 (n = 6) groups.

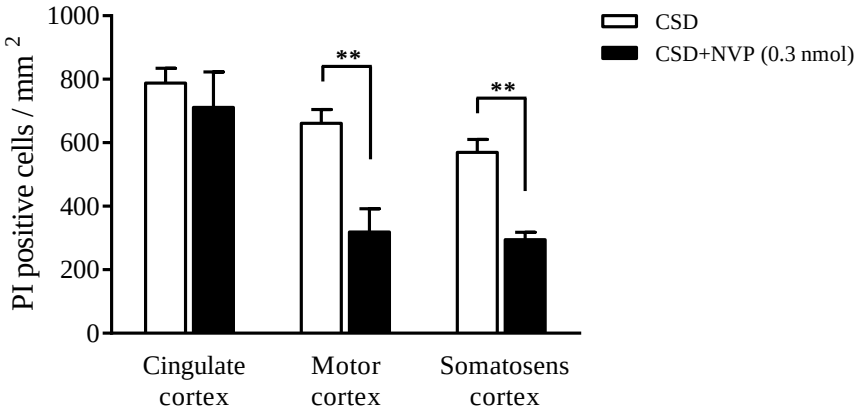

Figure 43. Effect of NVP-AAM077 (0.3 nmol) on PI staining in the presence of CSD in cingulate, motor and somatosensory cortices. All values shown were means ± SEM. Unpaired t-test with two-tailed calculation was used for statistical analysis for significance between CSD (n = 6) and NVP-AAM077 (n = 5) groups ($^{**}p < 0.01$).

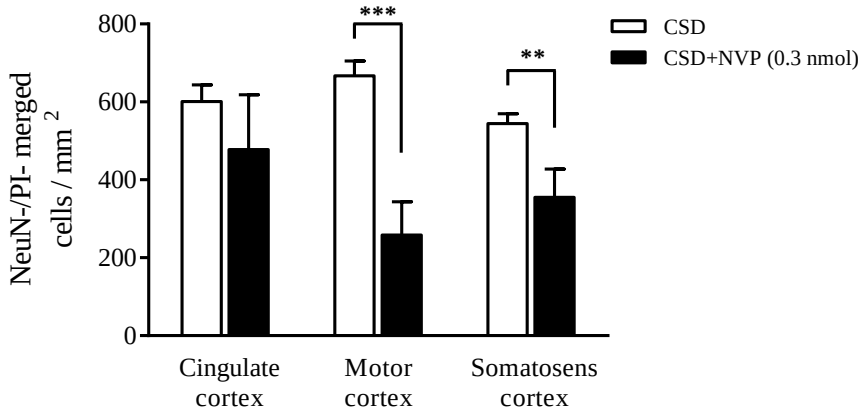

Figure 44. Effect of NVP-AAM077 (0.3 nmol) on NeuN staining in the presence of CSD in cingulate, motor and somatosensory cortices of rats. All values shown were means ± SEM. Unpaired t-test with two-tailed calculation was used for statistical analysis for significance between CSD (n = 6) and NVP-AAM077 (n = 5) groups ($^{**}p < 0.01$, $^{***}p < 0.001$).

6.2.2 CSD promoted ipsilateral cortical SFKs and Panx1 interaction

A unique band was observed at 60 kDa after incubating PY416 SFKs antibody with the protein from the sham group (Figure 45), indicating the immunoreactive specificity of PY416 SFKs in our preparation. In addition, there was no band observed if incubating the control agarose resin with Panx1 antibody complex in the process of IP'd purification, suggesting that PY416 SFKs are specifically purified from Panx1 complex in our preparation.

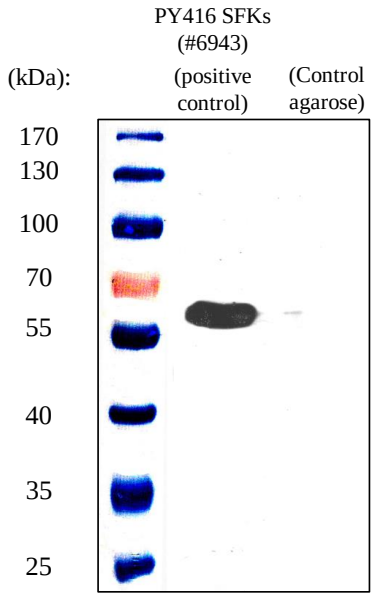

Figure 45. Control study for the immunoreactive specificity of PY416 SFKs for co-IP. PY416 SFKs was indicated by the 60 kDa protein bands from the ipsilateral cortex by western blot.

Immunoprecipitation followed by western blot study showed that intensive bands at the size of 60 kDa were detected in all 3 groups (Figure 46), indicating that PY416 SFKs are present in the Panx1 complex of the cerebral hemisphere. Similarly, total Panx1 was also observed (Figure 46) with the same molecular weight (45 kDa) as that described before when samples were not immune-precipitated with the Panx1 antibody (Figure 33).

In the sham group, the relative intensity of PY416 SFKs in Panx1 complex was 0.55 ± 0.13 (n = 3, Figure 47). In the CSD group, marked increase in the intensity was observed and the level of PY416 SFKs protein was 1.74 ± 0.13, which is significantly different from that of the sham group (n = 4, $^{*}p < 0.05$, Figure 47), indicating CSD promotes the interaction between phosphorylated SFKs and Panx1 protein in the ipsilateral cortex.

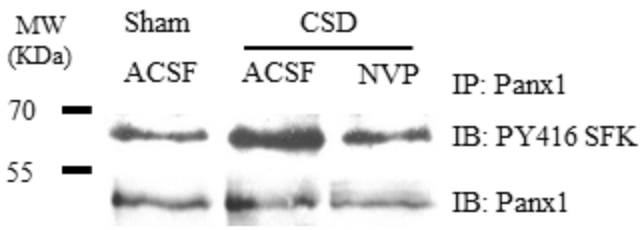

Figure 46. Co-immunoprecipitation assays from ipsilateral cortex of rats treated with ACSF or NVP-AAM077 (0.3 nmol) after CSD induction. Panx1 was immunoprecipitated and pulldown of Panx1 and PY416 SFKs was assessed by immunoblotting. Equal loading was indicated by total Panx1 immunoblotting.

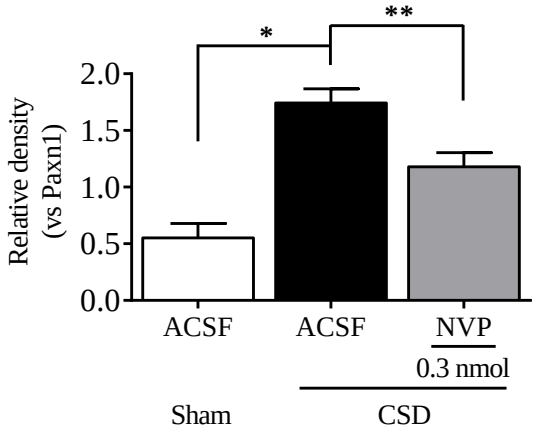

Figure 47. Quantitative analysis of relative intensity of IP'ed PY416 SFKs normalized to total Panx1 in ipsilateral cortex of rats treated with ACSF or NVP-AAM077 (0.3 nmol) after CSD. All the values shown were means ± SEM. Mann-Whitney test with two-tailed calculation was used for statistical analysis between sham (n = 3) and CSD (n = 4) groups ($^{*}p < 0.05$). Unpaired t-test with two-tailed calculation was used for statistical analysis between CSD and NVP-AAM077 (n = 4) groups ($^{**}p < 0.01$).

6.2.3 NR2A antagonist suppressed CSD-induced cortical Src and Panx1 interaction

No change in CSD-induced total Panx1 expression was observed under NVP-AAM077 application (Figure 46). Similar to the SFKs inhibitor, *i.c.v.*

perfusion of 0.3 nmol NVP-AAM077 resulted in a reduction of phosphorylated SFKs at Y416 amino acid in the Panx1 complex from the ipsilateral cortex with the relative density of 1.18 ± 0.13 and this was significantly different from that of CSD group ($n = 4$, $^{**}p < 0.01$, Figure 47).

6.3 Discussion

This study, for the first time, demonstrated that CSD-induced SFKs coupling to neuronal Panx1 channels in the ipsilateral cortex of rats. The interaction of SFKs and Panx1 was attenuated by inhibition of NR2A. Corresponds to this, the CSD-induced Panx1 channels opening was also reduced by NR2A inhibition. These results provide strong evidence to support that CSD-induced interaction of activated SFKs and Panx1 contributes to Panx1 channels opening, which can be regulated by NR2A-containing NMDA receptor.

CSD triggers Panx1 opening via coupling to SFKs

A key finding in this study is that CSD promotes the interaction of activated SFKs and Panx1 in cortex. SFKs are known to directly interact with the putative Y308 site on the intracellular C-terminus of Panx1 channels in hippocampus (Weilinger et al., 2012, Weilinger et al., 2016, Thompson, 2015) and that CSD is reported to promote Panx1 channels activity in cortex (Karatas et al., 2013). I therefore propose that activated SFKs may functional link to Panx1 channels during CSD. This study shows that there is a physical link of the activation state of SFKs and Panx1 in the rat ipsilateral cortical protein complex where Panx1 is immunoprecipitated with agarose resin. More importantly, the coupling of activated SFKs to Panx1 channel is largely promoted by CSD, suggesting a functionally link between SFKs and Panx1 during CSD. That CSD-induced neuronal Panx1 opening is prevented by the SFKs inhibitor (Chapter 5) further emphasizes the importance of the functional link between SFKs coupling to Panx1 activity during CSD and highlights that the interaction is of neuronal origin. These results are consistent with a model in which SFKs are involved in migraine pathogenesis in part the initiation of CSD-induced inflammatory response induced by CSD via neuronal Panx1 channels (Karatas et al., 2013).

Mechanism underlying CSD-induced SFKs coupling to Panx1

As expected, inhibition of NR2A not only prevented CSD-induced SFKs phosphorylation (Figure 31), but also attenuated SFKs coupling to Panx1 (Figure 47) and Panx1 channels opening (Figure 44). These evidences identified a link between NR2A and Panx1 during CSD, in which the CSD-activated SFKs coupling to Panx1 channels is regulated by NR2A-containing NMDA receptor.

The CSD-induced Panx1 opening is not altered by NR2A inhibition in cingulate cortex (Figure 43 and d), although SFKs inhibition prevents CSD-induced Panx1 opening in this region (Figure 38 and 40). It is assumed that NR2B rather than NR2A subunit may function to Panx1 activation via SFKs in cingulate cortex based on three considerations: (i) pan-NMDA receptor antagonist prevents CSD-induced Panx1 channels opening (Karatas et al., 2013); (ii) NR2B contributes to cortex susceptibility to CSD in rats (Menniti et al., 2000) and (iii) NR2A/B have synergistic effect on CSD as co-application of NR2A and NR2B antagonists have stronger inhibitory effect on CSD than individual used alone *in vitro* (Jia et al., 2015). However, given in the absence of direct evidence for the action of NR2B in the SFKs-Panx1 signaling in response to CSD, further investigation will be required in the future.

It is relevant to consider that a region of activated Panx1 channels remains even when SFKs or NR2A activity was inhibited in motor and somatosensory cortices (Figure 38 and 40, Figure 43 and 44). This may be attributed to the extracellular high K^+ with the following evidences: (i) Panx1 channels can be activated at resting potential when the concentration of extracellular K^+ at near 100 mM (Silverman et al., 2009); (ii) during CSD attack, the concentration of extracellular K^+ rapidly rises and reach levels as high as near 80 mM (Smith et al., 2006). Alternatively, the remained activated Panx1 is probably attributed to the cleavage of the C-terminal of Panx1 channels as breaking the C-terminus of Panx1 by proteolytic action of caspases can open the channel pore (Chekeni et al., 2010). The above considerations imply the variability and complexity of the modulation of Panx1 during CSD.

In summary, this work reveals a previously unknown migraine mechanism

involving SFKs. It concludes that NR2A regulates CSD-induced SFKs coupling to neuronal Panx1 in the cortex of rat (Figure 48), which extends the previous study that CSD triggered Panx1 channels opening and subsequently inflammatory response and the trigeminovascular mechanism of migraine in the animal model (Karatas et al., 2013). Targeting the elements of NR2A/SFKs/Panx1 signaling pathway might constitute an effective strategy preventing migraine and other neurological diseases associated with CSD.

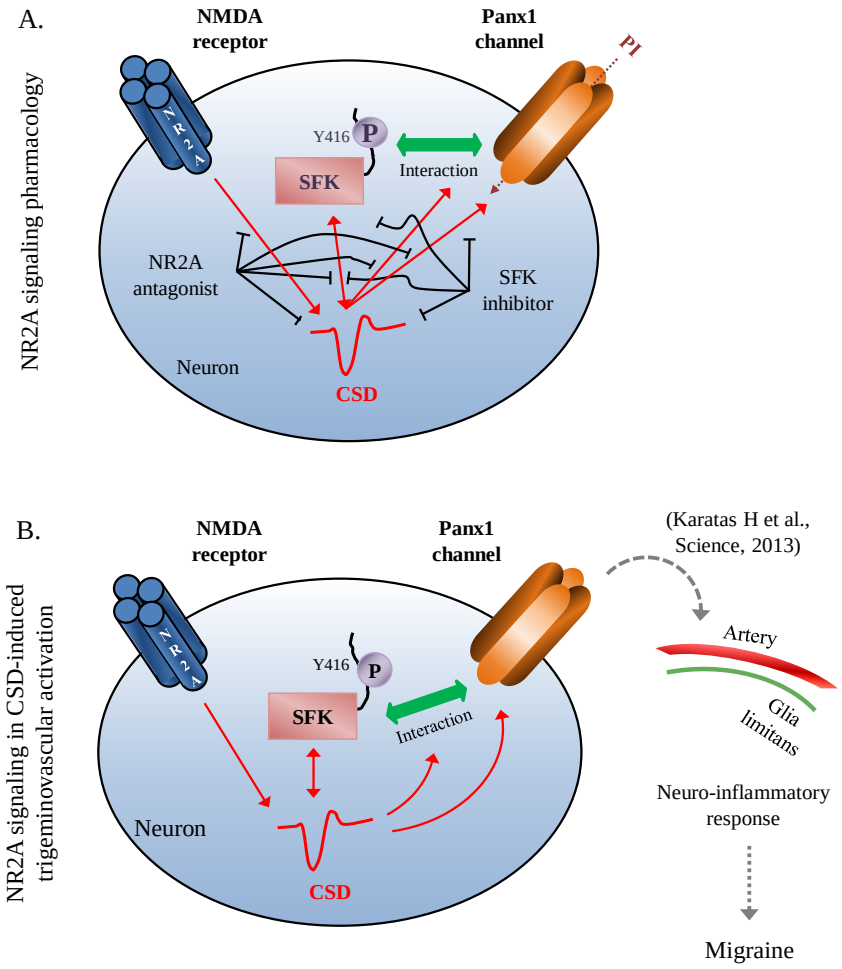

Figure 48. Schematic depiction of NR2A signaling regulates CSD-induced rapid SFKs activation coupling to neuronal Panx1 channels in cortex of rats. (A) The pharmacological inhibition of NR2A signaling in our investigation. (B) The demonstrated signaling pathway in the study may trigger subsequent inflammatory response in the meninges leading to migraine headache. Red arrows-bars indicate the steps that CSD triggered. Black T-bars indicate the

inhibitory effect by inhibitors. Dotted lines indicate the cascades referring to other study. Abbreviations: NMDA, N-methyl-D-aspartic acid; SFK, sarcoma family kinase; CSD, cortical spreading depression; Panx1, pannexin1.

Chapter 7 NR2A contributes to CSD-induced CGRP gene expression

CGRP mRNA is significantly increased in motor, somatosensory and visual cortices of the ipsilateral hemisphere of rats 24 hours after multiple, but not single CSD (Wang et al., 2016b). In addition, the increase of CGRP gene expression in trigeminal ganglion, medulla pons and cervical spinal cord can be prevented by NMDA antagonist in nitroglycerin-induced migraine model of rats (Greco et al., 2016). Furthermore, my data showed the critical role of NR2A-containing receptor in mediating CSD. In the light of the above findings, it is plausible to propose that NR2A could regulate CSD-induced CGRP gene expression in ipsilateral discrete cortices 24 hours after multiple CSD.

7.1 Objectives

7.1.1 To investigate whether NR2A inhibition could suppress multiple CSD.

7.1.2 To investigate whether the elevation of CGRP mRNA in motor, somatosensory and visual cortices 24 hours after CSD could be prevented by NR2A inhibition.

7.2 Results

7.2.1 Multiple CSD was suppressed by NR2A inhibition

In the sham group, ACSF administration was insufficient to elicit CSD in all sham rats (n = 3). In the CSD group, 1 μl of topical 3 M KCl onto the dura resulted in the first CSD wave that began ~2 – 3 minutes after administration. The number and magnitude of CSD in the 1st 5 minutes-K^+ application was 2.0 ± 0.41 (n = 4, Figure 49 A) and 5.04 ± 0.41 mV × minutes (n = 4, Figure 49 B) in respective order. There was no significant difference in the number or magnitude of CSD

episodes over the 5 high-K^+ applications, indicating CSD was not altered throughout experiment under isoflurane anesthesia. When summed up, the accumulative number and magnitude of CSD for each rat were 8.50 ± 1.32 (n = 4, Figure 50 A) and 72.35 ± 15.07 mV × minutes (n = 4, Figure 50 B) in the CSD group. 0.3 nmol NVP-AAM077 significantly suppressed the CSD magnitude to 42.56 ± 0.62 mV × minutes (n = 4, $^{*}p < 0.05$, Figure 50 B), whereas CSD number (6.40 ± 0.51, n = 5, Figure 50 A) was not altered compared to the CSD group.

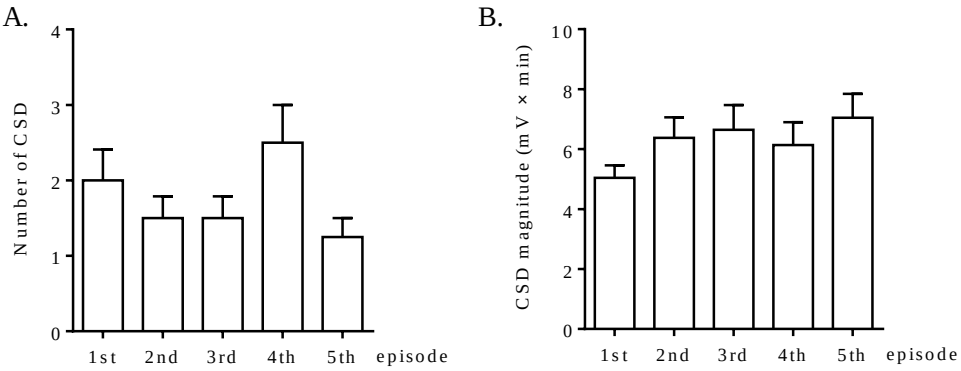

Figure 49. Statistical analysis of the magnitude and number of CSD propagation waves induced by topical application of 3 M KCl into the burr hole with dura intact on the parietal bone of the rats. There was no significant difference in the number or magnitude of CSD episodes over the 5 high-K^+ applications if *i.c.v.* perfusion of ACSF prior to the 1st high-K^+ applications (n = 4). One-way ANOVA was used for comparing among the CSD episodes.

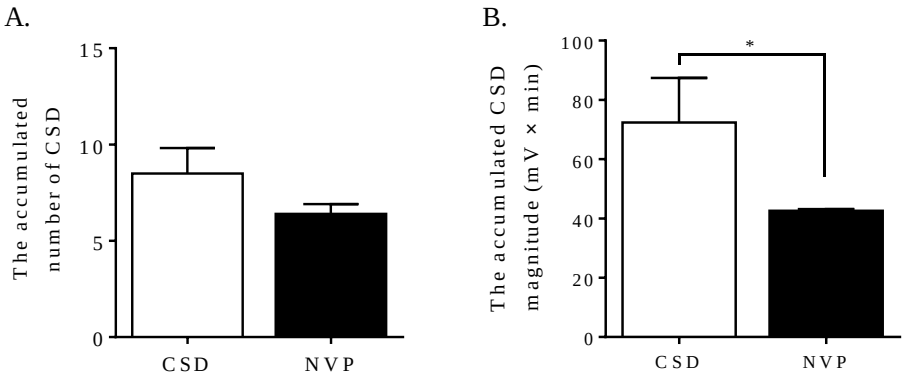

Figure 50. Effects of NVP-AAM077 (0.3 nmol) *i.c.v.* perfused prior to the 1st KCl applications on the cortical susceptibility to CSD and the accumulated magnitude of CSD. All the values shown are means ± SEM. Unpaired t-test with one-tailed calculation was used for statistical analysis for significance between NVP-AAM077 ($n = 4$) and CSD ($n = 4$) group ($^{*}p < 0.05$).

7.2.2 NVP-AAM077 suppressed CSD-induced CGRP mRNA expression in visual cortex, but not motor or somatosensory cortex.

In the sham group, CGRP mRNA levels in the ipsilateral motor, somatosensory, and visual cortices were similar (Figure 51). In CSD group, The CGRP mRNA levels were significantly increased in the ipsilateral motor (9.26 ± 1.2, $n = 3$), somatosensory (16.29 ± 1.51, $n = 3$) and visual cortices (11.72 ± 1.79, $n = 3$) 24 hours after multiple CSD when compared with sham group with 1.0 ± 0.36 ($n = 3$, $^{*}p < 0.05$), 1.0 ± 0.41 ($n = 3$, $^{*}p < 0.05$) and 1.0 ± 0.36 ($n = 3$, $^{*}p < 0.05$) in respective order (Figure 51), which was consistent with our previous study (Wang et al., 2016b). Interestingly, 0.3 nmol NVP-AAM077 significantly suppressed the CGRP mRNA levels to 5.85 ± 1.31 ($n = 5$, $^{*}p < 0.05$) in visual cortex compared to the corresponding CSD group (Figure 51). However, the CGRP mRNA levels in motor (5.95 ± 2.14, $n = 5$) and somatosensory cortex (10.85 ± 4.471, $n = 4$) was not altered by NVP-AAM077 (Figure 51).

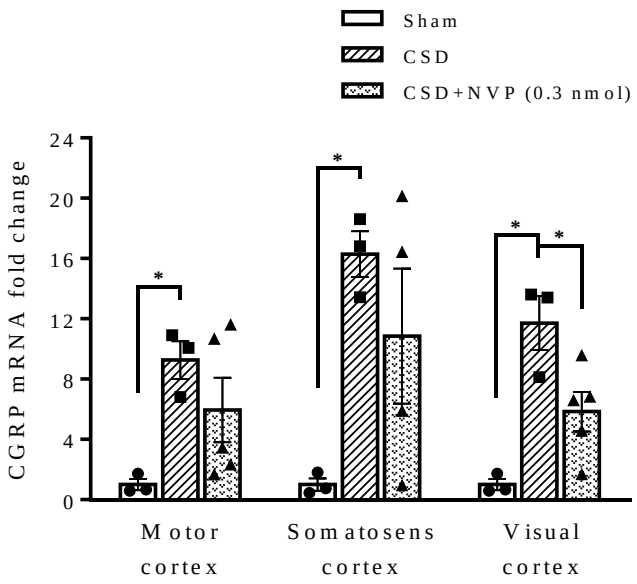

Figure 51. Effect of NR2A (0.3 nmol) to CGRP mRNA expression 24 hours after multiple CSD in ipsilateral motor, somatosensory and visual cortices. Mann-Whitney test with two-tailed calculation was used for statistical analysis, $^{*}p < 0.05$, sham ($n = 3$) vs CSD ($n = 3$) groups, CSD vs NVP-AAM077 ($n = 5$) groups.

7.3 Discussion

This data firstly confirmed that NR2A mediates multiple CSD. Further quantification of CGRP mRNA demonstrated that multiple CSD-induced CGRP gene expression in ipsilateral motor, somatosensory and visual cortices. This elevation of CGRP mRNA was inhibited by the inhibition of NR2A-containing NMDA receptors in visual, but not motor and somatosensory cortices, suggesting a critical role of NR2A in mediating CSD-induced CGRP gene expression in discrete cerebral cortices.

Validation of multiple CSD model for NR2A pharmacology

Herein, neither the cortical susceptibility to CSD nor the magnitude of CSD is altered among the 5 CSD episodes (Figure 49) under isoflurane anesthesia in the control group, which is consistent with our previous study (Wang et al., 2016b),

suggesting a stable and consistent procedure of multiple CSD elicitation in our preparation. Importantly, *i.c.v.* perfusion of 0.3 nmol NVP-AAM077 prior to the 1st high-K^+ application significantly suppresses the accumulated magnitude of CSDs is consistent with that single CSD is suppressed by NR2A inhibition in the chick retina (Wang et al., 2012) and rats (Bu et al., 2016), confirming the validity of the CSD mode for NR2A pharmacology.

Different with the typical single CSD event accompanied with migraine aura in human (Hadjikhani et al., 2001), this experimental protocol was designed to elicit multiple CSD similar to that used in other laboratories (Peeters et al., 2007, Sukhotinsky et al., 2011, Bu et al., 2016). The two facts that up to hundreds of CSD waves occur over days following the brain injury (Hartings et al., 2016), and that a subset of migraineurs suffer episodic migraine attack over months (Dodick et al., 2014), suggesting a clinical relevance of multiple CSD.

CSD-induced CGRP gene expression

A significant increase in CGRP mRNA in the ipsilateral motor, somatosens and visual cerebral cortices is observed 24 hour after multiple CSD, suggesting that unilateral multiple CSD is sufficient to induce CGRP gene expression in these cerebral cortical regions. In addition, the fact that CGRP mRNA levels are similarly increased in multiple cortical regions indicates that the elevation is attributed to CSD, rather than depolarization in the immediate area of K^+ application (Del Bianco et al., 1991).

It is reported that CGRP receptor inhibition suppresses the magnitude of CSD and the tissue susceptibility to CSD both in the chick retina (Wang et al., 2016a) and the brain slice (Tozzi et al., 2012). In addition, application of exogenous CGRP reverses the inhibitory effect of CGRP receptor antagonist to CSD (Tozzi et al., 2012), suggesting a critical role of CGRP/CGRP receptor signaling in CSD elicitation. More limited studies also report that CGRP is elevated in plasma and jejunum of rodent TBI models (Hang et al., 2004), and that both peripheral and central administration of CGRP antibodies attenuates CGRP-induced light aversive behavior as a measure of migraine-associated photophobia in mice (Mason et al., 2016), raising the possibility that the CGRP gene expression post

multiple CSD may involve in the associated diseases.

Mechanism underlying NR2A regulated CGRP gene expression induced by CSD

A key finding is that multiple CSD-induced CGRP gene expression is mediated by NR2A-containing receptor in visual cortex. The mechanism remains unknown, however, several possibilities may account for the elevation of CGRP by CSD. Firstly, mitogen-activated protein kinase (MAPK) pathway is probably an output for NR2A signaling in mediating CSD-induced CGRP gene expression based on the following observations: (i) a proteomic analysis isolates NMDA receptor multiprotein complexes of the sequential protein kinases of the MAPK pathway, including Raf, MAPK and extracellular signal–regulated kinase (ERK) from mouse brain (Husi et al., 2000), which may involve in synaptic plasticity by regulating various transcription factors and controlling gene expression (Adams and Sweatt, 2002); (ii) CSD can upregulate the level of ERK phosphorylation in the trigeminal ganglion (Iwashita et al., 2013) where the CSD-induced CGRP synthesis (Yisarakun et al., 2015) and release (Akerman et al., 2002) are observed as well; and (iii) in an nitroglycerin-induced migraine model of rat, phosphor-ERK are up-regulated in the brain neurons, whereas their expression levels are decreased in headache-free intervals of the migraine compared to the stages of migraine attack (Guo et al., 2016).

Another possibility is that NR2A may mediate CSD-induced CGRP gene expression through a SFKs mechanism for two reasons: (i) NR2A contributes to CSD-induced SFKs activation in cortex of rats (Figure 30 and 31); and (ii) the nerve growth factor (NGF)-induced increase in capsaicin evoked release of CGRP is blocked by the SFKs inhibitor in acute isolated DRG of rats (Park et al., 2010). However, given the mediation of Src to the NGF-induced release of CGRP is observed within several hours (Park et al., 2010), whether SFKs involve in the CGRP expression at the later phase of CSD, i.e. at the 24^{th} hour, requires further investigation.

It is relevant to consider that a region of CGRP gene expression even remains when NR2A activity is inhibited in somatosensory and motor cortices (Figure 51), which implies other unrevealed signals in mediating CSD-induced CGRP gene

expression in these regions. While speculative, one mechanism may be the generation of reactive oxygen species (ROS). A recent analysis of the literature concludes that oxidative stress is a shared feature of most migraine triggers encountered in clinical practice (Borkum, 2016). Likewise, the ROS-responsive cyclo-oxygen-ase-2 (COX-2) gene is reported to be upregulated by CSD (Urbach et al., 2006). Moreover, ROS-induced CGRP gene expression can be inhibited with antioxidant treatment in rat trigeminal ganglia (Raddant and Russo, 2014). In light of these observations, I speculate that CSD-induced ROS production may lead to upregulation of CGRP gene in cortex. However, this does not mean that the assumed ROS/CGRP signaling pathway is specific in the somatosensory and motor cortical regions as ROS is widely expressed in the whole cortex (Bolognin et al., 2013). The distinct signaling involving CGRP gene expression after CSD in discrete cortices requires further investigation.

In summary, I conclude that NR2A-containing receptor contributes to the CSD-induced upregulation of CGRP gene in the visual cortex. The significance of this finding is that NR2A may be a mechanism by which CGRP levels become elevated post CSD for a prolonged period in some migraine patients with visual aura. These data extends my early study showing NR2A mediates a rapid cellular response post CSD, i.e. NR2A contributes to the CSD-induced SFKs coupling to Panx1 channels, and highlight the essential involvement of NR2A in both repaid and later events post CSD.

Chapter 8 General discussion

This thesis demonstrates that the contribution of NR2A-containing NMDA receptor to CSD genesis and propagation, and reveals two strands of downstream signaling pathways of NR2A in CSD involving SFKs, Panx1 and CGRP in the rat cortex. It can be summarized as: (i) NR2A-containing NMDA receptor contributes to CSD genesis and propagation (chapter 3); (ii) SFKs play a critical role during CSD as SFKs can be activated by CSD and SFKs contribute to CSD propagation (chapter 4); (iii) CSD coupling activated SFKs to neuronal Panx1 channels, which is regulated by NR2A (chapters 4-6); and (iv) NR2A contributes to CSD-induced CGRP gene expression in visual cortex (chapter 7).

CSD has been demonstrated to be dependent on activation of the NMDA receptor in the neocortex of a variety of species (Gorji et al., 2001). In this project, NR2A-containing NMDA receptor inhibition not only suppresses CSD propagation but also genesis, implicating a therapeutic potential by blocking NR2A subunit in migraine. In addition, the specificity of targeting NR2A rather than blockade of channel pore of NMDA receptor in mediating CSD (Peeters et al., 2007, Olah et al., 2013) highlights the potential of clinical use of NR2A with less side effects.

Herein, I identify a previous unknown element SFK in mediating CSD. The fact that inhibition of SFKs activity can suppress the cortical susceptibility to CSD and CSD propagation (Chapter 5) probably could be attributed to the involvement of SFKs substrates (Yeatman, 2004). Among these, the NMDA receptors can be considered as a candidate because multiple C-terminal sites of tyrosine of both NR2A and NR2B subunits can be phosphorylated by SFKs (Salter and Kalia, 2004), and that both of the subunits contribute to the CSD propagation (Menniti et al., 2000, Bu et al., 2016). In addition, the contribution of NR2A to CSD-induced SFKs activation (Chapter 5) could be linked to the regulation of CSD by SFKs forming a positive loop, which leads to a better understanding of NR2A-containing NMDA receptor in mediating CSD.

This work also first links two important elements, i.e. NR2A and Panx1, in CSD,

which is demonstrated by that CSD couples activated SFKs to neuronal Panx1 channels, which is positively regulated by NR2A. It extends a previous study with CSD caused Panx1 channels opening followed by inflammatory factors (e.g. nuclear factor κB and interleukin-1β) releasing to meninges and consequently triggered headache-like behavior in mice (Karatas et al., 2013). The significance is that clarifies a mechanism of CSD-induced Panx1 channels opening and provides an evidence for the involvement of NR2A in the CSD-induced headache in animal model.

Furthermore, this study gives an explanation to the CSD-induced CGRP gene expression in visual cortex, as evidenced by the suppressing effect of NR2A inhibition to CSD propagation and the elevation of CGRP mRNA. The less efficiency of NR2A inhibition to the CSD-induced CGRP gene expression in motor and somatosens cortices may imply the distinct roles of NR2A to the consequences of CSD through CGRP in the discrete regions of cortex.

In conclusion, this project demonstrates the contribution of NR2A-containing NMDA receptor to CSD genesis and propagation and identifies a signaling pathway, which extends the previous understanding of NR2A in CSD pathology. In addition, given the critical roles of NR2A, Panx1 channels and CGRP in the generation and consequences of CSD, the revealed element, i.e. SFKs, for CSD physiopathology may represent a hub that widely participants in the diseases associated with CSD via a range of signaling transduction. Targeting the NR2A signaling pathway involving SFKs, Panx1 and CGRP may be a potential strategy to prevent and/or relieve migraine and TBI. Nonetheless, a limitation of animal CSD studies remains extrapolation to humans, especially as CSD propagation is limited by prominent sulci in the human brain that are absent in the lissencephalic rodent brain (James et al., 1999). Within this limitation, whether NR2A and its relative signaling could function to migraine in human still needs further investigation.

Chapter 9 Further work

(i) *Is CSD suppressed by the NR2A antagonist applied through clinical route?*

Our data provides solid evidence showing both CSD genesis and propagation can be suppressed by central administration of NR2A antagonists. However, whether peripheral administration of chemicals antagonizing NR2A could suppress CSD remains controversy as that the BOLD response of CSD is not altered by intraperitoneal injection of TCN-201 with an estimated dosage at 10 mg/kg based on its similarity in potency to ifenprodil in rats (Shatillo et al., 2015). I assume that the ineffectiveness of peripheral application of TCN-201 on CSD may be caused by (i) low efficiency of TCN-201 to CSD; (ii) lack of exploring effective concentration of TCN-201 in the guaranty of its selectivity of NR2A; (iii) the different methods applied for CSD recording: BOLD fMRI (Shatillo et al., 2015) vs electrophysiology. In this case, it would be worthwhile to further investigate whether CSD could be suppressed by NR2A antagonist applied through clinical acceptable route.

In the preliminary experiment, I carried out one experiment in a rat using caudal vein injection of NVP-AAM077 at 2.4 mg/kg, at which the drug is selective for NR2A subunit (Fox et al., 2006). Five repeated CSD episodes were induced by topical application of 2 M KCl for 15 minutes, each followed by 40 minutes tissue recovery. With expected, at this dose, the drug injected 40 minutes prior to the 2nd CSD induction, has an inhibitory tendency to tissue susceptibility to CSD as reflected by the reduced CSD number, propagation rate and prolonged CSD latency (Figure 52). Maximum inhibitory effects of NVP-AAM077 on CSD were observed at the 110th minutes after drug application. This result further supports the key role of NR2A in mediating CSD, indicating drug-alike candidates targeting NR2A may constitute a highly specific strategy for the treatment of migraine. More data is required for studying the pharmacokinetic profile of the drug in the future.

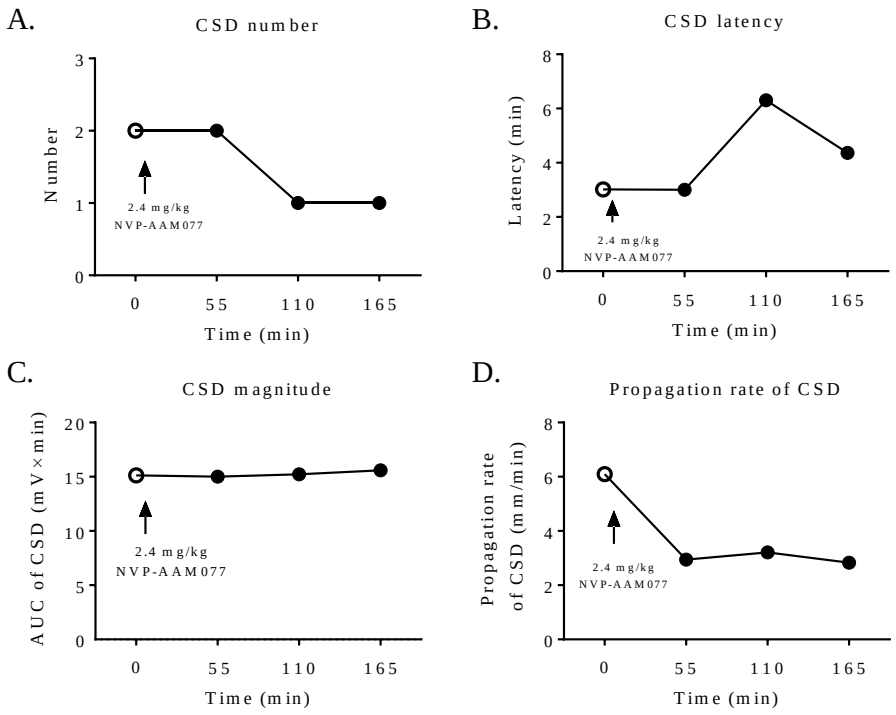

Figure 52. This figure shows inhibitory effects of pre-treatment of NVP-AAM077 2.4 mg/kg through caudal vein on cortex susceptibility to CSD induced by topical application of 2 M KCl in the rat (*n*=1). Reducing tendency to CSD number, propagation rate and increasing tendency on CSD latency were observed, whereas the CSD magnitude was not altered after drug application.

(ii) *Does SFKs inhibition suppress CSD-induced interaction of SFKs and Panx1?*

The present study shows that CSD promotes the SFKs-Panx1 interaction and Panx1 channels opening. Inhibition of SFKs by PP2 significantly suppresses Panx1 channels opening, suggesting that CSD triggers Panx1 opening via activating SFKs. However, it lacks a direct evidence as whether SFKs inhibitor could prevent CSD-induced SFKs-Panx1 interaction to further confirm that SFKs functioning to Panx1 channels by physical interaction.

(iii) *Are CSD-induced SFKs activation and phospho-SFKs coupling to Panx1*

channels different between parts of cortex?

It has been demonstrated that CSD propagation is inhomogeneous in ipsilateral cortex (Eiselt et al., 2004). Specifically, the amplitudes of K^+-induced CSD in the cortical parts nearby middle line, e.g. cingulate cortex, was much smaller than that in the lateral cortical parts (Eiselt et al., 2004). Herein, the IHC data showed that CSD-induced Panx1 channels opening is not mediated by NR2A in ipsilateral cingulate cortex, although Western blotting result shows that NR2A contributes to CSD-induced phospho-SFKs coupling to Panx1 in whole ipsilateral cortex, which raising the possibility that the NR2A/SFKs/Panx1 signaling is regional specific. In this case, it is necessary to investigate whether CSD-induced NR2A/SFKs/Panx1 cascade differs among cingulate, motor and somatosensory cortices.

(iv) *How do SFKs mediate CSD?*

This study reveals a critical role of SFKs in mediating CSD. Although the mechanism remains unknown, it is likely that SFKs may mediate CSD via interacting with NR2A, and especially with the Y1325 and/or Y1387 amino acid(s) of NR2A as discussed in chapter 4. It would be worth investigating that whether CSD could recruit phospho-SFKs to activate NR2A and whether disrupting the interaction of SFKs and NR2A could suppress CSD.

(v) *Does NR2A mediate CSD-induced CGRP gene expression via SFKs?*

It is known that NR2A contributes to single CSD-induced SFKs activation and multiple CSD-induced CGRP gene expression. In addition, a previous study shows a Src/CGRP signaling as Src inhibition suppressed the NGF-induced release of CGRP in capsaicin-pretreated acute isolated DRG (Park et al., 2010). Based on the above evidences, I assume that NR2A may mediate the multiple CSD-induced CGRP gene expression via SFKs.

(vi) The requirement of more data for further confirmation.

In order to make the conclusion that CSD activates SFKs more robust, further work is required to increase sample number for the sham, PP2 and PP3 groups used in western blotting (Figure 27). Besides that, more sample number is also required for PP2 and PP3 groups of IHC to confirm the contribution of SFKs to CSD-induced Panx1 channels opening (Figure 38 and 40).

Reference

ADAMS, J. P. & SWEATT, J. D. 2002. Molecular psychology: roles for the ERK MAP kinase cascade in memory. *Annu Rev Pharmacol Toxicol,* 42**,** 135-63.

ADDAE, J. I., EVANS, S. M., ALI, N. & STONE, T. W. 2000. NMDA-induced changes in a cortical network in vivo are prevented by AMPA. *Brain Res,* 869**,** 211-5.

AIBA, I., CARLSON, A. P., SHELINE, C. T. & SHUTTLEWORTH, C. W. 2012. Synaptic release and extracellular actions of Zn2+ limit propagation of spreading depression and related events in vitro and in vivo. *J Neurophysiol,* 107**,** 1032-41.

AKERMAN, S., WILLIAMSON, D. J., KAUBE, H. & GOADSBY, P. J. 2002. Nitric oxide synthase inhibitors can antagonize neurogenic and calcitonin gene-related peptide induced dilation of dural meningeal vessels. *Br J Pharmacol,* 137**,** 62-8.

ARULMANI, U., MAASSENVANDENBRINK, A., VILLALON, C. M. & SAXENA, P. R. 2004. Calcitonin gene-related peptide and its role in migraine pathophysiology. *Eur J Pharmacol,* 500**,** 315-30.

AUBERSON, Y. P., ALLGEIER, H., BISCHOFF, S., LINGENHOEHL, K., MORETTI, R. & SCHMUTZ, M. 2002. 5-Phosphonomethylquinoxalinediones as competitive NMDA receptor antagonists with a preference for the human 1A/2A, rather than 1A/2B receptor composition. *Bioorg Med Chem Lett,* 12**,** 1099-102.

AYATA, C. 2010. Cortical spreading depression triggers migraine attack: pro. *Headache,* 50**,** 725-30.

AYATA, C. & LAURITZEN, M. 2015. Spreading Depression, Spreading Depolarizations, and the Cerebral Vasculature. *Physiol Rev,* 95**,** 953-93.

BACK, T., KOHNO, K. & HOSSMANN, K. A. 1994. Cortical negative DC deflections following middle cerebral artery occlusion and KCl-induced spreading depression: effect on blood flow, tissue oxygenation, and electroencephalogram. *J Cereb Blood Flow Metab,* 14**,** 12-9.

BAIN, J., MCLAUCHLAN, H., ELLIOTT, M. & COHEN, P. 2003. The specificities of protein

kinase inhibitors: an update. *Biochem J,* 371**,** 199-204.

BASARSKY, T. A., FEIGHAN, D. & MACVICAR, B. A. 1999. Glutamate release through volume-activated channels during spreading depression. *J Neurosci,* 19**,** 6439-45.

BETTINI, E., SAVA, A., GRIFFANTE, C., CARIGNANI, C., BUSON, A., CAPELLI, A. M., NEGRI, M., ANDREETTA, F., SENAR-SANCHO, S. A., GUIRAL, L. & CARDULLO, F. 2010. Identification and characterization of novel NMDA receptor antagonists selective for NR2A- over NR2B-containing receptors. *J Pharmacol Exp Ther,* 335**,** 636-44.

BIGAL, M., RAPOPORT, A., SHEFTELL, F., TEPPER, D. & TEPPER, S. 2008. Memantine in the preventive treatment of refractory migraine. *Headache,* 48**,** 1337-42.

BIGAL, M. E., WALTER, S. & RAPOPORT, A. M. 2015. Therapeutic antibodies against CGRP or its receptor. *Br J Clin Pharmacol,* 79**,** 886-95.

BOLAY, H., REUTER, U., DUNN, A. K., HUANG, Z., BOAS, D. A. & MOSKOWITZ, M. A. 2002. Intrinsic brain activity triggers trigeminal meningeal afferents in a migraine model. *Nat Med,* 8**,** 136-42.

BOLOGNIN, S., ZATTA, P., LORENZETTO, E., VALENTI, M. T. & BUFFELLI, M. 2013. beta-Amyloid-aluminum complex alters cytoskeletal stability and increases ROS production in cortical neurons. *Neurochem Int,* 62**,** 566-74.

BORKUM, J. M. 2016. Migraine Triggers and Oxidative Stress: A Narrative Review and Synthesis. *Headache,* 56**,** 12-35.

BOWYER, S. M., OKADA, Y. C., PAPUASHVILI, N., MORAN, J. E., BARKLEY, G. L., WELCH, K. M. & TEPLEY, N. 1999a. Analysis of MEG signals of spreading cortical depression with propagation constrained to a rectangular cortical strip. I. Lissencephalic rabbit model. *Brain Res,* 843**,** 71-8.

BOWYER, S. M., TEPLEY, N., PAPUASHVILI, N., KATO, S., BARKLEY, G. L., WELCH, K. M. & OKADA, Y. C. 1999b. Analysis of MEG signals of spreading cortical depression with propagation constrained to a rectangular cortical strip. II. Gyrencephalic swine model. *Brain Res,* 843**,** 79-86.

BRAIN, S. D., WILLIAMS, T. J., TIPPINS, J. R., MORRIS, H. R. & MACINTYRE, I. 1985. Calcitonin gene-related peptide is a potent vasodilator. *Nature,* 313**,** 54-6.

BRAVO, D., MATURANA, C. J., PELISSIER, T., HERNANDEZ, A. & CONSTANDIL, L. 2015. Interactions of pannexin 1 with NMDA and P2X7 receptors in central nervous system pathologies: Possible role on chronic pain. *Pharmacol Res,* 101**,** 86-93.

BREDT, D. S. & SNYDER, S. H. 1992. Nitric oxide, a novel neuronal messenger. *Neuron,* 8**,** 3-11.

BREE, D. & LEVY, D. 2016. Development of CGRP-dependent pain and headache related behaviours in a rat model of concussion: Implications for mechanisms of post-traumatic headache. *Cephalalgia*.

BRENNAN, K. C., BELTRAN-PARRAZAL, L., LOPEZ-VALDES, H. E., THERIOT, J., TOGA, A. W. & CHARLES, A. C. 2007. Distinct vascular conduction with cortical spreading depression. *J Neurophysiol,* 97**,** 4143-51.

BU, F., DU, R., LI, Y., QUINN, J. P. & WANG, M. 2016. NR2A contributes to genesis and propagation of cortical spreading depression in rats. *Sci Rep,* 6**,** 23576.

CAHILL, J., CALVERT, J. W. & ZHANG, J. H. 2006. Mechanisms of early brain injury after subarachnoid hemorrhage. *J Cereb Blood Flow Metab,* 26**,** 1341-53.

CAO, Y., WELCH, K. M., AURORA, S. & VIKINGSTAD, E. M. 1999. Functional MRI-BOLD of visually triggered headache in patients with migraine. *Arch Neurol,* 56**,** 548-54.

CHANG, J. C., SHOOK, L. L., BIAG, J., NGUYEN, E. N., TOGA, A. W., CHARLES, A. C. & BRENNAN, K. C. 2010. Biphasic direct current shift, haemoglobin desaturation and neurovascular uncoupling in cortical spreading depression. *Brain,* 133**,** 996-1012.

CHAZOT, P. L., GODUKHIN, O. V., MCDONALD, A. & OBRENOVITCH, T. P. 2002. Spreading depression-induced preconditioning in the mouse cortex: differential changes in the protein expression of ionotropic nicotinic acetylcholine and glutamate receptors. *J Neurochem,* 83**,** 1235-8.

CHEKENI, F. B., ELLIOTT, M. R., SANDILOS, J. K., WALK, S. F., KINCHEN, J. M.,

LAZAROWSKI, E. R., ARMSTRONG, A. J., PENUELA, S., LAIRD, D. W., SALVESEN, G. S., ISAKSON, B. E., BAYLISS, D. A. & RAVICHANDRAN, K. S. 2010. Pannexin 1 channels mediate 'find-me' signal release and membrane permeability during apoptosis. *Nature,* 467**,** 863-7.

CHEN, H. S. & LIPTON, S. A. 2005. Pharmacological implications of two distinct mechanisms of interaction of memantine with N-methyl-D-aspartate-gated channels. *J Pharmacol Exp Ther,* 314**,** 961-71.

CHEN, H. S. & LIPTON, S. A. 2006. The chemical biology of clinically tolerated NMDA receptor antagonists. *J Neurochem,* 97**,** 1611-26.

CHEN, Q. X., PERKINS, K. L., CHOI, D. W. & WONG, R. K. 1997. Secondary activation of a cation conductance is responsible for NMDA toxicity in acutely isolated hippocampal neurons. *J Neurosci,* 17**,** 4032-6.

CHESLER, M. & KRAIG, R. P. 1987. Intracellular pH of astrocytes increases rapidly with cortical stimulation. *Am J Physiol,* 253**,** R666-70.

CHEUNG, H. H. & GURD, J. W. 2001. Tyrosine phosphorylation of the N-methyl-D-aspartate receptor by exogenous and postsynaptic density-associated Src-family kinases. *J Neurochem,* 78**,** 524-34.

CHOUDHURI, R., CUI, L., YONG, C., BOWYER, S., KLEIN, R. M., WELCH, K. M. & BERMAN, N. E. 2002. Cortical spreading depression and gene regulation: relevance to migraine. *Ann Neurol,* 51**,** 499-506.

CLASADONTE, J., DONG, J., HINES, D. J. & HAYDON, P. G. 2013. Astrocyte control of synaptic NMDA receptors contributes to the progressive development of temporal lobe epilepsy. *Proc Natl Acad Sci U S A,* 110**,** 17540-5.

COLONNA, D. M., MENG, W., DEAL, D. D. & BUSIJA, D. W. 1994. Calcitonin gene-related peptide promotes cerebrovascular dilation during cortical spreading depression in rabbits. *Am J Physiol,* 266**,** H1095-102.

CRUZ, N. F., ADACHI, K. & DIENEL, G. A. 1999. Rapid efflux of lactate from cerebral cortex during K+ -induced spreading cortical depression. *J Cereb Blood Flow Metab,* 19**,** 380-92.

CULL-CANDY, S. G. & LESZKIEWICZ, D. N. 2004. Role of distinct NMDA receptor subtypes at central synapses. *Sci STKE,* 2004**,** re16.

CURTIS, D. R. & WATKINS, J. C. 1961. Analogues of glutamic and gamma-amino-n-butyric acids having potent actions on mammalian neurones. *Nature,* 191**,** 1010-1.

CUTRER, F. M. 2010. Pathophysiology of migraine. *Semin Neurol,* 30**,** 120-30.

DAHLEM, M. A. & MULLER, S. C. 2000. Image processing techniques applied to excitation waves in the chicken retina. *Methods,* 21**,** 317-23.

DAHLEM, Y. A., DAHLEM, M. A., MAIR, T., BRAUN, K. & MULLER, S. C. 2003. Extracellular potassium alters frequency and profile of retinal spreading depression waves. *Exp Brain Res,* 152**,** 221-8.

DE LIMA, D. S., MAIA, L. M., BARBOZA EDE, A., DUARTE RDE, A., DE SOUZA, L. S. & GUEDES, R. C. 2009. L-glutamine supplementation during the lactation period facilitates cortical spreading depression in well-nourished and early-malnourished rats. *Life Sci,* 85**,** 241-7.

DEFELIPE, J., ALONSO-NANCLARES, L. & ARELLANO, J. I. 2002. Microstructure of the neocortex: comparative aspects. *J Neurocytol,* 31**,** 299-316.

DEL BIANCO, E., SANTICIOLI, P., TRAMONTANA, M., MAGGI, C. A., CECCONI, R. & GEPPETTI, P. 1991. Different pathways by which extracellular Ca2+ promotes calcitonin gene-related peptide release from central terminals of capsaicin-sensitive afferents of guinea pigs: effect of capsaicin, high K+ and low pH media. *Brain Res,* 566**,** 46-53.

DINGLEDINE, R., BORGES, K., BOWIE, D. & TRAYNELIS, S. F. 1999. The glutamate receptor ion channels. *Pharmacol Rev,* 51**,** 7-61.

DODICK, D. W., GOADSBY, P. J., SILBERSTEIN, S. D., LIPTON, R. B., OLESEN, J., ASHINA, M., WILKS, K., KUDROW, D., KROLL, R., KOHRMAN, B., BARGAR, R., HIRMAN, J., SMITH, J. & INVESTIGATORS, A. L. D. S. 2014. Safety and efficacy of ALD403, an antibody to calcitonin gene-related peptide, for the prevention of frequent episodic migraine: a randomised, double-blind, placebo-controlled, exploratory phase 2 trial. *Lancet Neurol,* 13**,** 1100-7.

DREIER, J. P. 2011. The role of spreading depression, spreading depolarization and spreading ischemia in neurological disease. *Nat Med,* 17**,** 439-47.

DREIER, J. P., KORNER, K., EBERT, N., GORNER, A., RUBIN, I., BACK, T., LINDAUER, U., WOLF, T., VILLRINGER, A., EINHAUPL, K. M., LAURITZEN, M. & DIRNAGL, U. 1998. Nitric oxide scavenging by hemoglobin or nitric oxide synthase inhibition by N-nitro-L-arginine induces cortical spreading ischemia when K+ is increased in the subarachnoid space. *J Cereb Blood Flow Metab,* 18**,** 978-90.

EDVINSSON, L. 2008. CGRP blockers in migraine therapy: where do they act? *Br J Pharmacol,* 155**,** 967-9.

EDVINSSON, L. 2015. CGRP receptor antagonists and antibodies against CGRP and its receptor in migraine treatment. *Br J Clin Pharmacol,* 80**,** 193-9.

EFTEKHARI, S. 2016. changes in the contralateral cerebral hemisphere in response to cortical spreading depression *5th European Headache and Migraine Trust International Congress,* 381.

EISELT, M., GIESSLER, F., PLATZEK, D., HAUEISEN, J., ZWIENER, U. & ROTHER, J. 2004. Inhomogeneous propagation of cortical spreading depression-detection by electro- and magnetoencephalography in rats. *Brain Res,* 1028**,** 83-91.

FABRICIUS, M., JENSEN, L. H. & LAURITZEN, M. 1993. Microdialysis of interstitial amino acids during spreading depression and anoxic depolarization in rat neocortex. *Brain Res,* 612**,** 61-9.

FARIA, L. C. & MODY, I. 2004. Protective effect of ifenprodil against spreading depression in the mouse entorhinal cortex. *J Neurophysiol,* 92**,** 2610-4.

FARINELLI, I., DE FILIPPIS, S., COLOPRISCO, G., MISSORI, S. & MARTELLETTI, P. 2009. Future drugs for migraine. *Intern Emerg Med,* 4**,** 367-73.

FARKAS, E., BARI, F. & OBRENOVITCH, T. P. 2010. Multi-modal imaging of anoxic depolarization and hemodynamic changes induced by cardiac arrest in the rat cerebral cortex. *Neuroimage,* 51**,** 734-42.

FARKAS, E., PRATT, R., SENGPIEL, F. & OBRENOVITCH, T. P. 2008. Direct, live imaging of cortical spreading depression and anoxic depolarisation using a fluorescent, voltage-sensitive dye. *J Cereb Blood Flow Metab,* 28**,** 251-62.

FERGUS, A. & LEE, K. S. 1997. Regulation of cerebral microvessels by glutamatergic mechanisms. *Brain Res,* 754**,** 35-45.

FEUERSTEIN, D., BACKES, H., GRAMER, M., TAKAGAKI, M., GABEL, P., KUMAGAI, T. & GRAF, R. 2016. Regulation of cerebral metabolism during cortical spreading depression. *J Cereb Blood Flow Metab,* 36**,** 1965-1977.

FLORES-SOTO, M. E., CHAPARRO-HUERTA, V., ESCOTO-DELGADILLO, M., VAZQUEZ-VALLS, E., GONZALEZ-CASTANEDA, R. E. & BEAS-ZARATE, C. 2012. [Structure and function of NMDA-type glutamate receptor subunits]. *Neurologia,* 27**,** 301-10.

FOX, C. J., RUSSELL, K. I., WANG, Y. T. & CHRISTIE, B. R. 2006. Contribution of NR2A and NR2B NMDA subunits to bidirectional synaptic plasticity in the hippocampus in vivo. *Hippocampus,* 16**,** 907-15.

FURUKAWA, H., SINGH, S. K., MANCUSSO, R. & GOUAUX, E. 2005. Subunit arrangement and function in NMDA receptors. *Nature,* 438**,** 185-92.

GARRY, M. G., WALTON, L. P. & DAVIS, M. A. 2000. Capsaicin-evoked release of immunoreactive calcitonin gene-related peptide from the spinal cord is mediated by nitric oxide but not by cyclic GMP. *Brain Res,* 861**,** 208-19.

GARTHWAITE, J., CHARLES, S. L. & CHESS-WILLIAMS, R. 1988. Endothelium-derived relaxing factor release on activation of NMDA receptors suggests role as intercellular messenger in the brain. *Nature,* 336**,** 385-8.

GIELEN, M., SIEGLER RETCHLESS, B., MONY, L., JOHNSON, J. W. & PAOLETTI, P. 2009. Mechanism of differential control of NMDA receptor activity by NR2 subunits. *Nature,* 459**,** 703-7.

GILL, R., ANDINE, P., HILLERED, L., PERSSON, L. & HAGBERG, H. 1992. The effect of MK-801 on cortical spreading depression in the penumbral zone following focal ischaemia in the

rat. *J Cereb Blood Flow Metab,* 12**,** 371-9.

GINGRICH, J. R., PELKEY, K. A., FAM, S. R., HUANG, Y., PETRALIA, R. S., WENTHOLD, R. J. & SALTER, M. W. 2004. Unique domain anchoring of Src to synaptic NMDA receptors via the mitochondrial protein NADH dehydrogenase subunit 2. *Proc Natl Acad Sci U S A,* 101**,** 6237-42.

GODUKHIN, O. V. & OBRENOVITCH, T. P. 2001. Asymmetric propagation of spreading depression along the anteroposterior axis of the cerebral cortex in mice. *J Neurophysiol,* 86**,** 2109-11.

GORJI, A., SCHELLER, D., STRAUB, H., TEGTMEIER, F., KOHLING, R., HOHLING, J. M., TUXHORN, I., EBNER, A., WOLF, P., WERNER PANNECK, H., OPPEL, F. & SPECKMANN, E. J. 2001. Spreading depression in human neocortical slices. *Brain Res,* 906**,** 74-83.

GRECO, R., DEMARTINI, C., ZANABONI, A. M., REDAVIDE, E., PAMPALONE, S., TOLDI, J., FULOP, F., BLANDINI, F., NAPPI, G., SANDRINI, G., VECSEI, L. & TASSORELLI, C. 2016. Effects of kynurenic acid analogue 1 (KYNA-A1) in nitroglycerin-induced hyperalgesia: Targets and anti-migraine mechanisms. *Cephalalgia*.

GUO, J. Q., DENG, H. H., BO, X. & YANG, X. S. 2016. Involvement of BDNF/TrkB and ERK/CREB axes in nitroglycerin-induced rat migraine and effects of estrogen on these signals in the migraine. *Biol Open*.

HADJIKHANI, N., SANCHEZ DEL RIO, M., WU, O., SCHWARTZ, D., BAKKER, D., FISCHL, B., KWONG, K. K., CUTRER, F. M., ROSEN, B. R., TOOTELL, R. B., SORENSEN, A. G. & MOSKOWITZ, M. A. 2001. Mechanisms of migraine aura revealed by functional MRI in human visual cortex. *Proc Natl Acad Sci U S A,* 98**,** 4687-92.

HANG, C. H., SHI, J. X., LI, J. S., WU, W., LI, W. Q. & YIN, H. X. 2004. Levels of vasoactive intestinal peptide, cholecystokinin and calcitonin gene-related peptide in plasma and jejunum of rats following traumatic brain injury and underlying significance in gastrointestinal dysfunction. *World J Gastroenterol,* 10**,** 875-80.

HANKE, J. H., GARDNER, J. P., DOW, R. L., CHANGELIAN, P. S., BRISSETTE, W. H., WERINGER, E. J., POLLOK, B. A. & CONNELLY, P. A. 1996. Discovery of a novel, potent, and

Src family-selective tyrosine kinase inhibitor. Study of Lck- and FynT-dependent T cell activation. *J Biol Chem,* 271**,** 695-701.

HANKE, W. & DE LIMA, V. M. 2008. Central nervous tissue: an excitable medium. a study using the retinal spreading depression as a tool. *Philos Trans A Math Phys Eng Sci,* 366**,** 359-68.

HANSEN, A. J. & LAURITZEN, M. 1984. The role of spreading depression in acute brain disorders. *An Acad Bras Cienc,* 56**,** 457-79.

HANSEN, J. M., HAUGE, A. W., OLESEN, J. & ASHINA, M. 2010. Calcitonin gene-related peptide triggers migraine-like attacks in patients with migraine with aura. *Cephalalgia,* 30**,** 1179-86.

HANSEN, K. B., OGDEN, K. K. & TRAYNELIS, S. F. 2012. Subunit-selective allosteric inhibition of glycine binding to NMDA receptors. *J Neurosci,* 32**,** 6197-208.

HARGREAVES, R. 2007. New migraine and pain research. *Headache,* 47 Suppl 1**,** S26-43.

HARTINGS, J. A., SHUTTLEWORTH, C. W., KIROV, S. A., AYATA, C., HINZMAN, J. M., FOREMAN, B., ANDREW, R. D., BOUTELLE, M. G., BRENNAN, K. C., CARLSON, A. P., DAHLEM, M. A., DRENCKHAHN, C., DOHMEN, C., FABRICIUS, M., FARKAS, E., FEUERSTEIN, D., GRAF, R., HELBOK, R., LAURITZEN, M., MAJOR, S., OLIVEIRA-FERREIRA, A. I., RICHTER, F., ROSENTHAL, E. S., SAKOWITZ, O. W., SANCHEZ-PORRAS, R., SANTOS, E., SCHOLL, M., STRONG, A. J., URBACH, A., WESTOVER, M. B., WINKLER, M. K., WITTE, O. W., WOITZIK, J. & DREIER, J. P. 2016. The continuum of spreading depolarizations in acute cortical lesion development: Examining Leao's legacy. *J Cereb Blood Flow Metab*.

HARTINGS, J. A., STRONG, A. J., FABRICIUS, M., MANNING, A., BHATIA, R., DREIER, J. P., MAZZEO, A. T., TORTELLA, F. C., BULLOCK, M. R. & CO-OPERATIVE STUDY OF BRAIN INJURY, D. 2009. Spreading depolarizations and late secondary insults after traumatic brain injury. *J Neurotrauma,* 26**,** 1857-66.

HELLIER, J. L., WHITE, A., WILLIAMS, P. A., DUDEK, F. E. & STALEY, K. J. 2009. NMDA receptor-mediated long-term alterations in epileptiform activity in experimental chronic epilepsy.

Neuropharmacology, 56**,** 414-21.

HERNANDEZ-CACERES, J., MACIAS-GONZALEZ, R., BROZEK, G. & BURES, J. 1987. Systemic ketamine blocks cortical spreading depression but does not delay the onset of terminal anoxic depolarization in rats. *Brain Res,* 437**,** 360-4.

HOF, P. R., PASCALE, E. & MAGISTRETTI, P. J. 1988. K+ at concentrations reached in the extracellular space during neuronal activity promotes a Ca2+-dependent glycogen hydrolysis in mouse cerebral cortex. *J Neurosci,* 8**,** 1922-8.

HOLLAND, P. R., AKERMAN, S. & GOADSBY, P. J. 2010. Cortical spreading depression-associated cerebral blood flow changes induced by mechanical stimulation are modulated by AMPA and GABA receptors. *Cephalalgia,* 30**,** 519-27.

HUANG, L., BOCEK, M., JORDAN, J. K. & SHEEHAN, A. H. 2014. Memantine for the prevention of primary headache disorders. *Ann Pharmacother,* 48**,** 1507-11.

HUSI, H., WARD, M. A., CHOUDHARY, J. S., BLACKSTOCK, W. P. & GRANT, S. G. 2000. Proteomic analysis of NMDA receptor-adhesion protein signaling complexes. *Nat Neurosci,* 3**,** 661-9.

ISAKSON, B. E. & THOMPSON, R. J. 2014. Pannexin-1 as a potentiator of ligand-gated receptor signaling. *Channels (Austin),* 8**,** 118-23.

IWASHITA, T., SHIMIZU, T., SHIBATA, M., TORIUMI, H., EBINE, T., FUNAKUBO, M. & SUZUKI, N. 2013. Activation of extracellular signal-regulated kinase in the trigeminal ganglion following both treatment of the dura mater with capsaicin and cortical spreading depression. *Neurosci Res,* 77**,** 110-9.

JAMES, M. F., SMITH, M. I., BOCKHORST, K. H., HALL, L. D., HOUSTON, G. C., PAPADAKIS, N. G., SMITH, J. M., WILLIAMS, A. J., XING, D., PARSONS, A. A., HUANG, C. L. & CARPENTER, T. A. 1999. Cortical spreading depression in the gyrencephalic feline brain studied by magnetic resonance imaging. *J Physiol,* 519 Pt 2**,** 415-25.

JIA, Y., ZHOU, J., BU, F. & WANG, M. 2015. Synergistic Suppression of Cortical Spreading Depression under NR2A and NR2B Inhibition. *Pharmacology & Pharmacy,* 6**,** 573-579.

KARATAS, H., ERDENER, S. E., GURSOY-OZDEMIR, Y., LULE, S., EREN-KOCAK, E., SEN, Z. D. & DALKARA, T. 2013. Spreading depression triggers headache by activating neuronal Panx1 channels. *Science,* 339**,** 1092-5.

KATSURA, H., OBATA, K., MIZUSHIMA, T., SAKURAI, J., KOBAYASHI, K., YAMANAKA, H., DAI, Y., FUKUOKA, T., SAKAGAMI, M. & NOGUCHI, K. 2006. Activation of Src-family kinases in spinal microglia contributes to mechanical hypersensitivity after nerve injury. *J Neurosci,* 26**,** 8680-90.

KAUBE, H., HERZOG, J., KAUFER, T., DICHGANS, M. & DIENER, H. C. 2000. Aura in some patients with familial hemiplegic migraine can be stopped by intranasal ketamine. *Neurology,* 55**,** 139-41.

KEMP, J. A. & MCKERNAN, R. M. 2002. NMDA receptor pathways as drug targets. *Nat Neurosci,* 5 Suppl**,** 1039-42.

KERTESZ, S., KAPUS, G., GACSALYI, I. & LEVAY, G. 2010. Deramciclane improves object recognition in rats: potential role of NMDA receptors. *Pharmacol Biochem Behav,* 94**,** 570-4.

KIM, M. J., DUNAH, A. W., WANG, Y. T. & SHENG, M. 2005. Differential roles of NR2A- and NR2B-containing NMDA receptors in Ras-ERK signaling and AMPA receptor trafficking. *Neuron,* 46**,** 745-60.

KITAHARA, Y., TAGA, K., ABE, H. & SHIMOJI, K. 2001. The effects of anesthetics on cortical spreading depression elicitation and c-fos expression in rats. *J Neurosurg Anesthesiol,* 13**,** 26-32.

KOHR, G. & SEEBURG, P. H. 1996. Subtype-specific regulation of recombinant NMDA receptor-channels by protein tyrosine kinases of the src family. *J Physiol,* 492 (Pt 2)**,** 445-52.

KRIVANEK, J. 1961. Some metabolic changes accompanying Leao's spreading cortical depression in the rat. *J Neurochem,* 6**,** 183-9.

KUCHARZ, K., SONDERGAARD RASMUSSEN, I., BACH, A., STROMGAARD, K. & LAURITZEN, M. 2016. PSD-95 uncoupling from NMDA receptors by Tat-N-dimer ameliorates neuronal depolarisation in cortical spreading depression. *J Cereb Blood Flow Metab*.

KUDO, C., NOZARI, A., MOSKOWITZ, M. A. & AYATA, C. 2008. The impact of anesthetics and hyperoxia on cortical spreading depression. *Exp Neurol,* 212**,** 201-6.

KUGE, Y., HASEGAWA, Y., YOKOTA, C., MINEMATSU, K., HASHIMOTO, N., MIYAKE, Y. & YAMAGUCHI, T. 2000. Effects of single and repetitive spreading depression on cerebral blood flow and glucose metabolism in cats: a PET study. *J Neurol Sci,* 176**,** 114-23.

KUMAR, A., JAGGI, A. S. & SINGH, N. 2014. Pharmacological investigations on possible role of Src kinases in neuroprotective mechanism of ischemic postconditioning in mice. *Int J Neurosci,* 124**,** 777-86.

KURTH, T., CHABRIAT, H. & BOUSSER, M. G. 2012. Migraine and stroke: a complex association with clinical implications. *Lancet Neurol,* 11**,** 92-100.

LASHLEY, K. 1941. Patterns of cerebral integration indicated by the scotoma of migraine. *Arch Neurol Psychiatry***,** 259-264.

LASSEN, L. H., HADERSLEV, P. A., JACOBSEN, V. B., IVERSEN, H. K., SPERLING, B. & OLESEN, J. 2002. CGRP may play a causative role in migraine. *Cephalalgia,* 22**,** 54-61.

LAURITZEN, M. 1994. Pathophysiology of the migraine aura. The spreading depression theory. *Brain,* 117 (Pt 1)**,** 199-210.

LAURITZEN, M., DREIER, J. P., FABRICIUS, M., HARTINGS, J. A., GRAF, R. & STRONG, A. J. 2011. Clinical relevance of cortical spreading depression in neurological disorders: migraine, malignant stroke, subarachnoid and intracranial hemorrhage, and traumatic brain injury. *J Cereb Blood Flow Metab,* 31**,** 17-35.

LAURITZEN, M. & HANSEN, A. J. 1992. The effect of glutamate receptor blockade on anoxic depolarization and cortical spreading depression. *J Cereb Blood Flow Metab,* 12**,** 223-9.

LAURITZEN, M., HANSEN, A. J., KRONBORG, D. & WIELOCH, T. 1990. Cortical spreading depression is associated with arachidonic acid accumulation and preservation of energy charge. *J Cereb Blood Flow Metab,* 10**,** 115-22.

LAURITZEN, M., RICE, M. E., OKADA, Y. & NICHOLSON, C. 1988. Quisqualate, kainate and

NMDA can initiate spreading depression in the turtle cerebellum. *Brain Res,* 475**,** 317-27.

LEAO, A. A. P. 1944a. Pial circulation and spreading depression of activity in the cerebral cortex *J. Neurophysiol. ,* 7**,** 391-396.

LEAO, A. A. P. 1944b. Spreading Depression of Activity in the Cerebral Cortex. *J. Neurophysiol.,* 359-390.

LEAO, A. A. P. 1947. Further observations on the spreading depression of activity in the cerebral cortex. *J Neurophysiol,* 10**,** 409-14.

LEVY, D., BURSTEIN, R. & STRASSMAN, A. M. 2005. Calcitonin gene-related peptide does not excite or sensitize meningeal nociceptors: implications for the pathophysiology of migraine. *Ann Neurol,* 58**,** 698-705.

LIPTON, R. B., BIGAL, M. E., STEINER, T. J., SILBERSTEIN, S. D. & OLESEN, J. 2004. Classification of primary headaches. *Neurology,* 63**,** 427-35.

LIU, L., WONG, T. P., POZZA, M. F., LINGENHOEHL, K., WANG, Y., SHENG, M., AUBERSON, Y. P. & WANG, Y. T. 2004. Role of NMDA receptor subtypes in governing the direction of hippocampal synaptic plasticity. *Science,* 304**,** 1021-4.

LIU, X. J., GINGRICH, J. R., VARGAS-CABALLERO, M., DONG, Y. N., SENGAR, A., BEGGS, S., WANG, S. H., DING, H. K., FRANKLAND, P. W. & SALTER, M. W. 2008. Treatment of inflammatory and neuropathic pain by uncoupling Src from the NMDA receptor complex. *Nat Med,* 14**,** 1325-32.

LIU, Y., BISHOP, A., WITUCKI, L., KRAYBILL, B., SHIMIZU, E., TSIEN, J., UBERSAX, J., BLETHROW, J., MORGAN, D. O. & SHOKAT, K. M. 1999. Structural basis for selective inhibition of Src family kinases by PP1. *Chem Biol,* 6**,** 671-8.

LIU, Y., WONG, T. P., AARTS, M., ROOYAKKERS, A., LIU, L., LAI, T. W., WU, D. C., LU, J., TYMIANSKI, M., CRAIG, A. M. & WANG, Y. T. 2007. NMDA receptor subunits have differential roles in mediating excitotoxic neuronal death both in vitro and in vivo. *J Neurosci,* 27**,** 2846-57.

LYNCH, D. R. & GUTTMANN, R. P. 2001. NMDA receptor pharmacology: perspectives from molecular biology. *Curr Drug Targets,* 2**,** 215-31.

MACVICAR, B. A. & THOMPSON, R. J. 2010. Non-junction functions of pannexin-1 channels. *Trends Neurosci,* 33**,** 93-102.

MARRANNES, R., WILLEMS, R., DE PRINS, E. & WAUQUIER, A. 1988. Evidence for a role of the N-methyl-D-aspartate (NMDA) receptor in cortical spreading depression in the rat. *Brain Res,* 457**,** 226-40.

MARTIN, G. S. 2001. The hunting of the Src. *Nat Rev Mol Cell Biol,* 2**,** 467-75.

MASON, B. N., KAISER, E. A., KUBURAS, A., LOOMIS, M. M., LATHAM, J. A., GARCIA-MARTINEZ, L. F. & RUSSO, A. F. 2016. Induction of migraine-like photophobic behavior in mice by both peripheral and central CGRP mechanisms. *J Neurosci*.

MATSUSHIMA, K., HOGAN, M. J. & HAKIM, A. M. 1996. Cortical spreading depression protects against subsequent focal cerebral ischemia in rats. *J Cereb Blood Flow Metab,* 16**,** 221-6.

MAYEVSKY, A. & WEISS, H. R. 1991. Cerebral blood flow and oxygen consumption in cortical spreading depression. *J Cereb Blood Flow Metab,* 11**,** 829-36.

MENNITI, F. S., PAGNOZZI, M. J., BUTLER, P., CHENARD, B. L., JAW-TSAI, S. S. & FROST WHITE, W. 2000. CP-101,606, an NR2B subunit selective NMDA receptor antagonist, inhibits NMDA and injury induced c-fos expression and cortical spreading depression in rodents. *Neuropharmacology,* 39**,** 1147-55.

MICHAELIS, E. K. 1998. Molecular biology of glutamate receptors in the central nervous system and their role in excitotoxicity, oxidative stress and aging. *Prog Neurobiol,* 54**,** 369-415.

MIES, G. & PASCHEN, W. 1984. Regional changes of blood flow, glucose, and ATP content determined on brain sections during a single passage of spreading depression in rat brain cortex. *Exp Neurol,* 84**,** 249-58.

MILNER, P. M. 1958. Note on a possible correspondence between the scotomas of migraine and spreading depression of Leao. *Electroencephalogr Clin Neurophysiol,* 10**,** 705.

MULDERRY, P. K., GHATEI, M. A., BISHOP, A. E., ALLEN, Y. S., POLAK, J. M. & BLOOM, S. R. 1985. Distribution and chromatographic characterisation of CGRP-like immunoreactivity in the brain and gut of the rat. *Regul Pept,* 12**,** 133-43.

MUTCH, W. A. & HANSEN, A. J. 1984. Extracellular pH changes during spreading depression and cerebral ischemia: mechanisms of brain pH regulation. *J Cereb Blood Flow Metab,* 4**,** 17-27.

NASSTROM, J., BOO, E., STAHLBERG, M. & BERGE, O. G. 1993. Tissue distribution of two NMDA receptor antagonists, [3H]CGS 19755 and [3H]MK-801, after intrathecal injection in mice. *Pharmacol Biochem Behav,* 44**,** 9-15.

NELLGARD, B. & WIELOCH, T. 1992. NMDA-receptor blockers but not NBQX, an AMPA-receptor antagonist, inhibit spreading depression in the rat brain. *Acta Physiol Scand,* 146**,** 497-503.

NEYTON, J. & PAOLETTI, P. 2006. Relating NMDA receptor function to receptor subunit composition: limitations of the pharmacological approach. *J Neurosci,* 26**,** 1331-3.

NOH, J., LEE, E. S. & CHUNG, J. M. 2009. The novel NMDA receptor antagonist, 2-hydroxy-5-(2,3,5,6-tetrafluoro-4-trifluoromethyl-benzylamino)-benzoic acid, is a gating modifier in cultured mouse cortical neurons. *J Neurochem,* 109**,** 1261-71.

NORN, S., PERMIN, H., KRUSE, E. & KRUSE, P. R. 2015. [On the history of barbiturates]. *Dan Medicinhist Arbog,* 43**,** 133-51.

NOSEDA, R. & BURSTEIN, R. 2013. Migraine pathophysiology: anatomy of the trigeminovascular pathway and associated neurological symptoms, cortical spreading depression, sensitization, and modulation of pain. *Pain,* 154 Suppl 1**,** S44-53.

OBRENOVITCH, T. P., RICHARDS, D. A., SARNA, G. S. & SYMON, L. 1993. Combined intracerebral microdialysis and electrophysiological recording: methodology and applications. *J Neurosci Methods,* 47**,** 139-45.

OBRENOVITCH, T. P. & ZILKHA, E. 1995. High extracellular potassium, and not extracellular glutamate, is required for the propagation of spreading depression. *J Neurophysiol,* 73**,** 2107-14.

OBRENOVITCH, T. P. & ZILKHA, E. 1996a. Inhibition of cortical spreading depression by L-701,324, a novel antagonist at the glycine site of the N-methyl-D-aspartate receptor complex. *Br J Pharmacol,* 117**,** 931-7.

OBRENOVITCH, T. P. & ZILKHA, E. 1996b. Intracerebral microdialysis markedly inhibits the propagation of cortical spreading depression. *Acta Neurochir Suppl,* 67**,** 21-3.

OGDEN, K. K. & TRAYNELIS, S. F. 2011. New advances in NMDA receptor pharmacology. *Trends Pharmacol Sci,* 32**,** 726-33.

OKUTANI, D., LODYGA, M., HAN, B. & LIU, M. 2006. Src protein tyrosine kinase family and acute inflammatory responses. *Am J Physiol Lung Cell Mol Physiol,* 291**,** L129-41.

OLAH, G., HEREDI, J., MENYHART, A., CZINEGE, Z., NAGY, D., FUZIK, J., KOCSIS, K., KNAPP, L., KRUCSO, E., GELLERT, L., KIS, Z., FARKAS, T., FULOP, F., PARDUTZ, A., TAJTI, J., VECSEI, L. & TOLDI, J. 2013. Unexpected effects of peripherally administered kynurenic acid on cortical spreading depression and related blood-brain barrier permeability. *Drug Des Devel Ther,* 7**,** 981-7.

PAOLETTI, P. & NEYTON, J. 2007. NMDA receptor subunits: function and pharmacology. *Curr Opin Pharmacol,* 7**,** 39-47.

PARK, K. A., FEHRENBACHER, J. C., THOMPSON, E. L., DUARTE, D. B., HINGTGEN, C. M. & VASKO, M. R. 2010. Signaling pathways that mediate nerve growth factor-induced increase in expression and release of calcitonin gene-related peptide from sensory neurons. *Neuroscience,* 171**,** 910-23.

PEETERS, M., GUNTHORPE, M. J., STRIJBOS, P. J., GOLDSMITH, P., UPTON, N. & JAMES, M. F. 2007. Effects of pan- and subtype-selective N-methyl-D-aspartate receptor antagonists on cortical spreading depression in the rat: therapeutic potential for migraine. *J Pharmacol Exp Ther,* 321**,** 564-72.

PEIXOTO, N. L., FERNANDES DE LIMA, V. M. & HANKE, W. 2001. Correlation of the electrical and intrinsic optical signals in the chicken spreading depression phenomenon. *Neurosci Lett,* 299**,** 89-92.

PENUELA, S., GEHI, R. & LAIRD, D. W. 2013. The biochemistry and function of pannexin channels. *Biochim Biophys Acta,* 1828**,** 15-22.

PIETROBON, D. & MOSKOWITZ, M. A. 2014. Chaos and commotion in the wake of cortical spreading depression and spreading depolarizations. *Nat Rev Neurosci,* 15**,** 379-93.

PIPER, R. D. & LAMBERT, G. A. 1996. Inhalational anesthetics inhibit spreading depression: relevance to migraine. *Cephalalgia,* 16**,** 87-92.

PROESCHOLDT, M. G., HUTTO, B., BRADY, L. S. & HERKENHAM, M. 2000. Studies of cerebrospinal fluid flow and penetration into brain following lateral ventricle and cisterna magna injections of the tracer [14C]inulin in rat. *Neuroscience,* 95**,** 577-92.

PUSIC, K. M., PUSIC, A. D., KEMME, J. & KRAIG, R. P. 2014. Spreading depression requires microglia and is decreased by their M2a polarization from environmental enrichment. *Glia,* 62**,** 1176-94.

RADDANT, A. C. & RUSSO, A. F. 2014. Reactive oxygen species induce procalcitonin expression in trigeminal ganglia glia. *Headache,* 54**,** 472-84.

READ, S. J., HIRST, W. D., UPTON, N. & PARSONS, A. A. 2001. Cortical spreading depression produces increased cGMP levels in cortex and brain stem that is inhibited by tonabersat (SB-220453) but not sumatriptan. *Brain Res,* 891**,** 69-77.

READ, S. J., SMITH, M. I., HUNTER, A. J. & PARSONS, A. A. 1997. The dynamics of nitric oxide release measured directly and in real time following repeated waves of cortical spreading depression in the anaesthetised cat. *Neurosci Lett,* 232**,** 127-30.

RODRIGUES, P. S., GUIMARAES, A. P., DE AZEREDO, F. A. & MARTINS-FERREIRA, H. 1988. Involvement of GABA and ACh in retinal spreading depression: effects of "low calcium-high magnesium" solutions. *Exp Brain Res,* 73**,** 659-64.

RODRIGUES, P. S. & MARTINS-FERREIRA, H. 1980. Cholinergic neurotransmission in retinal spreading depression. *Exp Brain Res,* 38**,** 229-36.

ROSKOSKI, R., JR. 2004. Src protein-tyrosine kinase structure and regulation. *Biochem Biophys*

Res Commun, 324**,** 1155-64.

RUSSO, A. F. 2015. Calcitonin Gene-Related Peptide (CGRP): A New Target for Migraine. *Annu Rev Pharmacol Toxicol,* 55**,** 533-52.

SALTER, M. W. & KALIA, L. V. 2004. Src kinases: a hub for NMDA receptor regulation. *Nat Rev Neurosci,* 5**,** 317-28.

SALTER, M. W. & PITCHER, G. M. 2012. Dysregulated Src upregulation of NMDA receptor activity: a common link in chronic pain and schizophrenia. *FEBS J,* 279**,** 2-11.

SANZ-CLEMENTE, A., NICOLL, R. A. & ROCHE, K. W. 2013. Diversity in NMDA receptor composition: many regulators, many consequences. *Neuroscientist,* 19**,** 62-75.

SASAKI, Y. F., ROTHE, T., PREMKUMAR, L. S., DAS, S., CUI, J., TALANTOVA, M. V., WONG, H. K., GONG, X., CHAN, S. F., ZHANG, D., NAKANISHI, N., SUCHER, N. J. & LIPTON, S. A. 2002. Characterization and comparison of the NR3A subunit of the NMDA receptor in recombinant systems and primary cortical neurons. *J Neurophysiol,* 87**,** 2052-63.

SCHOCK, S. C., MUNYAO, N., YAKUBCHYK, Y., SABOURIN, L. A., HAKIM, A. M., VENTUREYRA, E. C. & THOMPSON, C. S. 2007. Cortical spreading depression releases ATP into the extracellular space and purinergic receptor activation contributes to the induction of ischemic tolerance. *Brain Res,* 1168**,** 129-38.

SEIDEL, J. L., ESCARTIN, C., AYATA, C., BONVENTO, G. & SHUTTLEWORTH, C. W. 2016. Multifaceted roles for astrocytes in spreading depolarization: A target for limiting spreading depolarization in acute brain injury? *Glia,* 64**,** 5-20.

SEIDEL, J. L. & SHUTTLEWORTH, C. W. 2011. Contribution of astrocyte glycogen stores to progression of spreading depression and related events in hippocampal slices. *Neuroscience,* 192**,** 295-303.

SHATILLO, A., SALO, R. A., GINIATULLIN, R. & GROHN, O. H. 2015. Involvement of NMDA receptor subtypes in cortical spreading depression in rats assessed by fMRI. *Neuropharmacology,* 93**,** 164-70.

SHEARDOWN, M. J. 1993. The triggering of spreading depression in the chicken retina: a pharmacological study. *Brain Res,* 607**,** 189-94.

SHENG, M. & KIM, M. J. 2002. Postsynaptic signaling and plasticity mechanisms. *Science,* 298**,** 776-80.

SHI, H., LI, J. H., JI, C. F., SHANG, H. Y., QIU, E. C., WANG, J. J. & JING, X. H. 2010. [Effect of electroacupuncture on cortical spreading depression and plasma CGRP and substance P contents in migraine rats]. *Zhen Ci Yan Jiu,* 35**,** 17-21.

SHINOHARA, M., DOLLINGER, B., BROWN, G., RAPOPORT, S. & SOKOLOFF, L. 1979. Cerebral glucose utilization: local changes during and after recovery from spreading cortical depression. *Science,* 203**,** 188-90.

SILVERMAN, W. R., DE RIVERO VACCARI, J. P., LOCOVEI, S., QIU, F., CARLSSON, S. K., SCEMES, E., KEANE, R. W. & DAHL, G. 2009. The pannexin 1 channel activates the inflammasome in neurons and astrocytes. *J Biol Chem,* 284**,** 18143-51.

SINTAS, C., FERNANDEZ-CASTILLO, N., VILA-PUEYO, M., POZO-ROSICH, P., MACAYA, A. & CORMAND, B. 2016. Transcriptomic Changes in Rat Cortex and Brainstem After Cortical Spreading Depression With or Without Pretreatment With Migraine Prophylactic Drugs. *J Pain*.

SMART, J. E., OPPERMANN, H., CZERNILOFSKY, A. P., PURCHIO, A. F., ERIKSON, R. L. & BISHOP, J. M. 1981. Characterization of sites for tyrosine phosphorylation in the transforming protein of Rous sarcoma virus (pp60v-src) and its normal cellular homologue (pp60c-src). *Proc Natl Acad Sci U S A,* 78**,** 6013-7.

SMITH, J. M., BRADLEY, D. P., JAMES, M. F. & HUANG, C. L. 2006. Physiological studies of cortical spreading depression. *Biol Rev Camb Philos Soc,* 81**,** 457-81.

SMITH, M. I., READ, S. J., CHAN, W. N., THOMPSON, M., HUNTER, A. J., UPTON, N. & PARSONS, A. A. 2000. Repetitive cortical spreading depression in a gyrencephalic feline brain: inhibition by the novel benzoylamino-benzopyran SB-220453. *Cephalalgia,* 20**,** 546-53.

SOMJEN, G. G. 2005. Aristides Leao's discovery of cortical spreading depression. *J Neurophysiol,* 94**,** 2-4.

SOMJEN, G. G., AITKEN, P. G., CZEH, G. L., HERRERAS, O., JING, J. & YOUNG, J. N. 1992. Mechanism of spreading depression: a review of recent findings and a hypothesis. *Can J Physiol Pharmacol,* 70 Suppl**,** S248-54.

STEENBERGH, P. H., HOPPENER, J. W., ZANDBERG, J., VISSER, A., LIPS, C. J. & JANSZ, H. S. 1986. Structure and expression of the human calcitonin/CGRP genes. *FEBS Lett,* 209**,** 97-103.

STORER, R. J. & GOADSBY, P. J. 1997. Microiontophoretic application of serotonin (5HT)1B/1D agonists inhibits trigeminal cell firing in the cat. *Brain,* 120 (Pt 12)**,** 2171-7.

STRONG, A. J., TOMLINSON, B. E., VENABLES, G. S., GIBSON, G. & HARDY, J. A. 1983. The cortical ischaemic penumbra associated with occlusion of the middle cerebral artery in the cat: 2. Studies of histopathology, water content, and in vitro neurotransmitter uptake. *J Cereb Blood Flow Metab,* 3**,** 97-108.

SUGRUE, M. M., BRUGGE, J. S., MARSHAK, D. R., GREENGARD, P. & GUSTAFSON, E. L. 1990. Immunocytochemical localization of the neuron-specific form of the c-src gene product, pp60c-src(+), in rat brain. *J Neurosci,* 10**,** 2513-27.

SUKHOTINSKY, I., DILEKOZ, E., WANG, Y., QIN, T., EIKERMANN-HAERTER, K., WAEBER, C. & AYATA, C. 2011. Chronic daily cortical spreading depressions suppress spreading depression susceptibility. *Cephalalgia,* 31**,** 1601-8.

TAKAGI, N., CHEUNG, H. H., BISSOON, N., TEVES, L., WALLACE, M. C. & GURD, J. W. 1999. The effect of transient global ischemia on the interaction of Src and Fyn with the N-methyl-D-aspartate receptor and postsynaptic densities: possible involvement of Src homology 2 domains. *J Cereb Blood Flow Metab,* 19**,** 880-8.

TEPE, N., FILIZ, A., DILEKOZ, E., AKCALI, D., SARA, Y., CHARLES, A. & BOLAY, H. 2015. The thalamic reticular nucleus is activated by cortical spreading depression in freely moving rats: prevention by acute valproate administration. *Eur J Neurosci,* 41**,** 120-8.

TERASAKI, Y., SASAKI, T., YAGITA, Y., OKAZAKI, S., SUGIYAMA, Y., OYAMA, N., OMURA-MATSUOKA, E., SAKODA, S. & KITAGAWA, K. 2010. Activation of NR2A receptors

induces ischemic tolerance through CREB signaling. *J Cereb Blood Flow Metab,* 30**,** 1441-9.

TFELT-HANSEN, P. C. 2010. History of migraine with aura and cortical spreading depression from 1941 and onwards. *Cephalalgia,* 30**,** 780-92.

THOMAS, S. M. & BRUGGE, J. S. 1997. Cellular functions regulated by Src family kinases. *Annu Rev Cell Dev Biol,* 13**,** 513-609.

THOMPSON, R. J. 2015. Pannexin channels and ischaemia. *J Physiol,* 593**,** 3463-70.

THOMPSON, R. J., JACKSON, M. F., OLAH, M. E., RUNGTA, R. L., HINES, D. J., BEAZELY, M. A., MACDONALD, J. F. & MACVICAR, B. A. 2008. Activation of pannexin-1 hemichannels augments aberrant bursting in the hippocampus. *Science,* 322**,** 1555-9.

THOMPSON, R. J., ZHOU, N. & MACVICAR, B. A. 2006. Ischemia opens neuronal gap junction hemichannels. *Science,* 312**,** 924-7.

TORRENTE, D., MENDES-DA-SILVA, R. F., LOPES, A. A., GONZALEZ, J., BARRETO, G. E. & GUEDES, R. C. 2014. Increased calcium influx triggers and accelerates cortical spreading depression in vivo in male adult rats. *Neurosci Lett,* 558**,** 87-90.

TOZZI, A., DE IURE, A., DI FILIPPO, M., COSTA, C., CAPRONI, S., PISANI, A., BONSI, P., PICCONI, B., CUPINI, L. M., MATERAZZI, S., GEPPETTI, P., SARCHIELLI, P. & CALABRESI, P. 2012. Critical role of calcitonin gene-related peptide receptors in cortical spreading depression. *Proc Natl Acad Sci U S A,* 109**,** 18985-90.

UNEKAWA, M., TOMITA, Y., TORIUMI, H. & SUZUKI, N. 2012. Suppressive effect of chronic peroral topiramate on potassium-induced cortical spreading depression in rats. *Cephalalgia,* 32**,** 518-27.

URBACH, A., BRUEHL, C. & WITTE, O. W. 2006. Microarray-based long-term detection of genes differentially expressed after cortical spreading depression. *Eur J Neurosci,* 24**,** 841-56.

VAN DONGEN, R. M., ZIELMAN, R., NOGA, M., DEKKERS, O. M., HANKEMEIER, T., VAN DEN MAAGDENBERG, A. M., TERWINDT, G. M. & FERRARI, M. D. 2016. Migraine biomarkers in cerebrospinal fluid: A systematic review and meta-analysis. *Cephalalgia*.

VAN HARREVELD, A. 1959. Compounds in brain extracts causing spreading depression of cerebral cortical activity and contraction of crustacean muscle. *J Neurochem,* 3**,** 300-15.

VANDESOMPELE, J., DE PRETER, K., PATTYN, F., POPPE, B., VAN ROY, N., DE PAEPE, A. & SPELEMAN, F. 2002. Accurate normalization of real-time quantitative RT-PCR data by geometric averaging of multiple internal control genes. *Genome Biol,* 3**,** Research0034.

VECSEI, L., SZOK, D., CSATI, A. & TAJTI, J. 2015. CGRP antagonists and antibodies for the treatment of migraine. *Expert Opin Investig Drugs,* 24**,** 31-41.

VIANA, M., LINDE, M., SANCES, G., GHIOTTO, N., GUASCHINO, E., ALLENA, M., TERRAZZINO, S., NAPPI, G., GOADSBY, P. J. & TASSORELLI, C. 2016. Migraine aura symptoms: Duration, succession and temporal relationship to headache. *Cephalalgia,* 36**,** 413-21.

VON BAUMGARTEN, L., TRABOLD, R., THAL, S., BACK, T. & PLESNILA, N. 2008. Role of cortical spreading depressions for secondary brain damage after traumatic brain injury in mice. *J Cereb Blood Flow Metab,* 28**,** 1353-60.

VON ENGELHARDT, J., COSEREA, I., PAWLAK, V., FUCHS, E. C., KOHR, G., SEEBURG, P. H. & MONYER, H. 2007. Excitotoxicity in vitro by NR2A- and NR2B-containing NMDA receptors. *Neuropharmacology,* 53**,** 10-7.

WANG, H., CAO, Y., CHIANG, C. Y., DOSTROVSKY, J. O. & SESSLE, B. J. 2014a. The gap junction blocker carbenoxolone attenuates nociceptive behavior and medullary dorsal horn central sensitization induced by partial infraorbital nerve transection in rats. *Pain,* 155**,** 429-35.

WANG, J. Q., GUO, M. L., JIN, D. Z., XUE, B., FIBUCH, E. E. & MAO, L. M. 2014b. Roles of subunit phosphorylation in regulating glutamate receptor function. *Eur J Pharmacol,* 728**,** 183-7.

WANG, M., CHAZOT, P. L., ALI, S., DUCKETT, S. F. & OBRENOVITCH, T. P. 2012. Effects of NMDA receptor antagonists with different subtype selectivities on retinal spreading depression. *Br J Pharmacol,* 165**,** 235-44.

WANG, M., LI, Y. & LIN, Y. 2015. GABAA receptor alpha2 subtype activation suppresses retinal spreading depression. *Neuroscience,* 298**,** 137-44.

WANG, M., OBRENOVITCH, T. P. & URENJAK, J. 2003. Effects of the nitric oxide donor, DEA/NO on cortical spreading depression. *Neuropharmacology,* 44**,** 949-57.

WANG, Y., LI, Y. & WANG, M. 2016a. Involvement of CGRP receptors in retinal spreading depression. *Pharmacol Rep,* 68**,** 935-8.

WANG, Y., TYE, A. E., ZHAO, J., MA, D., RADDANT, A. C., BU, F., SPECTOR, B. L., WINSLOW, N. K., WANG, M. & RUSSO, A. F. 2016b. Induction of calcitonin gene-related peptide expression in rats by cortical spreading depression. *Cephalalgia*.

WATANABE, M., MISHINA, M. & INOUE, Y. 1994. Distinct spatiotemporal expressions of five NMDA receptor channel subunit mRNAs in the cerebellum. *J Comp Neurol,* 343**,** 513-9.

WEILINGER, N. L., LOHMAN, A. W., RAKAI, B. D., MA, E. M., BIALECKI, J., MASLIEIEVA, V., RILEA, T., BANDET, M. V., IKUTA, N. T., SCOTT, L., COLICOS, M. A., TESKEY, G. C., WINSHIP, I. R. & THOMPSON, R. J. 2016. Metabotropic NMDA receptor signaling couples Src family kinases to pannexin-1 during excitotoxicity. *Nat Neurosci,* 19**,** 432-42.

WEILINGER, N. L., TANG, P. L. & THOMPSON, R. J. 2012. Anoxia-induced NMDA receptor activation opens pannexin channels via Src family kinases. *J Neurosci,* 32**,** 12579-88.

WILLETTE, R. N., LYSKO, P. G. & SAUERMELCH, C. F. 1994. A comparison of (+)SK&F 10047 and MK-801 on cortical spreading depression. *Brain Res,* 648**,** 347-51.

WIMALAWANSA, S. J., MORRIS, H. R., ETIENNE, A., BLENCH, I., PANICO, M. & MACINTYRE, I. 1990. Isolation, purification and characterization of beta-hCGRP from human spinal cord. *Biochem Biophys Res Commun,* 167**,** 993-1000.

WOLF, H. K., BUSLEI, R., SCHMIDT-KASTNER, R., SCHMIDT-KASTNER, P. K., PIETSCH, T., WIESTLER, O. D. & BLUMCKE, I. 1996. NeuN: a useful neuronal marker for diagnostic histopathology. *J Histochem Cytochem,* 44**,** 1167-71.

YAN WANG, A. E. T., JUNLI ZHAOA, DONGQING MAAB, ANN C RADDANT, FAN BUA, BENJAMIN L SPECTOR, NOLAN K WINSLOW, MINYAN WANG, ANDREW F RUSSO 2016. Induction of calcitonin gene-related peptide expression in rats by cortical spreading depression.

Cephalalgia, 0**,** 9.

YANG, M. & LEONARD, J. P. 2001. Identification of mouse NMDA receptor subunit NR2A C-terminal tyrosine sites phosphorylated by coexpression with v-Src. *J Neurochem*, 77**,** 580-8.

YAVICH, L. & YLINEN, A. 2005. Spreading depression in the cortex differently modulates dopamine release in rat mesolimbic and nigrostriatal terminal fields. *Exp Neurol*, 196**,** 47-53.

YEATMAN, T. J. 2004. A renaissance for SRC. *Nat Rev Cancer*, 4**,** 470-80.

YILDIRIM, T., EYLEN, A., LULE, S., ERDENER, S. E., VURAL, A., KARATAS, H., OZVEREN, M. F., DALKARA, T. & GURSOY-OZDEMIR, Y. 2015. Poloxamer-188 and citicoline provide neuronal membrane integrity and protect membrane stability in cortical spreading depression. *Int J Neurosci*, 125**,** 941-6.

YISARAKUN, W., CHANTONG, C., SUPORNSILPCHAI, W., THONGTAN, T., SRIKIATKHACHORN, A., REUANGWECHVORACHAI, P. & MANEESRI-LE GRAND, S. 2015. Up-regulation of calcitonin gene-related peptide in trigeminal ganglion following chronic exposure to paracetamol in a CSD migraine animal model. *Neuropeptides*, 51**,** 9-16.

ZHANG, F., LI, C., WANG, R., HAN, D., ZHANG, Q. G., ZHOU, C., YU, H. M. & ZHANG, G. Y. 2007. Activation of GABA receptors attenuates neuronal apoptosis through inhibiting the tyrosine phosphorylation of NR2A by Src after cerebral ischemia and reperfusion. *Neuroscience*, 150**,** 938-49.

ZHANG, X., LEVY, D., KAINZ, V., NOSEDA, R., JAKUBOWSKI, M. & BURSTEIN, R. 2011. Activation of central trigeminovascular neurons by cortical spreading depression. *Ann Neurol*, 69**,** 855-65.

ZHANG, X., LEVY, D., NOSEDA, R., KAINZ, V., JAKUBOWSKI, M. & BURSTEIN, R. 2010. Activation of meningeal nociceptors by cortical spreading depression: implications for migraine with aura. *J Neurosci*, 30**,** 8807-14.

ZHOU, N., GORDON, G. R., FEIGHAN, D. & MACVICAR, B. A. 2010. Transient swelling, acidification, and mitochondrial depolarization occurs in neurons but not astrocytes during spreading depression. *Cereb Cortex*, 20**,** 2614-24.

ZOIDL, G., PETRASCH-PARWEZ, E., RAY, A., MEIER, C., BUNSE, S., HABBES, H. W., DAHL, G. & DERMIETZEL, R. 2007. Localization of the pannexin1 protein at postsynaptic sites in the cerebral cortex and hippocampus. *Neuroscience,* 146**,** 9-16.

List of Abbreviations

Acetycholine	ACh
Alternating current	AC
α-amino-3-hydroxy-5-methyl-4-isoxazolepropionic acid	AMPA
Area of interest	AOI
Area under the curve	AUC
Artificial cerebral spinal fluid	ACSF
Blood-oxygen level-dependent	BOLD
Calmodulin	CaM
Cerebral blood flow	CBF
Calcitonin gene-related peptide	CGRP
Central nervous system	CNS
Cerebral metabolic rate of O_2	$CMRO_2$
Cortical spreading depression	CSD
Direct current	DC
Delay	D
Direct current	DC
Dimethylsulfoxide	DMSO
Electroencephalogram	EEG
Height	H
High-mobility group box 1	HMGB1
Intracerebroventricular	i.c.v.
Immunohistochemistry	IHC
Kainite	KA
Latency	L
Slope of depolarization	Sld
Magnetic resonance imaging	MRI
Slope of repolarization	Slr
NADH dehydrogenase subunit 2	ND2
N-methyl-D-aspartic	NMDA
Nitric oxide	NO

Neuronal nitric oxide synthase	nNOS
Pannexin	Panx
Paraformaldehyde fixative	PFA
Peptidylprolyl isomerase A	PPIA
Postsynaptic density protein 95	PSD95
Pre-amplifier	PREAMP
Propidium iodide	PI
Quantitative polymerase chain reaction	qPCR
Retinal spreading depression	RSD
Room temperature	RT
Sarcoma family kinases	SFKs
Sodium phosphate buffer	PBS
Traumatic brain injury	TBI
Tris-buffered saline	TBS
Width at half height	W

Publications and Presentations

Publications

BU, F., DU, R., LI, Y., QUINN, J. P. & WANG, M. 2016. NR2A contributes to genesis and propagation of cortical spreading depression in rats. Sci Rep, 6, 23576.

WANG, Y., TYE, A. E., ZHAO, J., MA, D., RADDANT, A. C., **BU, F.**, SPECTOR, B. L., WINSLOW, N. K., WANG, M. & RUSSO, A. F. 2016b. Induction of calcitonin gene-related peptide expression in rats by cortical spreading depression. Cephalalgia.

Poster Presentations

BU, F., QUINN, J. P. & WANG, M. 09/2016. Critical Role of Src Family Kinases in Cortical Spreading Depression. The 5th European Headache and Migraine Trust International Congress. Glasgow, UK.

WANG, M., **BU, F.** & QUINN, J. P. 09/2016. NR2A-containing NMDA Receptors Contribute to CSD-induced Panx1 Channels Opening via Src Family Kinases. The 5th European Headache and Migraine Trust International Congress. Glasgow, UK.

BU, F., QUINN, J. P. & WANG, M. 09/2015. NR2A Regulates PANX1 and Src Activation in Early Stage of Migraine. The 6th FAONS Congress and 11th Biennial Conference of CNS. Tongxiang, China.

BU, F., QUINN, J. P. & WANG, M. 05/2014. NR2A Plays a Key Role in Mediating CSD Genesis - a potential strategy against migraine with aura. BIT's 5th World Congress of Neuro Talk. Nanjing, China.

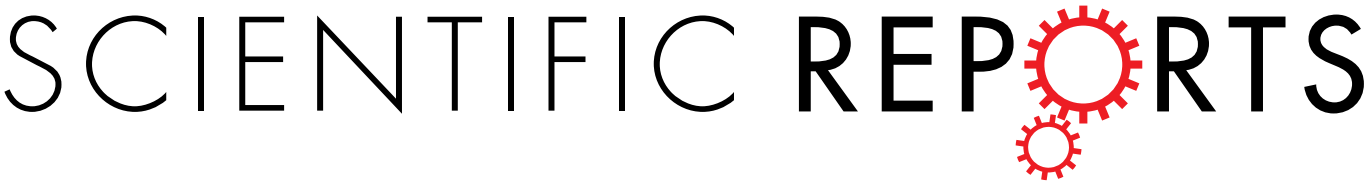

OPEN

NR2A contributes to genesis and propagation of cortical spreading depression in rats

Received: 05 November 2015
Accepted: 08 March 2016
Published: 22 March 2016

Fan Bu[1,2], Ruoxing Du[2], Yi Li[3], John P Quinn[4] & Minyan Wang[1,2]

Cortical spreading depression (CSD) is a transient propagating excitation of synaptic activity followed by depression, which is implicated in migraine. Increasing evidence points to an essential role of NR2A-containing NMDA receptors in CSD propagation *in vitro*; however, whether these receptors mediate CSD genesis *in vivo* requires clarification and the role of NR2A on CSD propagation is still under debate. Using *in vivo* CSD in rats with electrophysiology and *in vitro* CSD in chick retina with intrinsic optical imaging, we addressed the role of NR2A in CSD. We demonstrated that NVP-AAM077, a potent antagonist for NR2A-containing receptors, perfused through microdialysis probes, markedly reduced cortex susceptibility to CSD, but also reduced magnitude of CSD genesis in rats. Additionally, NVP-AAM077 at 0.3 nmol perfused into the contralateral ventricle, considerably suppressed the magnitude of CSD propagation wave and propagation rate in rats. This reduction in CSD propagation was also observed with TCN-201, a negative allosteric modulator selective for NR2A, at 3 μM, in the chick retina. Our data provides strong evidence that NR2A subunit contributes to CSD genesis and propagation, suggesting drugs selectively antagonizing NR2A-containing receptors might constitute a highly specific strategy treating CSD associated migraine with a likely better safety profile.

Cortical Spreading Depression (CSD) is a temporary excitation of synaptic activity[1,2], followed by depression that propagates slowly across the cerebral cortex. CSD is implicated in pathophysiological mechanisms of migraine aura[3–5] and may lead to migraine headache via central modulation involving the activation of neuronal PANX1 protein[6]. CSD is accompanied by a rapid disruption of ionic homeostasis, release of neurotransmitters, neuropeptides and changes in cerebral blood flow; however, the molecular pathways that mediate the initial phase of CSD and its role in the development of migraine are still poorly understood.

N-methyl-D-aspartate (NMDA) receptor activation is known to contribute to CSD genesis and propagation as the non-competitive inhibitor, MK801, appears to be the most effective anti-CSD compound in rats[7,8]. However, this drug is perceived as an unlikely anti-CSD candidate for migraine aura treatment because of unacceptable side effects resulting from the blockade of normal neuronal function[9,10]. The NMDA receptor is composed of two mandatory NR1 subunits and at least two NR2 (A-D) or a NR3 (A-B) subunit[11]. NR2A typically mediate synaptic transmission whereas NR2B-containing receptors are located extrasynaptically[12,13] on astrocytes[14]. Increasing evidence has demonstrated that these two major receptor subunits, NR2A[15] and NR2B[8,16] play critical roles in CSD modulation, thus drugs selectively antagonizing these subunits have been proposed as potential candidates for migraine therapy, having better efficacy and a better safety profile[8,15].

However, whether NR2A-containing receptors modulate susceptibility of the cortex to CSD is unknown. Additionally, whether NR2A-containing receptors contribute to CSD propagation is still a matter of debate[15,16]. We have demonstrated that inhibition of NR2A-containing receptors by NVP-AAM077, an antagonist that is preferably selective for NR2A at the concentration applied, resulted in suppression of CSD propagation in chick retina, a tissue which lacks blood vessels[15], suggesting involvement of neuronal and glial activity. However, using blood oxygen level dependent (BOLD) fMRI approach, NR2A inhibition under TCN-201, a negative allosteric modulator selective for NR2A-containing NMDA receptors, application did not alter CSD propagation features in rats[16]. Therefore, the role of NR2A in CSD propagation requires further clarification *in vivo*.

[1]Department of Biological Sciences, Xi'an Jiaotong-Liverpool University, Suzhou, 215123, China. [2]Centre for Neuroscience, Xi'an Jiaotong-Liverpool University, Suzhou, 215123, China. [3]Department of Applied Chemistry, Xi'an Jiaotong-Liverpool University, Suzhou, 215123, China. [4]Department of Molecular and Clinical Pharmacology, Institute of Translational Medicine, University of Liverpool, Liverpool, L69 7ZB, UK. Correspondence and requests for materials should be addressed to M.W. (email: Minyan.wang@xjtlu.edu.cn)

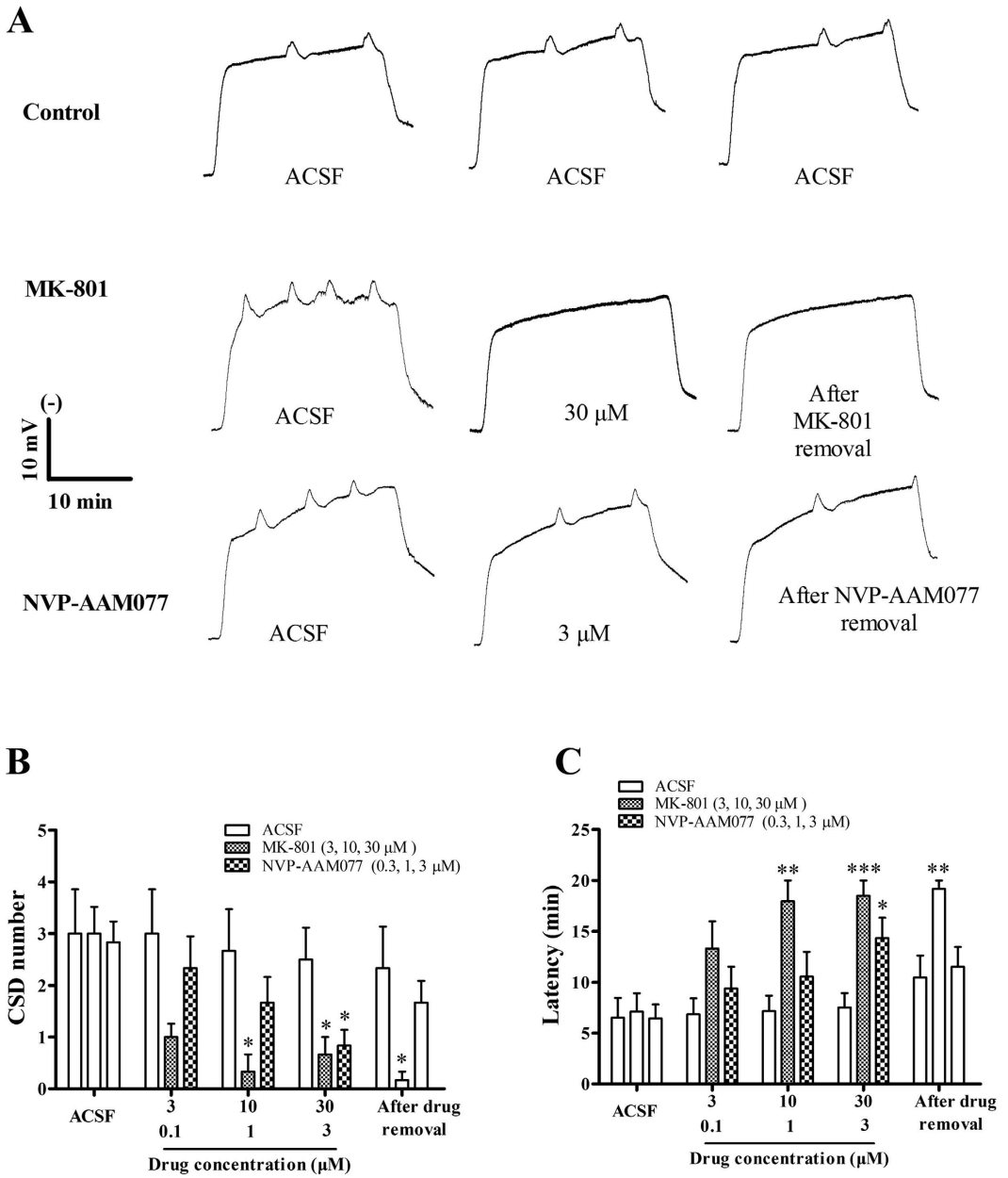

Figure 1. Representative CSD traces (**A**) and effects of MK-801 and NVP-AAM077 on tissue susceptibility to CSD induced by high K^+ perfused through the microdialysis probe. Three groups including ACSF solution ($n = 6$) as control, MK-801 ($n = 6$) and NVP-AAM077 ($n = 6$) were considered. All the values given are means ± SEM. One-way ANOVA test was used for statistics of multiple comparisons, with subsequent Bonferonni test for significance between control and drug treatment groups ($*p < 0.05$, $**p \leq 0.01$, $***p \leq 0.001$). Paired *t*-test used to test whether tissue was restored after drug removal between the 4th and 5th CSD episodes.

The primary aim of this study was to explore the role of NR2A-containing receptors in CSD genesis and propagation in rats by investigating effects of NVP-AAM077. The involvement of NR2A in CSD propagation was subsequently confirmed using another pharmacological tool TCN-201 at concentrations selective for binding to NR2A in chick retina.

Results

Validation of microdialysis-based CSD model under isoflurane anaesthesia. At the CSD genesis site of the control group (ACSF, $n = 6$), the average number, latency and the magnitude of the 1st CSD episode was 3.0 ± 0.86 (Fig. 1B), 6.53 ± 1.93 minutes (Fig. 1C) and 4.95 ± 1.06 mV × minute (Fig. 2A, $n = 6$), in respective order. There was no significant difference in any of these parameters over the five repeated CSD episodes (Figs 1B,C and 2A). To validate the CSD model under anesthesia with isoflurane, the non-competitive NMDA

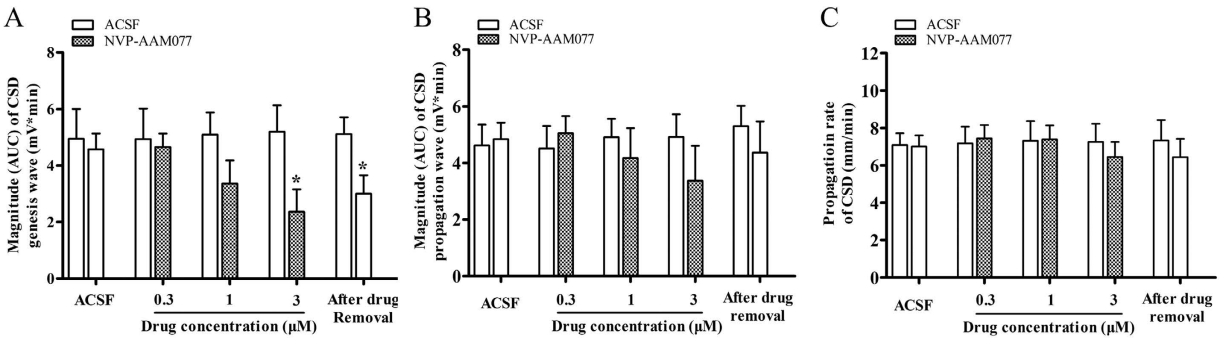

Figure 2. Effects of NVP-AAM077 perfused through the microdialysis probe on the magnitude of both CSD genesis (**A**), propagation waves (**B**) and propagation rate (**C**). All the values shown are means ± SEM. Unpaired t-test was used for statistical analysis for significance between the drug ($n = 6$) and control group ($n = 6$) (*$p < 0.05$). Paired *t*-test used to test whether tissue was restored after drug removal between the 4th and 5th CSD episodes.

receptor antagonist, MK801, with known anti-CSD effect[7,15], was examined through the microdialysis probe. MK-801 suppressed CSD genesis in a concentration dependent manner (Fig. 1, $n = 6$). MK801 at 30 μM significantly reduced CSD number (0.67 ± 0.33) compared to the control group (2.5 ± 0.62) (One-Way ANOVA, $p = 0.019$, $F = 5.236$) (Fig. 1B). At this concentration, CSD latency increased 2.5-folds by MK801 compared to the control group (One-Way ANOVA, $p = 0.001$, $F = 9.88$) (Fig. 1C) and CSD waves were completely abolished in five out of six experiments during the 20-minute recording period (Fig. 1A). This inhibitory effect of MK801 on CSD was persistent after the drug removal (*i.e.* in the 5th CSD episode, Fig. 1A–C).

Suppression of CSD genesis by NVP-AAM077 applied through microdialysis. To investigate whether NVP-AAM077 alters CSD genesis, the microdialysis-based CSD model was used for local application of both K^+-medium and the drug. In the control group, CSD number in the 2nd, 3rd and 4th episodes was 3.0 ± 0.86, 2.67 ± 0.8, and 2.53 ± 0.62 respectively (Fig. 1A,B, $n = 6$). NVP-AAM077 at 0.3, 1 and 3 μM perfused through microdialysis probes concentration dependently reduced CSD number to 2.33 ± 0.61, 1.67 ± 0.49 and 0.83 ± 0.31 in respectively order (Fig. 1A,B, $n = 6$). At the highest concentration applied, the reduction in CSD number reached significance ($p = 0.036$, $F = 5.236$, $n = 6$, Fig. 1B).

In the control group, CSD latency in the 2nd, 3rd and 4th CSD episodes was 6.85 ± 1.57, 7.18 ± 1.52, and 7.52 ± 1.41 minutes, in respective order (Fig. 1A). Conversely to CSD number, NVP-AAM077 all three concentrations applied prolonged CSD latency to 9.39 ± 2.15, 10.56 ± 2.43 and 13.94 ± 2.23 minutes in the corresponding CSD episodes. The drug at 3 μM perfused through the microdialysis probe significantly prolonged CSD latency when compared with the corresponding control ($p = 0.041$, $F = 9.88$, Fig. 1A,C, $n = 6$). There was no significant effect of NVP-AAM077 on CSD number and latency after the drug removal.

In the control group, CSD magnitude in the 2nd, 3rd and 4th CSD episodes was 4.94 ± 1.08, 5.45 ± 0.86, and 5.20 ± 0.94 mV × minute, in respective order. NVP-AAM077 also significantly reduced CSD magnitude in a concentration dependent manner (Fig. 2A, $n = 6$). NVP-AAM077 at 0.3, 1 and 3 μM reduced the magnitude to 4.66 ± 0.48, 3.36 ± 0.82 and 2.36 ± 0.79 (t-test, $p = 0.043$, $F = 1.411$) mV × minute, in respective order. This inhibitory effect slightly recovered to 3.00 ± 0.67 mV × minute after the drug removal, which, however, did not reach significance when compared with that of the 4th episode in NVP-AAM077 (3 μM) group.

Suppression of CSD propagation by NVP-AAM077 perfused into contralateral ventricle but not via the microdialysis probe. Distinct from that of NVP-AAM077 on CSD genesis, perfusion of NVP-AAM077 through the microdialysis probe was unable to alter the magnitude of CSD propagation wave at the propagation site (Fig. 2B, $n = 6$). This route of delivery did not alter the velocity of CSD at all concentrations tested when compared with the control group (Fig. 2C, $n = 6$).

To allow NVP-AAM077 diffusing to distant cortical layer for investigating CSD propagation under NR2A inhibition, perfusion of the drug into contralateral ventricle was performed (see methods). In the control group, the magnitude of CSD propagation wave at the anterior recording site (0.4 mm to bregma) and propagation rate was 5.67 ± 0.64 mV × minute, and 4.0 ± 0.2 mm/minute respectively (Fig. 3A,B, $n = 6$). There was no change of these parameters throughout the experiment. In contrast to that perfused via microdialysis probe, 0.3 nmol of NVP-AAM077 perfused into the contralateral ventricle significantly suppressed both the magnitude of CSD propagation wave (Fig. 3A, t-test, $p = 0.044$, $t = 2.302$) and propagation rate (Fig. 3B, t-test, $p = 0.013$, $t = 3.008$). In the drug group, the magnitude of CSD propagation wave was reduced to 4.20 ± 0.80 mV × minute compared to 6.37 ± 0.50 mV × minute in the control group (Fig. 3A, $n = 6$). Similarly, the propagation rate slowed down to 2.64 ± 0.27 mm/minutes compared to 4.02 ± 0.37 mm/minutes in the control group (Fig. 3B, $n = 6$) when measured between the two recording electrode implantation sites.

Suppression of CSD by TCN-201 in chick retina. To confirm NR2A-containing NMDA receptors are involved in CSD propagation, we examined the effect of TCN-201 that was previously reported to have better

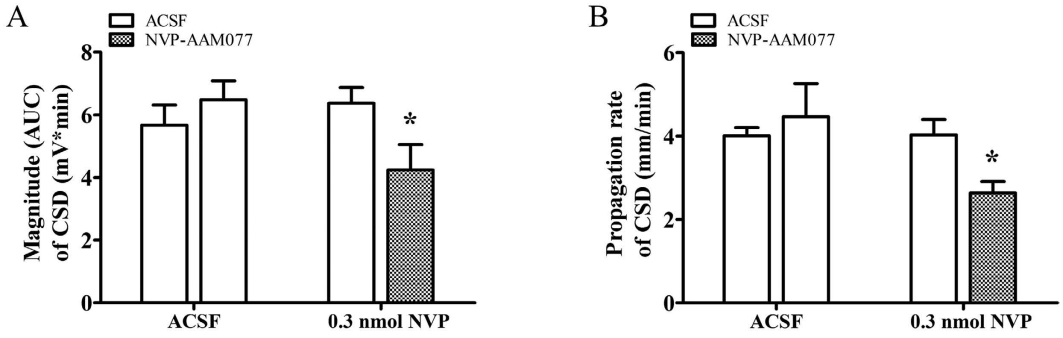

Figure 3. Effects of NVP-AAM077 perfused into the left lateral ventricle on the magnitude of CSD propagation (**A**) and propagation rate (**B**). All the values shown are means ± SEM. Unpaired t-test was used for statistical analysis for significance between the drug ($n = 6$) and control group ($n = 6$) ($^{*}p < 0.05$).

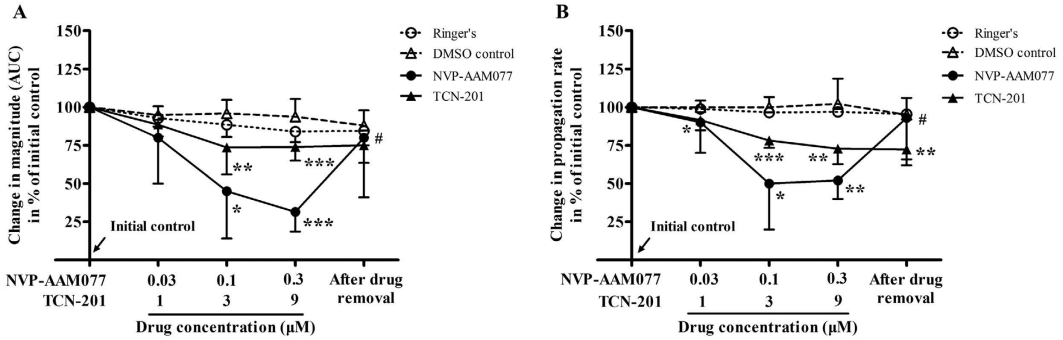

Figure 4. Effects of NVP-AAM077 ($n = 6$) and TCN-201 ($n = 6$) on the magnitude (**A**) and propagation rate (**B**) of CSD propagation induced by K^+ in the chick retina. Data was plotted as percentage of their initial levels and indicated as mean ± SD. Kruskal–Wallis test was used for statistical analysis of multiple comparisons, with subsequent Dunns test for significance ($^{*}p < 0.05$, $^{**}p \leq 0.01$, $^{***}p \leq 0.001$, TCN-201 *vs.* DMSO control ($n = 8$) or NVP-AAM077 *vs.* Ringer's control ($n = 6$)). Wilcoxon matched pairs test was used to test whether tissue was restored after drug removal ($^{\#}p < 0.05$, 0.3 μM NVP-AAM077 *vs.* drug removal).

selectivity for NR2A than NVP-AAM077[17] in CSD propagation in chick retina. Effect of NVP-AAM077 on CSD propagation was also designed for comparison.

In the Ringer's group, there was no significant change in the magnitude and propagation rate over repeated CSD episodes throughout the experiment (Fig. 4, $n = 6$). Compared with the Ringer's group, both CSD magnitude and propagation rate were markedly suppressed by NVP-AAM077 in a concentration-dependent manner (Fig. 4A,B, $n = 6$), which is in consistent with that reported previously[15]. At the maximum concentration tested (0.3 μM), the magnitude and propagation rate of CSD was reduced to 31.5% (Kruskal–Wallis test, $p = 0.0001$, $H = 20.47$) and 52% (Kruskal–Wallis test, $p = 0.003$, $H = 18.97$) of initial level respectively. This inhibitory effect significantly recovered to 80.2% (Wilcoxon matched pairs test, $p = 0.03$, $W = 21$) and 88.2% (Wilcoxon matched pairs test, $p = 0.032$, $W = 20.56$) of initial level after drug removal (high concentration *vs* drug removal).

Similar to the result of NVP-AAM077, but to a lesser extent, TCN-201 at both the medium and highest concentrations applied, markedly reduced the magnitude and propagation rate (Fig. 4A,B, $n = 6$), when compared with their respective DMSO group ($n = 8$). At 9 μM, the magnitude and propagation rate of RSD was reduced to 73.8% (Kruskal–Wallis test, $p = 0.0001$, $H = 20.47$) and 72.8% (Kruskal–Wallis test, $p = 0.003$, $H = 18.97$) of the initial level respectively. This inhibitory effect did not recover after drug removal (Fig. 4).

Discussion

Our *in vivo* data reveals, for the first time, a critical role of NR2A-containing receptors in CSD genesis as demonstrated by that NVP-AAM077 perfused via microdialysis probes not only reduced cortex susceptibility to K^+-induced CSD but also suppressed the magnitude of CSD elicitation in rats (Figs 1 and 2). Additionally, the electrophysiology study with NVP-AAM077 in rats (Fig. 3) and the application of TCN-201 in chick retina (Fig. 4) extended our previously findings on NR2A-containing receptor activation contributing to CSD propagation[15].

Validation of microdialysis-based CSD model under isoflurane anesthesia. Several studies reported that inhalational anaesthetics suppress CSD[18,19]. In this study, we still considered isoflurane anesthesia, but not pentobarbitone, which has the least action on CSD[20], for studying genesis and propagation of CSD for the following reasons: (1) our *in vivo* experiment lasted almost 7 hours, whereas barbiturates usually only

maintain anesthesia from several minutes to 4 hours[21], which did not meet our requirement; (2) Isoflurane has been widely used in other studies for studying CSD[8,16,22,23]; indeed, isoflurane provided a stable and consistent depth of anesthesia throughout the experiment and the concentration could be adjusted according to surgical and CSD recording procedures under study; whereas barbiturates generally result in uneven levels of anesthesia[21]; (3) Under isoflurane anaesthesia, the profound inhibitory effects of MK801 on CSD magnitude and susceptibility of the cortex to CSD (Fig. 1) were consistent with those reported previously[24,25]; (4) The fact that neither genesis nor propagation of CSD was altered in the control group yet was suppressed by NVP-AAM077, suggests that the suppression of CSD was due to NR2A inhibition, rather than to isoflurane. Collectively, the above evidence validates that the *in vivo* study under isoflurane anaesthesia is feasible and valid for assessing CSD genesis and propagation for NMDA receptor pharmacology.

NR2A-containing receptors mediate both CSD genesis and propagation. NVP-AAM077 markedly suppressed K^+-induced CSD number and increased CSD latency when perfused via microdialysis probes at 0.3 μM (Fig. 1). The reduced cortex susceptibility to CSD under NR2A inhibition extended our previous finding on the crucial role NR2A-containing receptors in mediating CSD propagation[15].

Surprisingly, local application of NVP-AAM077 at 0.3 μM through the microdialysis probe did not alter the magnitude of CSD propagation wave and propagation rate in rats (Fig. 2B,C), which is in contrast to that was reported in chick retina, in that NVP-AAM077 was effective in suppressing CSD propagation rate and magnitude[15]. We suspected that this negative result *in vivo* may be attributed to the fact that the anterior CSD propagation site was not exposed to NVP-AAM077 when the drug was locally perfused through microdialysis probes at the CSD elicitation site (Fig. 5A). To clarify whether NVP-AAM077 was effective in CSD propagation *in vivo*, contralateral ventricle perfusion of NVP-AAM077 (total 0.3 nmol) was considered as this would allow the drug to diffuse to distant cortex by following cerebrospinal fluid flow. Indeed, it has previously been demonstrated in rats that a larger molecule, insulin, could flow to almost the whole cortex in rats within 2 hours after contralateral ventricle injection, with approximate 1/100 of the drug distributed to the contralateral cortical tissue 30 minutes after injection[26]. In our study, as expected, the 0.3 nmol of NVP-AAM077 perfused into the contralateral ventricle was found to markedly suppress both the magnitude of CSD propagation wave (Fig. 3A) and propagation rate in rats (Fig. 3B), confirming NR2A mediates CSD propagation[15].

The importance of NR2A in CSD propagation was further supported by the action of TCN-201 (Fig. 4), which has 300-fold selectivity to NR2A compared with NR2B-containing receptors[17]. Indeed, at the medium concentration of 3 μM of the drug applied, suppressive effects on both propagation rate and magnitude of CSD propagation wave was observed in chick retina (Fig. 4). As the chick retina is devoid of blood vessels, the fact that the inhibitory effect of TCN-201 and NVP-AAM077 on CSD propagation under our study suggests an involvement of neuronal or glial mechanism under NR2A inhibition. Interestingly, this data on TCN-201 in chick retina is in contrast to a recent study employing BOLD fMRI approach, which showed that TCN-201 was ineffective in CSD BOLD response in rats[16]. The discrepancy may be attributed to different methods applied for CSD recording: BOLD fMRI[16] that is largely based on brain-specific hemodynamic responses *versus* intrinsic optical signal that is based on neuronal activity of chick retina (Fig. 4). Whether TCN-201 could alter CSD *in vivo* using an electrophysiology approach where neuronal activities could be monitored requires further investigation. It is noted that the efficacy of TCN-201 against CSD in chick retina is >30-fold lower than that of NVP-AAM077 (Fig. 4A). This suggests that a much higher concentration of TCN-201 may be needed for sufficient binding to its receptors in future *in vivo* studies for effectiveness of the drug on CSD. Further studies using NR2A knockout animals will also help to elucidate the role of NR2A in CSD.

Elucidation of the inhibitory effects of NVP-AAM077 on CSD in *in vivo* suggests that NVP-AAM077 or such drug-alike candidates targeting NR2A may constitute a highly specific strategy with better efficacy and safety profile for treating CSD associated migraine aura, relative to non-subtype selective NMDA receptors[15]. This possibility is likely due to the following reasons: (1) NVP-AAM077 suppressed CSD in chick retina (Fig. 4) with approximately 320-fold more potency than memantine[8], a clinically acceptable drug for treating migraines[27]. (ii) Partial inhibition of CSD by NVP-AAM077 in rats was also observed with the non-competitive NR2A subunit antagonist, memantine[8,9]. (iii) The rapid reversibility of NVP-AAM077 after the drug withdrawal (Figs 1–3) resulting from its competitive antagonism supports a likely better safety profile. (iv) Our latest preliminary data demonstrated that using a clinical acceptable route of administration (intravenous), pre-treatment of NVP-AAM077, at a dose of 2.4 mg/kg that preferably antagonizes NR2A-containing receptors[28], suppressed tissue susceptibility to CSD induced by topical application of KCl (data was not shown).

Mechanism contributing to the role of NR2A in CSD. The present data suggests activation of NR2A-containing receptors contributes to CSD genesis and propagation. There are several mechanisms which may explain the nature of CSD modulation by NVP-AAM077 and TCN-201 *in vivo* and *in vitro*. It is likely that inhibition of CSD genesis and propagation wave under NR2A inhibition is attributed to their ability to desensitize neurons (as NVP-AAM077 competitively blocks steady-state NR1/NR2A receptor currents from a cortical neuron)[29]; whereas TCN-201 accelerates NR1/NR2A receptor deactivation[30]. This notion was supported by that the inhibitory effect of NVP-AAM077 and TCN-201 on CSD propagation was observed in the chick retina, a tissue devoid of blood vessels, suggesting neuronal mechanism under NR2A inhibition. Alternatively, the suppression of CSD in response to NR2A inhibition may be based on the NR2A-mediated steady-state current permitting calcium ion influx in neurons[31]; whilst the increased calcium influx triggers and accelerates CSD in rats[32]. Finally, the role of NR2A in CSD may also be associated with its interaction with postsynaptic density protein 95 (PSD95) as NMDA receptor desensitization can be regulated by direct binding of NR2 to PDZ1-2 domains of PSD95 in neuronal and non-neuronal cells[33]. Further investigations are required to understand mechanism underlying NR2A-containing receptors in mediating CSD genesis and propagation. It is known that the NR2B

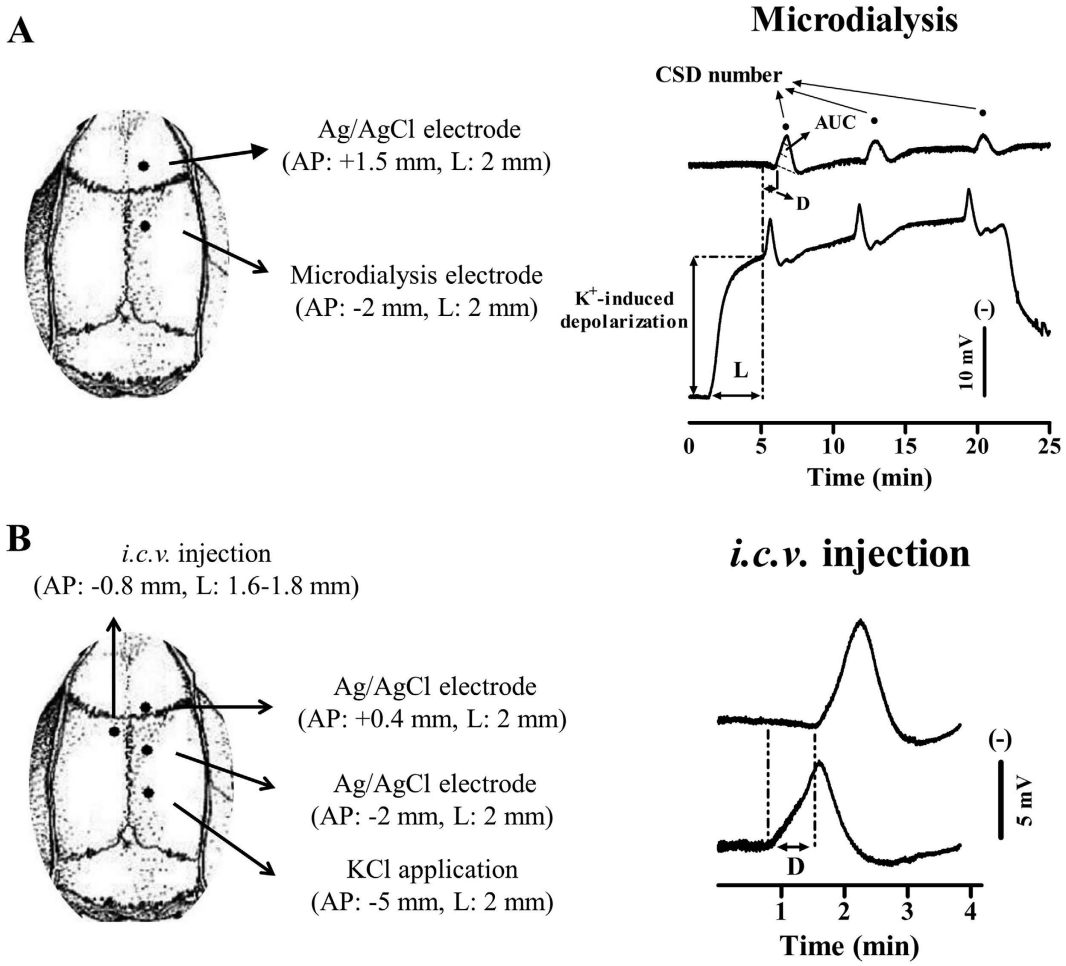

Figure 5. Schematic representation of electrode implantation sites (left) and representative traces in DC potential of CSD (right) induced by K^+ through microdialysis probe (upper) and topical application (lower) in the anaesthesized rat. (**A**) In microdialysis based CSD experiment (upper), CSD wave in the genesis site was recorded by perfusion of 250 mM KCl through the microdialysis probe implanted at 2 mm posterior to bregma in the rat right cortex. CSD propagation wave was simultaneously recorded through the Ag/AgCl electrode implanted at 1.5 mm anterior to bregma. Drugs or ACSF was perfused through the microdialysis probe for pharmacology study. (**B**) In intracerebral ventricle (*i.c.v*) based experiment (lower), CSD was induced by topical application of 3 M KCl through the hole with dura intact at 5 mm posterior to bregma in the right skull. CSD propagation wave was recorded at both 2 mm posterior to and 0.4 mm anterior to bregma. The drug or ACSF was perfused into contralateral ventricle through a cannula implanted (lower left). CSD magnitude is indicated as Area under the curve (AUC, dotted line, right upper trace). CSD latency (L) and CSD number are used to assess the susceptibility of the cortex to K^+ induced CSD. CSD propagation rate is used to assess the susceptibility of the cortex to CSD propagation as calculated by the distance dividing by the time delay (D, right).

containing NMDA receptor is also involved in CSD elicitation and propagation in rats using electrophysiology[8] and BOLD fMRI[16]. Therefore, it is reasonable to propose that CSD genesis and propagation requires both NR2A and NR2B activation. Further synergistic effect on CSD under both NR2A and NR2B inhibition *in vivo* remains to be examined.

In summary, our data provides strong evidence that NR2A subunit contributes to CSD genesis and propagation, suggesting drugs selectively antagonizing NR2A-containing receptors might constitute a highly specific strategy treating CSD associated migraine with a likely better safety profile.

Methods

All animal procedures were approved by the Ethical Review Panels of Soochow University and performed in accordance with the associated guidelines. All efforts were made to minimize animal suffering to reduce the number of animals used.

***In vivo* CSD in rats with electrophysiology.** *Animal use and anaesthesia.* Adult, male Sprague Dawley rats ($n = 30$, 317 ± 40 g, mean $\pm$ SD, Shanghai SLAC Laboratory Animal Corporation Ltd) were housed with food

and water available *ad libitum*. Rats were anaesthetised with isoflurane (5% for induction, 2.5–3.5% during the surgery, 1–1.5% for maintenance) in O_2:N_2O (1:2), with the animal breathing spontaneously. The depth of anaesthesia was monitored and adjusted through careful examination of the electroencephalogram (EEG) signal and through observation of the animal. Rectal temperature of animals was maintained at 37 °C. CSD induction was carried out one hour after the surgery for tissue stabilization.

Microdialysis-based CSD experiment. To record CSD genesis and propagation waves, two burr holes were drilled on the right parietal bone (Fig. 5A). (i) Microdialysis probes incorporating an electrode (ME-H1, Applied Neuroscience, London) were implanted through the posterior burr hole (coordinates: 2 mm posterior and 2 mm lateral to bregma, 1.4–1.5 mm deep from the cortical surface) for recording of CSD genesis waves; (ii) Ag/AgCl electrodes (0.1 mm i.d, Applied Neuroscience, London) were implanted into the ipsilateral cortex through the anterior burr hole (coordinates: 1.5 mm anterior and 2 mm lateral to bregma, 0.9 mm deep from the cortical surface) for recording of CSD propagation waves; separate Ag/AgCl reference electrodes were placed under the scalp of rats. EEG and Direct Current (DC) potential were derived from the potential between microdialysis probes or Ag/AgCl electrodes and reference electrodes. The microdialysis probe was perfused with artificial cerebrospinal fluid (ACSF) at 1 µl/minute with a syringe pump (CMA100, CMA/Microdialysis, Solna, Sweden). For CSD elicitation, a medium containing 250 mM K^+ (K^+-medium, composition in mM: 2.5 NaCl, 250 KCl, 1.18 $MgCl_2$, 1.26 $CaCl_2$; pH 7.3 adjusted with 1 M NaOH, not buffered) was used; It is noted that a higher concentration of K^+ at 250 mM was required to induce CSD compared to 160 mM employed when halothane was used as the anaesthetic[34]. This difference in K^+ requirement could be due to the anaesthetics (isoflurane *vs* halothane) having different effects on CSD[18], but this effect can be ignored as all experiments were carried out under the same anesthetic condition.

One hour after the surgery, drugs or ACSF were perfused through the microdialysis probe at 1 µl/minute. In order to examine the effects of NVP-AAM07 on CSD genesis and propagation, the following series of experiments were carried out. The known non-competitive NMDA receptor antagonist, MK801, was used as the reference. These series are: (i) ACSF (Control, $n = 6$); (ii) MK801 (Sigma-Aldrich, Dorset, UK, $n = 6$); (iii) NVP-AAM077 ($n = 6$), which was synthesized following the procedures described in the literature[35] and further purified by HPLC. It should be noted that the microdialysis probe used in this study has ~10% recovery rate, *i.e.* the ratio of the drug penetration through the semi-permeable membrane of the probe into the cortex relative to its original concentration. An estimation of 0.3 µM of NVP-AAM077 was expected to diffuse into the cortex surrounding the microdialysis probe implantation site when the maximum concentration at 3 µM of the drug was applied, at which, the drug is preferably selective for NR2A subunit[36].

Five consecutive CSD episodes were elicited in each experiment by perfusion of K^+-medium through microdialysis probes for 20 minutes followed by 40 minutes ACSF perfusion to allow tissue recovery. These five episodes were: (i) initial ACSF control; (ii) low concentration of the drug or ACSF; (iii) medium concentration of the drug or ACSF; (vi) high concentration of the drug or ACSF; (v) post-treatment with ACSF solution. The drug at each concentration (0.3, 1, 3 µM for NVP-AAM077 or 3, 10, 30 µM for MK801) was perfused through microdialysis probes for 20 minutes before and during high K^+-medium perfusion for the 2nd, 3rd and 4th CSD episodes.

Intracerebroventricular injection experiment. To ensure NVP-AAM077 diffusion to a wider cortical region for investigation of CSD propagation under NR2A inhibition, a separate set of *in vivo* experiment by perfusion of NVP-AAM077 into the left lateral ventricle was designed. Three burr holes were drilled in the right and left parietal bones (Fig. 5B) for the following purposes: (i) one burr hole (1 mm i.d) with dura intact was drilled in the right parietal bone (coordinates: 5 mm posterior and 2 mm lateral to bregma) for inducing CSD by topical application of 1 µl of 3 M KCl for 1 minute; (ii and iii) two burr holes were drilled on the ipsilateral area (coordinates: 2 mm posterior and 0.4 mm anterior to bregma respectively, 2 mm lateral) and Ag/AgCl recording electrodes were implanted into the cortex (0.9 mm deep from the cortical surface) through these burr holes for recording CSD propagation waves. The DC potential was derived between the Ag/AgCl electrodes and a reference electrode placed under the scalp; (vi) A stainless steel cannula (inner diameter: 0.38 mm, RWD Life Science, Shenzhen, China) was implanted into the contralateral ventricle (coordinates: 0.8 mm posterior and 1.6–1.8 mm lateral to bregma, 3.5 mm deep from the cortical surface) and held in place by acrylic dental cement for the drug or ACSF perfusion. These burr holes were kept moisture with ACSF throughout the experiment.

After one hour stabilization post-surgery, two CSD episodes were induced by topical application of 1 µ1 of KCl at 3 M with 40 minute interval. NVP-AAM077 (0.3 nmol, $n = 6$) or ACSF (Control, $n = 6$) was perfused at 1 µl/minute for 10 minutes using a syringe pump (CMA100, CMA/Microdialysis, Solna, Sweden) into the contralateral ventricle immediately after the 1st CSD wave of each episode was completed.

Recording of EEG and extracellular direct current potential. EEG and DC signal recording was as reported previously[34]. Briefly, EEG and DC signals were amplified using an AC/DC pre-amplifier (NL834, Neurolog System, Digitimer Ltd., Welwyn Garden City, UK). All the recorded variables were continuously digitised, displayed and recorded by a computer using Labview 11.0 (NI Instruments) via an analogue/digital-converter (USB6009, NI Instruments). In the microdialysis-based experiment, CSD at the induction site was recognized as a transient, negative shift superimposed on the sustained shift resulting from the imposed high extracellular K^+ concentration (Fig. 5A, lower trace). CSD propagation wave was recognized by a transient, negative shift but in the absence of the sustained depolarization shift (Fig. 5A, upper trace and 5B).

In vivo data presentation and statistical analysis. Details on CSD number, latency and magnitude in rats were quantified as that described previously (Wang *et al.*[34]). Labview program was used to determine (i) CSD number in each episode; (ii) Latency (minute), the time required to elicit the 1st CSD wave from the start of depolarization

induced by high K^+-medium. In the case of the CSD wave being completely abolished by drug(s), the latency was counted as 20 minutes. CSD number and latency were used to reflect cortex susceptibility to CSD; (iii) Area under the curve (AUC, mV × minute) of CSD waves was used to reflect CSD magnitude. The magnitude of each CSD wave in each CSD episode was averaged for data comparison. Values were counted as zero when CSD waves were abolished; (vi) CSD propagation rate (mm/minute). The velocity of each CSD wave in each CSD episode was averaged for data comparison. All values were given in mean ± SEM. CSD number and latency was analysed using one-way ANOVA with subsequent Bonferonni test for significance between drugs and control group. CSD magnitude and propagation rate were analysed using unpaired t-test between the drug and control group. Paired t-test was used to test the significance of the effect of drug removal.

***In vitro* CSD in chick retina with intrinsic optical imaging.** *CSD induction in chick retina and intrinsic optical imaging.* Twenty six male chicks (purchased at 1 day old, WuXi Yangzichang Ltd, Wuxi, China) were housed for at least a week before use (aged 8–28 days). As described previously[37], posterior eyeball was positioned in a chamber, which was perfused at 0.5 ml/minute with Ringer's solution. The tissue was stabilized for at least 30 minutes before CSD induction and temperature kept constant at 32 °C.

Retinal CSD was induced as previously described[15,37]. Briefly, ten repeated CSD episodes were induced by ejection of 1 μl of KCl (0.1 μM) at the eyeball with 20-minute interval for tissue recovery. The retina was illuminated for 25 ms at 1 Hz using a high-power LED spotlight (625 nm peak wavelength, SLS-0307-A, Mightex; Pleasanton, CA, USA) and the illumination was driven by a computer-controlled power supply (Sirius LED controller, SLC-SA04-U; Mightex, Pleasanton, USA). The reflected light was simultaneously recorded with a monochrome camera (QIC-F-M-12, Media Cybernetics, Marlow, UK). Image sequences were taken at 1 Hz over a 3-minute period, started as CSD was elicited. Camera exposure and illumination were synchronized using the same external trigger (TG5011, TTi, UK). Image Pro Plus software (IPP 7.0; Media Cybernetics UK, China) was used for image acquisition, storage and analysis.

In vitro experimental design for drug testing. Four groups were designed and the concentration range of each drug was carefully selected to ensure that each drug tested was preferably selective for NR2A subunit: (i) TCN-201 (Tocris, Bristol, UK) at 1, 3 and 9 μM ($n = 6$); (ii) NVP-AAM077, at 0.03, 0.1 and 0.3 μM ($n = 6$) as the positive control; (iii) DMSO (Sigma-Aldrich, Dorset, UK) at 0.001%, 0.03% and 0.1% as the TCN-201 vehicle group in respective order ($n = 8$); It should be noted the maximum concentration of DMSO without affecting CSD in chick retina was 0.1% DMSO per our preliminary experiment; (vi) Ringer's solution as the control ($n = 6$) for NVP-AAM077 group.

For each group tested, ten CSD episodes were induced in each experiment, with two separate CSDs for each of the different and consecutive tests: (i) initial Ringer's control; (ii) low concentration of drug or vehicle; (iii) medium concentration of drug or vehicle; (vi) high concentration of drug or vehicle; (v) post-treatment with Ringer's control (*i.e.* drug removal). For each test sequence, the perfusion medium was changed immediately after the end of the 2nd, 4th, 6th, and 8th CSD recording when required, so that the preparation was adequately perfused with the proper drug, vehicle, or Ringer's medium for the subsequent test.

In vitro data presentation and statistical analysis. As reported previously (Wang *et al.*[15]), for each image sequence, an area of interest (AOI) parallel to the CSD wave front was delineated manually. For each image within the sequence, the gray levels of the pixels constituting the AOI were averaged and plotted against the time as an indicator to characterize CSD. For each CSD wave, the area under the curve (AUC, gray levels × minute) of the transient cellular depolarization was calculated and used as an index of the magnitude of propagating CSD. For each CSD wave, propagation rate was also calculated to reflect the degree of tissue excitability. The calculated values within each different test were averaged and all corresponding data were given as mean ± SD in percentages of their respective baselines. Kruskal–Wallis test was used with subsequent Dunn's test for comparison of the magnitude and propagation rate of RSD between the drug and respective control group. Wilcoxon matched pairs test was used to test the significance of the difference for the last two tests with each drug (*i.e.* effect of drug removal).

References

1. Seidel, J. L., Escartin, C., Ayata, C., Bonvento, G. & Shuttleworth, C. W. Multifaceted roles for astrocytes in spreading depolarization: A target for limiting spreading depolarization in acute brain injury? *Glia*. **64,** 5–20 (2016).
2. Somjen, G. G. Aristides Leao's discovery of cortical spreading depression. *J Neurophysiol*. **94,** 2–4 (2005).
3. Hadjikhani, N. *et al.* Mechanisms of migraine aura revealed by functional MRI in human visual cortex. *Proc Natl Acad Sci USA* **98,** 4687–92 (2001).
4. Lauritzen, M. Pathophysiology of the migraine aura. The spreading depression theory. *Brain*. **117** (Pt 1), 199–210 (1994).
5. Moskowitz, M. A. Pathophysiology of headache–past and present. *Headache*. **47** Suppl 1, S58–63 (2007).
6. Karatas, H. *et al.* Spreading depression triggers headache by activating neuronal Panx1 channels. *Science* **339,** 1092–5 (2013).
7. Marrannes, R., Willems, R., De Prins, E. & Wauquier, A. Evidence for a role of the N-methyl-D-aspartate (NMDA) receptor in cortical spreading depression in the rat. *Brain Res*. **457,** 226–40 (1988).
8. Peeters, M. *et al.* Effects of pan- and subtype-selective N-methyl-D-aspartate receptor antagonists on cortical spreading depression in the rat: therapeutic potential for migraine. *J Pharmacol Exp Ther*. **321,** 564–72 (2007).
9. Chen, H. S. & Lipton, S. A. Pharmacological implications of two distinct mechanisms of interaction of memantine with N-methyl-D-aspartate-gated channels. *J Pharmacol Exp Ther*. **314,** 961–71 (2005).
10. Chen, H. S. & Lipton, S. A. The chemical biology of clinically tolerated NMDA receptor antagonists. *J Neurochem*. **97,** 1611–26 (2006).
11. Paoletti, P. & Neyton, J. NMDA receptor subunits: function and pharmacology. *Curr Opin Pharmacol*. **7,** 39–47 (2007).
12. Sanz-Clemente, A., Nicoll, R. A. & Roche, K. W. Diversity in NMDA receptor composition: many regulators, many consequences. *Neuroscientist*. **19,** 62–75 (2013).
13. von Engelhardt, J., Doganci, B., Seeburg, P. H. & Monyer, H. Synaptic NR2A- but not NR2B-Containing NMDA Receptors Increase with Blockade of Ionotropic Glutamate Receptors. *Front Mol Neurosci*. **2,** 19 (2009).

14. Dzamba, D., Honsa, P. & Anderova, M. NMDA Receptors in Glial Cells: Pending Questions. *Curr Neuropharmacol*. **11,** 250–62 (2013).
15. Wang, M., Chazot, P. L., Ali, S., Duckett, S. F. & Obrenovitch, T. P. Effects of NMDA receptor antagonists with different subtype selectivities on retinal spreading depression. *Br J Pharmacol*. **165,** 235–44 (2012).
16. Shatillo, A., Salo, R. A., Giniatullin, R. & Grohn, O. H. Involvement of NMDA receptor subtypes in cortical spreading depression in rats assessed by fMRI. *Neuropharmacology*. **93c,** 164–170 (2015).
17. Bettini, E. *et al.* Identification and characterization of novel NMDA receptor antagonists selective for NR2A- over NR2B-containing receptors. *J Pharmacol Exp Ther*. **335,** 636–44 (2010).
18. Piper, R. D. & Lambert, G. A. Inhalational anesthetics inhibit spreading depression: relevance to migraine. *Cephalalgia*. **16,** 87–92 (1996).
19. Verhaegen, M., Todd, M. M. & Warner, D. S. The influence of different concentrations of volatile anesthetics on the threshold for cortical spreading depression in rats. *Brain Res*. **581,** 153–5 (1992).
20. Kitahara, Y., Taga, K., Abe, H. & Shimoji, K. The effects of anesthetics on cortical spreading depression elicitation and c-fos expression in rats. *J Neurosurg Anesthesiol*. **13,** 26–32 (2001).
21. Vogler, G. A. In *Anesthesia and Analgesia* (eds Mashwl, F.) Ch. 19, 627–664 (Academic Press, 2006).
22. Chang, J. C. *et al.* Biphasic direct current shift, haemoglobin desaturation and neurovascular uncoupling in cortical spreading depression. *Brain*. **133,** 996–1012 (2010).
23. Unekawa, M., Tomita, Y., Toriumi, H. & Suzuki, N. Suppressive effect of chronic peroral topiramate on potassium-induced cortical spreading depression in rats. *Cephalalgia*. **32,** 518–27 (2012).
24. Obrenovitch, T. P. & Zilkha, E. Intracerebral microdialysis markedly inhibits the propagation of cortical spreading depression. *Acta Neurochir Suppl*. **67,** 21–3 (1996).
25. Willette, R. N., Lysko, P. G. & Sauermelch, C. F. A comparison of (+)SK&F 10047 and MK-801 on cortical spreading depression. *Brain Res*. **648,** 347–51 (1994).
26. Proescholdt, M. G., Hutto, B., Brady, L. S. & Herkenham, M. Studies of cerebrospinal fluid flow and penetration into brain following lateral ventricle and cisterna magna injections of the tracer [14C]inulin in rat. *Neuroscience*. **95,** 577–92 (2000).
27. Huang, L., Bocek, M., Jordan, J. K. & Sheehan, A. H. Memantine for the prevention of primary headache disorders. *Ann Pharmacother*. **48,** 1507–11 (2014).
28. Fox, C. J., Russell, K. I., Wang, Y. T. & Christie, B. R. Contribution of NR2A and NR2B NMDA subunits to bidirectional synaptic plasticity in the hippocampus *in vivo*. *Hippocampus*. **16,** 907–15 (2006).
29. Noh, J., Lee, E. S. & Chung, J. M. The novel NMDA receptor antagonist, 2-hydroxy-5-(2,3,5,6-tetrafluoro-4-trifluoromethyl-benzylamino)-benzoic acid, is a gating modifier in cultured mouse cortical neurons. *J Neurochem*. **109,** 1261–71 (2009).
30. Hansen, K. B., Ogden, K. K. & Traynelis, S. F. Subunit-selective allosteric inhibition of glycine binding to NMDA receptors. *J Neurosci*. **32,** 6197–208 (2012).
31. von Engelhardt, J. *et al.* Excitotoxicity *in vitro* by NR2A- and NR2B-containing NMDA receptors. *Neuropharmacology*. **53,** 10–7 (2007).
32. Torrente, D. *et al.* Increased calcium influx triggers and accelerates cortical spreading depression *in vivo* in male adult rats. *Neurosci Lett*. **558,** 87–90 (2014).
33. Sornarajah, L. *et al.* NMDA receptor desensitization regulated by direct binding to PDZ1-2 domains of PSD-95. *J Neurophysiol*. **99,** 3052–62 (2008).
34. Wang, M., Obrenovitch, T. P. & Urenjak, J. Effects of the nitric oxide donor, DEA/NO on cortical spreading depression. *Neuropharmacology*. **44,** 949–57 (2003).
35. Auberson, Y. P. *et al.* 5-Phosphonomethylquinoxalinediones as competitive NMDA receptor antagonists with a preference for the human 1A/2A, rather than 1A/2B receptor composition. *Bioorg Med Chem Lett*. **12,** 1099–102 (2002).
36. Paoletti, P. *et al.* Molecular organization of a zinc binding n-terminal modulatory domain in a NMDA receptor subunit. *Neuron*. **28,** 911–25 (2000).
37. Wang, M., Li, Y. & Lin, Y. GABAA receptor alpha2 subtype activation suppresses retinal spreading depression. *Neuroscience*. **298,** 137–44 (2015).

Acknowledgements

This work was supported by Wangwenli Charitable foundation, China (RD0006), Xi'an Jiaotong-Liverpool University (XJTLU) PhD studentship for Fan Bu, a registered PhD student at University of Liverpool and the XJTLU research development fund. The author thank colleagues in the animal unit of Soochow University for offering animal facility, Yanli Li for her technical training of Fan Bu on *in vitro* study and Dr. Shangbin Chen from Huangzhong Science Technology University for his tutoring the labview program.

Author Contributions

F.B. performed experiments, analyzed data and drafted manuscript; R.D. analysed data, edited and revised manuscript. Y.L. synthesized NVP-AAM077 and revised manuscript. J.P.Q. revised manuscript. M.W. conception and design of research; drafted and edited manuscript.

Additional Information

Competing financial interests: The authors declare no competing financial interests.

How to cite this article: Bu, F. *et al.* NR2A contributes to genesis and propagation of cortical spreading depression in rats. *Sci. Rep.* **6**, 23576; doi: 10.1038/srep23576 (2016).

Original Article

Cephalalgia
An International Journal of Headache

International Headache Society

Cephalalgia
0(0) 1–9

DOI: 10.1177/0333102416678388
cep.sagepub.com

SAGE

Induction of calcitonin gene-related peptide expression in rats by cortical spreading depression

Yan Wang[1,*], Anne E Tye[2,*], Junli Zhao[1], Dongqing Ma[1,3], Ann C Raddant[4], Fan Bu[1,3], Benjamin L Spector[4], Nolan K Winslow[4], Minyan Wang[1,3,#] and Andrew F Russo[2,4,5,6,#]

Abstract

Objective: The neuropeptide calcitonin gene-related peptide (CGRP) has now been established as a key player in migraine. However, the mechanisms underlying the reported elevation of CGRP in the serum and cerebrospinal fluid of some migraineurs are not known. A candidate mechanism is cortical spreading depression (CSD), which is associated with migraine with aura and traumatic brain injury. The aim of this study was to investigate whether CGRP gene expression may be induced by experimental CSD in the rat cerebral cortex.

Methods: CSD was induced by topical application of KCl and monitored using electrophysiological methods. Quantitative PCR and ELISA were used to measure CGRP mRNA and peptide levels in discrete ipsilateral and contralateral cortical regions of the rat brain 24 hours following CSD events and compared with sham treatments.

Results: The data show that multiple, but not single, CSD events significantly increase CGRP mRNA levels at 24 hours post-CSD in the ipsilateral rat cerebral cortex. Increased CGRP was observed in the ipsilateral frontal, motor, somatosensory, and visual cortices, but not the cingulate cortex, or contralateral cortices. CSD also induced CGRP peptide expression in the ipsilateral, but not contralateral, cortex.

Conclusions: Repeated CSD provides a mechanism for prolonged elevation of CGRP in the cerebral cortex, which may contribute to migraine and post-traumatic headache.

Keywords

CGRP, migraine, traumatic brain injury, post-traumatic headache, gene expression

Date received: 2 May 2016; revised: 23 September 2016; accepted: 2 October 2016

Introduction

Migraine is a complex, multifactorial neurological disorder that is conservatively estimated to affect ~12% of Americans (1). The most prominent characteristic of migraine is the disabling headache, which manifests as a throbbing, unilateral pain made worse with routine activity, and coincident with nausea/vomiting and/or photophobia/phonophobia. Approximately one-third of migraineurs experience a premonitory aura, which typically manifests as a disruption in the ipsilateral visual hemifield (2). The pathophysiological substrate of the visual aura is cortical spreading depression (CSD), a transient wave of neuronal and glial depolarization, followed by a sustained depression of electrical activity (3,4). CSD is associated with a massive translocation of ions and release of nitric oxide, arachidonic acid, glutamate, and ATP (5,6). The sudden rise in extracellular K^+, arachidonic acid and nitric oxide is the likely trigger for CSD-induced activity in meningeal nociceptors (7) and central trigeminovascular neurons (8).

[1]Centre for Neuroscience and [3]Department of Biological Sciences, Xi'an Jiaotong-Liverpool University (XJTLU), SIP, Suzhou 215123, China; [2]Neuroscience Program, Departments of [4]Molecular Physiology and Biophysics, and [5]Neurology, University of Iowa, Iowa City, IA 52242, USA; [6]Veterans Affairs Medical Center, Iowa City, IA 52246, USA

*Yan Wang and Anne E Tye are equal contributors.

#Minyan Wang and Andrew F Russo are shared last authors.

Corresponding author:
Andrew Russo, Department of Molecular Physiology and Biophysics, University of Iowa, Iowa City, IA 52242, USA.
Email: andrew-russo@uiowa.edu

CSD may also lead to migraine by potentiation of an inflammatory response in the dura (9).

In addition to the connection between migraine and CSD, it is well accepted that CSD also occurs following acute brain injuries, such as traumatic brain injury (TBI) and strokes (10–12). Whereas the pattern of brain injury-triggered CSD is heterogeneous and influenced by many factors, a common feature is that there are multiple CSD events, often about every 30 minutes for many hours to days (11). For example, 72% of subarachnoid hemorrhage patients experience clusters of repetitive CSD events (13), and 56% of TBI patients experience repeated spreading depression events (mostly CSD), with a total of 1328 events observed in 58 patients over 67 hours (14). Hence, brain injury in humans can lead to tens to hundreds of CSD events over days. Repeated CSD events have also been observed for hours to days in some, but not all, animal TBI models (12).

It has been shown that multiple CSD events can modulate many genes at early (hours) and late (days to weeks) time points across a variety of gene ontologies (15,16). A potential candidate for regulation by CSD is calcitonin gene-related peptide (CGRP). CGRP is a vasoactive neuropeptide that is widely distributed in the central and peripheral nervous systems. Clinical and preclinical studies have established CGRP as a key player in migraine (17). Intravenous CGRP administration to migraineurs is sufficient to elicit a migraine-like headache (18,19), and CGRP levels have been reported to be elevated in both the serum and CSF of migraineurs (20). Importantly, CGRP receptor antagonists and CGRP-blocking antibodies can ameliorate migraine symptoms (21,22).

In this report, we have asked whether CSD is sufficient to alter CGRP expression. Such a link would fit in the context of interesting, but limited, evidence of CGRP involvement in CSD (17,23). In particular, a calcium-dependent release of CGRP was observed during CSD and inhibition of CGRP receptors reduced the magnitude of CSD in rat neocortical slices (24). Elevated CGRP may modulate neurotransmission and possibly contribute to sensory hypersensitivity (17,25). For this scenario, we reasoned that the elevated synthesis, if it occurred, would likely be maintained for a relatively long time (24 hours). Similar prolonged times were also required for activation of CGRP gene expression in trigeminal ganglia organ cultures (26), and by epigenetic reprogramming of glial cells (27). We therefore proposed that CSD might be a mechanism by which cortical levels of CGRP become elevated for a prolonged period in migraine and TBI patients.

Materials and methods

Animals

Adult male Sprague–Dawley rats ($n = 36$, 240–440 g; Shanghai SLAC Laboratory Animal Corporation, Ltd.) with food and water *ad libitum* were used. Experimental procedures were performed in the animal unit of Soochow University. All rats were healthy, with no drug treatments or previous tests carried out prior to experimentation. Animals were housed two per cage in specific pathogen-free conditions with standard bedding material and rat special synthetic feed. Animals were allowed to acclimate to the housing room for 7 days prior to the experiment, then matched by body weight into experimental groups of sham and CSD, which were performed randomly on different days using one rat per day at various times during the day. No animals were excluded from the analysis. During the experiment, rats were given isoflurane anesthesia, which was monitored by absence of whisker movements and lack of reaction to brief tail pinches. After surgeries, animals were given an antibiotic and anti-inflammatory, as described below, and outwardly appeared healthy. Euthanasia was by excess isoflurane exposure. All procedures were approved by the Ethic Review Panel of Soochow University under agreement with XJTLU, and performed in accordance with Chinese national guidelines and in adherence to ARRIVE guidelines.

CSD induction

Animals were anesthetized with isoflurane (5% induction, 2.5–3.5% during surgery, 1.0–1.5% maintenance) in O_2: N_2O (1:2). A small incision was made and two small burr holes were drilled carefully in the skull right frontoparietal region (1 mm i.d.; Figure 1). The posterior hole (4 mm posterior, 2 mm lateral to bregma) was prepared with extra care to minimize damage to the underlying dura. A silver chloride recording electrode was implanted through the anterior hole (3 mm anterior, 2 mm lateral to bregma) for recording of CSD waves. A reference electrode was placed under the scalp. Both holes were moisturized with artificial cerebrospinal fluid (ACSF; 125 mM NaCl, 2.5 mM KCl, 1.18 mM $MgCl_2$, 1.26 mM $CaCl_2$, pH 7.3). Rectal temperature was maintained at 37°C. Upon completion of surgery, rats were maintained under anesthesia for at least 1 hour to allow for stabilization and tissue recovery.

For the multiple CSD group ($n = 14$), 1 µl of 3 M KCl was carefully dropped into the posterior hole for single CSD wave elicitation. As soon as the first CSD wave was detected at the recording site, KCl was removed using a tissue, followed by washout with

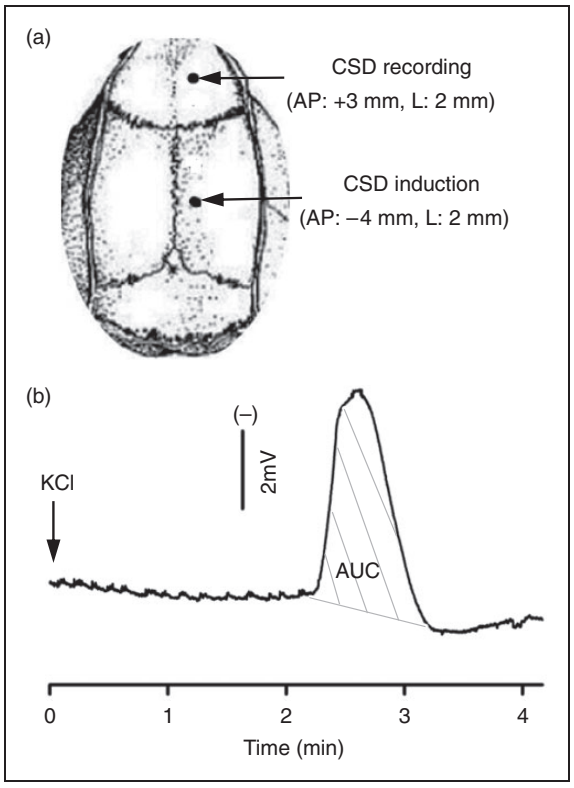

Figure 1. Cortical spreading depression (CSD) induction and propagation in the rat cortex. (A) CSD was induced with topical application of 1 μl 3 M KCl (or artificial cerebrospinal fluid for sham) onto the dura via a posterior burr hole. An anterior hole was used for CSD recording. A total of 36 rats were used. Of these, 26 rats were used for multiple CSD experiments including 14 for CSD induction and 12 for sham. To minimize the animal use, three of 14 rats in the CSD group and three of 12 in the sham group were also used for measuring calcitonin gene-related peptide (CGRP) levels in addition to CGRP mRNA. In the single CSD group, 10 rats were used with five for CSD and sham, respectively. (B) A representative trace showing CSD propagation and magnitude (indicated as area under the curve, AUC, grey lines).

ACSF and placement of ACSF-moistened cotton over the hole. For the sham group ($n = 12$), 1 μl ACSF was used. In both groups, five repeated CSD or sham episodes were elicited at 40-minute intervals. Both electroencephalogram (to monitor depth of anesthesia) and direct current potentials (to monitor CSD events) were recorded and analyzed using LabVIEW. The electrode was removed and wound sutured after the fifth CSD episode. Ibuprofen (5–10 mg) and mupirocin ointment (0.4–0.8 mg) were applied. At 24 hours after the fifth CSD episode, the rat was re-anesthetized for euthanasia and tissue removal.

For the single CSD group ($n = 5$), CSD induction, CSD recording, and post-surgery care were the same as that for the repeated CSD, except that only one CSD episode was elicited by 1 μl of 3 M KCl. For the sham group ($n = 5$), 1 μl ACSF was used. At 24 hours, the rat was re-anesthetized for euthanasia and tissue removal.

qPCR

All quantitative polymerase chain reaction (qPCR) assays on multiple CSD tissue samples were performed blinded at the University of Iowa using coded samples shipped from XJTLU. Some of those samples were also tested at XJTLU as an internal control for measurements on the single CSD samples, which were done at XJTLU. In both locations, the same protocols and reagents were used. Whole cortex or cortical regions (50–100 mg) were homogenized in 1 ml TRIzol (Sigma-Aldrich) and RNA concentration and purity measured by Nano-Drop (Thermo Scientific); 1 μg total RNA was reverse transcribed into cDNA using the GoScript™ RT system (Promega). qPCR was performed in duplicate using 1/20th of the cDNA reaction on a Bio-Rad CFX Connect using SYBR-Green Master Mix (Takara Clontech), except for 18S rRNA, which used 1/20,000th of the cDNA. Primers (forward, reverse) were: CGRP (NM_001033953.2) 5′AACCTTGGAAAGCAGCCCAGGCATG3′, 5′GTGGGCACAAAGTTGTCCTTCACCA3′; and three reference genes: peptidylprolyl isomerase A (PPIA) (NM_017101.1) 5′TTGCTGCAGACATGGTCAAC3′, 5′TGTCTGCAAACAGCTCGAAG3′; β-actin (ACTB) (NM_001101.3) 5′ACGGTCAGGTCATCACTATGG3′, 5′AGCCACCAATCCACACAG3′; and 18S rRNA (NR_046237.1) 5′ATGGCCGTTCTTAGTTGGTG3′, 5′AACGCCACTTGTCCCTCTAA3′. All qPCR data from multiple CSD samples were analyzed using both absolute quantification of CGRP mRNA (with standard curves) and relative fold change ($2^{-\Delta\Delta Cq}$ method) normalized to each contralateral hemisphere. The single CSD samples were analyzed only by the relative fold change ($2^{-\Delta\Delta Cq}$ method) normalized to the sham tissue. Standard curves were generated using plasmids containing PCR products in pCR2.1 (Invitrogen) (confirmed by sequence). CGRP mRNA levels were normalized to the product-based geometric mean of the three reference genes (28), calculated as the cube-root of the product of the reference genes $(\text{PPIA} \times \beta\text{-actin} \times 18\text{S})^{1/3}$ divided by 10,000. Similar results were observed when CGRP levels were normalized to each individual reference gene. CGRP levels are mean ± SEM.

ELISA

Protein extraction and detection from cortex homogenates followed the manufacturer's instructions using the

rat CGRP enzyme-linked immunosorbent assay (ELISA) kit (Bertin Pharma). To minimize the number of animals, cortical regions were snap frozen, pulverized, and split to allow both protein and RNA extractions. Due to the small amounts of tissue, it was necessary to combine motor, somatosensory, and visual cortices for protein, and set aside cingulate and frontal cortices for only RNA. All protein samples were rapidly homogenized within 15 seconds in 2 N acetic acid at 2 ml/100 mg tissue, then heated at 90°C for 10 minutes, centrifuged at 10,000 *g* for 30 minutes, dried for 1 hour, and stored at −80°C. Immediately before assay, samples were reconstituted with enzyme immunoassay (EIA) buffer, and analyzed using a microplate reader. CGRP levels are mean ± SEM.

Data analysis

For qPCR data, statistical analyses were performed using GraphPad Prism software as follows: comparisons across groups were done using an ordinary one-way analysis of variance (ANOVA) Kruskal–Wallis test; comparisons between ipsilateral *versus* contralateral hemispheres within the group were done using one-tailed Wilcoxon –*t*-test; comparisons between CSD and sham groups were done using one-tailed Mann–Whitney *t*-test. For ELISA data, normal distribution was confirmed by SPSS 16.0 software, and statistical analyses were performed using GraphPad Prism software with comparisons across groups using one-way ANOVA; comparisons between ipsilateral versus contralateral hemisphere within the group using one-tailed paired *t*-test; comparisons between CSD and sham groups using one-tailed unpaired *t*-test.

Results

Detection of experimentally induced CSD in rats

In the sham group, ACSF administration was insufficient to elicit CSD. In the CSD group, 1 µl of topical 3 M KCl onto the dura resulted in a CSD wave that began ~2–3 minutes after administration (Figures 1A and 1B). CSD propagation was identified by a transient, negative shift of the direct current–potential, which was observed in all CSD rats monitored by this means. For the rats that underwent multiple CSD events, the magnitude of each event was approximately 9 mV × minutes and there was no significant difference in the number or magnitude of CSD episodes over the 5 KCl applications ($p = 0.89$) (not shown). When summed up, the mean accumulative magnitude of CSD for each rat was 53.0 ± 10.2 mV × minutes in the multiple CSD group ($n = 14$) and 5.9 ± 1.8 mV × minutes ($n = 5$) in the single CSD group. Generally, only a single CSD wave was observed after each of the applications; although in four rats a second wave was observed after one of the applications in the multiple CSD group.

Increased cortical CGRP gene expression at 24 hours post-multiple CSD

In the sham group, the copy number of contralateral and ipsilateral CGRP mRNA was 13.5 ± 2.9 and 14.1 ± 2.2, respectively ($p = 0.69$), indicating that the surgical procedure did not significantly change CGRP gene expression (Figure 2A).

In the CSD group, the copy number of CGRP mRNA in the contralateral hemisphere was 18.6 ± 2.2, which is not significantly different from that of contralateral hemisphere in sham rats ($p = 0.14$; Figure 2A), demonstrating that repeated unilateral CSD does not affect CGRP gene expression in the contralateral hemisphere. In contrast, repeated CSD events in the ipsilateral hemisphere significantly increased the CGRP mRNA copy number to 79.1 ± 22.7 at 24 hours post-CSD ($p < 0.001$; Figure 2A). Comparison of relative ipsilateral CGRP levels normalized to the contralateral hemisphere of each rat agrees with the measured absolute levels. The sham group showed a 1.3 ± 0.4-fold increase between hemispheres, whereas the CSD group had a significantly greater 3.8 ± 0.8-fold increase ($p = 0.004$; Figure 2B).

No increased CGRP gene expression at 24 hours post-single CSD

In the single CSD group, CSD ipsilateral cortex did not show a significant change in CGRP mRNA levels. There was a 1.28 ± 0.06-fold change compared with that in sham ipsilateral group ($p = 0.11$; Figure 3). Contralateral samples were not included in this test, as it was shown that surgery did not significantly alter CGRP gene expression during the multiple CSD tests (Figure 2). Thus, it is very unlikely an elevation of CGRP gene expression in the contralateral cortex would be observed with single CSD.

Regional induction of CGRP in the cortex

We then examined CGRP mRNA levels in discrete regions of the cortex. In the sham group, CGRP mRNA levels in the contralateral and ipsilateral frontal, motor, somatosensory, and visual cortices were similar (Figure 4A). The cingulate had slightly higher CGRP mRNA levels in the sham contralateral (16.7 ± 4.0) and ipsilateral (32.9 ± 12.0) cortices (Figure 4A), which is consistent with a previous report that the rat cingulate has elevated CGRP relative to other cortical regions (29). There was no significant

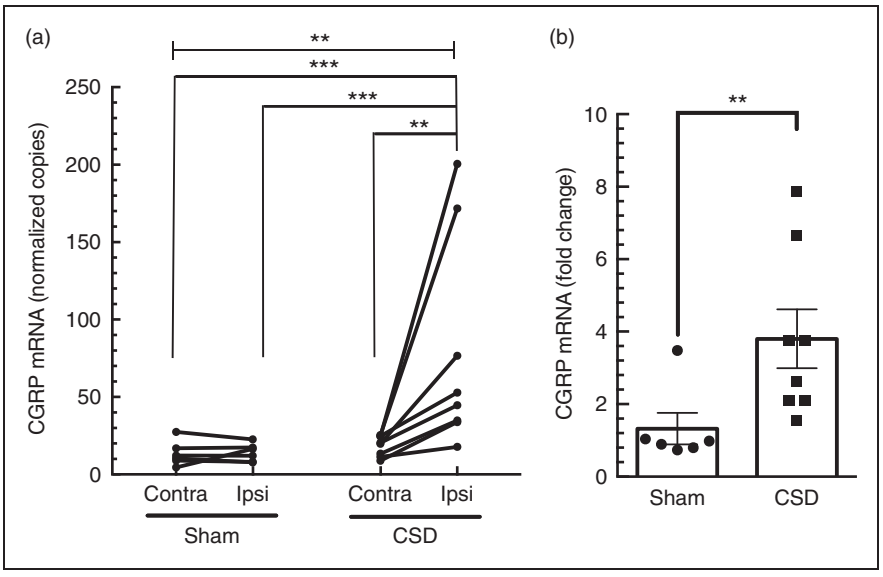

Figure 2. Ipsilateral calcitonin gene-related peptide (CGRP) mRNA is upregulated 24 hours post-multiple cortical spreading depression (CSD). (a) Absolute levels of CGRP mRNA were significantly elevated in the ipsilateral (ipsi), but not contralateral (contra), cortex post-CSD. There was no significant increase in the sham-treated rats. Data for individual rats are shown with lines connecting the paired cortices. (b) Comparison of CGRP mRNA levels between contralateral and ipsilateral cortices shown for individual rats (left panel) and as the fold change (right panel). Increased relative expression of CGRP mRNA in the ipsilateral normalized to contralateral cortex. In both (a) and (b), sham ($n = 6$), CSD ($n = 8$), $^{**}p < 0.01$; $^{***}p < 0.001$.

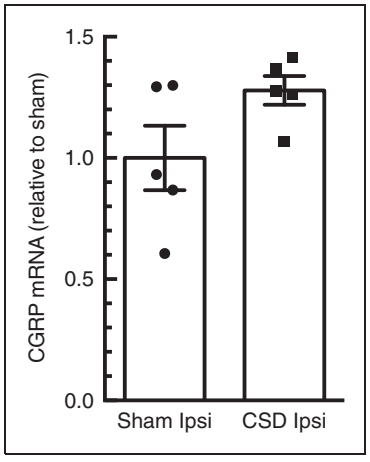

Figure 3. Ipsilateral calcitonin gene-related peptide (CGRP) mRNA is not altered 24 hours post-single cortical spreading depression (CSD). Comparison of CGRP levels between ipsilateral (ipsi) cortices of CSD rats ($n = 5$) normalized to sham rats ($n = 5$). There was no significant difference ($p = 0.11$).

change in CGRP mRNA content between contralateral and ipsilateral hemispheres of sham frontal, cingulate, or somatosensory cortices ($p = 0.16$, 0.11, and 0.22, in respective order), indicating that the surgery does not alter CGRP mRNA expression in these regions. However, a slight, but significant, increase in CGRP mRNA was observed in the motor and visual cortices of sham rats ($p = 0.016$ and 0.031, respectively; Figure 4A).

Following CSD, CGRP mRNA levels were significantly increased in the ipsilateral frontal, motor, somatosensory, and visual cortices when compared with sham ($p = 0.013$, 0.001, 0.001, and 0.001, respectively; Figure 4A). In contrast, CSD did not alter CGRP mRNA levels in the ipsilateral cingulate cortex compared with sham ($p = 0.45$; Figure 4A). As with the whole cortex, comparison between CSD and sham cohorts of the relative CGRP levels normalized to the contralateral hemisphere of each rat agreed with the absolute levels. In the CSD rats, there were significant increases in the ipsilateral compared with contralateral hemispheres of the frontal cortex (8.0 ± 1.8, $p = 0.013$), motor cortex (9.5 ± 3.1, $p = 0.013$), somatosensory cortex (15.3 ± 4.0, $p = 0.001$), and visual (14.5 ± 5.4, $p = 0.001$) compared with sham rats (Figure 4B). Also, as seen with absolute expression data, the normalized cingulate cortex did not exhibit a CSD-induced increase over sham (1.6 ± 0.3, $p = 0.45$; Figure 4B).

Increased CGRP peptide expression at 24 hours post-multiple CSD

Aliquots of somatosensory, motor, and visual cortices used for RNA analyses were combined and used for parallel peptide measurements (see Methods). In the sham group, CGRP peptide levels were 1.4 ± 0.5 ng/g tissue in the ipsilateral hemisphere and 1.8 ± 0.1 ng/g tissue in contralateral ($p = 0.27$), indicating that surgical procedures do not alter overall CGRP expression

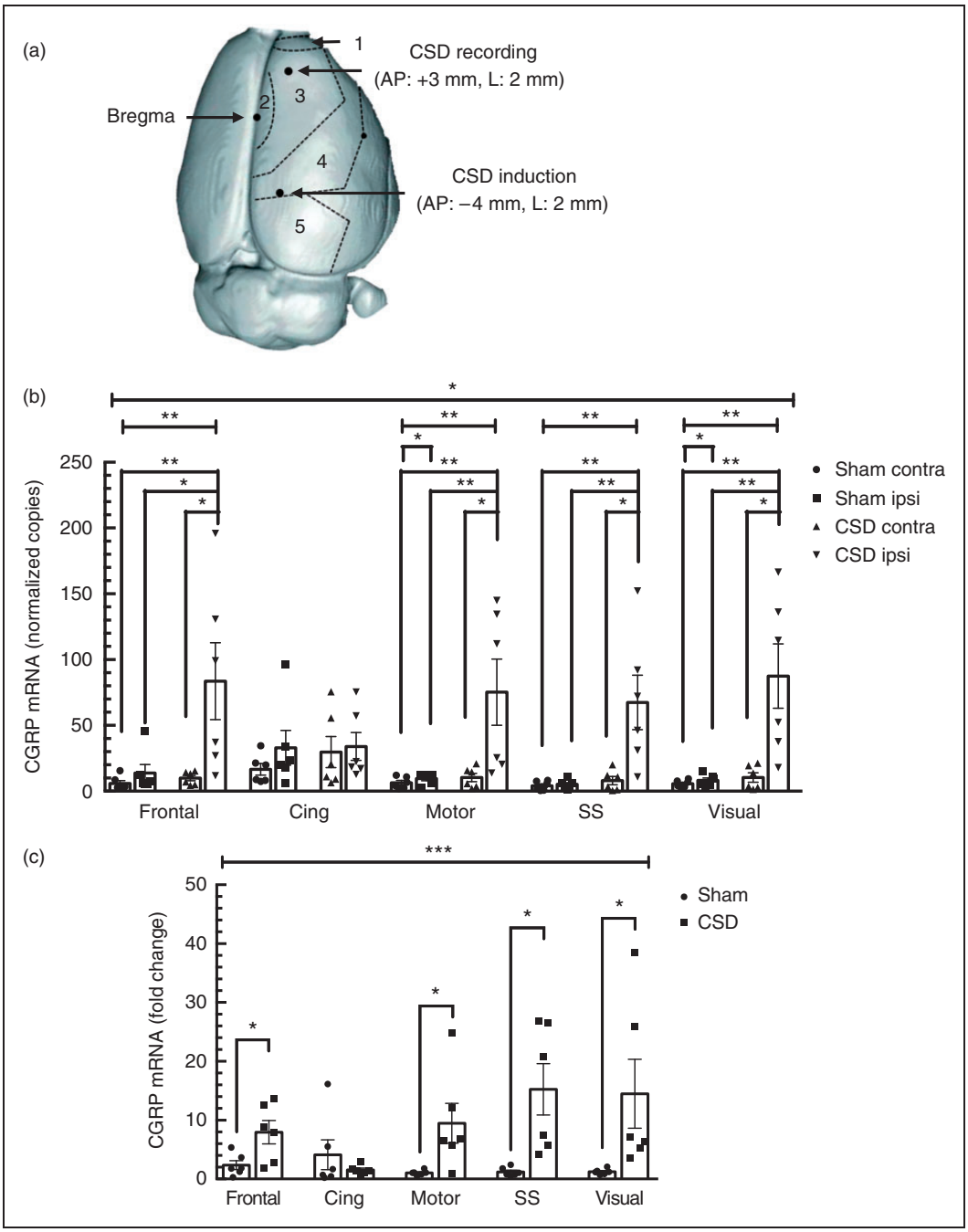

Figure 4. Multiple cortical spreading depression (CSD)-induced calcitonin gene-related peptide (CGRP) mRNA expression shows regional specificity. (a) Top view of rat brain cortical regions used for dissections. Cortical regions are designated as 1 = frontal, 2 = cingulate, 3 = motor, 4 = somatosensory, and 5 = visual. The CSD recording and induction sites are also indicated. (b) Absolute levels of CGRP mRNA were significantly elevated in ipsilateral (ipsi) frontal, motor, somatosensory (SS), and visual cortices, but not in the cingulate (Cing) cortex, or the contralateral (contra) hemispheres, 24 hours post-multiple CSD. (c) Significant increases in relative ipsilateral CGRP mRNA were observed in the frontal, motor, somatosensory, and visual cortices, but not in the cingulate cortex, at 24 hours post-multiple CSD. In both panels, sham ($n = 6$), CSD ($n = 6$), $^{*}p < 0.05$; $^{**}p < 0.01$; $^{***}p < 0.001$.

under these conditions (Figure 4). In the CSD ipsilateral cortex, the CGRP level was 4.0 ± 0.6 ng/g tissue, which was about 2.9-fold higher than sham ipsilateral cortex ($p = 0.014$; Figure 5).

Discussion

In this study, we have shown that unilateral multiple CSD is sufficient to upregulate CGRP mRNA and peptide levels in the ipsilateral cerebral cortex. The RNA

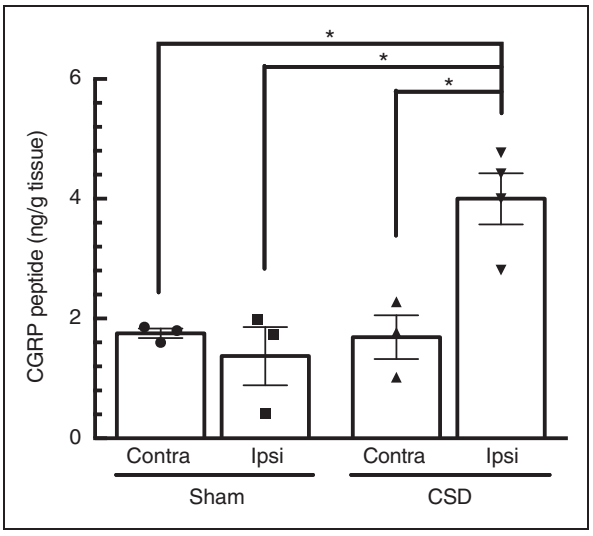

Figure 5. Ipsilateral calcitonin gene-related peptide (CGRP) peptide levels are upregulated post-multiple cortical spreading depression (CSD). CGRP peptide levels are significantly elevated in ipsilateral (ipsi) cortex 24 hours post-CSD ($n = 3$), but not the contralateral (contra) hemispheres, nor in sham rats ($n = 3$), $^*p < 0.05$.

induction was widespread across much of the cerebral cortex: in the frontal, motor, somatosensory, and visual cortices, but not in the cingulate cortex. The lack of induction in the cingulate is consistent with reports that CSD propagation is less efficient in this region (30). Importantly, the fact that CGRP mRNA levels were similarly increased in multiple cortical regions indicates that the elevated expression is attributed to CSD, rather than depolarization in the immediate area of KCl application. These data extend an earlier *in vitro* study showing that CSD induced CGRP release in rat neocortical slices (24). Thus, CSD might contribute to the elevated CGRP in the CSF of some migraine patients. However, it is very unlikely that cortical CGRP contributes to the elevation of CGRP in the external jugular vein during migraine. Indeed, Piper et al. (31) clearly documented that CGRP release into the external jugular vein was not increased by experimental CSD in the cat. Whether CSD increases synthesis in the trigeminal ganglia remains to be determined. A recent study reported that CSD increases the number of CGRP-positive cells in rat trigeminal ganglia (32), which may point to increased synthesis. Overall, these data provide evidence linking CSD and CGRP expression that may contribute to migraine pathogenesis.

A key finding of our study was that multiple CSD events were required for robust induction of the CGRP gene. The experimental protocol we used was designed to elicit multiple CSD events similar to that used in other laboratories (9,23,33–35), but which also likely differs from human migraine. Indeed migraine aura is believed to involve only a single CSD event. On the other hand, TBI is commonly associated with up to hundreds of CSD waves that can occur over days following the injury (10–12). To our knowledge, the possibility that individuals with a history of head trauma and spreading depression exhibit elevated CGRP levels has not been investigated. However, in a recent study, Elliott and colleagues observed a sustained elevation of CGRP in the brainstem (most likely from the trigeminal nerve) for at least 4 weeks in rodents exposed to controlled cortical impact injury (36). This injury can cause one to four CSD events over several hours (37). More limited studies have also reported elevated CGRP in other rodent TBI models (38,39). Whether from TBI or migraine, there is increasing evidence that CSD affects behavior and likely potentiates nociception that may in part involve CGRP. CSD activates meningeal nociceptors and central trigeminovascular neurons (7,8,40), and an immediate effect of CSD is reduced movement and freezing responses (41,42). Nonetheless, a limitation of animal CSD studies remains extrapolation to humans, especially as CSD propagation is limited by prominent sulci in the human brain that are absent in the lissencephalic rodent brain. Within this limitation, we predict that TBI may increase CGRP levels to alter brain plasticity and predispose patients to migraine-like post-traumatic headaches.

How might CSD increase cortical CGRP gene expression? While speculative, one mechanism may be generation of reactive oxygen species (ROS). Migraineurs have elevated plasma levels of a ROS-induced lipid peroxidation products (43). In rats, CSD produces ROS in the cortex and trigeminal nerve (44,45). Likewise, the ROS-responsive COX2 gene has been reported to be upregulated by CSD (16). Moreover, ROS-induced CGRP gene expression can be inhibited with antioxidant treatment in rat trigeminal ganglia (26). In light of these observations, we speculate that CSD-induced ROS production can lead to pro-inflammatory cascades that upregulate the CGRP gene. Interestingly, a recent analysis of the literature concluded that oxidative stress is a shared feature of most migraine triggers (43).

We have provided evidence showing that CSD upregulates CGRP gene expression in the cortex. Given the promising potential of CGRP-based therapeutics for treating and preventing migraine, a link between CSD and CGRP further emphasizes the importance of CSD as a target for migraine drug development (46,47). The significance of our finding is that CSD may be a mechanism by which CGRP levels become elevated for a prolonged period in some migraine patients. While there are multiple mechanisms that can potentially increase CGRP expression, including nitric oxide (48) and cytokines (33,48,49), this is the first report of a

physiological *in vivo* mechanism that may elevate cortical CGRP gene expression in migraine and post-traumatic headache. Given CGRP's role as a neuromodulator (17), this elevation may potentially contribute to cortical hyperexcitability and sensory abnormalities in migraine.

Article highlights

- Multiple CSD events can trigger CGRP gene expression in discrete regions of the rat cerebral cortex.
- This is the first *in vivo* evidence for a mechanism to initiate and maintain elevated CGRP levels in migraine and post-traumatic headache.

Acknowledgements

We are grateful for advice and training from Dan Kaufmann and KC Brennan (University of Utah) and advice from Sajedeh Eftekhari (UCLA) and Karin Warfvinge and Lars Edvinsson (Lund University). We also thank Liwen Jiang (XJTLU) for technical support on single CSD experiments.

Declaration of conflicting interests

The authors declared no potential conflicts of interest with respect to the research, authorship, and/or publication of this article.

Funding

The authors disclosed receipt of the following financial support for the research, authorship, and/or publication of this article: Wangwenli Charitable Foundation (RD0006), NIH (NS075599), Veterans Affairs Medical Center (1IO1RX002101), and Department of Defense USAMRAA (W81XWH-16-1-0071).

References

1. Lipton RB, Bigal ME, Diamond M, et al. Migraine prevalence, disease burden, and the need for preventive therapy. *Neurology* 2007; 68: 343–349.
2. Cutrer FM and Huerter K. Migraine aura. *Neurologist* 2007; 13: 118–125.
3. Ayata C and Lauritzen M. Spreading depression, spreading depolarizations, and the cerebral vasculature. *Physiol Rev* 2015; 95: 953–993.
4. Hadjikhani N, Sanchez Del Rio M, Wu O, et al. Mechanisms of migraine aura revealed by functional MRI in human visual cortex. *Proc Natl Acad Sci U S A* 2001; 98: 4687–4692.
5. Charles A and Brennan K. Cortical spreading depression-new insights and persistent questions. *Cephalalgia* 2009; 29: 1115–1124.
6. Pietrobon D and Moskowitz MA. Pathophysiology of migraine. *Annu Rev Physiol* 2013; 75: 365–391.
7. Zhang X, Levy D, Noseda R, et al. Activation of meningeal nociceptors by cortical spreading depression: Implications for migraine with aura. *J Neurosci* 2010; 30: 8807–8814.
8. Zhang X, Levy D, Kainz V, et al. Activation of central trigeminovascular neurons by cortical spreading depression. *Ann Neurol* 2011; 69: 855–865.
9. Karatas H, Erdener SE, Gursoy-Ozdemir Y, et al. Spreading depression triggers headache by activating neuronal Panx1 channels. *Science* 2013; 339: 1092–1095.
10. Dreier JP. The role of spreading depression, spreading depolarization and spreading ischemia in neurological disease. *Nat Med* 2011; 17: 439–447.
11. Lauritzen M, Dreier JP, Fabricius M, et al. Clinical relevance of cortical spreading depression in neurological disorders: Migraine, malignant stroke, subarachnoid and intracranial hemorrhage, and traumatic brain injury. *J Cereb Blood Flow Metab* 2011; 31: 17–35.
12. Hartings JA, Shuttleworth CW, Kirov SA, et al. The continuum of spreading depolarizations in acute cortical lesion development: Examining Leao's legacy. *J Cereb Blood Flow Metab*, Epub ahead of print 21 June 2016. DOI: 10.1177/0271678X16654495.
13. Dreier JP, Woitzik J, Fabricius M, et al. Delayed ischaemic neurological deficits after subarachnoid haemorrhage are associated with clusters of spreading depolarizations. *Brain* 2006; 129: 3224–3237.
14. Hartings JA, Bullock MR, Okonkwo DO, et al. Spreading depolarisations and outcome after traumatic brain injury: A prospective observational study. *Lancet Neurol* 2011; 10: 1058–1064.
15. Takizawa T, Shibata M, Kayama Y, et al. Temporal profiles of high-mobility group box 1 expression levels after cortical spreading depression in mice. *Cephalalgia* 2016; 36: 44–52.
16. Urbach A, Bruehl C and Witte OW. Microarray-based long-term detection of genes differentially expressed after cortical spreading depression. *Eur J Neurosci* 2006; 24: 841–856.
17. Russo AF. Calcitonin gene-related peptide (CGRP): A new target for migraine. *Annu Rev Pharmacol Toxicol* 2015; 55: 533–552.
18. Hansen JM, Hauge AW, Olesen J, et al. Calcitonin gene-related peptide triggers migraine-like attacks in patients with migraine with aura. *Cephalalgia* 2010; 30: 1179–1186.
19. Lassen LH, Haderslev PA, Jacobsen VB, et al. CGRP may play a causative role in migraine. *Cephalalgia* 2002; 22: 54–61.
20. van Dongen RM, Zielman R, Noga M, et al. Migraine biomarkers in cerebrospinal fluid: A systematic review and meta-analysis. *Cephalalgia*. Epub ahead of print 17 February 2016. DOI: 10.1177/0333102415625614.

21. Bigal ME, Walter S and Rapoport AM. Therapeutic antibodies against CGRP or its receptor. *Br J Clin Pharmacol* 2015; 79: 886–895.
22. Edvinsson L. CGRP receptor antagonists and antibodies against CGRP and its receptor in migraine treatment. *Br J Clin Pharmacol* 2015; 80: 193–199.
23. Wang M. Cortical spreading depression and calcitonin gene-related peptide: A brief review of current progress. *Neuropeptides* 2013; 47: 463–466.
24. Tozzi A, de Iure A, Di Filippo M, et al. Critical role of calcitonin gene-related peptide receptors in cortical spreading depression. *Proc Natl Acad Sci U S A* 2012; 109: 18985–18990.
25. Hansen JM and Ashina M. Calcitonin gene-related peptide and migraine with aura: A systematic review. *Cephalalgia* 2014; 34: 695–707.
26. Raddant AC and Russo AF. Reactive oxygen species induce procalcitonin expression in trigeminal ganglia glia. *Headache* 2014; 54: 472–484.
27. Park KY, Fletcher JR, Raddant AC, et al. Epigenetic regulation of the calcitonin gene-related peptide gene in trigeminal glia. *Cephalalgia* 2011; 31: 614–624.
28. Vandesompele J, De Preter K, Pattyn F, et al. Accurate normalization of real-time quantitative RT-PCR data by geometric averaging of multiple internal control genes. *Genome Biol* 2002; 3RESEARCH0034.
29. Bhatt DK, Gupta S, Ploug KB, et al. mRNA distribution of CGRP and its receptor components in the trigeminovascular system and other pain related structures in rat brain, and effect of intracerebroventricular administration of CGRP on Fos expression in the TNC. *Neurosci Lett* 2014; 559: 99–104.
30. Eiselt M, Giessler F, Platzek D, et al. Inhomogeneous propagation of cortical spreading depression-detection by electro- and magnetoencephalography in rats. *Brain Res* 2004; 1028: 83–91.
31. Piper RD, Edvinsson L, Ekman R, et al. Cortical spreading depression does not result in the release of calcitonin gene-related peptide into the external jugular vein of the cat: Relevance to human migraine. *Cephalalgia* 1993; 13: 180–183. discussion 49.
32. Yisarakun W, Chantong C, Supornsilpchai W, et al. Up-regulation of calcitonin gene-related peptide in trigeminal ganglion following chronic exposure to paracetamol in a CSD migraine animal model. *Neuropeptides* 2015; 51: 9–16.
33. Jander S, Schroeter M, Peters O, et al. Cortical spreading depression induces proinflammatory cytokine gene expression in the rat brain. *J Cereb Blood Flow Metab* 2001; 21: 218–225.
34. Ayata C. Pearls and pitfalls in experimental models of spreading depression. *Cephalalgia* 2013; 33: 604–613.
35. Rangel YM, Kariko K, Harris VA, et al. Dose-dependent induction of mRNAs encoding brain-derived neurotrophic factor and heat-shock protein-72 after cortical spreading depression in the rat. *Brain Res Mol Brain Res* 2001; 88: 103–112.
36. Elliott MB, Oshinsky ML, Amenta PS, et al. Nociceptive neuropeptide increases and periorbital allodynia in a model of traumatic brain injury. *Headache* 2012; 52: 966–984.
37. von Baumgarten L, Trabold R, Thal S, et al. Role of cortical spreading depressions for secondary brain damage after traumatic brain injury in mice. *J Cereb Blood Flow Metab* 2008; 28: 1353–1360.
38. Song Y, Bi L, Zhang Z, et al. Increased levels of calcitonin gene-related peptide in serum accelerate fracture healing following traumatic brain injury. *Mol Med Rep* 2012; 5: 432–438.
39. Hang CH, Shi JX, Li JS, et al. Levels of vasoactive intestinal peptide, cholecystokinin and calcitonin gene-related peptide in plasma and jejunum of rats following traumatic brain injury and underlying significance in gastrointestinal dysfunction. *World J Gastroenterol* 2004; 10: 875–880.
40. Bolay H, Reuter U, Dunn AK, et al. Intrinsic brain activity triggers trigeminal meningeal afferents in a migraine model. *Nat Med* 2002; 8: 136–142.
41. Fioravanti B, Kasasbeh A, Edelmayer R, et al. Evaluation of cutaneous allodynia following induction of cortical spreading depression in freely moving rats. *Cephalalgia* 2011; 31: 1090–1100.
42. Tepe N, Filiz A, Dilekoz E, et al. The thalamic reticular nucleus is activated by cortical spreading depression in freely moving rats: Prevention by acute valproate administration. *Eur J Neurosci* 2015; 41: 120–128.
43. Borkum JM. Migraine triggers and oxidative stress: A narrative review and synthesis. *Headache* 2016; 56: 12–35.
44. Shatillo A, Koroleva K, Giniatullina R, et al. Cortical spreading depression induces oxidative stress in the trigeminal nociceptive system. *Neuroscience* 2013; 253: 341–349.
45. Viggiano A, Viggiano E, Valentino I, et al. Cortical spreading depression affects reactive oxygen species production. *Brain Res* 2011; 1368: 11–18.
46. Costa C, Tozzi A, Rainero I, et al. Cortical spreading depression as a target for anti-migraine agents. *J Headache Pain* 2013; 14: 62.
47. Noseda R and Burstein R. Migraine pathophysiology: Anatomy of the trigeminovascular pathway and associated neurological symptoms, cortical spreading depression, sensitization, and modulation of pain. *Pain* 2013; 154(Suppl 1): S44–S53.
48. Bellamy J, Bowen EJ, Russo AF, et al. Nitric oxide regulation of calcitonin gene-related peptide gene expression in rat trigeminal ganglia neurons. *Eur J Neurosci* 2006; 23: 2057–2066.
49. Richter F, Lutz W, Eitner A, et al. Tumor necrosis factor reduces the amplitude of rat cortical spreading depression in vivo. *Ann Neurol* 2014; 76: 43–53.

Critical Role of Src Family Kinases in Cortical Spreading Depression in Rats

Fan Bu[1,2], John P Quinn[2], Minyan Wang[1,*]
[1] Department of Biological Sciences, Centre for Neuroscience, Xi'an Jiaotong-Liverpool University (XJTLU), Suzhou, China;
[2] Department of Molecular and Clinical Pharmacology, Institute of Translational Medicine, Liverpool University (UoL), Liverpool, UK
Corresponding author: Dr Minyan Wang, minyan.wang@xjtlu.edu.cn

Background:

- Cortical spreading depression (CSD) is a propagating excitation of both neurons and glia followed by depression in cortex and subcortical regions, which may promote migraine attacks and the progression of stroke lesions.
- NR2A/B-containing NMDA receptors contribute to CSD genesis and propagation [1,2], whereas their mechanism remains unknown.
- Src Family Kinases (SFKs) can increase NMDA receptor currents by phosphorylation of one or more tyrosine residues in C-tails of NR2A/B subunits [3]. Activation of NMDA receptors lead to activation of SFKs during anoxia [4].

Aim:

To investigate whether SFKs are involved in cortical spreading depression.

Methods:

- Electrophysiology was performed to detect the effect of a SFKs inhibitor PP2 (PP3 as the inactive analog) at 5 μM on CSD.
- Western blotting (WB) was then performed to analyze the protein level of SFKs.

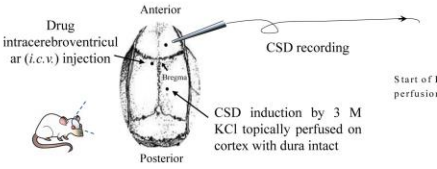

Figure 1. Schematic representation of surgical coordinates on parietal bone of isoflurane anaesthetic rats.

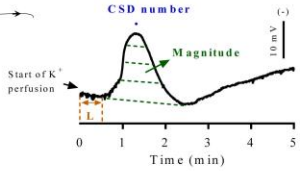

Figure 2. Representative trace in DC potential of CSD.

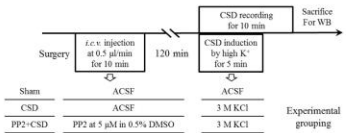

Figure 3. *in vivo* experimental protocol.

Results:

1. CSD increased SFKs phosphorylation at Y416 (PY416) in ipsilateral cortex, which was reversed by PP2.

2. PP2 reduced cortex susceptibility to CSD and the magnitude of CSD.

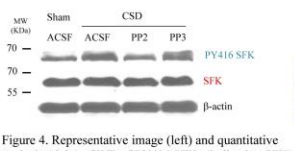

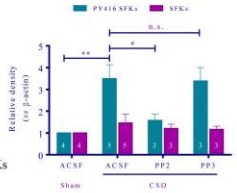

Figure 4. Representative image (left) and quantitative analysis (right) of WB of PY416 SFKs (indicating SFKs activation) and total SFKs. mean±SEM

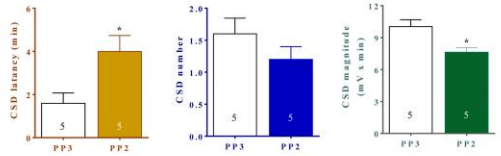

Figure 5. Quantitative analysis of CSD weaves. mean±SEM

Conclusion and Further Work:

- **This study reveals a previously unknown migraine mechanism involving SFKs.**
- **Whether SFKs activation regulates NR2A-mediated CSD requires further investigation.**

References: 1. BU, F et al., *Scientific reports* 6:23576, 2016. 2. PEETERS, M. et al., *J Pharmacol Exp Ther,* 321, 564-72, 2007. 3. SALTER, M. et al., *Nat Rev Neurosci,* 5, 317-28, 2007. 4. WEILINGER, N. L. et al., *J Neurosci,* 32, 12579-88, 2012.

First author information: Fan Bu, fan.bu13@student.xjtlu.edu.cn, the final PhD student in XJTLU and UoL.

Acknowledgment: primary supervisor Dr. Minyan Wang , co-supervisor Professor John P Quinn, Yan Wang, Dongqing Ma and Liwen Jiang; Funding from XJTLU and Wenli Wang charitable foundation.

NR2A-containing NMDA Receptors Contribute to CSD-induced Panx1 Channels Opening via Src Family Kinases

Minyan Wang[1], Fan Bu[1,2], John P Quinn[2]
[1] Department of Biological Sciences, Centre for Neuroscience, Xi'an Jiaotong-Liverpool University (XJTLU), Suzhou, China;
[2] Department of Molecular and Clinical Pharmacology, Institute of Translational Medicine, Liverpool University, Liverpool, UK

Background:

- Cortical spreading depression (CSD) is a propagating excitation of both neurons and glia followed by depression in cortex and subcortical regions, which is the underlying cause of migraine attacks.
- CSD may lead to migraine headache via activating Pannexin1 (Panx1) channels [1], whereas the mechanism remains unknown.
- NR2A-containing NMDA receptors contribute to CSD genesis and propagation [2,3].
- CSD can activate Src Family Kinases (SFKs). (Unpublished data, refer to poster EHMTC-0379)
- Anoxia-induced NMDA receptor activation opens Panx1 channels via SFKs [4].

Aims:

To explore whether NR2A could regulate CSD-induced Panx1 channels opening involving SFKs.

Methods:

- Pharmacological treatment via intracerebroventricular (*i.c.v*) injection.
- CSD induction by topical application of 3 M KCl on cortex with dura intact for 5 minutes in isoflurane anaesthetic rats.
- Immunohistochemistry (IHC), western blotting (WB) and co-immunoprecipitation (co-IP) were then performed using pre-treated tissue.

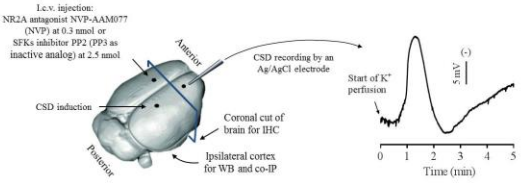

Figure 1. Schematic representation of surgical coordinates on rat cortex (left) and representative trace in direct current potential of CSD (right).

Results:

1. CSD-induced SFKs phosphorylation at amino acid Y416 (PY416) was suppressed by NR2A inhibition.

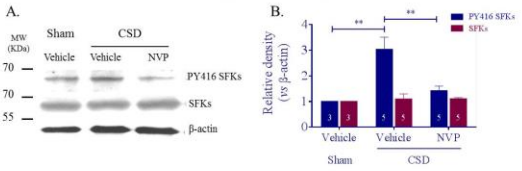

Figure 2. Representative image (A) and quantitative analysis (B) of western blotting of PY416 SFK (indicating SFKs activation) and total SFKs in the absence or presence of NVP. mean ± SEM.

2. CSD-induced interaction between PY416 SFKs and Panx1 was suppressed by NR2A inhibition.

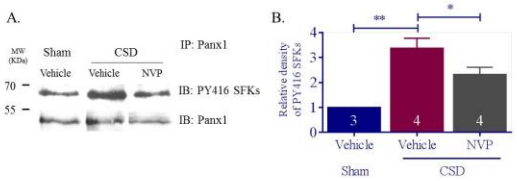

Figure 3. Representative image (A) and quantitative analysis (B) of western blotting of PY416 SFKs that was co-IP'd by Panx1 Ab. Equal loading is indicated by Panx1. mean ± SEM.

3. Both NR2A inhibition and SFKs inhibition prevented CSD-induced PI influx in NeuN-positive cells.

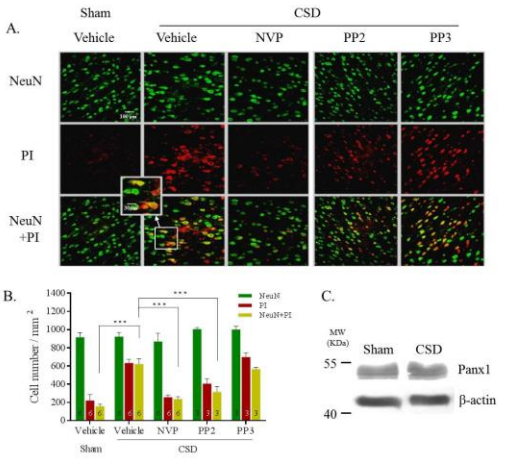

Figure 4. (A) Representative image of propidium iodide (PI)- (red) and NeuN- (green) staining cells at layers V and VI of ipsilateral motor cortex observed at 400X. PI indicates cells with activated Panx1 channels. NeuN indicates neurons. (B) The averaged number of cells (mm²) in layers V and VI of ipsilateral motor, cingulate and somatosensory cortical regions in the absence or presence of NVP and PP2. (C) The protein expression of Panx1 was not altered after CSD. mean ± SEM.

Conclusion:

- CSD induces SFKs and Panx1 channels interaction.
- CSD-induced SFKs activation and its interaction with neuronal Panx1 channels can be mediated by NR2A, reveals a previously unknown pathway in migraine pathophysiology.

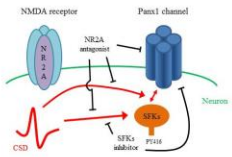

References: 1. KARATAS, H et al., *Science*, 339: 1092-1095, 2013. 2. BU, F et al., *Scientific reports* 6:23576, 2016. 3. WANG MY et al., *Br J Pharmacol*, 165: 235–244, 2012. 4. WEILINGER, N. L. et al., *J Neurosci*, 32, 12579-88, 2012.

Contact: Dr Minyan Wang Minyan.wang@xjtlu.edu.cn;

Acknowledgment: Yan Wang, Dongqing Ma and Liwen Jiang; Yi Li for gift, NVP-AAM077; Funding from XJTLU and Wenli Wang Charitable Foundation.

NR2A Regulates PANX1 and Src Activation in Early Stage of Migraine

Fan Bu[1], John Quinn[2], Minyan Wang[1,*]

1 Biological Sciences Department, Xi'an Jiaotong-Liverpool University, Su Zhou, China; 2 Institute of Translational Medicine, University of Liverpool, Liverpool, UK

Background

- Migraine is a common neurologic disorder, characterized by recurrent, unilateral, throbbing headache often with cutaneous allodynia, photophobia, phonophobia and numbness.
- Cortical spreading depression (CSD) is a propagating excitation of both neurons and glia followed by depression in cortex and subcortical regions, which may lead to migraine in human being. CSD is accompanied with the release of various neurotransmitters, ion disturbance and change in blood flow.
- NR2A-containing NMDA receptors (NR2A) contribute to genesis and propagation of CSD [1].
- CSD triggers Pannexin 1 (Panx 1) channels opening followed by the release of inflammatory factors in glia limitans of meninges and further lead to headache-like behavior in rats [2].
- Panx 1 channels opening is Src kinase (Src) activation dependent [3].

Aim

To investigate whether NR2A mediates CSD-induced Panx 1 channels opening and Src activation

Methods

CSD induction and recording in cortex of rats

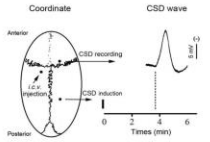

Figure 1. (A) Diagram showing coordinates of CSD induction, recording and drug injection on skull of anaesthetic rats. CSD was induced by 3 M KCl applied on the surface of right cortex and recorded by Ag/AgCl electrode on the ipsilateral side. Drug was intracerebroventricularly (*i.c.v.*) injected on the contralateral side. (B) Representative direct current potential of CSD wave.

Experimental design

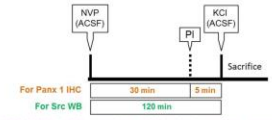

NVP-AAM077 (NVP), competitive NR2A-preferring receptors antagonist; Propidium iodide (PI), red-fluorescent stain, indicating activated Panx 1.

Figure 2. Two sets of Experiments were designed for Panx1 immunohistochemistry (IHC) and Src western blot (WB). Three groups for each experimental set: sham (ACSF+PI+ACSF), CSD (ACSF+PI+KCl), NVP (NVP+PI+KCl).

For Panx 1 IHC, NVP (0.3 nmol) and PI (2 μg) were *i.c.v.* injected 30 and 5 min before CSD induction respectively.

For Src WB, NVP was *i.c.v.* injected 120 min before CSD induction. Ipsilateral cortex was dissected for WB use.

Results

1.CSD was suppressed by NVP.

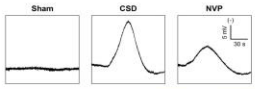

2. NVP prevented CSD-induced PI uptake in cells of cortical layers V & VI

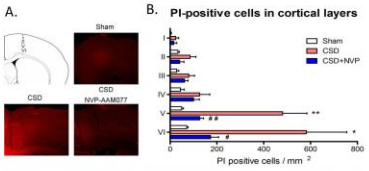

Figure 4. (A) PI-staining cells (red) in coronal planes of ipsilateral cortex observed at 40X; (B) The number of PI-positive cells in unit area (mm^2) in each layer. mean±SEM. n = 6

3. NVP prevented CSD-induced PI influx in NeuN-labeled cells.

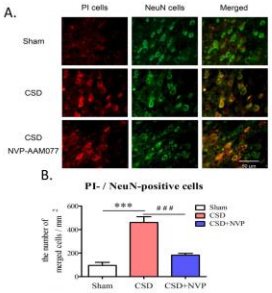

Figure 5. (A) PI- (red) and NeuN- (green) staining cells observed at 400X. Anti-NeuN (1:1000) antibody was for labeling neurons. (B) The number of merged cells in unit area (mm^2) in layers V and VI. Merged cells is ~ 90% of PI-staining cells. mean±SEM. n = 6

4. NVP reversed CSD-induced Src tyrosine phosphorylation.

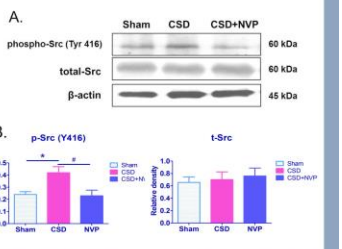

Figure 6. (A) Bands of phospho- / total- Src assayed by WB. Anti-phospho-Src (Tyr 416) (1:500) and Src (1:1000) antibodies, indicating activated and total Src respectively. (B) Quantitative analysis of relative density of p- and t- Src in (A) compared with β-actin levels. mean±SEM. n = 3 ~ 5

Conclusion and further work

- **NR2A activates CSD-induced neuronal Panx 1 channels in cortex.**
- **CSD induces cortical Src activation.**
- **NR2A contributes to CSD-induced Src activation.**
- Whether NR2A opens Panx 1 channels via Src during CSD requires further investigation.

Acknowledgment Dr. Minyan Wang (primary supervisor) and Professor John Quinn (co-supervisor); Yan Wang for IHC guidance; Novartis Pharmas (Switzerland) for gift, NVP-AAM077; Funding from XJTLU and Wenli Wang charitable foundation.

References 1. Wang et al., Br J Pharmacol, 165: 235–244, 2012. 2. Karatas et al., Science, 339: 1092-1095, 2013. 3. Weilinger et al., J Neurosci, 32:12579-88, 2012.

Contact Fan Bu (卜凡) e-mail: fan.bu13@student.xjtlu.edu.cn

NR2A Plays a Key Role in Mediating CSD Genesis - a potential strategy against migraine with aura?

Fan Bu[1,2], John Quinn[2], Minyan Wang[1,*]

1. Centre of Neuroscience, Biological Sciences Department, Xi'an Jiaotong-Liverpool University, Su Zhou, China
2. Institute of Translational Medicine, Liverpool University, Liverpool, UK;
* Corresponding author. E-mail address: Minyan.wang@xjtlu.edu.cn

Background

- Cortical spreading depression (CSD) is a transient disruption of local ionic homeostasis, followed by depression that may promote migraine attacks and the progression of stroke lesions .
- NMDA receptor inhibition by MK-801 decreases magnitude and propagation rate of CSD in rat [1].
- Competitive NR2A-preferring receptor antagonist, NVP-AAM077, decreases the magnitude and propagation rate of retinal spreading depression[2].

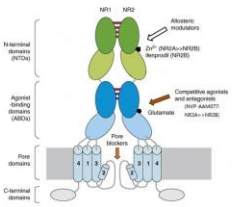

Figure 1. Functional binding sites of NR2A [3]

Aim To determine whether NR2A inhibition suppresses CSD *in vivo*.

Method

- Microdialysis probes and Ag/AgCl electrodes were implanted respectively into the right cortex of rats for recording CSD genesis and propagation.
- Five repeated CSD episodes were induced by high potassium through the microdialysis probe with 40-minute recovery interval.

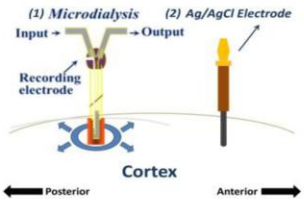

Figure 2. Diagram showing microdialysis probe and Ag/AgCl electrode implantations

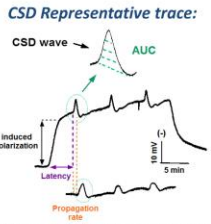

Figure 3. Representative traces to indicate area under the curve (AUC), Latency, and Propagation rate during CSD elicitation (1) and propagation (2).

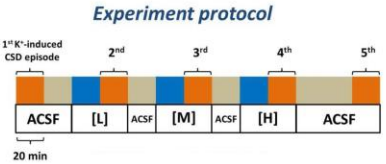

Figure 4. Experimental design showing 5 repeated CSD episodes were induced by high potassium for 20 minutes, each followed by 40-minutes recovery. The drug at 3 different concentrations was applied 20 minutes before and during the 2nd, 3rd and 4th episodes.

Results

- MK-801 markedly suppressed the magnitude of CSD genesis and propagation and reduced susceptibility of CSD, however, it did not alter the velocity of CSD propagation.
- NVP-AAM077 also significantly decreased the magnitude of CSD genesis, however, it did not alter susceptibility of the cortex to CSD, nor change the propagation rate.

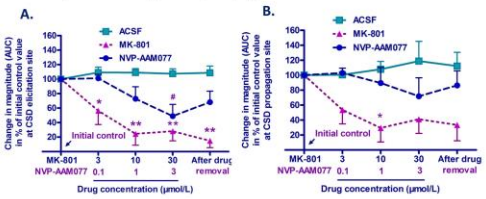

Figure 5. Averaged data showing effects of MK801 and NVP-AAM077 on magnitude of CSD genesis and propagation (n=6 respectively)

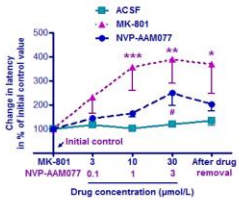

Figure 6. Averaged data showing effects of MK801 and NVP-AAM077 (n=6 respectively) on CSD latency.

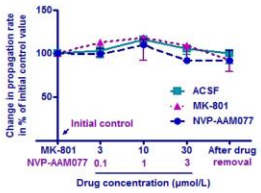

Figure7. Neither NVP-AAM077 (n=6) nor MK-801 (n=6) altered CSD propagation rate.

Conclusion and Further Work

- NR2A inhibition suppresses CSD elicitation suggesting that NR2A plays a key role in mediating CSD genesis.
- Whether NR2A mediates CSD propagation and how NR2A-mediated CSD process are regulated requires further investigation.

Reference

1. Peeters et al. The Journal of Pharmacology and Experimental, 321:564–572, 2007.
2. Wang et al. British Journal of Pharmacology, 165: 235–244, 2012.
3. Pierre Paoletti and Jacques Neyton. Current Opinion in Pharmacology, 7:39–47, 2007.

Acknowledgement

Novartis Pharmas (Switzerland) for gift, NVP-AAM077;
My primary supervisor Dr. Minyan Wang for supervision and co-supervisor Dr. John Quinn.